SYNTHESIS AND PHOTOPHYSICAL PROPERTIES OF ORGANIC DIPOLAR MOLECULAR NANO/MICROPARTICLES

A Thesis
Submitted for the Degree of

DOCTOR OF PHILOSOPHY

by

Ravi Kumar Kanaparthi

School of Chemistry
University of Hyderabad
Hyderabad - 500 046
INDIA

June 2011

To
My Parents

"A person who never made a mistake never tried anything new."

-Albert Einstein

" Things are simple, we should not make them complex."

-Anunay Samanta

STATEMENT

I hereby declare that the matter embodied in the thesis entitled *"Synthesis and Photophysical Properties of Organic Dipolar Molecular Nano/Microparticles"* is the result of investigations carried out by me in the School of Chemistry, University of Hyderabad, Hyderabad, India under the supervision of **Prof. Anunay Samanta**.

In keeping with the general practice of reporting scientific investigations, due acknowledgements have been made wherever the work described is based on the findings of other investigators. Any omission or error that might have crept in is regretted.

June 2011
Kanaparthi

Ravi Kumar

SCHOOL OF CHEMISTRY
UNIVERSITY OF HYDERABAD
HYDERABAD-500 046, INDIA

Phone: +91-40-2313 4813 (O)
+91-40-2313 0715 (R)
Fax: +91-40-2301 1594
Email: assc@uohyd.ernet.in
anunay.samanta@gmail.com

Prof. Anunay Samanta
FNASc, FASc, FNA
J.C. Bose Fellow

30th June, 2011

CERTIFICATE

Certified that the work embodied in the thesis entitled ***"Synthesis and Photophysical Properties of Organic Dipolar Molecular Nano/Microparticles"*** has been carried out by **Mr. Ravi Kumar Kanaparthi** under my supervision and that the same has not been submitted elsewhere for any degree.

Anunay Samanta
(Thesis Supervisor)

Dean
School of Chemistry
University of Hyderabad

Acknowledgement

It gives me immense pleasure to express my sincere gratitude and deep respect to **Prof. Anunay Samanta**, my research supervisor, for his constant cooperation, encouragement and kind guidance. He has been quite helpful to me in both academic and personal fronts. His hard work and positive thinking are inspirational to my research career.

Studying at School of Chemistry was a great exciting experience in my life. I would like to thank the former and present Deans, School of Chemistry, for providing infrastructure and research facilities and all the faculty members of the school for their cooperation during my Master's and Doctoral studies. Their creative and enthusiastic lectures are the driving forces for my research my carrier.

Financial assistance from UGC, New Delhi is greatly acknowledged. I am also thankful to DST (PURSE grant) for providing financial assistance to attend international conference held at Honolulu, Hawaii, U.S.A.

I value my association with my lab seniors: Sandip, Tamal, Prasun, Moloy, Aniruddha and Bhaswati from whom I have learned many unwritten aspects of research. I would like to specially thank Sandip for introducing me to research giving me useful research tips. My hearty thanks to Moloyda for helping me to overcome all the depressing experiences I went through during my research tenure. I acknowledge my junior friends Dinesh (sincere), Santhosh (Mr.perfect and cool), Sanghamitra, Soumya, Satyajit (wikipedia), Ashok (naughty) and Chandra Sekhar (jovial) for maintaining friendly and cooperative atmosphere in the lab. I am really lucky to have them as my juniors. My special thanks to Dinesh and Santhosh for their useful discussions.

I also thank all non-teaching staff for their timely help, Raghavaiah for X-ray data collection, Satyannarayana for recording NMR data, A.R. Shetty and Mallaiah Shetty for their help in purchasing chemicals in particular.

I am thankful to all my colleagues in the School of Chemistry for helping and supporting me in various issues. My sincere thanks to Srinivas (SKD lab) and Ranjit (AN lab) for helping with single crystal X-ray data collection and analysis.

I would like thank Pavan Kumar, Manjunath, Murthy, Ahmad and Nalini of Central Instrumentation Laboratory of *University of Hyderabad*, for helping with SEM and Fluorescence Microscopy experiments. My hearty thanks to Muvva Durga Prasad and Manohar Reddy for their help in TEM measurements. I also thank M. Laxminanrayana for FESEM experiments.

Today I stand as chemist because of Kutumba Rao of *SVRM College* who taught organic chemistry. It is because of his enthusiastic lectures, I have chosen *chemistry* as a major subject for my higher studies. I also thank K. Surendra Babu, Neerajanabhaiah, G. Srinivasa Rao, P. Srinivasa Rao and Sudhkar in particular for

their excellent lectures. I extend my sincere thanks to other teachers, Prabhakara Rao, Panchumarthi Srinivasa Rao, G. Srinivasa Rao of Physics Department; Bhavannarayana and Subrahmanyam of Mathematics Department for their timely help and discussions during my intermediate and graduation study. I would also like to thank Ratna Raju of Telugu Department; Das and Supriya of English Department.

I would also like to express my sincere thanks to Krishna Kishore, KV Rao, Suneel (Vamsam) and Suresh for their timely help in both academics and financial aspects. Without these persons I would not have even think of *study in UoH*. I extend my sincere thanks to G. Pulla Rao who actually laid a road to UoH with his excellent teaching.

I thank Mr. Sivaranjan Reddy (he is something special) who has associated with me more than any one during my stay. He is more than a friend, stood with my all the time. I would like to thank all my MSc classmates and juniors, especially, Prasanth, Venkatram, Lachaiach, Yarabarla, Pavan, Ravi, Leela, Rakesh, Mitta, KVS, Dev, Ganipisetti, Taagubotu Mallesh, Ganesh, Hari, Koppolu Srinu, Guru, Laxman, Vijiyendar, and Ravi. I also thank my MSc senior students, Phani Phavan, Sekhar Reddy, Venu Srinivas, Naga Raju, Vikram, Ramu, Rama Kumar, Sridhar Reddy, Venkata Reddy and Korella for their valuable suggestions during my MSc.

My close association with Galla Karunakar, Jaya Prakash, DLV Prasad, Venkat (Director), G.V.Ramesh, Gupta, Hari, Balu, Rajesh, Narahari, Pavan, Rajeswar Singh, Yadaiah, Krishna Rao, Anji, Rams, Ramesh, Bhuvan, Ramesh Reddy, Veera Raghavaiah, Tanmoy, RajaGopal[2], NagaPrasad, Ghanta, Naba Kamal, Ranjith, Jagadeesh, Arun, Arindam, Sandip, Sudangshu, Karunakar, SrinivasaRao, Sanjeev, Vikranth, Narayana, Ramu Yadav, Venu, Ramakrishna, Rambabu, GDP, Kishore, Bharat, Satish, Chaitanya, Vijji, Anand, P. Kishore, Ganesh, Sekhar Reddy, Praveen, DK Sheshagiri, Ramesh, Israel, Venkaiah, and Sundar is really sweet and memorable during my stay and I am thankful to them for various reasons.

I am also grateful for the valuable friendship of Nalla Babai (Kiran), Ratna Joseph, Jagapathi, Prasanna, Ratna Kumari, Matte, Naraiah, Basavapatuni who are still my buddies. I must acknowledge the valuable friendship of Salman, PotuRaj, Bujji Babu, Jyothi, Gangadhar, Chukka Ravi, Satyannarayana, Koteswara rao, Kode Kiran (stats), Kanaka Raju, Srikanth and Suresh.

I want to pay sincere gratitude from the bottom of my heart to my uncle (Nirikshana Rao). He is a role model to me since my childhood. His constant support for my higher studies is always memorable and valuable. I would like to thank all my relatives, Anjaiah babai & family; Stalin mama & family; Sastry pedananna& family, Bulli babai & family. I cherished with my cousins, Sekhar, Pani, Manoj, RaghuRam, ManiRam, Nikhil Chakravarthy, Avinash, Sravani, Sandhya, Naresh, Jayanth, Raji, Jyothi.

My special thanks my mama Babu Rao & his family. I value my brother-in-laws Venu, Ramesh, Suresh, Sarath and Das for their love and affection.

This thesis would have not been possible without the selfless love and support of my parents (Ratam & Ratna Kumari), brothers (Anand & Sasi) and sister (JayaSri). I value the blessings of my grandparents.

Last but not least, I am thankful to my wife, Sudeena and son, Suhas.

-Ravi Kumar

List of Publications

1. "Ratiometric fluorescence signaling of fluoride ions by an amidophthalimide derivative." M. Sarkar, Y. Raghavendra, B. Bhattacharya**, Ravi Kumar K.** and A. Samanta *J. Chem. Sci.* **2007,** *119*, 91-97.
2. "Polarity dependence of the radiative and nonradiative rates of flavone derivatives comprising structurally similar amino moieties: Change in the nature of the emitting state." M. Sarkar, **Ravi Kumar K.**, B. Bhattacharya and A. Samanta *J. Phys. Chem. A* **2008**, *112*, 3302-3310.
3. "Probing the Aggregated State of 4-(9-anthryl)-*N*,*N*-dimethylaniline by UV-Vis Absorption and Fluorescence Spectroscopy, Microscopy, and Crystallography. " **Ravi Kumar K.**, M. Sarkar and A. Samanta *J. Phys. Chem. B* **2009**, *113,* 15189-15195.
4. "Folding and Unfolding Movements in a [2]Pseudorotaxane". M. Suresh, A. K. Mandal, M. K. Kesharwani, N. N. Adarsh, B. Ganguly, **Ravi Kumar K.** A. Samanta and A. Das. *J. Org. Chem.* **2011**, *76*, 138-144.
5. "Synthesis, structure and luminescence behavior of a mononuclear cadmium(II) dicyanamide and a coordination polymer of mercury(II) dicyanamide containing 2,2'-dipyridylamine (dpaH) as end-capping ligand/anion of dpaH as binucleating bridge. Variance in coordination numbers, nuclearities and architectures with metal ion templates." S. Das, K. Bhar, S. Chantrapromma, H-K. Fun, **Ravi Kumar K.**, A. Samanta and B. K. Ghosh, *Inorganica Chimica Acta*, **2011***,367*, 199-206.

6. "Controlled fabrication and optical properties of highly fluorescent nano-/micro-particles of dipolar molecular system." **Ravi Kumar K.**, S. Patra and A. Samanta (*communicated*)
7. "How diverse the nanostructures of a single molecular system can be?" **Ravi Kumar K.** and A. Samanta. (*communicated*)
8. "Self-assembled 2D-nanoplates of highly fluorescent molecule." **Ravi Kumar K.** and A. Samanta. (*in preparation*)
9. "Photophysical properties of 4-(9-Anthryl)-N,N-Dimethylaniline in room temperature ionic liquids." **Ravi Kumar K.**, K. Santhosh and A. Samanta. (*in preparation*)

Conference Presentations

1. Controlled fabrication and optical properties of highly fluorescent 1D and semi-2D nanostructures of a dipolar organic molecular system. **Ravi Kumar K.** and A. Samanta. – 2nd Pacifichem, 2010, organized by International Chemical Congress of Pacific Basin Societies, Honolulu, Hawaii, U.S.A., December 2010. **(Oral and poster presentations)**
2. Synthesis and optical properties of molecular nano/microparticles of 9-(4-cyanophenyl) carbazole. **Ravi Kumar K.** and A. Samanta. – 3rd Asia Pacific Symposium on Radiation Chemistry and 10th Biennial Trombay Symposium on Radiation & Photochemistry, organized by Bhabha Atomic Research Centre, (BARC), Lonavala, Maharashtra, India September 2010. **(Poster Presentation).**
3. Controlled synthesis of 1D or semi-2D molecular nanostructures and study of optical properties. **Ravi Kumar K.** and A. Samanta. – 7th Annual In-house symposium of School of Chemistry, ChemFest 2010, organized by School of Chemistry, University of Hyderabad, Hyderabad, India, January 2010 (**Oral Presentation**).
4. Optical properties of rectangular nanoparticles of 4-hexadecylamino-7-nitrobenz-oxa-1,3-diazole. **Ravi Kumar K.** and A. Samanta. – National Symposium on Radiation and Photochemistry (NSRP), 2009, organized by BARC Kumaun University, Ninital, India, March 2009. (**Poster Presentation**).

5. Photophysical properties of organic nanoparticles: **Ravi Kumar K.**, M. Sarkar and A. Samanta. – Trombay Symposium for Radiation and Photochemistry, 2009, BARC, Pune, India, January 2008. (**Poster Presentation**).

Thesis Layout

The thesis has been divided into seven chapters. ***Chapter 1*** provides a brief introduction on inorganic and semiconductor-nanomaterials. A comprehensive discussion on organic nano/microparticles, highlighting their fabrication methodologies, growth mechanism, optical properties and some of the applications is also provided. Some of the characteristics of electron donor-acceptor (EDA) systems, which are frequently used as molecular probes for studying complex environments, are discussed briefly. The design strategies behind the fabrication of the nanostructures of few EDA molecular systems are briefly outlined. The chapter also introduces the surfactant molecules and their role in the formation of nanoparticles. Motivation behind the present work has also been briefly discussed. ***Chapter 2*** provides the details of the experimental procedures and methodologies adopted in this investigation. The instrumental details and methods for different calculations have also been discussed in this chapter**.** ***Chapter 3*** describes the aggregation behavior of highly dipolar molecule in absence of additives. ***Chapter 4*** deals with the controlled fabrication of 1D and semi-2D nanostructures in the presence of additives. ***Chapter 5*** delineates the fabrication of multiple morphologies of a weakly dipolar molecule, 9-(4-cyanophenyl) carbazole. ***Chapter 6*** presents the self-assembled 2D-nanoplates of highly fluorescent 9,10-bis(4-cyanophenyl) anthracence and their optical properties. ***Chapter 7*** summarizes the findings of the present investigations by touching upon the achievements and looking into the future scope of the work.

Chapter 1

Introduction

This chapter introduces some basic concepts of the nanomaterials and provides a brief description of the inorganic and semiconductor nanoparticles. A comprehensive discussion on organic nano/microparticles, highlighting their fabrication methodologies, growth mechanism, optical properties and some of the applications is provided. As the electron donor-acceptor (EDA) molecular systems are the subject matter of the present work, some of the characteristics of EDA systems, which are frequently used as molecular probes for studying complex environments, are discussed briefly. The design strategies behind fabrication of the nanostructures of few EDA molecular systems are briefly outlined. The chapter also introduces surfactant molecules and their role in the formation of nanoparticles. The chapter is concluded after describing the motivation of the thesis and introducing the systems studied in this work.

1.1. Introduction to nanomaterials

Materials Chemistry is a branch of *Materials Science* which provides an overview of various types of materials, synthetic methodologies and relationship between the structures of materials and their overall properties.[1] Nanomaterials are described as *'novel materials whose size of elemental structure has been engineered at the nanometer scale*'. These nanomaterials exhibit different and interesting properties compared to the bulk material and single molecule and provide a bridge between the two. Moreover, intervention in the properties of materials at the nanoscale enables the creation of materials and devices with enhanced or completely new functionalities. The surface-to-volume ratio of the nanomaterials differs drastically compared to the bulk materials, and this leads to dramatic changes in magnetic, optical, electronic, mechanical and catalytic properties, with the sizes of the material. The dramatic enhancement of surface energy with decreasing particle size may be related to peculiar surface effects such as lowering of the melting point. For example, melting point of gold bulk crystal is about 1200 K, but

gold nanoparticles (2 nm) melts at 600 K.[2] A significant proportion of the atoms in the nanoscale structures are actually surface atoms.[2] As a result, the extent of any phenomenon or chemical reaction that occurs on the surface will be amplified in the nanoparticle. The nanomaterials can be broadly divided into three classes.

1.1.1. Inorganic nanoparticles

Nanoparticles made from inorganic metals and alloys fall in this category. The literature suggests that these nanoparticles have taken the lead over the nanoparticles of soft matter such as polymers and organic materials. In the case of inorganic nanostructures, the strong ionic or metallic bond is key factor which glues the building blocks of a nanostructure together. There are several methods available for the fabrication of inorganic nanoparticles. These synthetic methods are broadly based on "*top-down*" and "*bottom-up*" approaches. The *top-down* approach for fabrication is the one first suggested by Feynman in his famous American Physical Society lecture in 1959. This method is based on the division of a bulk solid into smaller portions. This can be achieved by milling or attrition, chemical methods, and volatilization of a solid followed by condensation of the volatilized components. Well known techniques such as *photolithography, electron beam lithography*, *anodization*, *ion- and plasma-etching* are few examples of top-down approach. The second one, "*bottom-up*" method of nanoparticle fabrication, involves condensation of atoms or molecules in a gas phase or in solution to create materials with *nano* dimensions. It requires a thorough understanding of the short range forces of attraction such as van der Waals forces, electrostatic forces, and a variety of interatomic or intermolecular forces. Relatively, this approach is far more popular in the nanoparticle synthesis than the other approach, primarily because one can exploit the short range forces in arranging the atoms or molecules in a controlled way and it is also possible to control the growth conditions for the fabrication of variety of nanostructures. As dispersions of nanoparticles are thermodynamically metastable,

primarily due to their very high surface area, which represents a positive contribution to the free enthalpy of the system, if the activation energies are not sufficiently high, there occurs an evolution of the nanoparticle causing an increase in nanoparticle size, known as Ostwald ripening process. This is why surface stabilization is often employed to hinder sintering, recrystallization and aggregation by using stabilizers or capping agents.

Transition-metal nanoparticles have been successfully used in applications in several areas of science and industry, including catalysis[3,4] and as chemical sensors.[5,6] In particular, Ir and Rh nanoparticles are used for olefin hydrogenation reactions.[7] The Au, Ag and Pt nanoparticles are having extensive applications in biology and nonlinear optics.[4] The optical property of the Au and Ag nanopartices has received attention for use in optical sensors, [8,9]color glasses,[10] photo-electrochemical cells.[11] One of the biggest advantages associated with these metal nanoparticles is surface enhanced raman scattering (SERS). It is difficult to observe Raman signals from a single molecule. But when the samples are coated with gold nanoparticle, Raman scattering intensity is increased by 14 times.[12] Au nanoparticles are also used for identification of diseased cells in body and drug delivery to the affected cells.[13] Silver nanoparticles show antiviral, antibacterial and antifungal activity.[14]

1.1.2. Semiconductor nanoparticles

These are well known as quantum dots (QDs), whose excitons (electron-hole pair) are confined in three dimensions. In a confined semiconductor, an electron-hole pair is typically bound within a characteristic length, called *exciton Bohr radius*. The energy states of the quantum dots are discrete with quantized energy levels. This phenomenon is called as *quantum confinement* and because of this confinement semiconductors behave like atoms; in fact, they are termed as artificial atoms.[15] QDs can be fabricated by three well-known methods: nanolithography,[16] molecular beam epitaxy[17,18] and solution chemical process (colloidal route).[19-21] However, the colloidal route is widely used for

synthesizing various quantum dots of different sizes. This method produces highly monodisperse and narrow size distributed QDs in gram quantities. Solution based colloidal synthesis process can be further classified into three major categories: controlled precipitation,[22-24] cluster build-up approach[25] and molecular precursor approach. Among the three, molecular precursor approach is widely used for various semiconductor nanoparticles.

Molecular precursor approach: Molecular precursor method is the most promising chemical route to the fabrication of the QDs for the semiconductor industry.[26] In this method, the molecular precursors are decomposed in a coordinating solvent at relatively high temperatures. The TOPO (tri-octylphosphine oxide) method has emerged as a significant and powerful chemical route to prepare high-quality nanocrystals for a wide range of semiconductors. Several modifications to this method have been reported of which two main approaches can be highlighted.[21,27,28] In the conventional Bawendi's TOPO method, a non-metal source (e.g., tri-n-octylphosphine selenide, TOPSe) and a metal[29] source (e.g., dimethylcadmium, $Cd(CH_3)_2$) are injected separately into hot TOPO to produce TOPO capped quantum dots.[21] An extension of this method is the injection of single molecule-precursors, which contain both elements of the final material within a single-molecule (e.g., alkyldithiocarbamates or alkyldiselenocarbamates of cadmium) into TOPO.[27] This approach avoids the use of toxic and highly pyrophoric compounds such as $Cd(CH_3)_2$ at high temperatures. Size-tuning is achieved during the synthetic process by adjusting the time and temperature of the synthesis. Accurate control of the synthetic parameters yields narrow size dispersions which can be further improved using post-synthetic treatments such as particle size fractionation. This method has also been used to produce size-tunable quantum confined luminescent core-shell nanocrystals.[30-32]

Quantum dots exhibit unique size dependent optical and electronic properties resulting from the quantum confinement of electrons in the QDs. For example, depending

on the size of the particles, they can emit at different regions in the visible region. Bigger QDs emit at low energy (red emission) while smaller dots emit at higher energy (blue emission). The coloration is directly related to the energy levels of the QD and these interesting optical properties can be understood by quantum mechanical treatment. As the quantum confinement originates from small size, electrons in the quantum dot behave like particle in a box. Hence, the band gap is indirectly proportional to the size of the QD and the larger quantum dots have more closely-spaced energy levels compared to the smaller QD. Because of their wide optical tunability QDs have been extensively used for labeling the proteins and bacteria cells.[33,34] Moreover, elongated structures such as rods and wires have been shown to emit linearly polarized light with a large energy separation between the absorption and emission maxima (Stokes shift), which reduce light reabsorption for light emission applications.[35] Two dimensional (nanoplates, nanodisks) semiconductor nanocrystal, known as, *quantum wells,* shown to be promising candidates for optoelectronic devices and piezoelectric applications.[36]

1.1.3. Organic nano/microparticles

The history of studies on organic nanoparticles is not long compared to those on metals and semiconductors and examples of organic nanoparticles are not many. Approximately 20 million organic compounds are synthesized in chemical laboratories and industries and many of these molecules play an important role in our daily life. Similar to the inorganic and semiconductor nanoparticles, organic nanoparticles are expected to show interesting chemical and physical properties when their sizes are brought down to mesoscopic regime. The conventional nanoparticles fabrication techniques which are used for inorganic/semiconductor materials cannot be applied to the organic materials due to the instability of organic molecules at elevated temperatures. Moreover it is reported that the particle size cannot be reduced less than 1 μm by one of the top-down method, crush technique, because of structural rearrangement in crystals

induced by a mechano-thermal effect.[37] Therefore, new synthetic methods are to be developed for the fabrication of nano/microrystals of low molecular weight organic molecules. Some of them are discussed in the following section.

1.1.3.1. Fabrication methods

1.1.3.1.1. Reprecipitation method: Ever since Nakanishi's first report on perylene nano/microparticles[38] in 1992, many organic molecular nano/microparticles have been successfully fabricated using this reprecipitation method and some of them were shown to have potential application. In a typical synthesis, a dilute solution of the target compound is dissolved in a good solvent (in terms of solubility) and a small quantity is rapidly injected into excess of poor solvent under vigorous stirring. The poor solvent for the target compound must be miscible with the good solvent infinitely, i.e. they should be miscible with each other at any ratio. As a result micro/nanocrystals are obtained in the poor solvent in dispersed state. Water usually serves as poor solvent for most of the organic compounds because of the low or negligible solubility of organic molecules. Using this method, micro/nanocrystals of diacetylene (**DA**) derivatives,[39,40] and many other molecules shown in Chart 1.1 have been successfully prepared.[41-46]

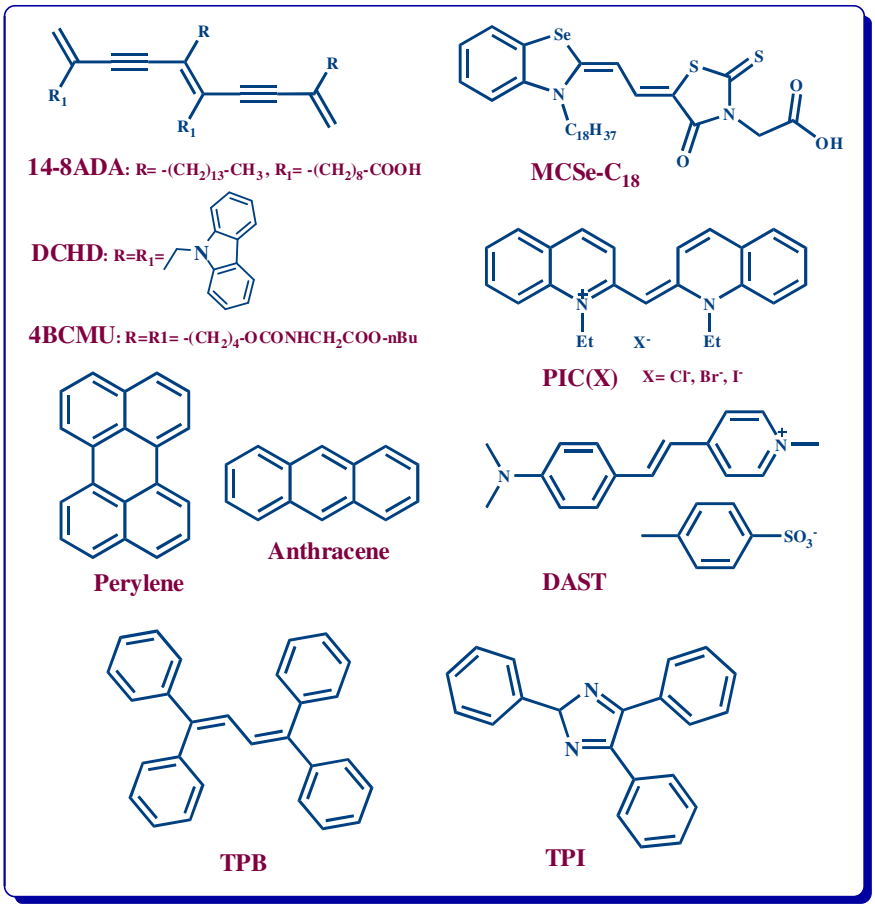

Chart 1.1

One example of the reprecipitation method (used for the preparation of **4BCMU** microcrystals) is described as follows.[39] In a typical experiment, 50 µl of ethanol solution of **4BCMU** is dispersed drop wise into 10 mL of vigorously stirred pure water at room temperature. Stirring is continued for a few more minutes for the completion of mixing and then the microcrystals are reprecipitated in dispersed water. Size tunability is achieved by various parameters like initial concentration of the compound, added

surfactant, solvent system, speed of the injection, temperature, mixing speed etc. For example, highly monodispersed microcrystals of **TPB** are obtained by irradiating the samples with microwaves.[47] After the addition of good solvent (acetone) to the poor solvent (water) the samples are irradiated with microwaves for a given time. Unlike the un-irradiated sample, microwave irradiated sample forms well-characterized rectangular micro/nanocrystals. It is proposed that the droplet formed after the addition of good solvent are homogeneously dispersed in the dispersion medium with the microwaves and rapid evaporation of acetone from the fine droplets prevents the aggregation between droplets and it results in the formation of highly monodispersed micro/nanoparticles.

Supercritical reprecipitation method (SCR)[46,48] and inverse reprecipitation (IR) method[42,49] are modified versions of original reprecipitation method. The former method is suitable for substances having low solubilities (such as titanyl-phthalocyanine) in organic solvents. In particular, the γ-form of titanyl-phthalocyanine nanocrystals were prepared by this method.[42] The later method (IR) is applicable to compounds which are soluble in water. In these cases, the water no longer serves as poor solvent and the two solvents to be chosen in such a way that one of them acts as a poor solvent and the other as good solvent. For example, **DAST** nanocrystals were prepared by this IR method.[49]

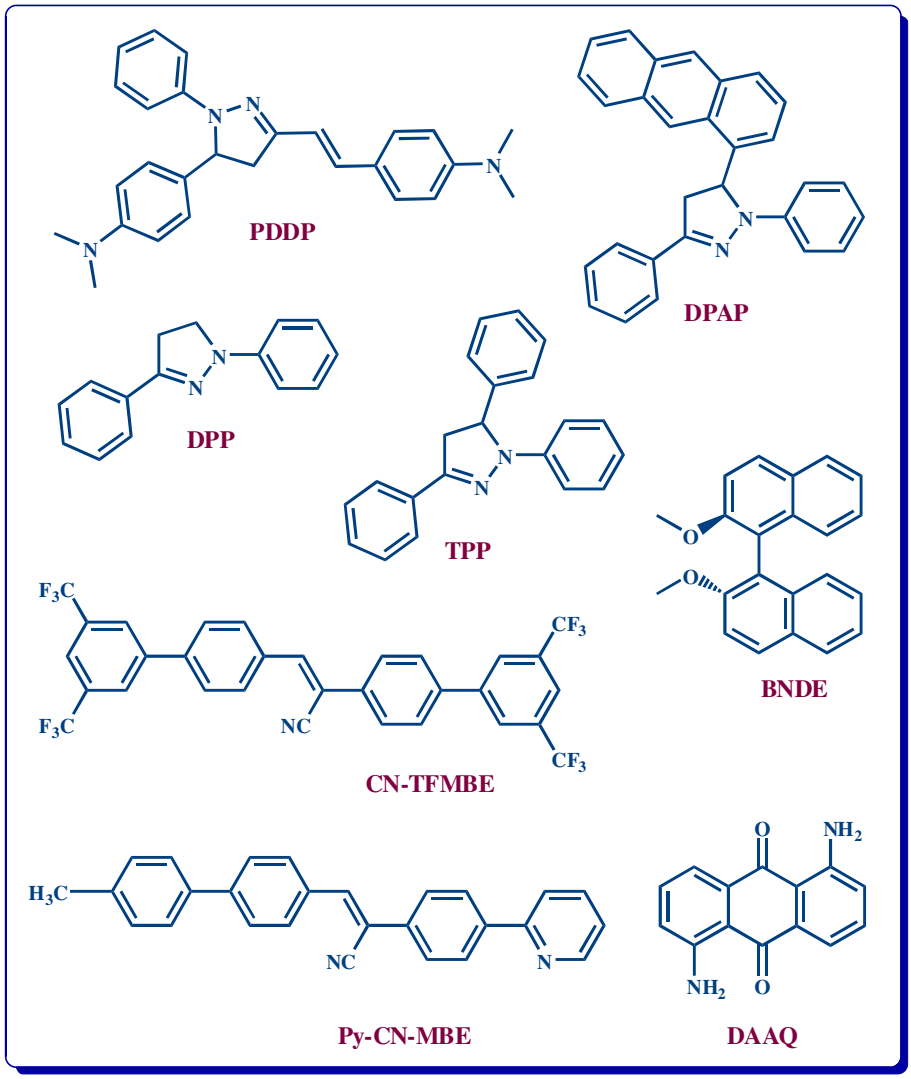

Chart 1.2

1.1.3.1.2. Hard template assisted synthesis: Ordered porous anodized alumina oxide (AAO) membranes have been considered as one of the most suitable host materials for the fabrication of nanotubes or nanowires. This is mainly because of their tunable pore

dimensions over a wide range of diameters (~ 7–300 nm), narrow pore size distribution, good mechanical and thermal stability. In a typical synthesis, AAO template is dipped into a solution of desired molecule, the capillary action of the alumina nanopores soak up the solution rapidly and expose the template to air for some time till the solvent evaporates. As a result, the solute will be deposited on nanopore walls and other places of the template. Then the template is to be annealed at a temperature below the melting point of the molecule. A nanopore wall has high surface energy which helps formation of tubular structure with the pore dimensions. These nanotubes are obtained by etching of the AAO template by aqueous sodium hydroxide solution or phosphoric acid. Yao and co-workers synthesized the nanotubes of perylene using this method.[50] Similarly, nanorods and nanowires can be prepared by annealing the template just above the solvent boiling temperatures. This solution based template (AAO) wetting approach has been reviewed recently.[51] Although this method is applicable to a variety of polymers and low molecular weight molecules, heating at higher temperatures may lead to decomposition of the molecules, and hence, the method is unsuitable for thermally unstable systems. Another drawback of this method is the 'size tunability'. As this aspect is controlled by the template dimensions it is not possible to have nanostructures of desired interest.

1.1.3.1.3. Physical vapor deposition (PVD) method: This is a facile method for preparing nanomaterials of thermally stable low molecular weight molecules and it has been used successfully for the preparation of various inorganic 1D nanomaterials and polymeric thin films.[52] However, the monodispersity of nanostructures is hard to control when small organic molecules are used as deposition sources. In this method, the degree of saturation is an important factor in controlling the morphology and dispersity of the products, and it is possible to process most solid materials into 1D nanostructures by controlling the vapor saturation at a low level.[53] Yao and co-workers synthesized single crystalline nanowires of **TPI**, from the adsorbent-assisted PVD method.[54] Adsorbents

such as neutral aluminum oxide or silica gel were introduced into this method to control the degree of saturation.

In a typical preparation, neutral aluminum oxide (or silica gel) and the sample are mixed uniformly with certain w/w ratio through grinding, and put into a quartz boat. The quartz boat loaded with the mixture is then put inside the center of a quartz tube, which is inserted into a horizontal tube furnace, maintained at temperature gradient. To avoid oxidation of the sample, nitrogen gas is flushed at constant rate during the process of vapor deposition. Various substrates are put along the downstream side of the flowing nitrogen to collect the products. Recently, Huang et al. reported direct growth of the vertically aligned organic nanowires of **DAAQ** without using any adsorbents on solid surfaces such as Si, glass, Au, Al, Fe, Cu foils, or W needle by PVD method.[55,56] The length and diameter of the nanowires were controlled by the growth conditions; the evaporation temperature and deposition time.

1.1.3.1.4. Self-Assembly through organogelation: A gel denotes a dilute mixture of at least two components, in which each of the components forms a separate continuous phase throughout the system. It has been realized that forming organogels is a very effective way to construct organic 1D nanomaterials with a variety of structures and properties. Park and coworkers reported a new class of low molecular weight organogel of **CN-TFMBE** with simple -CF_3 substituents (Chart 1.2).[57,58] The thermoreversible gels were obtained by the gelation of **CN-TFMBE** by dichloromethane and the microscopy experiments revealed the formation of entangled 3D networks consisting of bundles of fibrous aggregates. Interestingly, the gelation induced strong fluorescence emission, although **CN-TFMBE** monomers are totally nonfluorescent in 1,2-dichloroethane solution.[57] Experiments on analogous molecules indicate that the unique gelation capability of **CN-TFMBE** is influenced by the -CF_3 groups.

Though a few other methods (*chemical reaction method*, *self-assembly with solvent evaporation*, *self-assembly in the liquid phase*, *phase transfer*, *rapid solution dispersion*, *seed growth*, *and vapor diffusion)* are available, these are not discussed here because of their limited utility. Among the methods discussed for the fabrication of nano/microparticles of low molecular weight organic molecules, the reprecipitation method is most popular because of its simplicity, low cost and ability to produce various morphologies under ambient conditions.

1.1.3.2. Nucleation and crystal-growth mechanism

Based on the experimental results on **perylene** and **DCHD** microcrystals, Nakanishi et al. proposed a model for the growth mechanism (Scheme 1.1) of the microcrystals.[59] According to them, the crystallization in the reprecipitation method can be roughly divided into four stages.[39,40,44]

(I) Droplets formation

(II) Clusters formation

(III) Nucleation

(IV) Growth

When the probe solution is injected into the poor solvent under stirring/sonication, the probe solution disperses and forms droplet. As the two solvent systems are miscible at any given volume ratio, the good solvent elutes from liquid droplets to poor solvent and creates ‘clusters’. The clusters which are formed from the supersaturated state or by dissolution of the fine droplets are amorphous in nature. Then nucleation followed by growth of the nano/microparticles occurs by thermal collusion between super-fine particles. For controlling the crystal-size, one should have control on the size of the droplets or the amorphous microparticles. For example, by reducing the amount of injected probe solution or the initial concentration, the cluster particles size can be reduced and thus the crystal size is controlled. This picture has been established by static

light scattering (SLS) experiments in which the scattered light intensity is increased with the solution concentration and the quantity of the injected solution.

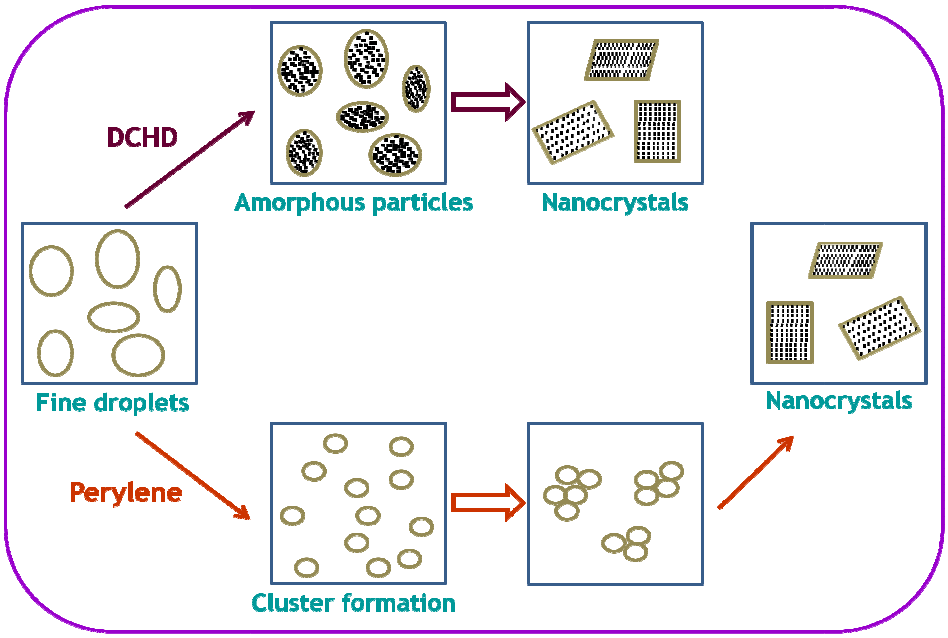

Scheme 1.1

1.1.3.3. Optical properties

1.1.3.3.1. Electronic absorption: It is not just the synthesis of the nanostructures but in fact many organic systems show interesting optical and electronic properties in the mesoscopic regime. Organic micro/nanoparticles exhibit interesting size- and morphology-dependent optical properties. Matsui and coworkers observed quantum confinement in the organic microsrystals for the first time.[60] Excitonic band of pyrene and anthracene microcrystals (2-10 nm) which were embedded in PMMA polymer

became narrower with decreasing particle size. Later, Nakanishi studied the effect of crystal size on the exciton absorption peak position of perylene, poly-**DCHD** and phthalocyanine microcrystals (20-100 nm).[43,45,61] In all cases, it was found that the excitonic band gap energy shifted to the higher-energy side with decreasing the crystal size. This phenomenon was termed as exciton confinement, which differs from the conventional quantum size effect observed for semi-conductor and inorganic nanoparticles. The conventional quantum confinement is observed for small particles with size < 10 nm, whereas the organic micro/nanocrystals are at least one order of magnitude larger than the semiconductor or inorganic nanoparticles. The size dependent spectral shift cannot be explained in terms of Mie scattering as it is the peak position which is affected here, not the width. The quantum confinement in organic microcrystals is attributed to lattice softening and interfacial interaction of the surface of the microcrystals with the surrounding media. Over the years, similar size dependent results have been observed for many molecular systems, pyrazolines[62], 2-(2′-hydroxyphenyl)benzothiazole,[63] etc. Yao et.al reported size-dependent optical properties of pyrazoline derivative, **PDDP**, and observed systematic growth of a new absorption band centered at 430-450 nm.[62] The new absorption is assigned to the aggregated state of the molecular microcrystals and the size dependent optical properties have been interpreted according to the Nakanishi's proposal.

1.1.3.3.2. Fluorescence emission: Size tunable fluorescence emission behavior of many organic molecular micro/nanocrystals has been observed. For example, fluorescence emission spectra of perylene microcrystals are found to be size dependent.[43,64] Although emission from self-trapping exciton levels to the ground state (~550 nm) is not influenced by the crystal size, the peak intensity from the free-exciton level becomes stronger and shifts to higher energy side with decreasing particles size. This has been explained by the lattice softening and electric field effect on the surrounding media through microcrystals.

With increasing the **PDDP** nanoparticle size, the intramolecular charge transfer (ICT) fluorescence emission is broadened and the peak position shifts towards longer wavelength compared to its molecular form.[62] In another report by the same group, multiple emissions from **DPP** nanoparticles, which are tunable from near UV to green by changing either the size of the particle or excitation wavelength, are observed.[65] The multiple emissions of **DPP** nanoparticles and its evolution as a function of size, is attributed to enhanced intermolecular interactions with increasing particle size. Another pyrazoline derivative, **DAP** which contains anthracene and pyrazoline groups, also exhibits size dependent optical properties.[66] It is interesting to note that a dilute solution of **DAP** exhibits only the fluorescence characteristic of the anthracene chromophore, while **DAP** nanoparticles exhibit multiple emissions from both anthracene and pyrazoline groups. The emission of **TPP** nanoparticles is tuned by doping technique. Blue emitting **TPP** is doped with red emitting **DCM** and by varying the dopant content the emission of the nanoparticles is tuned.[67] A similar strategy was applied for the generation of white emission.[68] Patra et.al reported tunable size dependent optical properties of **BCADQ** and attributed the same to the rigidification of the molecule on the formation of micro/nanoparthicles.[69] We also observed structural rigidification of an electron donor-acceptor (EDA) molecule **ADMA** on the formation of micro/nanocrystals.[70] Fluorescence polarization of the organic microcrystals provides important information of the crystal growth direction. Linearly polarized emission has been observed for the nanobelts fabricated from a perylenediimide derivative through both solution-based and surface-supported self-assembly.[71] A similar study on a slightly different perylenediimide derivative also reveals linearly polarized emission from nanofibers indicating well-defined π-stacking of the molecules and well-organized alignment of the crystal fibers.[72,73]

Apart from the size-tunable optical properties, Yao and coworkers investigated size-dependent exciton chirality in organic nanoparticles.[74] They prepared nanoparticles from a chiral auxiliary, **BNDE** with a range of particle sizes from 25 to 100 nm. The **BNDE** nanoparticles exhibited positive exciton chirality in the 200–260 nm region in circular dichroism (CD) spectra, which is completely opposite to the CD spectra of the dilute solution. The exciton chirality peaks evolved to the low-energy side with increase in particle size. The chirality inversion resulted from intermolecular exciton coupling between two adjacent **BNDE** molecules in the nanoparticles, and the bathochromic shift of the peaks was attributed to increased intermolecular interaction with increasing particle size. By doping red emitting **DCM** in the blue emitting nanorods of **DPP** white light emitting (WLE) nanorods have been fabricated.[75] Although triblock microrods show microarea heterogeneity of the striping pattern, macroscopically they generate high-quality white light in both colloidal suspension and solid state with high photo-luminescence efficiency.

1.1.3.4. Nonlinear optical properties

In addition to the linear optical properties, organic microcrystals also exhibit interesting nonlinear optical (NLO) properties. Nakanishi was the first to show some interesting nonlinear properties of the organic micro/nanoparticles using various techniques like third harmonic generation (THG), Z-scan, optical Kerr shutters and degenerate four-wave mixing (DFWM).[37] The measurements were carried out for organic microcrystals in the state of dispersion or in thin films. The THG properties of **MCSe-C$_{18}$** microcrystals with J-aggregated form were measured in polyvinylalcohol (PVA) matrix.[76] It is found that the third order susceptibility, $\chi^{(3)}$ is 20 times more than that of non J-state microcrystals. On the other hand the NLO properties of poly **DCHD** microcrystals (100 nm) in a gelatin film were studied by Z-scan method.[77] In this study, the $\chi^{(3)}$, non-linear refraction (n_2) and non-linear absorption (β) around the exciton peak were measured

using a tunable picosecond laser and the measured n_2 was as large as 0.024 cm^2/GW at resonant wavelengths. The one-dimensional π–conjugated main chain of the poly **DCHD** is responsible for large optical non-linearity. It is also found that the $\chi^{(3)}$ values at near resonant wavelength are as high as polydiacetylene single crystals.[77] Nanoparticles of an azo transition metal chelate compound were also prepared and the third order nonlinear optical (NLO) properties investigated.[78] The enhanced size-tunable off-resonant third-order NLO responses of these nanoparticles were observed. The NLO enhancement of the nanoparticles compared to that of the monomer was proved to originate from the increased intramolecular charge transfer (ICT) process due to the improved planarity of the ligands. The size-dependent NLO responses of the nanoparticles were attributed to the predominance of the intermolecular ICT at the expense of the intramolecular ICT with increasing particle size. Recently, Patra et.al reported appreciable optical limiting responses of **BCADQ** nano/microcrystals.[79] It is observed that colloids with larger particle sizes display improved damage thresholds. Open aperture Z-scan studies reveal appreciable 4-photon absorption in the colloidal materials and this is more prominent in the case of small particles. McNeill and coworkers demonstrated a new class of two-photon fluorescent nanoparticles based on conjugated fluorenone polymer which exhibit largest (2.0×10^5 GM) two-photon cross sections.[80] The nonlinear optical response in one-dimensional organic nanorods of a dipolar molecule have been examined by Goodson III and co-workers. It is found that the nanorods display an order of magnitude higher two-photon excited fluorescence when compared to the solution phase because of enhanced fluorescence quantum efficiency and two-photon cross-section in the aggregated state.[81]

1.1.3.5. Aggregation-induced emission enhancement

Most of the organic molecules fluoresce strongly in homogeneous solution than in their solid or aggregated state.[82,83] This reduction of fluorescence emission efficiency in the solid or aggregated state has been a major problem for device applications such as

organic light-emitting diodes. However, some molecules show very interesting fluorescence enhancement in the solid or aggregated state. For example, tetraphenylethylene is less-fluorescent in all solvents but its colloidal particles and solid show bright fluorescence. This is termed as aggregation induced emission enhancement (AIEE). Sometimes the molecules are non-fluorescent in solution but upon aggregation become fluorescent. This is called aggregation induced emission (AIE). Since the first aggregation-induced emission (AIE) active material, 1-methyl-1,2,3,4,5-pentaphenyl-silole, reported by Tang's group,[84] materials with AIE or AIEE properties have attracted much attention due to their potential applications in many fields.[85-87] In the past few years, several compounds with AIE or AIEE properties have been developed, such as silole derivatives,[88,89] 1-cyano-trans-1,2-bis-(40-methylbiphenyl)ethylene (CN-MBE) and its analogous molecules,[90,91] 2,5-diphenyl-1,4-distyrylbenzene (DPDSB) derivatives,[92,93] diphenyldibenzofulvene (DPDBF) derivatives,[94,95] conjugated polymers,[96,97] and others.[98-101] The AIE or AIEE in these systems resulted from the inhibition of the nonradiative channel, the vibrational/torsional energy relaxation process, blocked by the stacking of the intermolecular interaction in the aggregate state. Hence, the AIE or AIEE effect has been found to be usually associated with aromatic groups by rotatable C–C, C–N or N–N single bonds.[88-101] More recently, AIEE phenomenon is observed in the polycyclic aromatic alkaloid derivatives due to configuration changes in the excited state.[102,103] Tao et. al reported that AIE-active materials are promising candidates for OLED applications.[104]

1.1.3.6. Optoelectronic properties and applications

Tang and VanSlyke reported first electroluminescence (EL) devices using small organic fluorescent molecular material[105] and the first organic field-effect transistor (OFET)[106] was fabricated by Tsumura et al. using polythiophene thin film. Since then

many people are involved in the design and synthesis of new highly efficient molecular materials for EL devices and significant progress has been made during the past decades.[107-113] In the early days, more emphasis was placed on π-*conjugated systems,* which are considered as easily processable materials with high molecular ordering than the polymers[114-116] and molecular systems[117-119] for high-performance optoelectronic devices such as organic photovoltaics (OPV), organic light-emitting diodes (OLED) and organic field effect-transistors (OFET). However, in recent years, 1D-nanostructures (nanowires, nanoribbons, and nanotubes) of organic semiconductor molecules have been found as promising candidates for the development of miniaturized optoelectronic devices, interconnectors and molecular sensors.[120-125] Although, nanofibers fabricated from conducting polymers such as polyaniline[112], aniline oligomers[126] and polyacetylene,[111] showed interesting charge carrier mobility, the crystalline structure of polymer nanofibers is often difficult to control due to the complicated intermolecular interaction.

Charge-transport properties of organic semiconductor nanostructures are often measured by constructing an OFET.[122] These are usually fabricated either by aligning the structures between predeposited electrodes or by attaching electrodes to prealigned structures. For high charge carrier (electron/hole) mobility the nanostructure has to be defect free and should be highly crystalline in nature. Self-assembled single-crystalline nanowire/nanoribbon OFETs of pentacene derivatives and few aromatic molecules showed very high hole mobilities compared to their Thin-Film OFETs.[127-130] Such variations of the mobilities are assigned to the different crystalline nature of the Thin-Film and the nanostructure. The boundaries between crystalline domains in the Thin-Films could be responsible for the low carrier mobilities. The carrier mobilities are dependent on the morphology of the nanostructures is evident from the recent data on nanotubes, nanowires and nanoribbons.[131,132] Zhang and coworkers constructed OFET

from single crystalline nanoribbons and nanowires of 9,10-diphenylanthracene and observed high field-effect hole mobility for the nanoribbons while the nanowires show poor performance.[133] This was explained by considering the contact of these two nanostructures with the electrodes. π-π stacking interaction between planar aromatic molecules often leads to the formation of 1D- nanostructures, which permits high charge carrier mobility along the stacking direction.[134-138] A disruption of this π-π interaction in the molecular packing results in poor performance as evident by incorporation of a hetero atom in the planar perylene skeleton. On the other hand, devices constructed from single nanotubes or nanorods of a perylene derivative exhibit high resistance modulation.[139]

Imide-substituted perylene and perylenetetracarboxyldiimide (**PTCDI**) derivatives are another class of materials which show promising electronic and optoelectronic properties. Most of the **PTCDI** derivatives have a tendency to self-assemble into 1D-nanostructures because of strong π-π stacking interaction.[118,120,128,140-143] Free standing nanowires of **PTCDI** derivatives show poor conductivity while the immersed nanowires in basic condition show 3-fold enhancement.[143,144] Briseno et.al synthesized self-assembled nanowires of **PTCDI** derivative and demonstrated fabrication of n-channel semiconductor in OFETs for the first time. By combining n-channel nanowire (**PTCDI**) transistor with p-channel hexathiopentacene (**HTP**) nanowire transistors, they also constructed complementary inverter and achieved very high gain.[145]

1.1.3.7. Patterning of nanostructures

Arrangement of nanostructures in a desired fashion is essential for practical device applications. Few methods such as electrophoretic deposition,[146] lithographic patterning,[147] and ink-jet printing[148] are available for transferring the pre-formed organic/inorganic nanoparticles to arrange them in arrays. However, all these methods demand separate nanoparticle synthesis and complicated handling. Park and coworkers reported a promising new approach for the fabrication of photopatterned fluorescent

organic nanoparticles arrays in a polymer film, based on the principles of vapor-driven self-assembly (VDSA).[149] For this purpose, a strong self-assembling capable molecule, **Py-CN-MBE** doped thin poly(methyl methacrylate) (PMMA) polymer film was obtained by spin-coating from a filtered solution of **Py-CN-MBE** in 1,2-dichloroethane. When the thin film was exposed to dichloromethane vapor for 20 s, the vapor-exposed region of the film was found to exhibit slightly off-white turbidity. Scanning electron microscope measurements revealed the formation of nearly spherical nanoparticles (50 nm) and fluorescence measurements revealed huge AIEE. This interesting feature of the molecule has been utilized to pattern the nanoparticles in arrays of desired interest. For patterning, **Py-CN-MBE** and a photoacid doped thin PMMA films were spin-coated from filtered solution of 1,2-dichloroethane. The resulting film exhibited blue fluorescence emission and contained no aggregates. The film was then exposed to UV-light through a photomask. The irradiation gave rise to the transformation of the neutral form (**Py-CN-MBE**) into its quaternary salt form in the illuminated regions of the film. To generate the nanoparticles where neutral **Py-CN-MBE** is present, the photo-mask was removed and exposed to 1,2-dichloroethane vapors for 20 s.

Recently, Huang and his co-workers reported vertically aligned organic nanowire arrays of **DAAQ** dye molecules prepared by physical vapor transport method.[150] Later they showed patterned growth of these vertical nanowire arrays on substrates with predefined geometrical and chemical features.[56] The nanowires have been grown on high surface energy substrates such as sharp metal or AFM tips, and colloidal particles. Though the exact reason for such vertical alignment of the nanowires is not understood, its preferred nucleation and growth on high surface energy site has been utilized to obtain ordered arrays on pre-patterned substrates.

1.1.3.8. Optical waveguides

A *waveguide* is a structure which guides waves, such as electromagnetic waves or sound waves. There are different types of waveguides depending on the waves. The original and most common meaning is a hollow conductive metal pipe that carries high frequency radio waves, particularly microwaves. An *optical waveguide* is a physical structure that guides electromagnetic waves in the optical spectrum. Optical waveguides, usually made up of transparent media with higher refractive indices than their environment, can keep light transmit internally by total reflection at the interface. Transmission of light in fibers, is one of the most common examples of optical waveguiding, which is widely used in fiber-optic communications. Recently, it is found that 1D-nanostructures of fluorescent organic molecules are promising building blocks for the generation and propagation of light in future miniaturized optoelectronics.[151-154] It has been demonstrated[155] that light can only propagate within the transverse magnetic (TM) modes of nanowire waveguides, *i.e.* along the growth direction of the nano/microparticle. The performance of optical waveguides is often evaluated by measuring 'optical loss' in the light guiding process. For crystalline organic nano/microcrystals, relatively high optical loss is reported compared to inorganic or semiconductor counterparts. This is mainly due to lower refractive indices of the organic crystals ($n>1.5$) than those of the inorganic or semiconductors ($n>2$) crystals. Many attempts have been made to decrease the optical loss in an attempt to improve the waveguide performance. Most of them are focused on how to decrease the indices of the environment surrounding the waveguides, i.e., how best the total reflection can be utilized on the interface between the organic crystals and the air ($n>1$).[56] Rubahn and coworkers fabricated nanofibers of p-hexaphenyl up to 1 mm length by vacuum sublimation and guided the blue light.[151] H-aggregates of thiocyanine nanofibers (300 μm) serve as single-mode optical waveguides that propagate photo-luminescence in the range of 520 to 560

nm over 250 µm without any loss.[152] Three factors are responsible for the observation of high waveguiding performance of any material. Firstly, well-separated absorption and emission band of the molecule, which decreases the re-absorption of the emitted light. Secondly, smoothness of the surface of the nanofiber (as roughness of nanofiber surface causes scattering of light that propagates by total internal reflection at the boundary between the waveguide and external media) and finally, the high purity of the nanofibers which also helps to reduce the scattering.[153,156] Yao et. al demonstrated the nanowire of **TPI** as waveguides and ultraviolet lasers.[154] Studies on rod and tube morphologies of 9,10-bis(phenyl-ethynyl)anthracene, (**BPEA**) has revealed that the optical loss is minimized in tubes than in the rods due to decreasing re-absorption of the emitted light.[157] Although rods and tubes show waveguiding ability, the air inside the tubes can change the waveguiding behavior and help to reduce the optical loss. Very recently, high-quality microwires of **PTCDI** derivative have been fabricated and shown as low-loss optical waveguides.[72] The internal molecular alignment often results in the anisotropy of refractive index and produces strong birefringence and polarized PL emission with low propagation loss in light waveguiding. However, the optical waveguides based on small organic molecules with 2D structures have not progressed much despite of their ability to show bidirectional waveguiding property.[158]

1.1.3.9. Sensors

As discussed in the earlier sections, semiconductor organic 1D nanoparticles exhibit pronounced optical and optoelectronic properties compared to the bulk materials and thin films. Moreover, these properties are highly tunable and sensitive, which are essential for optimizing low cost effective sensor. Besides the tunability and sensitivity, large surface area-to-volume ratio of the small particles enhances the sensing element/analyte encounter probability of the organic nanowires. Signals representing the nanowire-analyte interactions must be in processable forms, such as current, color, or light, as

produced by a transduction mechanism.[159,160] Among the various transduction mechanisms, quenching of fluorescence and change of conductivity have been used widely in organic semiconductor nanowire sensors for various applications. Organic semiconductor nanowires as optical sensors can be fabricated by exploiting the exciton fluorescence and its modulation by interaction with the environment. When an analyte comes close to an organic nanowire, charge or energy transfer between the nanowire and the analyte occurs, resulting in quenching of the fluorescence. Such a detection mechanism is known to be very sensitive, especially when it comes to highly porous nanostructures such as a network of nanowires.[161] The limit of detection based on fluorescence quenching has been estimated to be less than one part per billion in the case of nanowires of **PTCDI** derivative. Such efficient sensing is attributed to efficient electron transfer process and the nature of the nanowires. Based on the same fluorescence quenching mechanism, arylene ethynylene macrocycle acts as effective sensor for oxidative molecules.[162] In this case, the strong electron donating ability of the molecule is utilized for sensing trinitrotoluene and other nitro-based explosives with extreme sensitivity. An electrical signal is thought to be more convenient for easy integration of the sensors into electronic circuits. 1D-nanostructure sensors of CuPc,[163] **PTCDI** derivatives,[143,144] and **DAAQ**[56,150] have been developed by monitoring the conductivity changes upon exposure to an analyte.

1.2. Electron donor-acceptor molecules and their characteristics

Considerable attention has been attached to the electron donor-acceptor (EDA) molecules in recent years primarily because of the fact that charge separation is one of the most fundamental processes involved in numerous chemical and biological transformations. A thorough understanding of the photoinduced charge separation process, which plays an important role in the photosynthesis phenomenon in plants,[164] helps in designing and developing of efficient systems for solar energy conversions in

modern days.[165-172] Moreover, the EDA systems find usage in sensing environments,[173] as nonlinear optical materials,[174] molecular electronic devices,[175] etc. EDA systems are also considered as a favorite testing ground for the theories of electron transfer and solvation dynamics.[176]

Mulliken was the first to introduce the concept of charge-transfer transition to describe the spectral and bonding interactions of molecular complexes formed between an electron donor and an acceptor.[177,178] The charge transfer can take place either through bond or through space. In systems where the electron donor and acceptor moieties are connected by a flexible spacer, a charge-transfer complex or exciplex is often formed due to the spatial overlap between the donor and acceptor orbitals.[82] But in cases where through-space interaction of the donor and acceptor orbitals is not possible due to limited configurational flexibility, charge separation is made possible by through-bond interaction of the two. In both cases, appropriate model systems[179-181] have been chosen to investigate the dependence of the electron transfer rate on the free energy of reaction, distance and orientation between the donor and acceptor and the medium. When the charge transfer (CT) state is luminescent, the CT emission provides an excellent opportunity to monitor the dynamics because internal structure and environment influence this luminescence in such a way that it could provide a detailed information of the thermodynamic and kinetics of photophysical properties. The simple photophysical techniques such as steady state and time-resolved fluorescence as well as transient absorption studies are generally employed for the study of the CT state.

An appreciable increase in the dipole moment is observed for a large majority of the EDA molecules, when they are subjected to photoexcitation. The emission maxima and quantum yields of these compounds are usually highly sensitive to the polarity of the medium. This sensitivity is often exploited to determine the polarity of unknown solvent mixtures or to estimate the polarity of the microenvironments in organized assemblies

such as micelles and membranes. Examples of these kinds of probes (Chart 1.3) are 6-propionyl-2-(N,N-dimethylamino)naphthalene (PRODAN),[182,183] 4-aminophthalimide (AP),[184-186] 1-anilinonaphthalene-8-sulfonate (ANS)[187] and hemicyanine dye.[188]

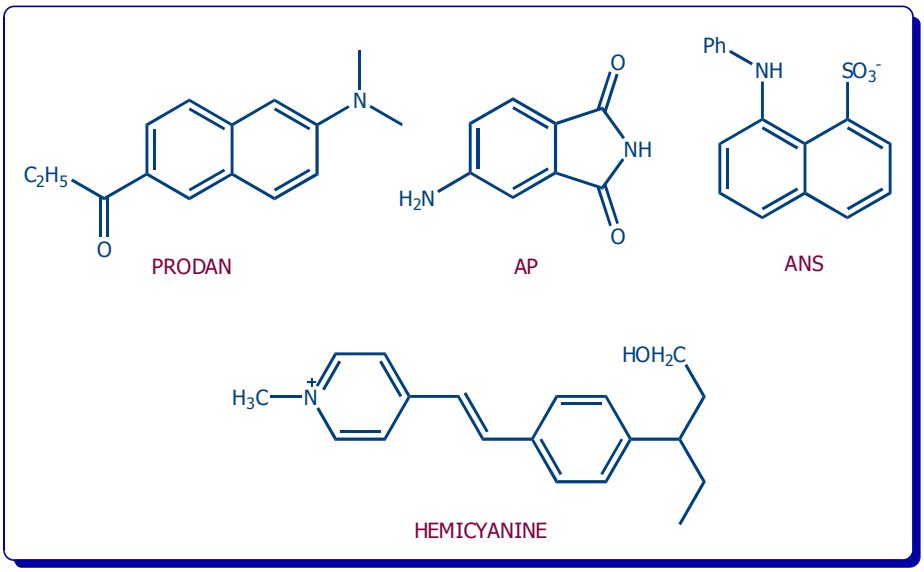

Chart 1.3. Examples of few common EDA probes used for estimation of polarity of environments.

1.2.1. Nonradiative processes

The nonradiative electronic processes in isolated molecules and condensed phase, take place without breaking of any chemical bond and generally involve the conversion of electronic energy to vibrational energy.[189] The nonradiative decay processes find many useful consequences in dye laser operation,[190] efficiency of fluorescence probes, stereomutation of 'push-pull' stilbenes, polyene and rhodopsin,[191-194] light fastness of dyeing agents,[195] effectiveness of photographic sensitizers[196] and molecular switching devices.[197] Radiationless transition between initial and final electronic states is known to occur at the point of intersection of potential energy surfaces. The nonradiative transition

happens irreversibly at this isoenergetic point to the higher vibrational level of the lower energy state and the excess vibrational energy cascades down the vibrational manifold. Thus, the radiationless conversion of energy involves two steps: (i) the transfer of energy at the isoenergetic point from the higher electronic state to the high vibrational level of the lower electronic state, and (ii) the rapid loss of excess vibrational energy after energy transfer. The efficiency of the radiationless transition is directly proportional to the value of the overlap integral (Franck-Condon integral) of the two interacting states. Apart from the Franck-Condon integral, the symmetry restrictions and spin multiplicity also dictate the efficiency of the crossover from one energy state to another. In addition, the *density of state* is another important factor for determining the efficiency of the nonradiative process. For example, in solution, the medium may provide a background of its own energy states which are nearly degenerate and in resonance with the initial state, which often facilitates the radiationless transition through the *quasicontinuum* of the final state. Solute-solvent interactions may further perturb the potential energy leading to crossing of surfaces. If such a crossing point was not present initially, then it promotes nonradiative transitions. But in the absence of specific solute-solvent interactions, the medium probably has very little effect on the rates of radiationless transitions. Thus, these three key factors, (1) energy gap between the interacting electronic states, (2) Franck-Condon overlap integral and (3) density of state govern the efficiency of the nonradiative processes. There are two major types of radiationless transitions: (i) *internal conversion*, and (ii) *intersystem crossing*. When the noradiative loss of energy occurs between electronic energy manifold of the same spin type i.e singlet-singlet or triplet-triplet then such transitions are called internal conversion. The intersystem crossing involves nonradiative energy loss between energy states of two different spin multiplicity. Structurally flexible systems often exhibits unusually high nonradiative rate due to their internal motion. There are several factors related to the internal motion of the molecule

that enhance the nonradiative rate in the systems. These factors are briefly touched upon by illustrating some of the well known fluorescent probes.

1.2.2. Rhodamines

These are a group of popular xanthene dyes (Chart 1.4), known for their interesting photophysical behavior. Rhodamines in frozen solutions or rhodamines with rigid amino group (such as rhodamine 101) show fluorescence quantum yield close to unity.[198,199] It is found that the internal conversion of these dyes is strongly associated with the rigidity of the xanthene-amine C-N bond. Several models have been proposed to explain the unusual dependence of the internal conversion rate on the solvent and molecular structure of the xanthene dyes. Among them the twisted intramolecular charge transfer (TICT) model[200,201] and umbrella like motion (ULM) model[202-204] are noteworthy. Whereas, the TICT model is mainly governed by the viscosity and polarity of the solvent, the ULM model stresses on the importance of specific solute-solvent interactions for unusually high internal conversion rate. Rettig and coworkers proposed the involvement of nonradiative TICT state for rhodamines and few other xanthene dyes.[200,201] A higher quantum yield and lifetime of the monoalkyl derivative compared to the dialkyl one is attributed to the higher energy of the TICT state of the former system. An alternative mechanism by Arbeloa et al.[203] effectively correlates the internal conversion with a change in the amino group configuration from planar to pyramidal one, known as ULM motion.

1.2.3. Coumarins

In order to account for the dependence of the fluorescence property of coumarins (Chart 1.4) on the structure of the amino moiety and on the polarity of the medium, Jones II and coworkers[205-207] suggested that the planar intramolecular charge transfer state is highly fluorescent, whereas twisted charge transfer state is nonemissive. Later, de Melo

et al.[208,209] have shown that the photophysical behavior of some coumarin derivatives is essentially determined by the relative location of two energetically close-lying n-π* and π-π* singlet states. A mixing between the two states depending upon the polarity of the media and the nature of the amino substitution controls the magnitude of the nonradiative rates in methoxycoumarin.

1.2.4. Squaraine

Squaraine is another class of popular dyes (Chart 1.4) emitting in the visible range, which shows interesting nonradiative decay behavior. The nonfluorescent nature of squaraine was interpreted in terms of twisting of the amino moiety around the C-N bond.[210,211] Essentially, the twisting leads to a region close to the funnel of conical intersection, which acts as a nonemissive decay channel.

1.2.5. Cyanine

Among the large organic molecules, cyanine dyes are interesting systems for the study of solvent and temperature dependent radiative and nonradiative processes. Fleming et al. have studied **DODCI** (Chart 1.4), a cyanine dye in a series of polar solvents at different temperatures as well as in rigid matrix and clarified the kinetics for the nonradiative decay.[212 49] The nonlinear Arrhenius plot was interpreted by invoking the

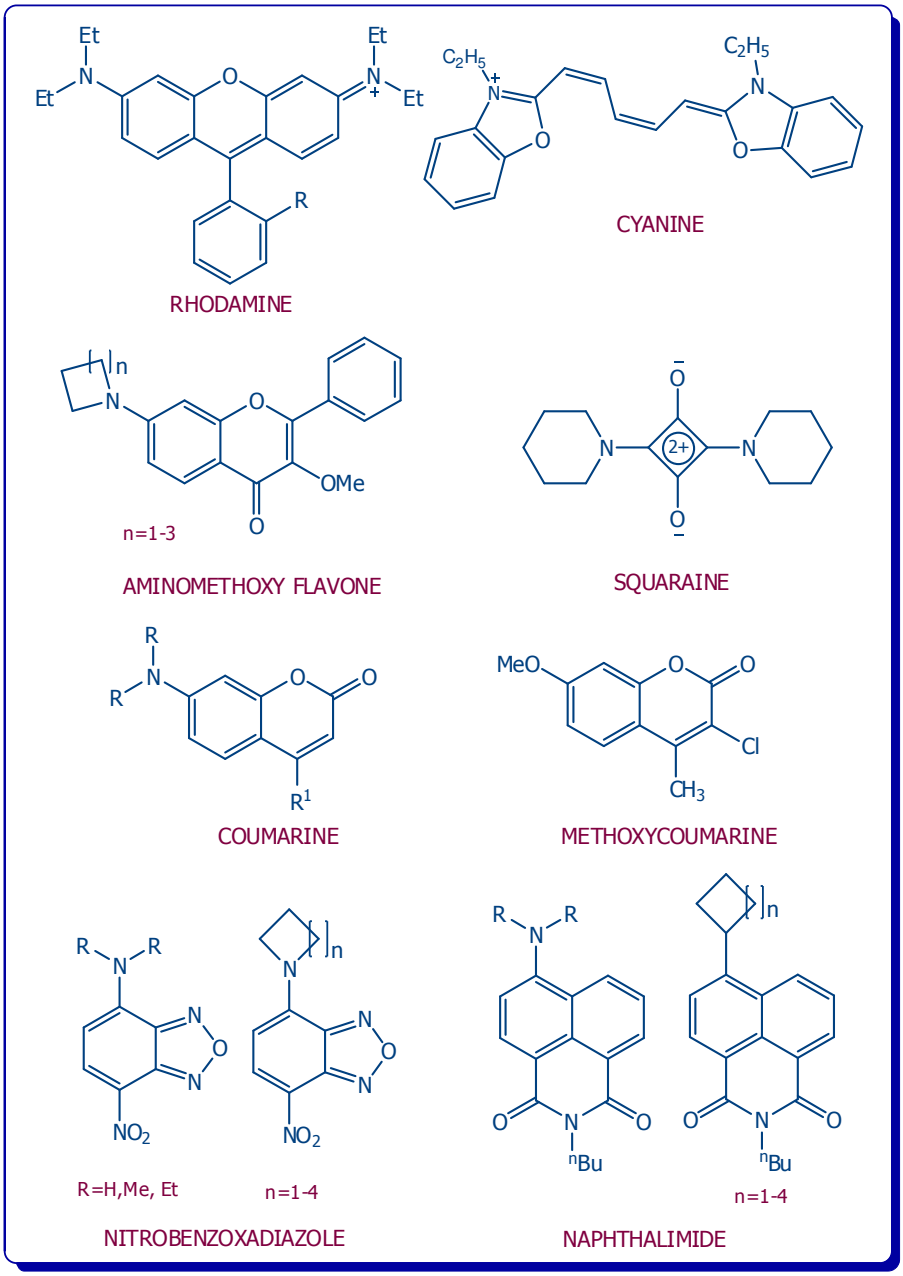

Chart 1.4. Examples of fluorophores known for efficient nonradiative processes.

involvement of a second nonradiative decay channel with a low activation energy barrier (~1.55 kcal/mol). This second nonradiative process with low activation barrier is supposed to be a direct internal conversion which at high temperature cannot compete with the twisting process.

1.2.6. Nitrobenzoxadiazole and naphthalimide derivatives

Recently, two sets of EDA systems, amine-terminated nitrobenzoxadiazole and naphthalimide derivatives (Chart 1.4), have been studied with a view to elucidate the nonradiative pathways in these systems.[213,214] It has been found that the nonradiative rate constants of these systems largely depend on the nature of the amino functionality. An increase in the length of the dialkyl groups connected to the amino nitrogen or an increase in the size of the ring containing the amino nitrogen enhances the nonradiative deactivation of the fluorescence state of the systems. It has also been shown that the variation in the nonradiative rate constants in both cases can be best explained in terms of the nitrogen inversion model.

1.2.7. Aminomethoxyflavone derivatives

Very recently Sarkar et al. studied some amine-terminated methoxyflavone derivatives to understand the solvent dependency of the nonradiative processes in these systems.[215] The nonradiative rate constants evaluated from the quantum yield and lifetime values show a decreasing trend with increasing polarity of the solvent. The observations have been accounted for taking into consideration the nature of the two excited states involved in the emission process. The results suggest a change in the nature of the emitting state from n-π^* to π-π^* with increase in the polarity of the medium.

1.3. Nanoparticles of few EDA molecular systems

Single crystalline 1D-nanostructures of highly dipolar molecule, **DPMM** (Chart 1.5) have been prepared by simple self-assembly process in solution without using any additives.[216] It is observed that the morphologies of **DPMM** can be easily controlled by varying the processing temperature. **DPMM** with D-A-D type architecture can be considered as having two dipole-dipole interactions in two different directions. Few other molecular systems (**DPPM** & **DSDC,** Chart 1.5) having similar arrangement also lead to the formation of ribbons. However, molecules having donor-acceptor (D-A) type architecture such as **DABM** & **DCM** (Chart 1.5) give rise to nanowire morphologies instead of nanoribbons. This showed that the direction(s) of the dipole moments govern the favored direction(s) of molecular stacking and thus the resulting morphologies. While two distinct directions of interaction (D-A-D type) promote the growth in two different orientations, one direction (D-A type) leads to growth in one orientation. Interestingly, these nanostructures show morphology dependent photoluminescence spectra. The change of semi-1D nanoribbons to 1D -nanotube and consequent change of emission behavior has been attributed to different pathways of low-energy molecular stacking at different temperatures.

Later it was demonstrated that the planarity of the system and strength of supramolecular interactions also dictate the shape of the 1-D or semi-2D nanoparticles.[217] Studies on a variety of intramolecular charge transfer molecules revealed that a stronger dipole-dipole interaction could increase the tendency of directional assembly. As molecular planarity decreases, rearrangement and stacking between molecules become difficult. Strong directional supramolecular interactions such as π-π stacking and hydrogen-bonding interactions are also effective in directing morphology of nanostructures. However, these interactions are believed to be effective only at the early stages of nucleation process and the final morphology is mostly governed by the growth

kinetics of the nanocrystal. In addition to the dipole-dipole and supramolecular interactions, other parameters can also be used to control the nanocrystal formation process. For example, supersaturation and nucleation can be induced by lowering solution temperature or decreasing the rate of solvent evaporation and initial concentration of the solution. Supersaturation and nucleation can also be controlled by stirring, or ultrasonication.

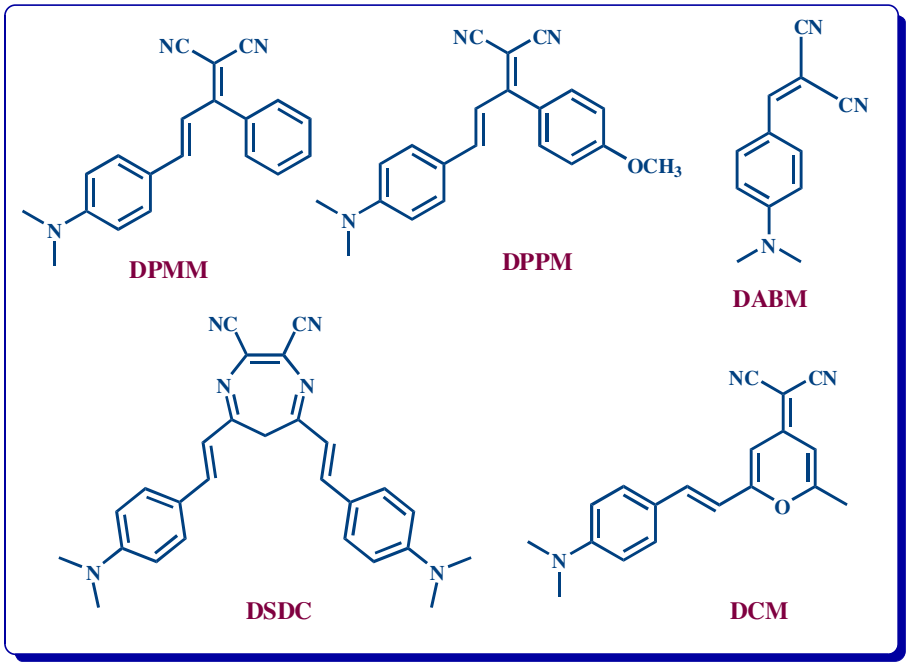

Chart 1.5

1.4. Surfactants and their role in aggregation

Surfactant and lipid molecules are amphiphathic molecules composed with one or more long alkyl chains (with at least six methylene units) and a polar head group.[218] The unique structure consisting of hydrophobic and hydrophilic groups give rise to associated

structures. Above certain concentration, the surfactant molecules segregate in aqueous solution to form very small particles, known as micelles and the concentration is known as critical micelle concentration (CMC). This micelle formation takes place over a narrow range of surfactant concentration and is accompanied by dramatic changes in various physical properties such as light scattering, viscosity, electrical conductivity, surface tension, osmotic pressure, and solubilization capacity of various solutes. Below the CMC, the monomeric surfactant acts as strong electrolyte (fully dissociated and unaggregated). However, at CMC small micelle formation begins and above CMC, any increase in the surfactant concentration leads to an increase in the number of micelles. Depending on the nature and strength of alkyl chain, head group, concentration, temperature and other additives, the size and shape of the micelles can be varied. Surfactants/lipids which consist of single alkyl chain form spherical micelles ($\leq$ 30 Å) while the surfactants/lipids with two or more alkyl chains form larger unilamellar or vesicles. When the surfactant concentration is extremely high, the spherical micelles transform to rod-like micelles. For example, the cationic surfactant cetyltrimethylammonium bromide (CTAB) forms spherical micelles above 0.9 mM. However, a further increase in concentration leads to increase the number of micelles and when the concentration exceeds 100 mM, these spherical micelles transform to give rod-like micelles and this concentration is known as second CMC.[219] The hydrocarbon chains align themselves to form an inner hydrophobic part while the polar head groups are located at the hydrocarbon-water interface. On the other hand, inverted micelles or reverse micelles are also possible in which the inner core consists of water pool and outer part is hydrophobic in nature.

A surfactant can influence the aggregation process of other solutes in two possible ways: providing a physical template,[220-222] and acting as a stabilizer.[223-227] The spherical and rodlike micelles are widely used as templates in the synthesis of inorganic

nanostructructures.[228-231] In these cases, rod-inducing co-surfactant is also necessary for the formation of rodlike micelles. The surfactant can also change the free energies for different crystallographic planes, and thus their relative growth rates.[229] For example, bromide ion is capable of adsorbing selectively onto the (100) planes of Ag, Au, Pd, and Pt nanocrystals with edge lengths < 25 nm to induce the formation of smaller nanocubes, rectangular nanobars, and octagonal nanorods.[232] Recently, using these soft micelle templates organic molecular 1D nanostructructures have been synthesized.[233-236] It is found that the organic molecule can induce the rod micelle formation even at lower concentration. It is observed that the surfactant molecules not only prevent the larger aggregates formation but they also selectively adsorb on the specific surfaces/planes and promote the growth of other planes.[227,236]

1.5. Motivation behind the thesis

The work embodied in the thesis has been undertaken with a two-dimensional objective: firstly, to find out how different the optical properties of some EDA molecular aggregates different from those in homogeneous solution and secondly, to identify the role of intermolecular interactions in the formation of the aggregates and in determining their morphology. The aggregation behavior of highly dipolar and weakly dipolar molecules have been probed in the absence and presence of additives to obtain insight into the mechanistic details of the intermolecular interactions in the aggregation process. The molecular systems investigated in this work are shown in Chart 1.6.

A substantial amount of work on **ADMA** is aimed at finding out the nature of the emitting state in the molecular form. However, these studies did not provide any information on the photophysical properties of the aggregated state of the molecule. Hence, we have embarked upon studies that explore the optical properties of **ADMA** in its aggregated state to find out whether/how these properties are related to the morphology of the aggregates. The aggregated state of **ADMA** has been probed using

electronic absorption and fluorescence spectroscopy, microscopy and crystallography. These results suggest that the morphologies and optical properties of the aggregates cannot be tuned without using any additive.

The study has been extended in the presence of various additives such as surfactants, polymer and ionic liquids in an attempt to control the morphologies of **ADMA** nanostructures. It is demonstrated that the sizes and shapes of the aggregates of **ADMA** can be tuned by the surfactants, but not by the other additives described above. The various morphologies (rods, ribbons and sheets/plates) captured in this work are shown to be the consequence of preferential adsorption of the surfactants to specific crystallographic planes of **ADMA**.

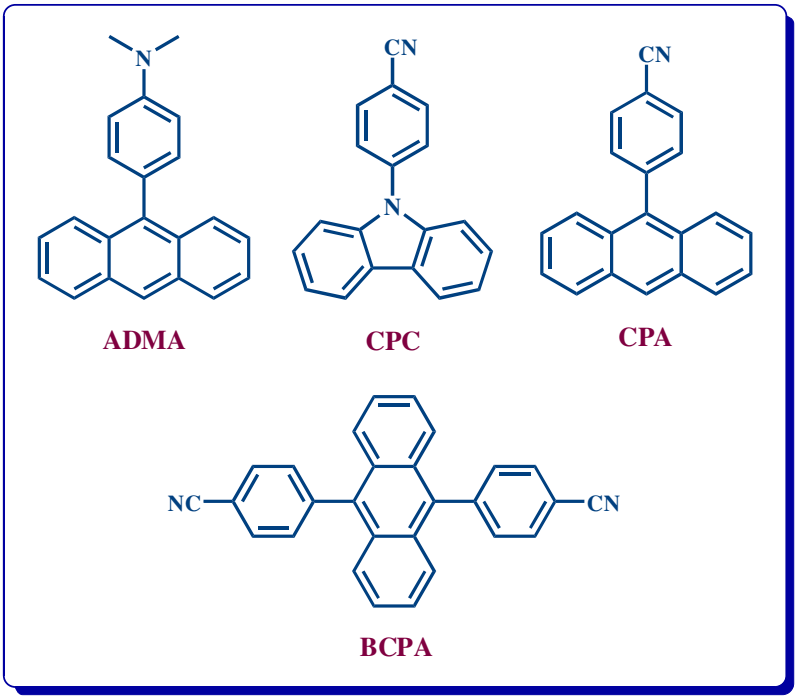

Chart 1.6: Molecular systems studied in this thesis

In order to accomplish large shape diversity of organic nanoparticles without using additives, but simply by manipulating the intermolecular interactions we realized that the EDA molecular system should be chosen such that its dipolar interaction should not be overwhelmingly larger than the supramolecular interactions. Using this strategy, we have demonstrated the fabrication of a large variety of nanostructures; rods, ribbons, tubes, rhombus crystals, hexagonal and rhombus plates of a single dipolar molecule, **CPC** (Chart 1.6) merely by changing temperature and solvent without using any templates.

With a view to obtain insight into the influence of the dipolar interaction in the nanoparticle formation and to understand the structure-property relation with the nano/microparticles morphology, two structurally related anthracene derivatives, CPA and BCPA (Chart 1.6) have been designed and synthesized. These investigations reveal that BCPA forms well-defined two-dimensional (2D) nanoplates while CPA gives aggregates with no well-defined shape.

References

(1) Fahlman, B. D. *Materials Chemistry* **2007**, *Springer*.
(2) Buffat, P.; Borel, J. P. *Phys. Rev. A* **1976**, *13*, 2287.
(3) Burda, C.; Chen, X.; Narayanan, R.; El-Sayed, M. A. *Chem. Rev.* **2005**, *105*, 1025.
(4) Daniel, M. C.; Astruc, D. *Chem. Rev.* **2004**, *104*, 293.
(5) Beer, P. D.; Cormode, D. P.; Davis, J. J. *Chem. Commun.* **2004**, 414.
(6) Chah, S.; Hammond, M. R.; Zare, R. N. *Chemistry & Biology* **2005**, *12*, 323.
(7) Redel, E.; Kramer, J.; Thomann, R. *J. Organometallic. Chem.* **2009**, *694*, 1069.
(8) McFarland, A. D.; Van Duyne, R. P. *Nano Lett.* **2003**, *3*, 1057.
(9) Ipe, B. I.; Yoosaf, K.; Thomas, K. G. *J. Am. Chem. Soc.* **2006**, *128*, 1907.
(10) Smoukov, S. K.; Bishop, K. J. M.; Kowalczyk, B.; Kalsin, A. M.; Grzybowski, B. A. *J. Am. Chem. Soc.* **2007**, *129*, 15623.
(11) He, C.; Xiong, Y.; Chen, J.; Zha, C.; Zhu, X. *J. Photochem. Photobiol. A: Chem.* **2003**, *157*.
(12) He, D.; Hu, B.; Yao, Q. F.; Wang, K.; Yu, S. H. *ACS Nano* **2009**, *3*, 3993.
(13) Shukla, R.; Hill, E.; Shi, X.; Kim, J.; Muniz, M. C.; Sunc, K.; R., J. B. J. *Soft Matter* **2008**, *4*, 2160.
(14) Panaek, A.; Kvitek, L.; Prucek, R.; Kolar, M.; Veerova, R.; Pizurova, N.; Sharma, V. K.; Nevena, T.; Zboril, R. *J. Phys. Chem. B* **2006**, *110*, 16248.
(15) Kastner, M. A. *Physics Today* **1993**, *46*, 24.
(16) Rogge, M. C.; Fuhner, C.; Keyser, U. F.; Haug, R. J.; Bichler, M.; Abstreiter, G.; Wegscheider, W. *Appl. Phys. Lett.* **2003**, *83*, 1163
(17) Jaeger, R. C. *Introduction to Microelectronic Fabrication.* **2002**, *Prentice Hall, New Jersey*.
(18) Franchi, S.; Trevisi, G.; Seravalli, L.; Frigeri, P. *Progress in Crystal Growth and Characterization of Materials* **2003**, *47*, 166.
(19) Rogach, A. L.; Talapin, D. V.; shevchenko, E. V.; Kornowski, A.; Hasse, M.; Weller, H. *Adv. Funct. mater.* **2002**, *12*.
(20) Talapin, D. V.; Jong-Soo Lee, J. S.; Kovalenko, M. V.; Shevchenko, E. V. *Chem. Rev.* **2010**, *110*, 389.
(21) Murray, C. B.; Noms, D. J.; Bawendi, M. G. *J. Am. Chem. Soc.* **1993**, *115*, 8706.
(22) Fojtik, A.; Weller, H.; Koch, U.; Henglein, A. *Phys. Chem.* **1984**, *88*, 969.
(23) Rossetti, R.; Ellison, J. L.; Gibson, J. M.; Brus, L. E. *J. Chem. Phys.* **1984**, *80*, 4464.
(24) Rossetti, R.; Hull, R.; Gibson, J. M.; Brus, L. E. *J. Chem. Phys.* **1985**, *82*, 552.
(25) Lover, T.; Bowmaker, G. A.; Seakins, J. M.; Cooney, R. P.; Henderson, W. *J. Mater. Chem.* **1997**, *7*, 647.
(26) Trindade, T.; O'Brien, P.; Pickett, N. L. *Chem. Mater.* **2001**, *13*, 3843.
(27) Trindade, T.; O'Brien, P. *Adv. Mater.* **1996**, *8*, 161.
(28) Trindade, T.; O'Brien, P. *Chem. Mater.* **1997**, *9*, 523.
(29) Manna, L.; Scher, E. C.; Alivisatos, A. P. *J. Am. Chem. Soc.* **2000**, *122*, 12700.
(30) Dabbousi, B. O.; Rodriguez-Viejo, J.; Mikulec, F. V.; Heine, J. R.; Mattoussi, H.; Ober, R. J., K. F.; Bawendi, M. G. *J. Phys. Chem. B* **1997**, *101*, 9463.

(31) Bruchez, J. M.; Moronne, M.; Gin, P.; Weiss, S.; Alivisatos, A. P. *Science* **1998**, *281*, 2013.
(32) Talapin, D. V.; Rogach, A. L.; Kornowski, A.; Haase, M.; Weller, H. *Nano Lett.* **2001**, *1*, 207.
(33) Zaman, M. B.; Toya Nath Baral, T. N.; Jianbing Zhang, J.; Dennis Whitfield, D.; Kui Yu, K. *J. Phys. Chem. C* **2009**, *113*, 496.
(34) Vannoy, C. H.; Xu, J.; Leblanc, R. M. *J. Phys. Chem. C* **2010**, *114*, 766.
(35) Scher, E. C.; Manna, L.; Alivisatos, A. P. *Philos. Trans. R. Soc. London, Ser. A* **2003**, *361*, 241.
(36) Ithurria, S.; Dubertret, B. *J. Am. Chem. Soc.* **2008**, *130*, 16504.
(37) Masuhara, H.; De Schryver, F. C.; (Eds.). *Organic Mesoscopic Chemistry* **1999**, *Blackwell Science*.
(38) Kasai, H.; Nalwa, H. S.; Oikawa, H.; Okada, S.; Matsuda, H.; Minami, N.; Kakuta, A.; Ono, K.; Mukoh, A.; Nakanishi, H. *Jpn. J. Appl. Phys.* **1992**, *31*, L1132.
(39) Katagi, H.; Kasai, H.; Okada, S.; Oikawa, H.; Matsuda, H.; Liu, Z. F.; Nakanishi, H. *Jpn. J. Appl. Phys* **1996**, *35*, L1364.
(40) Katagi, H.; Kasai, H.; Kamatani, H.; Okada, S.; Oikawa, H.; Matsuda, H.; Nakanishi, H. *J. Macromol. Sci. Pure & Appl. Chem.* **1997**, *A34*, 2013.
(41) Fujitsuka, M.; Kasai, H.; Masuhara, A.; Okada, S.; Oikawa, H.; Nakanishi, H.; Watanabe, A.; Ito, O. *Chem. Lett.* **1997**, 1211.
(42) Kamatani, H.; Kasai, H.; Okada, S.; Matsuda, H.; Oikawa, H.; MInami, N.; Kakuta, A.; Ono, K.; Mukoh, A.; Nakanishi, H. *Mol. Crys. Liq. Cryst.* **1994**, *252*, 233.
(43) Kasai, H.; Kamatani, H.; Okada, S.; Oikawa, H.; Matsuda, H.; Nakanishi, H. *Jpn. J. Appl. Phys* **1996**, *35*, L221.
(44) Kasai, H.; Oikawa, H.; Okada, S.; Nakanishi, H. *Bull. Chem. Soc. Jpn.* **1998**, *71*, 2597.
(45) Kasai, H.; Yoshikawa, Y.; Seko, T.; Okada, S.; Oikawa, H.; Matsuda, H.; Watanabe, A.; Ito, O.; Toyotama, H.; Nakanishi, H. *Mol. Crys. Liq. Cryst.* **1997**, *294*, 173.
(46) Komai, Y.; Kasai, H.; Hirakoso, H.; Okada, S.; Oikawa, H.; Adsciri, T.; Inomata, H.; Arai, K.; Nakanishi, H. *Mol. Crys. Liq. Cryst.* **1998**, *322*, 167.
(47) Baba, K.; Kasai, H.; Okada, S.; Oikawa, H.; Nakanishi, H. *Opti. Mater.* **2002**, *21*, 591.
(48) Komai, Y.; Kasai, H.; Hirakoso, H.; Hakuta, Y.; Katagi, H.; Okada, S.; Oikawa, H.; Adschiri, T.; Inomata, H.; Arai, K.; Nakanishi, H. *Jpn. J. Appl. Phys* **1999**, *38*, L81.
(49) Nakanishi, H.; Kasai, H. *Am. Chem. Soc. Sypm. Series* **1997**, *672*, 183.
(50) Zhao, L.; Yang, W.; Ma, Y.; Yao, J.; Lib, Y.; Liub, H. *Chem. Commun.* **2003**, 2442.
(51) Al-Kaysi, R. O.; Ghaddar, T. H.; Guirado, G. *J. NanoMater.* **2009**, *2009*, 1.
(52) Zhao, Y. S.; Fu, H.; Peng, A.; Ma, Y.; Xiao, D.; Yao, J. *Adv. Mater.* **2008**, *20*, 2859.
(53) Dai, Z. R.; Pan, Z. W.; Wang, Z. L. *Adv. Funct. Mater.* **2003**, *13*, 9.
(54) Zhao, Y. S.; Xiao, D.; Yang, W.; Peng, A.; Yao, J. *Chem. Mater.* **2006**, *18*, 2302.
(55) Zhao, Y. S.; Wu, J.; Huang, J. *J. Am. Chem. Soc.* **2009**, *131*, 3158.
(56) Zhao, Y. S.; Zhan, P.; Kim, J.; Sun, C.; Huang, J. *ACS Nano* **2010**, *4*, 1630.
(57) An, B. K.; Lee, D. S.; Lee, J. S.; Park, Y. S.; Song, H. S.; Park, S. Y. *J. Am. Chem. Soc.* **2004**, *126*, 10232.

(58) An, B. K.; Gihm, S. H.; Chung, J. W.; Park, C. R.; Kwon, S. K.; Park, S. Y. *J. Am. Chem. Soc.* **2009**, *131*, 3950.
(59) Masuhara, H.; Nakanishi, H.; Kasai, H. *Single Organic Nanoparticles (Ed.)*; Springer-Verlag: Berlin, 2003.
(60) Matsui, A. H.; Mizuno, K.; Nishi, O.; Matsushima, Y.; M. Shimizu, M.; Goto, T.; Takeshima, M. *Chem. Phys.* **1995**, *194*, 167.
(61) Nakanishi, H.; Katagi, H. *Supramole. Science* **1998**, *5*, 289.
(62) Fu, H.; Yao, J. *J. Am. Chem. Soc.* **2001**, *123*, 1434.
(63) Qian, Y.; Li, S.; Zhang, G.; Wang, Q.; Wang, S.; Xu, H.; Li, C.; Li, Y.; Yang, G. *J. Phys. Chem. B* **2007**, *111*, 5861.
(64) Kasai, H.; Kamatani, H.; Yashikawa, Y.; Okada, S.; Oikawa, H.; Watanabe, A.; Itoh, O.; Nakanishi, H. *Chem. Lett.* **1997**, 1181.
(65) Fu, H.; Loo, B. H.; Xiao, D.; Xie, R.; Ji, X.; Yao, J.; Zhang, B.; Zhang, L. *Angew. Chem. Int. Ed.* **2002**, *41*, 962.
(66) Xiao, D.; Xi, L.; Yang, W.; Fu, H.; Shuai, Z.; Fang, Y.; Yao, J. *J. Am. Chem. Soc.* **2003**, *125*, 6740.
(67) Peng, A. D.; Xiao, D. B.; Ma, Y.; Yang, W. S.; Yao, J. N. *Adv. Mater.* **2005**, *17*, 2070.
(68) Zhao, Y. S.; Fu, H.; Hu, F.; Peng, A.; Yang, W.; Yao, J. *Adv. Mater.* **2008**, *20*, 79.
(69) Patra, A.; Hebalkar, N.; Sreedhar, B.; Sarkar, M.; Samanta, A.; Radhakrishnan, T. P. *Small* **2006**, *2*, 650.
(70) Kanaparthi, R. K.; Sarkar, M.; Samanta, A. *J. Phys. Chem. B* **2009**, *113*, 15189.
(71) Datar, A.; Balakrishnan, K.; Yang, X.; Zuo, X.; Huang, J.; Oitker, R.; Yen, M.; Zhao, J.; Tiede, D. M.; Zang, L. *J. Phys. Chem. B* **2006**, *110*, 12327.
(72) Bao, Q.; Goh, B. M.; Yan, B.; Yu, T.; Shen, Z.; Loh, K. P. *Adv. Mater.* **2010**, *22*, 3661.
(73) Zhang, X.; Sun, B. *J. Phys. Chem. B* **2007**, 10.1021/jp0723517.
(74) Xiao, D.; Yang, W.; Yao, J.; Xi, L.; Yang, X.; Shuai, Z. *J. Am. Chem. Soc.* **2004**, *126*, 15439.
(75) Lei, Y.; Liao, Q.; Fu, H.; Yao, J. *J. Am. Chem. Soc.* **2010**, *132*, 1742.
(76) Matsuda, H.; Van Keruren, E.; Masaki, A. *Nonlinear Opt.* **1995**, *10*, 123.
(77) Matsuda, H.; Yamada, S.; Van Keruren, E. *Proc. SPIE* **1997**, *2998*, 241.
(78) Tian, Z. Y.; Huang, W. T.; Xiao, D. B.; Wang, S. Q.; Wu, Y. S.; Gong, Q. H.; Yang, W. S.; Yao, J. *Chem. Phys. Lett.* **2004**, *391*, 283.
(79) Patra, A.; Venkatram, N.; Narayana Rao, D.; Radhakrishnan, T. P. *J. Phys. Chem. C* **2008**, *112*, 16269.
(80) Wu, C.; Szymanski, C.; Cain, Z.; McNeill, J. *J. Am. Chem. Soc.* **2007**, *129*, 12904.
(81) Raymond, J. E.; Ramakrishna, G.; Twieg, R. J.; Goodson III, H. *J. Phys. Chem. C* **2008**, *112*, 7913.
(82) Birks, J. B. *In Photophysics of Aromatic Molecules*; John Wiley & Sons: London, 1970.
(83) Turro, N. J. *Modern Molecular Photochemistry*, 1 ed.; Benjamin/ Cummings Publishing Company, Inc.: California, 1978.
(84) Luo, J.; Xie, Z.; Lam, J. W. Y.; Cheng, L.; Chen, H.; Qiu, C.; Kwok, H. S.; Zhan, X.; Liu, Y.; Zhu, D.; Tang, B. Z. *Chem. Commun.* **2001**, 1740.

(85) Friend, R. H.; Gymer, R. W.; Holmes, A. B.; Burroughes, J. H.; Marks, R. N.; Taliani, C.; Bradley, D. D. C.; Santos, D. A. D.; Bredas, J. L.; Logdlund, M.; Salaneck, W. R. *Nature* **1999**, *397*, 121.
(86) Chen, J.; Law, C. C. W.; Lam, J. W. Y.; Dong, Y.; Lo, S. M. F.; Williams, I. D.; Zhu, D.; Tang, B. Z. *Chem. Mater.* **2003**, *15*, 1535.
(87) Qian, G.; Dai, B.; Luo, M.; Yu, D.; Zhan, J.; Zhang, Z.; Ma, D.; Wang, Z. Y. *Chem. Mater.* **2008**, *20*, 6208.
(88) Mi, B.; Dong, Y.; Li, Z.; Lam, J. W. Y.; Haussler, M.; Sung, H. H. Y.; Kwok, H. S.; Dong, Y.; Williams, I. D.; Liu, Y.; Luo, Y.; Shuai, Z.; Zhu, D. B.; Tang, B. Z. *Chem. Commun.* **2005**, 3583.
(89) Yu, G.; Yin, S.; Liu, Y.; Chen, J.; Xu, X.; Sun, X.; Ma, D.; Zhan, X.; Peng, Q.; Shuai, Z.; Tang, B. Z.; Zhu, D. B.; Fang, W.; Luo, Y. *J. Am. Chem. Soc.* **2005**, *127*, 6335.
(90) Li, S. J.; An, B. K.; Jung, S. D.; Chung, M. A.; Park, S. Y. *Angew. Chem., Int. Ed.* **2004**, *43*, 6346.
(91) An, B. K.; Kwon, S. K.; Jung, S. D.; Park, S. Y. *J. Am. Chem. Soc.* **2002**, *124*, 14410.
(92) Xie, Z.; Yang, B.; Cheng, G.; Liu, L.; He, F.; Shen, F.; Ma, Y.; Liu, S. *Chem. Mater.* **2005**, *17*, 1287.
(93) Li, Y.; Li, F.; Zhang, H.; Xie, Z.; Xie, W.; Xu, H.; Li, B.; Shen, F.; Ye, L.; Hanif, M.; Ma, D.; Y. Ma. *Chem. Commun.* **2007**, 231.
(94) Tong, H.; Dong, Y.; Haussler, M.; Lam, J. W. Y.; Sung, H. H. Y.; Williams, I. D.; Sun, J.; Tang, B. Z. *Chem. Commun.* **2006**, 1133.
(95) Tong, H.; Dong, Y.; Hong, Y.; Haussler, M.; Lam, J. W. Y.; Sung, H. H. Y.; Sun, X.; Yu, J.; Williams, I. D.; Kwok, H. S.; Tang, B. Z. *J. Phys. Chem. C* **2007**, *111*, 2287.
(96) Deans, R.; Kim, J.; Machacek, M. R.; Swager, T. M. *J. Am. Chem. Soc.* **2000**, *122*, 8565.
(97) Holzer, W.; Penzkofer, A.; Stockmann, R.; Meysel, H.; Liebegott, H.; Horhold, H. H. *Polymer* **2001**, *42*, 3183.
(98) Kim, S.; Zheng, Q.; He, G. S.; Bharali, D. J.; Pudavar, H. E.; Baev, A.; Prasad, P. N. *Adv. Funct. Mater.* **2006**, *16*, 2317.
(99) Kim, S.; Ohulchanskyy, T. Y.; Pudavar, H. E.; Pandey, R. K.; Prasad, P. N. *J. Am. Chem. Soc.* **2007**, *129*, 2669.
(100) Qin, A.; Lam, J. W. Y.; Mahtab, F.; Jim, C. K. W.; Tang, L.; Sun, J.; Sung, H. H. Y.; Williams, I. D.; Tang, B. Z. *Appl. Phys. Lett.* **2009**, *94*, 253308.
(101) Yuan, C. X.; Tao, X. T.; Ren, Y.; Li, Y.; Yang, J. X.; Yu, W. T.; Wang, L.; Jiang, M. H. *J. Phys. Chem. C* **2007**, *111*, 12811.
(102) Qian, Y.; Li, S.; Zhang, G.; Wang, Q.; Wang, S.; Xu, H.; Li, C.; Li, Y.; Yang, G. *J. Phys. Chem. B* **2007**, *111*, 5861.
(103) He, T.; Tao, A. T.; Yang, J. X.; Guo, D.; Xia, H. B.; Jiaac, J.; Jianga, M. *Chem. Commun.* **2011**, *47*, 2907.
(104) Liu, Y.; Tao, X.; Wang, F.; Dang, X.; Zou, D.; Ren, Y.; Jiang, M. *J. Phys. Chem. C* **2008**, *112*, 3975.
(105) Tang, C. W.; VanSlyke, S. A. *Appl. Phys. Lett.* **1987**, *51*, 913.
(106) Tsumura, A.; Koezuka, H.; Ando, T. *Appl. Phys. Lett.* **1986**, *49*, 1210—1212.

(107) Li, H. C.; Lin, Y. P.; Chou, P. T.; Cheng, Y. M.; Liu, R. S. *Adv. Funct. Mater.* **2007**, *17*, 520.
(108) Chen, S. Y.; Xu, X. J.; Liu, Y. Q.; Qiu, W. F.; Yu, G.; Wang, H. P.; Zhu, D. B. *J. Phys. Chem. C* **2007**, *111*, 1029.
(109) Zhang, H. Y.; Huo, C.; Zhang, J. Y.; Zhang, P.; Tian, W. J.; Wang, Y. *Chem. Commun.* **2006**, 281.
(110) Wang, R. Y.; Jia, W. L.; Aziz, H.; Vamvounis, G.; Wang, S. N.; Hu, N. X.; Popovic, Z. D.; Coggan, J. A. *Adv. Funct. Mater.* **2005**, *15*, 1483.
(111) Lee, H. J.; Jin, Z. X.; Aleshin, A. N.; Lee, J. Y.; Goh, M. J.; Akagi, K.; Kim, Y. S.; Kim, D. W.; Park, Y. W. *J. Am. Chem. Soc.* **2004**, *126*, 16722.
(112) Zhou, Y.; Freitag, M.; Hone, J.; Staii, C.; Jr. Johnson, A. T. *Appl. Phys. Lett.* **2003**, *83*, 3800.
(113) Lim, J. A.; Liu, F.; Ferdous, S.; Muthukumar, M.; Briseno, A. L. *Mater. Today* **2010**, *13*, 14.
(114) Peumans, P.; Yakimov, A.; Forrest, S. R. *J. Appl. Phys.* **2003**, *93*, 3693.
(115) Katz, H. E.; Bao, Z.; Gilat, S. L. *Acc. Chem. Res.* **2001**, *34*, 359.
(116) Peumans, P.; Uchida, S.; Forrest, S. R. *Nature* **2003**, *425*, 158.
(117) Meijer, E. W.; Schenning, A. P. H. J. *Nature* **2002**, *419*, 353.
(118) Hoeben, F. J. M.; Jonkheijm, P.; Meijer, E. W.; Schenning, A. P. H. J. *Chem. Rev.* **2005**, *105*, 1491−1546.
(119) Muller, C. D.; Falcou, A.; Reckefuss, N.; Rojahn, M.; Wiederhirn, V.; Rudati, P.; Frohne, H.; Nuyken, O.; Becker, H.; Meerholz, K. *Nature* **2003**, *421*, 829.
(120) Zang, L.; Che, Y.; Moore, J. S. *Acc. Chem. Res.* **2008**, *41*, 1596.
(121) Zhao, Y. S.; Fu, H.; Peng, A.; Ma, Y.; Liao, Q.; Yao, J. *Acc. Chem. Res.* **2010**, *43*, 409.
(122) Kim, F. S.; Ren, G.; Jenekhe, S. A. *Chem. Mater.* **2011**, *23*, 682.
(123) Briseno, A. L.; Mannsfeld, A. C. B.; Jenekhe, S. A.; Bao, Z.; Xia, Y. *Mater. Today* **2008**, *11*, 38.
(124) Huan, W.; ZengQi, X.; YuGuang, M.; JiaCong, S. *Sci. China. Series. B: Chemistry* **2007**, *50*, 433.
(125) Law, M.; Goldberger, J.; Yang, P. *Annu. Re . Mater. Res.* **2004**, *34*, 83.
(126) Wang, Y.; Tran, H. D.; Liao, L.; Duan, X.; Kane, R. B. *J. Am. Chem. Soc.* **2010**, *132*, 10365.
(127) Kim, D. H.; Lee, D. Y.; Lee, H. S.; Lee, W. H.; Kim, Y. H.; Han, J. I.; Cho, K. *Adv. Mater.* **2007**, *19*, 678.
(128) Briseno, A. L.; Mannsfeld, S. C. B.; Lu, X.; Xiong, Y.; Jenekhe, S. A.; Bao, Z.; Xia, Y. *Nano Lett.* **2007**, *7*, 668.
(129) Cavallini, M.; Stoliar, P.; Moulin, J. F.; Surin, M.; Leclere, P.; Lazzaroni, R.; Breiby, D. W.; Andreasen, J. W.; Nielsen, M. M.; Sonar, P.; Grimsdale, A. C.; Mullen, K.; Biscarini, F. *Nano Lett.* **2005**, *5*, 2422.
(130) Sun, Y.; Tan, L.; Jiang, S.; Qian, H.; Wang, C.; Yan, D.; Di, C.; Wang, Y.; Wu, W.; Yu, G.; Yan, S.; Wang, C.; Hu, W.; Liu, Y.; Zhu, D. *J. Am. Chem. Soc.* **2007**, *129*, 1882.
(131) Yamamoto, Y.; Jin, W.; Fukushima, T.; Minari, T.; Tsukagoshi, K.; Saeki, A.; Seki, S.; Tagawa, S.; Aida, T. *Chem. Lett.* **2009**, *38*, 888.

(132) Yamamoto, Y.; Fukushima, T.; Suna, Y.; Ishii, N.; Saeki, A.; Seki, S.; Tagawa, S.; Taniguchi, M.; Kawai, T.; Aida, T. *Science* **2006**, *314*, 1761.
(133) Zhang, X. J.; Yuan, G. D.; Li, Q. S.; Wang, B.; Zhang, X. H.; Zhang, R. Q.; Chang, J. C.; Lee, C. S.; Lee, S. T. *Chem. Mater.* **2008**, *20*, 6945.
(134) Nguyen, T. Q.; Martel, R.; Avouris, P.; Bushey, M. L.; Brus, L.; Nuckolls, C. *J. Am. Chem. Soc.* **2004**, *126*, 5234.
(135) Kastler, M.; Pisula, W.; Wasserfallen, D.; Pakula, T.; Mullen, K. *J. Am. Chem. Soc.* **2005**, *127*, 4286.
(136) Hill, J. P.; Jin, W.; Kosaka, A.; Fukushima, T.; Ichihara, H.; Shimomura, T.; Ito, K.; Hashizume, T.; Ishii, N.; Takuzo Aida, T. *Science* **2004**, *304*, 1481.
(137) Wurthner, F. *Chem. Commun.* **2004**, 1564.
(138) Jiang, W.; Zhou, Y.; Geng, H.; Jiang, S.; Yan, S.; Hu, W.; Wang, Z.; Shuai, Z.; Pei, J. *J. Am. Chem. Soc.* **2001**, *133*, 1.
(139) Huang, Y.; Quan, B.; Wei, Z.; Liu, G.; Sun, L. *J. Phys. Chem. C* **2009**, *113*, 3929.
(140) Chesterfield, R. J.; McKeen, J. C.; Newman, C. R.; Ewbank, P. C.; da Silva Filho, D. A.; Bredas, J. L.; Miller, L. L.; Mann, K. R.; Frisbie, C. D. *J. Phys. Chem. B* **2004**, *108*, 19281.
(141) Balakrishnan, K.; Datar, A.; Oitker, R.; Chen, H.; Zuo, J.; Zang, L. *J. Am. Chem. Soc.* **2005**, *127*, 10496.
(142) Datar, A.; Balakrishnan, K.; Yang, X.; Zuo, X.; Huang, J.; Oitker, R.; Yen, M.; Zhao, J.; Tiede, D. M.; Zang, L. *J. Phys. Chem. B* **2006**, *110*, 12327.
(143) Che, Y.; Datar, A.; Balakrishnan, K.; Zang, L. *J. Am. Chem. Soc.* **2007**, *129*, 7234.
(144) Che, Y.; Datar, A. X. Y.; Naddo, T.; Zhao, J.; Zang, L. *J. Am. Chem. Soc.* **2007**, *129*, 6354.
(145) Briseno, A. L.; Mannsfeld, S. C. B.; Reese, C.; Hancock, J. M.; Xiong, Y.; Jenekhe, S. A.; Bao, Z.; Xia, Y. *Nano Lett.* **2007**, *7*, 2847.
(146) Hayward, R. C.; Saville, D. A.; Aksay, I. A. *Nature* **2000**, *404*, 56.
(147) Hua, F.; Shi, J.; Lvov, Y.; Cui, T. *Nano Lett.* **2002**, *2*, 1219
(148) Magdassi, S.; Ben-Moshe, M. *Langmuir* **2003**, *19*, 939
(149) An, B. K.; Kwon, S. K.; Park, S. Y. *Angew. Chem. Int. Ed.* **2007**, *46*, 1978
(150) Zhao, Y. S.; Wu, J.; Huang, J. *J. Am. Chem. Soc.* **2009**, *131*, 3158.
(151) Balzer, F.; Bordo, V. G.; Simonsen, A. C.; Rubahnc, H. G. *Appl. Phys. Lett.* **2003**, *82*, 10.
(152) Takazawa, K. *J. Phys. Chem. C* **2007**, *111*, 8671.
(153) Takazawa, K.; Kitahama, Y.; Kimura, Y.; Kido, G. *Nano Lett.* **2005**, *5*, 1293.
(154) Zhao, Y. S.; Peng, A.; Fu, H.; Ma, Y.; Yao, J. *Adv. Mater.* **2008**, *20*, 1661.
(155) Zhao, Y. S.; Yang, W.; Xiao, D.; Sheng, X.; Yang, X.; Shuai, Z.; Luo, Y.; Yao, J. *Chem. Mater.* **2005**, *17*, 6430.
(156) Lebedenko, A. L.; Guralchuk, G. Y.; Sorokin, A. V.; Yefimova, S. L.; Malyukin, Y. V. *J. Phys. Chem. B* **2006**, *110*, 17772.
(157) Zhao, Y. S.; Xu, J.; Peng, A.; Fu, H.; Ma, Y.; Jiang, L.; Yao, J. *Angew. Chem. Int. Ed.* **2008**, *47*, 7301
(158) Huang, L.; Liao, Q.; Shi, Q.; Fu, H.; Mab, J.; Yao, J. *J. Mater. Chem.* **2010**, *20*.
(159) McQuade, D. T.; Pullen, A. E.; Swager, T. M. *Chem. Rev.* **2000**, *100*, 2537.

(160) Thomas, S. W.; Joly, G. D.; Swager, T. M. *Chem. Rev.* **2007**, *107*, 1339.
(161) Che, Y.; Yang, X.; Loser, S.; Zang, L. *Nano Lett.* **2008**, *8*, 2219.
(162) Naddo, T.; Che, Y.; Zhang, W.; Balakrishnan, K.; Yang, X.; Yen, M.; Zhao, J.; Moore, J. S.; Zang, L. *J. Am. Chem. Soc.* **2007**, *129*, 6978.
(163) Jung, J. S.; Lee, J. W.; Kim, K.; Cho, M. Y.; Jo, S. G.; Joo, J. *Chem. Mater.* **2010**, *22*, 2219.
(164) Michel-Beyerle, M. E. *In The Reaction Centre of Photosynthetic Bacteria* **1995**, *Springer-Verlag Berlin*.
(165) Bard, A.; Fox, M. A. *Acc. Chem. Res.* **1995**, *28*, 141.
(166) Diner, B. A.; Babcock, G. T.; Ed. *In Structure, Dynamics and Energy Conversion Efficiency in Photosystem II* **1996**, *Kluwer: Dordrecht*.
(167) Gust, D.; Moore, T. A.; Moore, A. L. *Acc. Chem. Res.* **1993**, *26*, 198.
(168) Kurreck, H.; Huber, M. *Angew. Chem. Int. Ed.* **1995**, *34*, 849.
(169) Memming, R.; Pelizetti, E.; Schiavello, M.; Ed. *In Photochemical Conversion and Storage of Solar Energy* **1991**, *Kluwer Holland*.
(170) Meyer, T. J. *Acc. Chem. Res.* **1989**, *22*, 163.
(171) Michel-Beyerle, M. E.; Finckh, P.; Heitele, H.; Volk, M. *J. Phys. Chem.* **1988**, *92*, 6584.
(172) Wasielewski, M. R. *Chem. Rev.* **1992**, *92*, 435.
(173) Fabbrizzi, L.; Poggi, A. *Chem. Soc. Rev.* **1995**, *24*, 197.
(174) Shelton, D. B.; Rice, J. E. *Chem. Rev.* **1994**, *94*, 3.
(175) Carter, F. L.; Siatoski, R. E.; Woltjen, H. *In Molecular Electronic Devices* **1988**, *North-Holland: Amsterdam*.
(176) Barbara, P. F.; Jarzeba, W. *Acc. Chem. Res.* **1988**, *21*, 195.
(177) Mulliken, R. S. *J. Am. Chem. Soc.* **1950**, *72*, 600.
(178) Mulliken, R. S. *J. Phys. Chem.* **1952**, *56*, 801.
(179) Fox, M. A.; Galoppini, E. *J. Am. Chem. Soc.* **1997**, *119*, 5277.
(180) Jordan, K. D.; Paddon-Row, M. N. *Chem. Rev.* **1992**, *92*, 395.
(181) Verhoeven, J. W.; Scherer, T.; Willemse, R. *J. Pure Appl. Chem.* **1993**, *65*, 1717.
(182) Yazdi, P.; McFann, G. J.; Fox, M. A.; Johnston, K. P. *J. Phys. Chem.* **1990**, *94*, 7224.
(183) Zhang, J.; Bright, F. V. *J. Phys. Chem.* **1992**, *96*, 5633.
(184) Saroja, G.; Ramachandram, B.; Saha, S.; Samanta, A. *J. Phys. Chem. B* **1999**, *103*, 2906.
(185) Saroja, G.; Soujanya, T.; Ramachandram, B.; Samanta, A. *J. Fluores.* **1998**, *8*, 405.
(186) Soujanya, T.; Krishma, T. S. R.; Samanta, A. *J. Phys. Chem.* **1992**, *96*, 8544.
(187) Slavik, J. *Biochem. Biophys. Acta* **1982**, *1*, 694.
(188) Narang, V.; Zhav, C. F.; Bhawalkar, J. D.; Bright, F. V.; Prasad, P. N. *J. Phys. Chem.* **1996**, *100*, 4521.
(189) Jortner, J.; Levine, R. D. *Adv. Chem. Phys.* **1981**, *47*, 1.
(190) Fletcher, A. N. *Appl. Phys.* **1983**, *B31*, 19.
(191) Baretz, B. H.; Singh, A. K.; Liu, R. S. H. *Nouv. J. Chim.* **1981**, *5*, 297.
(192) Gorner, H.; Schulte-Frohlinde, D. *J. Mol. Struct.* **1982**, *84*, 227.
(193) Keery, K. M.; Fleming, G. R. *Chem. Phys. Lett.* **1982**, *93*, 322.
(194) Salem, L. *Science* **1976**, *191*, 822.
(195) Allen, N. S.; Bentley, P.; McKellar, J. F. *J. Photochem.* **1976**, *5*, 225.

(196) O'Brien, D. F.; Kelly, T. M.; Costa, L. F. *Photogr. Sci. Eng.* **1974**, *18*, 76.
(197) Carter, F. L.; Lee, S. H.; Ed. *In Optical Information Processing Fundamentals*; Springer-Verlag: New York, 1981.
(198) Drexhage, K. H.; Schäfer, F. P.; Ed. *In Dye Laser*; Springer: Berlin, 1977.
(199) Kubin, R. F.; Fletcher, A. N. *J. Lumin.* **1982**, *27*, 455.
(200) Vogel, M.; Rettig, W.; Sens, R.; Drexhage, K. H. *Chem. Phys. Lett.* **1988**, *147*, 461.
(201) Vogel, M.; Rettig, W.; Sens, R.; Drexhage, K. H. *Chem. Phys. Lett.* **1988**, *148*, 452.
(202) Arbeloa, F. L.; Aguirresacona, U. I.; Arbeloa, I. L. *Chem. Phys.* **1989**, *130*, 371.
(203) Arbeloa, F. L.; Arbeloa, T. L.; Arbeloa, I. L.; De Schryver, F. C. *J. Photochem. Photobiol. A: Chem.* **1991**, *56*, 313.
(204) Onganer, Y.; Quitevis, E. L. *J. Phys. Chem.* **1992**, *96*, 7996.
(205) Jones II, G.; Jackson, W. R.; Choi, C. Y.; Bergmark, W. R. *J. Phys. Chem.* **1985**, *89*, 294.
(206) Jones II, G.; Jackson, W. R.; Halpern, A. M. *Chem. Phys. Lett.* **1980**, *72*, 391.
(207) Jones II, G.; Jackson, W. R.; Kanoktanaporn, S.; Halpern, A. M. *Opt. Commun.* **1980**, *33*, 315.
(208) de Melo, J. S.; Becker, R. S.; Elisei, F.; Macanita, A. L. *J. Chem. Phys.* **1997**, *107*, 6062.
(209) de Melo, J. S.; Becker, R. S.; Macanita, A. L. *J. Phys. Chem.* **1994**, *98*, 6054.
(210) Gude, C.; Rettig, W. *J. Phys. Chem. A* **2000**, *104*, 8050.
(211) Gude, C.; Rettig, W.; Lapouyade, R. *J. Phys. Chem. A* **1997**, *101*, 9673.
(212) Velsko, S. P.; Fleming, G. R. *Chem. Phys.* **1982**, *65*, 59.
(213) Saha, S.; Samanta, A. *J. Phys. Chem. A* **1998**, *102*, 7903.
(214) Saha, S.; Samanta, A. *J. Phys. Chem. A* **2002**, *106*, 4763.
(215) Sarkar, M.; Kanaparthi, R. K.; Bhattacharya, B.; Samanta, A. *J. Phys. Chem. A* **2008**, *112*, 3302.
(216) Zhang, X.; Zhang, X.; Zou, K.; Lee, C.-S.; Lee, S.-T. *J. Am. Chem. Soc.* **2007**, *129*, 3527.
(217) Zhang, X.; Zhang, X.; Wang, B.; Zhang, C.; Chang, J. C.; Lee, C. S.; Lee, S. T. *J. Phys. Chem. C* **2008**, *112*, 16264.
(218) Kalyanasundaram, K. *Photochemistry in Microheterogeneous Systems*; Academic Press INC.: London, 1987.
(219) Imae, T.; Kamiya, R.; Ikeda, S. *J. Colloid Interface Sci.* **1985**, *108*, 215.
(220) Andersson, M.; Pedersen, J. S.; Palmqvist, A. E. C. *Langmuir* **2005**, *21*, 11387.
(221) Petit, C.; Lixon, P.; Pileni, M.-P. *J. Phys. Chem.* **1993**, *97*.
(222) Setua, P.; Chakraborty, A.; Seth, D.; Bhatta, M. U.; Satyam, P. V.; Sarkar, N. *J. Phys. Chem. C* **2007**, *111*, 3901.
(223) Murphy, C. J.; Sau, T. K.; Gole, A. M.; Orendorff, C. J.; Gao, J.; Gou, L.; Hunyadi, S. E.; Li, T. *J. Phys. Chem. B* **2005**, *109*, 13857.
(224) Kuo, C.-H.; TChiang, T.-F.; Chen, L.-J.; M.H., H. H. *Langmuir* **2004**, *20*, 7820.
(225) Joseph, D.; Geckeler, K. E. *Langmuir* **2009**, *25*, 13224.
(226) Khanal, B. P.; Zubarev, E. R. *Angew. Chem. Int. Ed.* **2009**, *48*, 6888
(227) Zhang, X.; Yuan, G.; Li, Q.; Wang, B.; Zhang, X.; Zhang, R.; Chang, J. C.; Lee, C.; Lee, S. *Chem. Mater.* **2008**, *20*, 6945.
(228) Peng, X. G.; Manna, L.; Yang, W. D.; Wichham, J.; Scher, E.; Kadavanich, A.; Alivisatos, A. P. *Nature* **2000**, *404*, 59.

(229) Xia, Y.; Xiong, Y.; Lim, B.; Skrabalak, S. E. *Angew. Chem. Int. Ed.* **2009**, *48*, 60
(230) Jana, N. R.; Murphy, C. J. *Chem. Commun.* **2001**, 617.
(231) Murphy, C. J.; Jana, N. R. *Adv. Mater.* **2002**, *14*, 80.
(232) Xiong, Y.; Xia, Y. *Adv. Mater.* **2007**, *19*, 3385.
(233) Fu, H.; Xiao, D.; Yao, J.; Yang, G. *Angew. Chem. Int. Ed.* **2003**, *42*, 2883
(234) Hu, J.-S.; Guo, Y.-G.; Liang, H.-P.; Wan, L.-J.; Jiang, L. *J. Am. Chem. Soc.* **2005**, *127*, 17090.
(235) Jia, W.; ZuoLun, Z.; JunWei, Y.; JingYing, Z.; Yue, W. *Chinese Sci.Bull.* **2007**, *52*, 1307.
(236) Zhang, X.; Zhang, X.; Shi, W.; Meng, X.; Lee, C.; Lee, S. *J. Phys. Chem. B* **2005**, *109*, 18777.

Chapter 2

Materials, Methods and Instrumentation

This chapter lists the materials used in this study followed by the methods of purification of reagents and solvents. Synthesis of the electron donor-acceptor (EDA) molecules used in the studies is briefly described. Fabrication of nano/microparticles of the systems has been described. The instrumental details, especially the time-correlated single-photon counting technique (TCSPC) based picosecond setup, fluorescence lifetime imaging microscope (FLIM) and atomic force microscope (AFM) setup have been outlined. Various methodologies, like sample preparation for spectroscopy and microscopy experiments, measurements of fluorescence quantum yield and analysis of TCSPC data have been discussed. Theoretical methods for semi-empirical and density functional studies, based on which the ground state dipole moments of the different systems and energetics of molecular motifs have been evaluated, are discussed. The instrumental details, strategies for crystal growth and details concerning single crystal structure determination are also described at the end of this chapter.

2.1. Materials

Anthrone, tetrakis(triphenylphosphine)palladium(0) ($Pd(PPh_3)_4$), 4-bromo-*N*,*N*-dimethylaniline, 4-fluorobenzonitrile, 9,10-dibromoanthracene, 4-(cyano)phenylboricacid were procured from Sigma-Aldrich and used as received for the synthesis of electron donor-acceptor (EDA) systems. However, carbazole (Sigma-Aldrich) was recrystalized from hexane/acetone mixture and used in the synthesis of 9-cyanophenylcarbazole (CPC). 9-Bromoanthracene was prepared form anthracence (Avra Chemicals) using $CuBr_2$ (Avra Chemicals) by following a reported procedure.[1] Sodiumdodecylsulfate (SDS), triton-X100 (TX-100), polyvinylalcohol (PVA) cetyltrimethylammoniumbromide (CTAB) were also obtained from Sigma-Aldrich and used as received in the fabrication of nano/microparticles. The ionic liquids, [BMIM][Cl] and [BMIM][BF_4], were synthesized according to the literature method.[2] The purities of all compounds were

checked by single spot in thin layer chromatography (TLC), nuclear magnetic resonance spectroscopy (NMR) as well as by matching the absorption and emission spectra with literature.

The various drying agents and chemicals such as phosphorous pentoxide (P_2O_5), sodium metal, magnesium turnings and iodine used at different stages of the purification procedure, were purchased from local companies. Calcium hydride (CaH_2) was obtained from Spectrochem (India). GR grade solvents were obtained from Merck (India) for spectroscopic and synthetic purposes and their purification procedures are outlined in the following section. Deuteriated solvent, chloroform-d, was obtained from Merck (India).

2.2. Purification of conventional solvents and reagents

The solvents used at various stages of the study were purified using the procedures available in the literature.[3] We adopted the following procedures for the purification of various solvents.

Acetone, acetonitrile: The solvent was stirred with CaH_2 overnight or refluxed with P_2O_5 for 3-4 hr and then distilled. The distilled solvent was collected and stored under dry conditions.

Cyclohexane, tetrahydrofuran: The solvents were refluxed over metallic sodium for 3-4 hours and added benzophenone. The deep blue solution was refluxed for another one hour and collected under dry conditions.

Dimethylsulfoxide: The solvent was stored on dry molecular sieves for overnight and distilled under vacuum. Precautions were taken to store the solvent under dry conditions.

Water: MilliQ water produced from Millipore, SynergyPack, was used for the present study.

2.3. Synthesis of EDA systems

A brief description of the synthesis of electron donor-acceptor (EDA) molecules for the work in Chapter 3, 4, 5 and 6 is provided in this section.

4-(9-anthryl)-N,N-dimethylaniline (ADMA): Synthesis of ADMA was carried out following a standard procedure[4] (Scheme 1), which involves reaction between anthrone and the Grignard reagent obtained from 4-bromo-*N*,*N*-dimethylaniline (BDA). Briefly, a solution of anthrone (5.82 g, 0.03 mol) was added to a Grignard reagent, prepared from BDA (20.5 g, 0.1 mol) and magnesium flakes (2.5 g, 0.1 mol) in dry tetrahydrofuran (THF, 40 mL) at 0 °C under nitrogen atmosphere and stirred over a period of 30 min. After stirring for additional 1 h at room temperature, the reaction mixture was quenched with saturated NH_4Cl and worked up with diethyl ether (3 × 100 mL). The solvent was removed and the crude product was purified by column chromatography (neutral alumina column, hexane as an eluent) and recrystallized from ethyl acetate. The analytical data (LCMS, 1H NMR) of the purified compound confirmed the identity of the molecule.

9-(4-cyanophenyl)carbazole (CPC): CPC was prepared by following a reported procedure in the literature.[5] A mixture of carbazole (3 mmol) and NaH was stirred in dimethylformamide (DMF) at room temperature for 3 h. Then *in situ* formed sodiumcarbazole was heated with 4-fluorobenzonitrile (3 mmol) and NaI (6 mmol) at 120 °C for about 20 h. The crude product was precipitated by adding ice-cold water and filtered using a vacuum filtration setup. Then the dried product was purified by column chromatography using a silica gel as stationary phase and ethylacetate and *n*-hexane (50:50) as eluent. Final product was further purified by recrystallization from ethanol. The compound (colourless solid) was characterized by NMR spectroscopy and by comparing the absorption and fluorescence spectra in different solvents with the literature information.

9,10-Bis(4-cyanophenyl)anthracene (BCPA): The titled compound was synthesized by Suzuki-coupling reaction.[6] Briefly, a mixture of 9,10-dibromoanthracene (180 mg, 0.53 mmol), 4-cyanophenylboronic acid (240 mg, 1.64 mmol), [$Pd(PPh_3)_4$] (50 mg, 7 mol%), Na_2CO_3 (1.5 mL, 2 M) and solvent [THF (5 mL) and toluene (5 mL)] was heated at 85 °C under N_2 for ~24 h. On completion of the reaction (TLC monitoring), the reaction mixture was diluted with water and aqueous layer was extracted with diethylether (3×50 mL). The combined organic layers were dried over Mg_2SO_4 and the solvent was evaporated using rotary evaporator. The crude product was purified by a silica gel column chromatography. Elution of the column with 2% ethylacetate–hexane gave the desired coupling product (450 mg, 72%) as a pale yellow crystalline solid; mp 431 °C. The compound was characterized by 1H-NMR spectroscopy and single crystal X-ray diffraction study.

9-(4-cyanophenyl)anthracene (CPA): The desired compound was also synthesized by palladium catalyzed Suzuki-coupling reaction[6] (scheme 1). To a solution of 9-bromoanthracene (2 mmol, 517 mg) in toluene/THF (1:1 ratio, 10 ml), 4-(cyano)phenyl boric acid (2 mmol, 303 mg) and 3 ml 1M Na_2CO_3 and 50 mg [$Pd(PPh_3)_4$] were added. Then the reaction mixture was refluxed in oil bath for about 24 hours. The progress of the reaction was periodically monitored with TLC and after the completion of reaction, the reaction mixture was cooled to room temperature and 50 mL water was added. The organic layer was separated and aqueous layer was extracted with DCM (3×50 mL). The organic layers were combined and dried over anhydrous Na_2SO_4 and concentrated using rotary evaporator. The crude product was purified by column chromatography using alumina gel as stationary phase and 5% ethylacetate in hexane as mobile phase. Finally, the compound was recrystallized from hexane. The compound was characterized by 1H-NMR spectroscopy and single crystal X-ray diffraction study.

2.4. Fabrication of nano/microparticles

Self-assembled nano/microparticles of the systems were prepared by following reprecipitation method, which is available in the literatue.[7] The procedure is illustrated in Scheme 2.1. In a typical procedure, standard stock solution of the system is prepared and small amounts are injected rapidly into a large quantity of highly pure water (MilliQ) under ultra-sonication or stirring. After 2-3 minutes of sonication or stirring, the samples are kept as such without disturbing for some time for ageing of the nano/microstructures. For all the systems, water is used as poor solvent and depending on the system involved, the solvent for the stock solution is varied. Details of those solvents and concentrations are presented in the respective chapters.

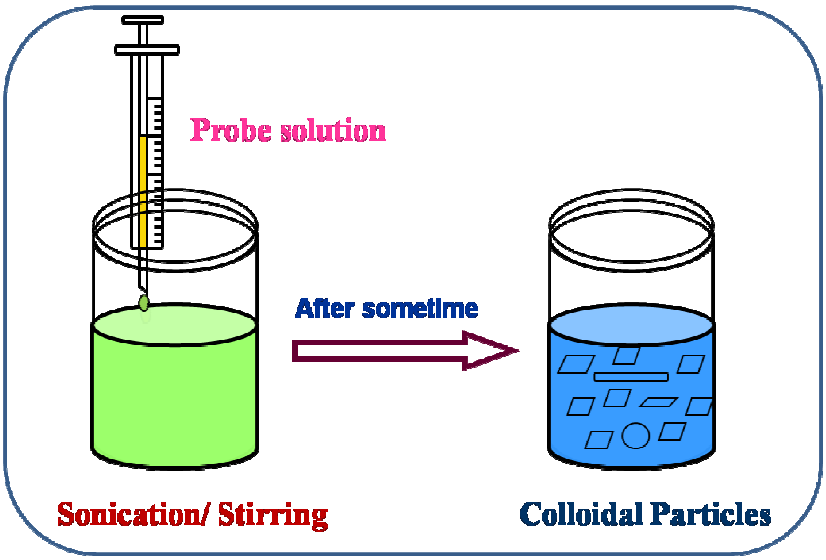

Scheme 2.1. Illustration of reprecipitation method

2.5. Instrumentation

The NMR spectra were measured using Bruker AVANCE 400 MHz NMR spectrometer. Steady-state absorption and fluorescence spectra were recorded on a UV-vis spectrophotometer (Cary100, Varian) and a spectrofluorimeter (FluoroLog-3, Jobin Yvon), respectively. The fluorescence spectra were corrected for the instrumental response.

Size and morphology of the nano/microparticles were examined by using a SolverPro-M (NT-MDT) atomic force microscope (AFM) and a Philips XL30 ESEM scanning electron microscope (SEM) using a beam voltage of 20 kV. Prior to SEM imaging, an ultra-thin layer of gold was coated using JEOL Fine coat Ion Sputter FC-1100 (operating at 1 kV and 10 mA for 3-5 minutes) to enhance the conductivity of the samples. Field emission scanning electron microscope (FESEM), ULTRA 55 (Carl Zeiss SMT) has been used to identify the morphology and size distribution of some of the colloidal samples prepared in Chapter 6. FEI TECNAI G2 S-TWIN transmission electron microscope (TEM) was used for high resolution imaging at an accelerating voltage of 200 kV. The fluorescent nanostructures were characterized by using Leica TCS SP2 AOBS DM6000 B upright laser scanning confocal microscope (λ_{ex}= 250-350 nm). The powder X-ray patterns of various nanostructures were measured by using Philips PW1830 Bragg-Brentano diffractometer with Cu Kα (1.5405 Å) and Cu Kα2 (1.5443 Å) radiation. Working principle and details of the some of the instrumental setups used in the present study are described in the following sections.

2.5.1. Picosecond time-correlated single-photon counting setup

Time-resolved fluorescence measurements were carried out using a time-correlated single-photon counting (TCSPC) spectrometer (5000, IBH)[8], the block diagram of which is shown in Scheme 2.2. Diode lasers or nanoLED were used as excitation sources and a micro-channel plate (MCP) photomultiplier tube was used as the detector. Depending on

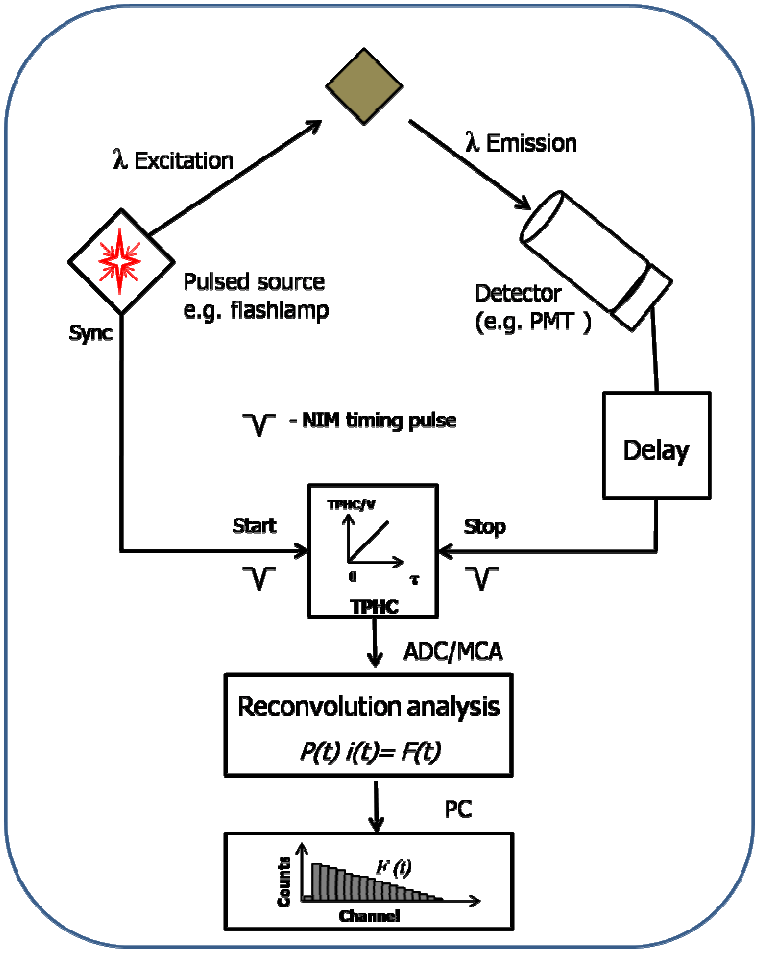

Scheme 2.2. Schematic block diagram for a TCSPC setup (Source: DataStation Hub User Manual, IBH).

the system involved, two different excitation sources, nanoLED (331 nm, FWHM = 1 ns) and diode laser (374 nm, FWHM = 65 ps) were employed. The maximum repetition rate of the diode lasers was 1 MHz. A Hamamatsu R3809U-50 MCP-PMT (160-850 nm range) was used as a detector.

The lamp profile was recorded by placing a scatterer (dilute solution of Ludox in water) in place of the sample. Decay curves were analyzed by nonlinear least-squares iteration procedure using IBH DAS6 (Version 2.2) decay analysis software.

2.5.2. Fluorescence lifetime imaging microscope

Fluorescence lifetime imaging microscope (FLIM) studies have been carried out using MicroTime 200, PicoQuant, typical block diagram of which is shown in Scheme 2.3 & 2.4. MicroTime 200 equipped with an XYZ piezoelectric scanning stage (P-733-2CL, Physik Instrumente), which was controlled by a dedicated software (SymPhoTime 5.1.3.1, PicoQuant). The output of a 405 nm pulsed picosecond laser diode (40 MHz; FWHM =175 ps) was coupled into the main optical unit using a polarization maintaining single mode optical fiber, guided through a 405 nm dichroic mirror (DM) and then the collimated laser beam was directed into the entrance port of an inverted microscope (IX 71, Olympus). The sample was mounted on specially made holders and the directed laser beam was focused onto the sample using 60X, NA= 1.2, water-immersion objective. Fluorescence was collected by the same objective and dichroic mirror, passed through 430 nm long pass filter and then the signal was spatially filtered by focusing onto a 50 μm diameter pinhole (PH) to cut the out-of-focus signals, re-collimated, and directed onto an avalanche photodiode (2MPD SPAD, dark count rate < 250 counts/sec ; Perkin-Elmer Inc.). The data acquisition was performed with PicoHarp 300 TCSPC module using software (PicoHarp300 version 2.3) in a Time-Tagged Time-Resolved (TTTR) mode, which stores all relevant information for each detected photon for further data analysis. All the images were scanned with highest possible resolution (512×512 pixel). The fluorescence lifetime images were constructed using the software. All the photons corresponding to one pixel were plotted into a histogram then fitted to an exponential

decay function for the exact lifetime information. This procedure is repeated for all the pixels in the image.

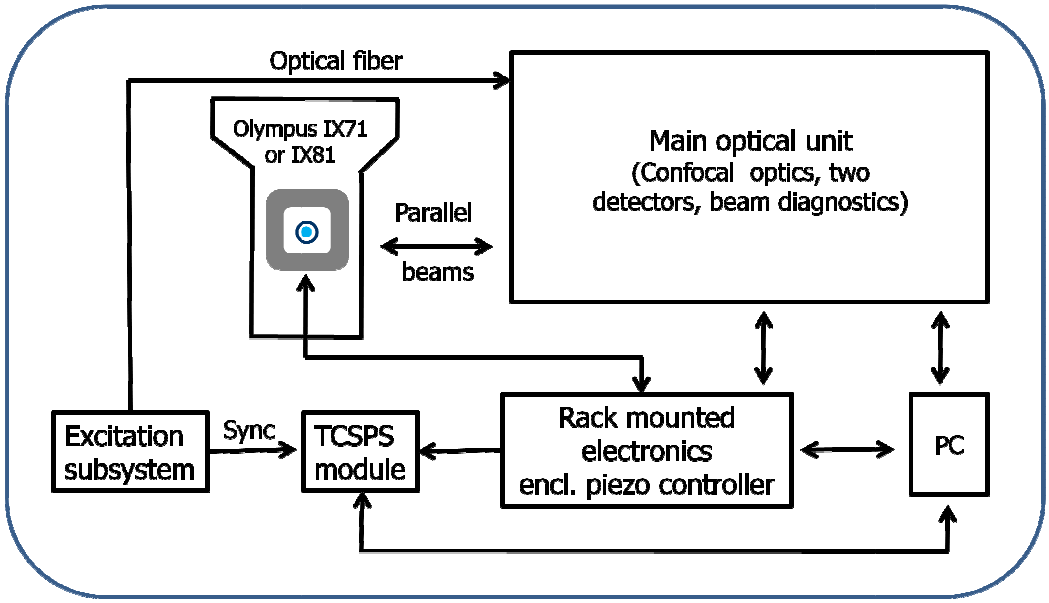

Scheme 2.3. Schematic block diagram for a MicroTime 200 setup (Source: PicoQuant User Manual).

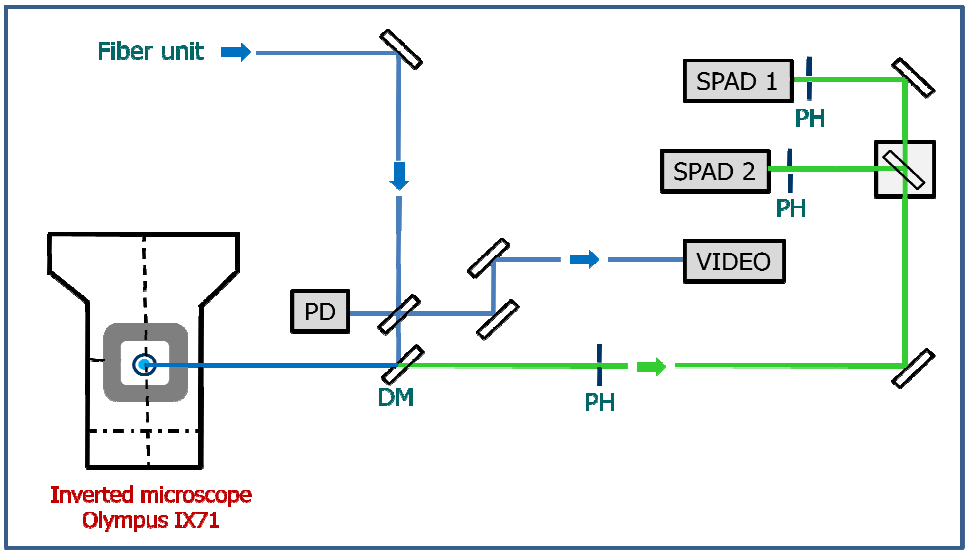

Scheme 2.4. Schematic block diagram for main optical unit of MicroTime 200 (Source: PicoQuant User Manual).

2.5.3. Atomic force microscope

Scanning probe microscopes (SPM) are defined as a broad group of instruments used to measure the surface properties of chemical and biological materials. Scanning tunneling microscopy (STM) and atomic force microscopy (AFM) are the two major classes of SPMs. Unlike STM, AFM enables the investigation of nonconductive material surfaces as well. For the present study, SolverPro-M (NT-MDT) atomic force microscope (AFM) has been employed to characterize nano/microparticles. SolverPro-M consisted of a cantilever having a sharp tip (probe, made from doped single crystal silicon, tip curvature radius is 6-10 nm) which was used to scan the specimen surface (Scheme 2.5). These were supported by a gold coated chip (3.4×1.6×0.3 mm) and the force constant of the cantilevers were in between 5.5-22.5 N/m. When the tip is brought (mechanically) close to the sample surface, forces between tip and surface such as mechanical contact forces, capillary forces, chemical bonding, electrostatic forces and Van der Waals forces

lead to the deflection of the cantilever according to Hooks-law. A laser beam (650 nm, <1 mW) focused at the rare side of the cantilever–tip was used to detect the cantilever deflections. Then the reflected laser beam from cantilever was detected by a series of photodiodes, position sensitive detector (PSD). Feedback mechanism was employed to maintain the constant force between tip and surface of the specimen. This was achieved by mounting the specimen on a piezoelectric tube which moves the specimen along z-direction for maintaining the constant force thorough out the measurement. All the measurements were performed using 10 µm bottom scanner (Z10162Y), which allowed to scan ~15×15 µm area on the sample in semicontact mode (tapping mode). The scanning was controlled by a dedicated software (Nova 1.26.0.1443).

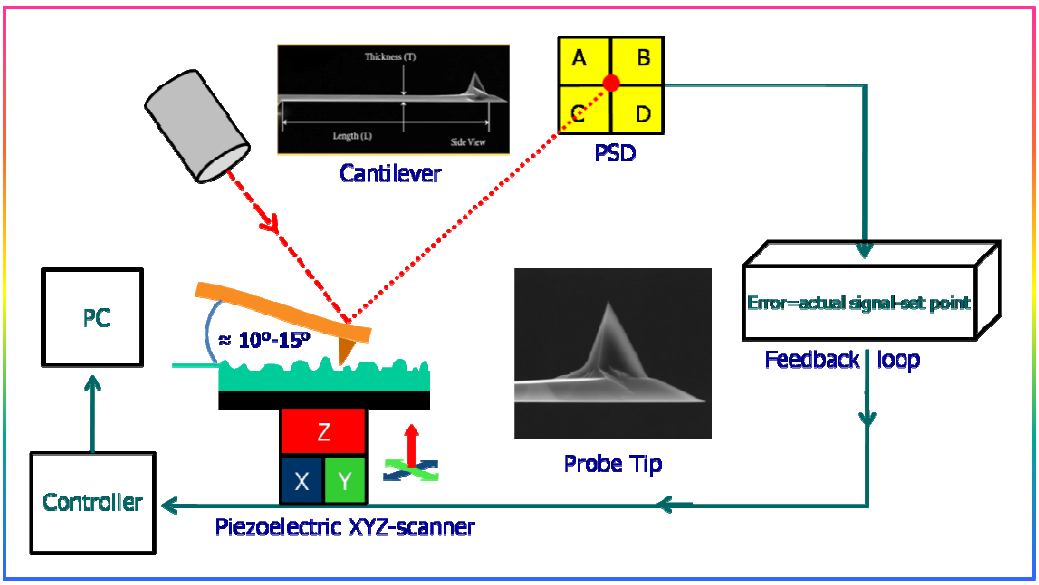

Scheme 2.5. Schematic block diagram for AFM SolverPro-M (Source: NTMDT User Manual).

2.6. Sample preparation

2.6.1. Spectral measurements

For measurements in conventional solvents, the solutions were prepared such that the absorbance of the solution (1 cm path length) at the excitation wavelength was around 0.05 - 0.1. The concentration of the probe molecules corresponding to an absorbance value of 0.2 was found to be in the range of 10^{-6} - 10^{-4} M. Nanoparticle absorbance values were maintained in between 0.1 - 0.3 at the excitation wavelength.

2.6.2. Microscopy analysis

The SEM, AFM and fluorescence microscopy samples were prepared by placing one or two drops of the colloidal solution onto a clean glass plate and subsequent evaporation of the solvent under vacuum. If necessary, the dried samples were washed with highly pure water to remove the residuals of additives and the samples were again dried under vacuum. When additives were used in the nanoparticles fabrication (Chapter 4), the samples were washed with milli-Q water to obtain the nano/microparticles. For TEM measurements, the colloidal solutions were casted on a carbon coated-copper grid and the dried samples were analyzed. For FLIM measurements, one or two drops of dilute colloidal samples were placed onto a cleaned cover slip (2×2 cm) and the solvent was dried fully under high vacuum.

2.7. Measurement of fluorescence quantum yield

For fluorescence quantum yield measurements, optically matched solutions (or solutions with very similar absorbances) of the sample and the standard at the excitation wavelength were prepared. The quantum yield was calculated by measuring the integrated area under the emission curves and by using the following equation,[9]

$$\Phi_{sample} = \frac{A_{sample} \times OD_{std} \times n^2_{sample}}{A_{std} \times OD_{sample} \times n^2_{std}} \times \Phi_{std} \quad (2.1)$$

where, Φ is the quantum yield, A is the integrated area of emission, OD is the optical density at the excitation wavelength, and n is the refractive index. The subscripts 'sample' and 'std' refer to the fluorophore of unknown quantum yield and the reference fluorophore of known quantum yield, respectively.

2.8. Data analysis of fluorescence lifetime

A brief outline of analysis of the fluorescence lifetimes is discussed.

The lifetimes of the samples were estimated from the measurements of fluorescence decay curves and the instrumental profiles using a nonlinear least-squares iterative fitting procedure (using decay analysis software IBH DAS6, Version 2.2). This program uses a reconvolution method for the analysis of experimental data.[10] When the decay time is long compared to the pulse width of the excitation pulse, the excitation may be described as a δ-function. However, when lifetime is short, distortion of the experimental data occurs by the finite decay time of the lamp pulse and response time of the photomultiplier and associated electronics. Since the measured decay function is convolution of the true fluorescence decay and the instrumental pulse, it is necessary to analyze the data by deconvolution in order to get the actual fluorescence lifetime. The mathematical statement of the problem is given by the following equation:

$$D(t) = \int_0^t P(t')G(t-t')dt' \quad (2.4)$$

where, D(t) is the fluorescence intensity at any given time t, P(t') is the intensity of the exciting light at time t' and G(t–t') is the response function of the experimental system. The experimental data D(t) and P(t') from the MCA were fed into a personal computer (PC) to determine the lifetime. We used the IBH program to analyze the multi-

exponential decays. An excitation pulse profile was recorded and then deconvolution started with mixing of the excitation pulse and a projected decay to form a new reconvoluted set. The data was compared with the experimental set and the difference between the data points was summed, generating χ^2 function for fitting. The deconvolution proceeded through a series of such iterations until an insignificant change of χ^2 occurred between iterations. The inspection of reduced χ^2, a plot of weighted residuals and autocorrelation function of the residuals allowed assessment of the quality of the fit.

2.9. Theoretical calculations

2.9.1. Semi-empirical calculations

Polarizability (α) and first order nonlinear hyperpolarizability (β) of ADMA were computed using Accelrys Materials Studio 4.3 software. The ground state dipole moments of the systems were obtained from the semi-empirical AM1 (Austin Model 1) method[11,12] using Gaussian 03 program package[13]. The geometries obtained from the single crystal X-ray studies were taken as input for the semiempirical calculations.

2.9.2. Density functional theory calculations

Single point energies and ground state dipole moments of the systems that are studied in the present work and their molecular motifs were also computed by density functional theory (DFT),[14-16] which is a more improved method of calculations than the Hartree-Fock theory in the sense that it includes terms for both exchange energy and the electron correlation. Instead of a pure DFT method, a hybrid method in which the exchange functional is a linear combination of the Hartree-Fock exchange and a functional integral was employed in the calculations. The energies of the various systems were determined using the hybrid DFT functional B3LYP[17,18] at the B3LYP/6-31G* or 6-31+G* level.

For all the calculations (single point energy), the geometries of the molecule and the motifs were obtained from the single crystal X-ray study and used as an input. Mercury (2.4 version, free version is available at CCDC website) software was used for the computation of energies of the motifs identification of intermolecular interactions and measuring the distances between the atoms of neighboring molecules.

The binding energy was calculated from the computed energies of the motifs (E_{motif}) and the molecule ($E_{molecule}$) using

$$E_S = [E_{motif} - N\ E_{molecule}]/\ N$$

Where, N represents the total number of molecules in a motif.
All the DFT calculations were performed using the Gaussian 03 program package.[13]

2.10. Single crystal X-ray crystallography

Single crystals of the compounds, suitable for X-ray diffraction studies, were grown from the slow evaporation of their dilute solutions. The raw data were collected on Bruker CCD and Xcalibur, Eos, Gemini X-ray diffractometers. The details of the collection and reduction of data for various compounds are as follows:

Collection and reduction of X-ray data from CCD difractometer: A tiny single crystal was mounted on the tip of glass fiber and transferred to a Bruker CCD X-ray diffraction system, which was equipped with a graphite-monochromatized Mo Kα radiation (λ = 0.71073 Å) source controlled by a Pentium-based PC running the SMART software package.[19] Data were collected at room temperature or at 100 K and the raw data frames were integrated by the SAINTPLUS program package.[20] Empirical absorption corrections were applied with the SADABS program[21] and the space group was determined by examining systematic absences and confirmed by the successful solution and refinement

of the structure.The structures were solved by direct methods and refined by full matrix least-squares and difference Fourier techniques with SHELXTL program package.[22] All non-hydrogen atoms were refined anisotropically. Relevant crystallographic parameters and thermal ellipsoid plots for various compounds are presented in the respective chapters.

Collection and reduction of X-ray data from Xcalibur, EOS, Gemini difractometer: Crystal structure of BCPA was collected on CrysAlisPro (Oxford Diffraction Ltd., Oxford, UK) version 1.171.33.55 with SCALE3 ABSPACK absorption correction, Xcalibur, EOS, Gemini measurement device, and Mo Kα (λ = 0.71073 Å) radiation. The crystal structure was solved by direct methods using SHELXS-9726 (University of Gottingen, Germany) and refined by full-matrix least-squares refinement on F^2 with anisotropic displacement parameters for non-hydrogen atoms using SHELXL-97.[23] Non-hydrogen atoms were refined anisotropically. After the final refinement, structure analysis and preparation of art works were carried out using MERCURY28 (Cambridge Crystallographic Date Centre, Cambridge, UK) and ORTEP-329 (Oakridge National laboratory, Oakridge, Tennessee, USA) softwares.

2.11. Standard error limits

Standard error limits involved in the measurements are:

λ_{max} (abs./fluo.)	± 1 nm
Φ_f	± 10%
τ_f (> 1 ns)	± 5%
τ_f (< 1 ns)	± 5-8% (depending on the excitation source used)

References

(1) Nonhebel, D. C. *J. Chem. Soc.* **1963**, 1216.
(2) Paul, A. *Ph.D. Thesis* **2008**, *University of Hyderabad*.
(3) Perrin, D. D.; Armerego, W. L. F.; Perrin, D. R. *In Purification of Laboratory Chemicals*; Pergamon Press: New York, 1980.
(4) Magita, M.; Okada, T.; Mataga, N.; Sakata, Y.; Misumi, S.; Nakashima, N.; Yashihara, K. *Bull. Chem. Soc. Jpn.* **1981**, *54*, 3304.
(5) Samanta, A.; Saha, S.; Fessenden, R. W. *J. Phys. Chem. A* **2001**, *105*, 5438.
(6) Kotha, S.; Ghosh, A. K.; Deodhar, K. D. *Synthesis* **2004**, *4*, 0549.
(7) Kasai, H.; Nalwa, H. S.; Oikawa, H.; Okada, S.; Matsuda, H.; Minami, N.; Kakuta, A.; Ono, K.; Mukoh, A.; Nakanishi, H. *Jpn. J. Appl. Phys.* **1992**, *31*, L1132.
(8) O'Connor, D. V.; Philips, D. *In Time-Correlated Single Photon Counting*; Academic Press: New York, 1984.
(9) Austin, E.; Gouterman, M. *Bioinorg. Chem.* **1978**, *9*, 281.
(10) Bevington, P. R. *In Data Reduction and Analysis for the Physical Sciences*; McGraw-Hill: New York, 1969.
(11) Dewar, M. J. S.; Dieter, K. M. *J. Am. Chem. Soc.* **1986**, *108*, 8075.
(12) Dewar, M. J. S.; Zoebisch, E. G.; Healy, E. F.; Stewart, J. J. P. *J. Am. Chem. Soc.* **1985**, *107*, 3902.
(13) Frisch, M. J. T., G. W.; Schlegel, H. B.; Scuseria, G. E.; Robb, M. A.; Cheeseman, J. R.; Zakrzewski, V. G.; Montgomery, J. A. Jr.; Stratmann, R. E.; Burant, J. C.; Dapprich, S.; Millam, J. M.; Daniels, A.D.; Kudin, K. N.; Strain, M. C.; Farkas, O.; Tomasi, J.; Barone, V.; Cossi, M.; Cammi, R.; Mennucci, B.; Pomelli, C.; Adamo, C.; Clifford, S.; Ochterski, J.; Petersson, G. A.; Ayala, P. Y.; Cui, Q.; Morokuma, K.; Malick, D. K.; Rabuck, A. D.; Raghavachari, K.; Foresman, J. B.; Cioslowski, J.; Ortiz, J. V.; Stefanov, B. B.; Liu, G.; Liashenko, A.; Piskorz, P.; Komaromi, I.; Gomperts, R.; Martin, R. L.; Fox, D. J.; Keith, T.; Al-Laham, M. A.; Peng, C. Y.; Nanayakkara, A.; Gonzalez, C.; Challacombe, M.; Gill, P. M. W.; Johnson, B.; Chen, W.; Wong, M. W.; Andres, J. L.; Gonzalez, C.; Head-Gordon, M.; Replogle, E. S.; Pople, J. A. *Gaussian 98*; Gaussian,Inc.: Pittsburgh, PA, 1998.
(14) Hohenberg, P.; Kohn, W. *Phys. Rev.* **1964**, *B864*, 136.
(15) Kohn, W.; Sham, L. J. *Phys. Rev.* **1965**, *A1133*, 140.
(16) Parr, R. G.; Yang, W. *In Density Functional Theory of Atoms and Molecules*; Oxford Univ. Press: Oxford, 1989.
(17) Becke, D. A. *J. Chem. Phys.* **1993**, *98*, 5648.
(18) Lee, C.; Yang, W.; Parr, R. G. *Phys. Rev. B* **1988**, *37*, 785.
(19) *SAINTPLUS, 6.45 Ed.*; Bruker AXS, Inc: Madison, WI, 2003.
(20) *SADABSRT, 5.629 Ed.*; Bruker AXS, Inc.: Madison, WI, 2003.
(21) *SAI, 2.10 Ed.*; Bruker AXS, Inc.: Madison, WI, 2003.
(22) *SHELXTL, 6.14 Ed.*; Bruker AXS, Inc.: Madison, WI, 2003.
(23) GM., S. *SHELXL-97: Program for crystal structure analysis*; University of Gottingen: Gottingen, Germany, 1997.

Chapter 3

Probing the Aggregated State of 4-(9-Anthryl)-N,N-Dimethylaniline by UV-vis Absorption and Fluorescence Spectroscopy, Microscopy and Crystallography

The aggregated state of electron donor-acceptor molecule, 4-(9-anthryl)-N,N-dimethylaniline (ADMA) has been studied by electronic absorption and fluorescence spectroscopy, microscopy and crystallography. Self-assembled aggregates have been prepared by reprecipitation method under various conditions without using any stabilizing agent and characterized by different microscopic techniques. These studies reveal spherical and plate-like morphologies and both amorphous and crystalline nature of the aggregates, whose sizes vary between 250 and 600 nm. The optical properties of these well-characterized aggregates have been studied and compared with those in molecular form. Intermolecular interaction in the aggregates induces remarkable change in the absorption and fluorescence properties of this dipolar system and the formation of stable aggregates can be conveniently followed by monitoring the spectral response of the system as a function of time. Intramolecular charge transfer process, which dominates the photophysical behavior of this molecular system, could not be observed in the solid or aggregated state. The nature of the intermolecular interactions responsible for the formation and stabilization of the aggregates has been identified from the spectral and crystal structure data of the system. The results highlight the scope of broadening the spectral response of the present system by exploiting the advantageous optical properties of the aggregated state of the molecule.

3.1. Introduction

Because of their unique properties, arising from the quantum-size effects,[1,2] the semiconductor or metal-based fluorescent inorganic nanoparticles serve as promising candidates for potential applications as fluorescent biological labels,[3,4] photovoltaic cells,[5] light emitting diodes[6] and optical sensors[7,8] and have received significant attention in recent years.[9-13] However, as stated earlier much less attention has so far been paid for the development of well characterized fluorescent organic nanoparticles. Strictly speaking, detailed studies on the fluorescent organic nanoparticles are still at their initial

stages despite the fact that the aggregates of fluorescent organic molecules play important roles in photography as sensitizers,[14-17] in mode-locking and Q-switching applications[18,19] and in exhibiting nonlinear properties.[20,21]

Among the recent studies on organic nanoparticles, the following are noteworthy. Park et. al synthesized a class of organic nanoparticles with mean diameter 30-40 nm, which exhibit enhanced fluorescence and later developed a method for the fabrication of photopatterned assemblies of fluorescent organic nanoparticles on the surfaces of solid substrates.[22,23] Luminescent 3-aminopropylmethyl (tetraphenyl)silole nanoparticles as a chemoselective sensor for Cr(VI) was reported.[24] Patra et. al synthesized a novel zwitterionic diaminodicyanoquinodimethane molecule and studied the intermolecular interactions involved in the formation of its nanoparticles.[25] Aggregation-induced enhancement of emission of various organic systems has been studied by several groups.[26-29] It is shown that site isolation and restriction of internal rotation can effectively suppress self quenching and the nonradiative process, and hence, give rise to large enhancement of the luminescent intensity in the aggregated or solid state.[30-36] In the case of electron donor-acceptor (EDA) molecules, wherein the donor and acceptor moieties are connected through π-conjugation, it is shown that some of them can form 1-D nanostructures like nanoribbons, nanotubes, and nanowires.[37-39] Fabrication of various 1-D crystalline nanostructures such as nanorods, nanotubes and nanoribbons has been reported in the case of other organic systems as well.[40-43]

Since the aggregates of organic molecules most often exhibit properties different from those in their molecular form, one can profitably exploit some of these properties in practical applications. However, since a large majority of the earlier studies were not backed by a parallel investigation of the structural characterization of the aggregates, presumably due to the nonavailability of high resolution microscopic techniques in early years, it is not known how/whether the properties of the aggregated state can be

controlled or tuned by modifying the nature of the aggregation. As the optical properties of the aggregates are expected to be intimately linked to the nature of aggregation, and hence, the morphology, one can address this issue only by combined microscopic and optical studies.

In this context, we have studied a highly fluorescent EDA molecule, 4-(9-anthryl)-N,N-dimethylaniline (ADMA) by covalently attaching the N,N-dimethylaniline donor to the anthracene acceptor. Ever since Mataga's group reported solvent-dependent photophysics of ADMA in the early seventies,[44] several groups have explored the photophysical properties of the molecule in solution in the context of exciplex photophysics, formation of twisted intramolecular charge-transfer (TICT) state, and solvent-induced electron-transfer reactions.[45-47] ADMA is a strongly twisted molecule in the ground state having a dipole moment around 5 D.[48] The dihedral angle between the two ring systems is estimated between 65 and 84° depending on the method.[46,47] No crystal structure data for ADMA is so far available. The absorption spectrum of ADMA is characterized by features suggestive of interaction between the anthracene and dimethylaniline moieties.[44] As far as the emission behavior is concerned, it is commonly accepted that ADMA exhibits a structured fluorescence in nonpolar solvents.[49] However, with increasing polarity of the solvent, the structure in the emission spectrum gradually disappears and the broad emission envelope shifts toward longer wavelength. The dipole moment of the locally excited (LE) and intramolecular charge transfer (ICT) states of the molecule are reported to be ca. 12.5 and 20.5 D, respectively.[50] In this paper, we report for the first time the photophysical behavior of ADMA in well-characterized mesoscopic regime.

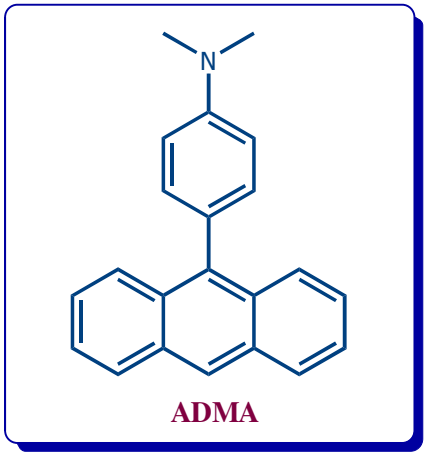

Chart 3.1. Molecular structure of 4-(9-anthryl)-N,N-dimethylaniline

3.2. Colloid Preparation and Microscopy

The self-assembled aggregates of ADMA have been prepared taking advantage of its poor solubility in aqueous solution. As described in the *chapter 2.3.*, injection of DMSO solution (100 μL, 2.7 mM) of ADMA into water (10 mL) under ultra-sonication results in the formation of colloidal aggregates, which is evident from the turbidity of the solution. Except for the first hour, during which aggregation process is completed, the colloids were found stable for several weeks without addition of any surfactant, capping agent, or stabilizing agent. Atomic force microscopy (AFM) measurements reveal particles of spherical and plate-like morphologies (Fig. 3.1). Scanning electron microscope (SEM) experiments reveal that these particles are having fine edges (Fig. 3.1), which is confirmed by TEM (Fig. 3.1) measurements. We investigated the sample for crystallinity and the selected area electron diffraction (SAED) pattern showed that these particles are indeed crystalline. The diameters of the spherical particles were found to vary from 250 to 600 nm.

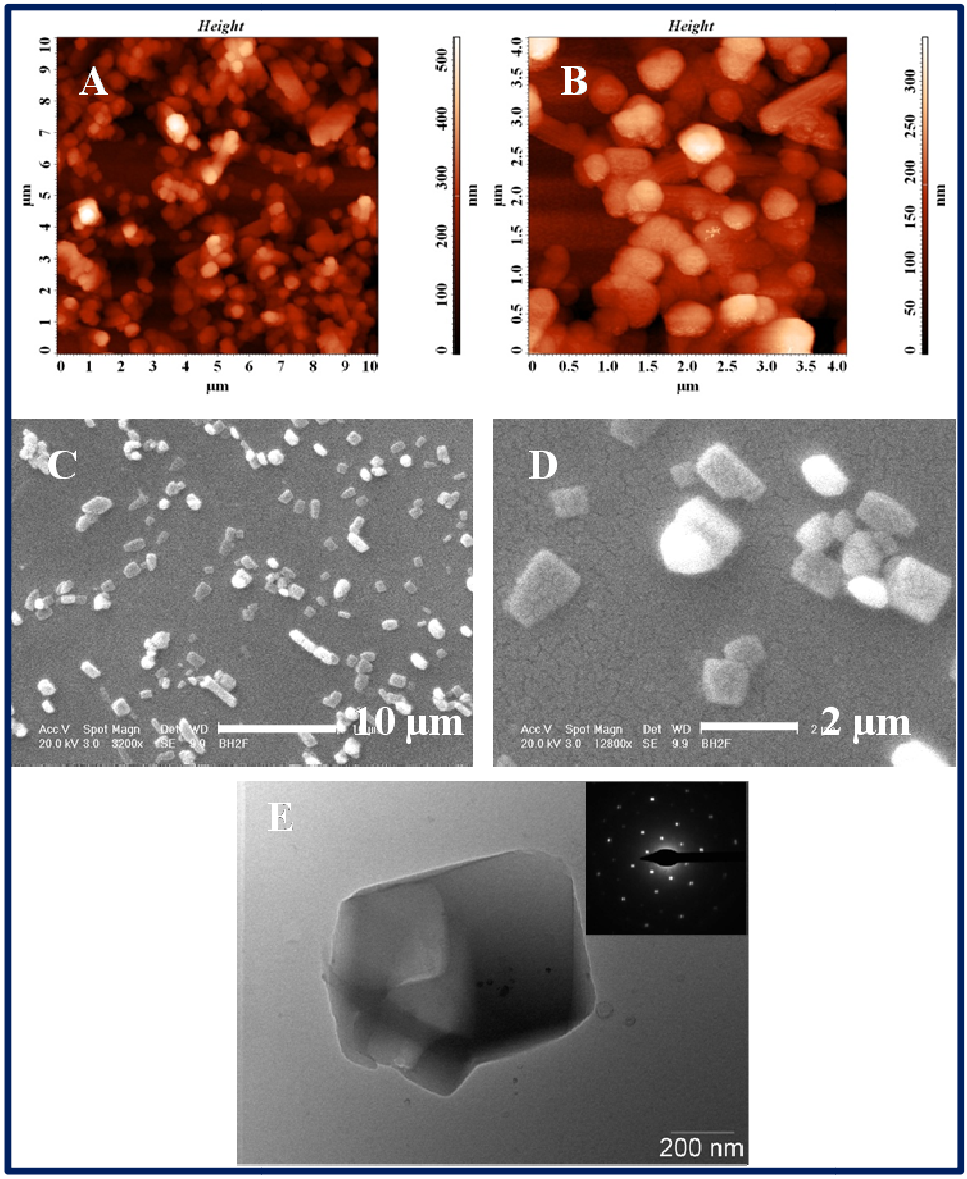

Fig. 3.1. AFM (A & B), SEM (C & D) and TEM (E) images of 100 µL ADMA colloids prepared in 10 mL of water. Inset in the TEM image shows selected area electron diffraction (SAED) pattern.

The aggregation of ADMA was investigated in a few other conditions as well. When the water to which the stock solution of ADMA was injected was stirred instead of being sonicated keeping other conditions identical, the nature of the formed particles remained similar with a wider size distribution (Fig. 3.2). The relative percentage of the plate-like crystalline particles was found to be higher in the case of stirring. However, when the same amount of stock solution was injected to a larger volume (25 mL) of water the particles became smaller (Fig. 3.3). In order to find out the effect of temperature, the same colloid was digested at 90 °C for 3 h. With the dige stion temperature, the size of particles increased slightly but the morphology was hardly affected (Fig. 3.3). On the other hand, when a larger amount of the stock solution (200 μL) was rapidly injected into the (i) same amount of water (10 mL), the particle size increased (Fig. 3.4) (ii) a larger volume (25 mL) of water two morphologies; hexagonal plates and irregular shaped particles (Fig. 3.5) were observed.

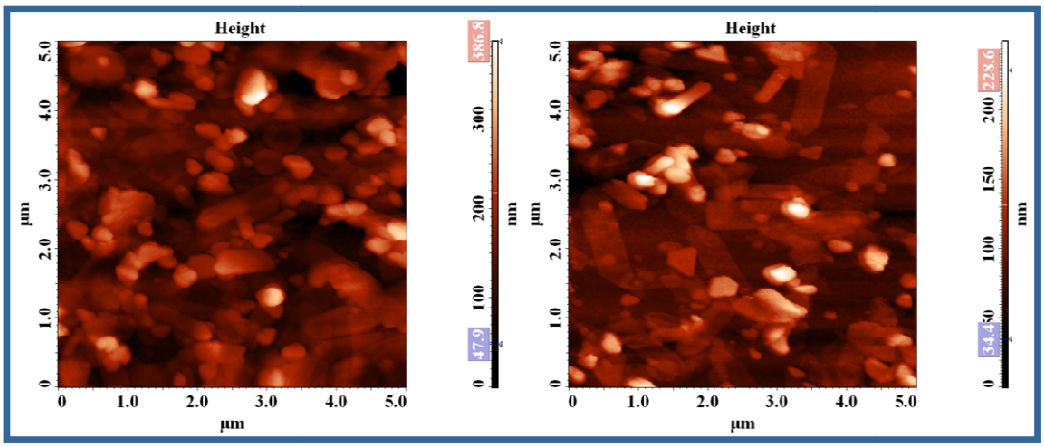

Fig. 3.2. AFM images (at two different locations) of colloids prepared by injecting 100 µL DMSO solution of ADMA (2.7 mM) into 10 mL water under vigorous *stirring*.

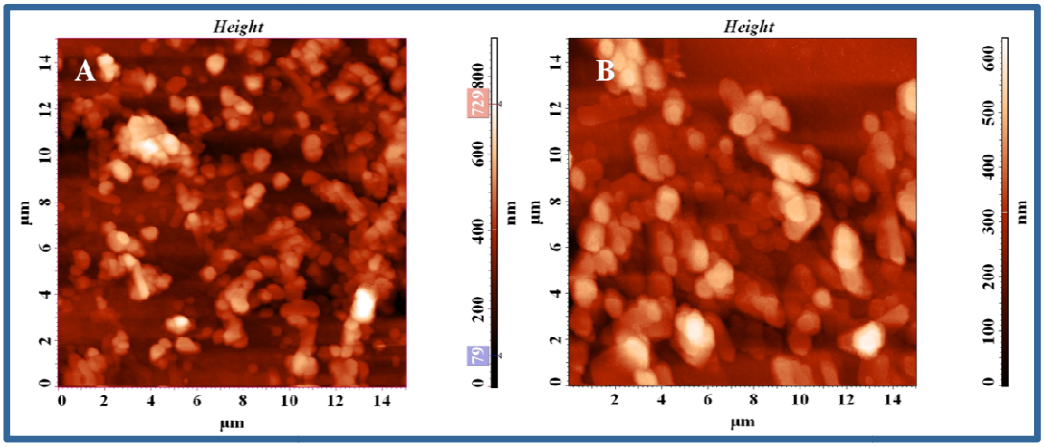

Fig. 3.3. AFM images of colloids prepared at room temperature by injecting 100 µL DMSO solution of ADMA (2.7 mM) into 25 mL water under ultra-sonication (A) and digested at 90 °C (B).

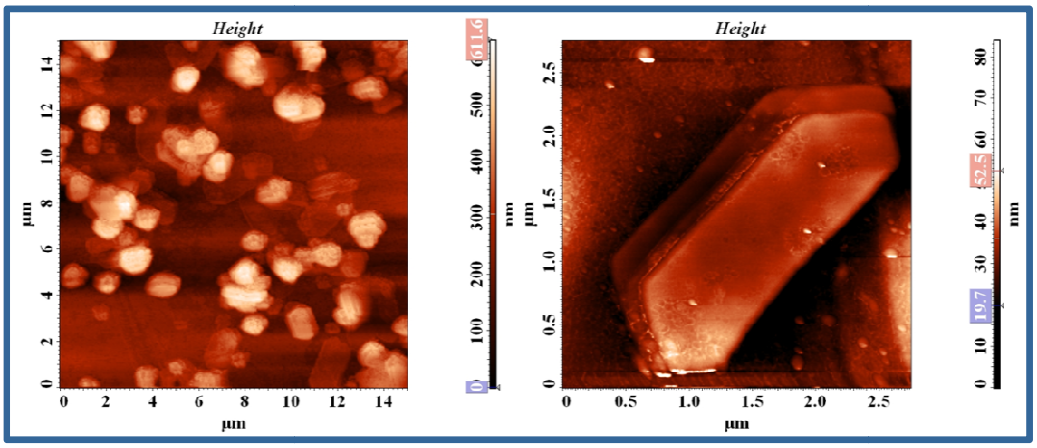

Fig. 3.4. AFM images (low and high magnification) of the colloids prepared by injecting 200 µL DMSO solution of ADMA (2.7 mM) into 10 mL water under ultra-sonication.

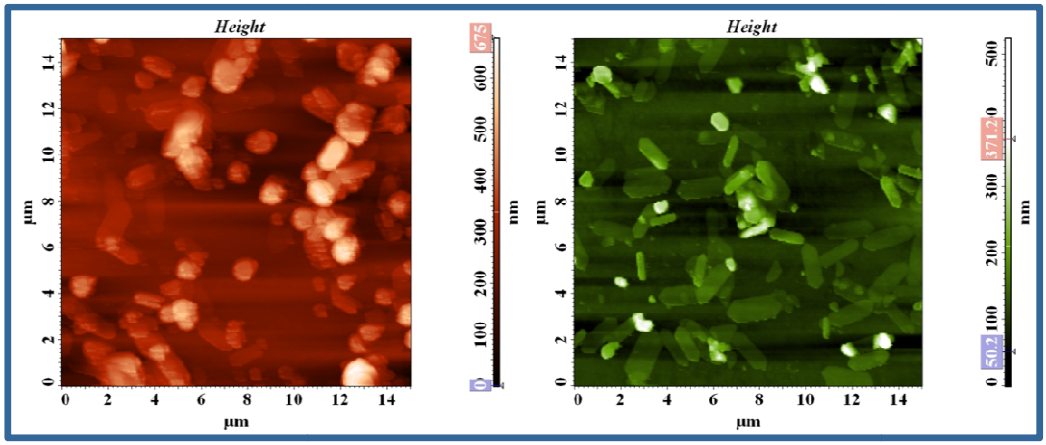

Fig. 3.5. AFM images of colloids at two different locations prepared by injecting 200 µL DMSO solution of ADMA (2.7 mM) into 25 mL water under ultra-sonication.

3.3. Steady state absorption and fluorescence behavior

3.3.1. Absorption

While the absorption spectrum of ADMA (Fig. 3.6) combines the spectral features of the constituent anthryl and *N*,*N*-dimethylanilino moieties, the presence of additional features, which cannot be attributed to these constituents, indicates interaction between the two moieties. For example, the short-wavelength region of the electronic spectrum of ADMA in cyclohexane resembles the vibronic structure of anthracene. However, in moderately polar or highly polar solvents (such as in tetrahydrofuran and dimethyl sulfoxide), one can observe considerable enhancement of absorbance in the long-wavelength region. These spectral features of ADMA are consistent with the literature.[44] The structureless broad absorption in the 400-450 nm region is attributable to the transition to an intramolecular charge transfer (ICT) state arising from the interaction between the constituent moieties. The ICT nature of the transition is evident from the bathochromic shift of the broadband with increase in solvent polarity, as depicted in Fig.

3.6. Figure 3.7 compares the absorption characteristics of homogeneous solutions of ADMA with those in the colloidal and solid (as thin-film) states. The absorption spectra of the thin film and colloidal solution of ADMA are distinctly different from those in the homogeneous solutions. A significant enhancement of the absorption intensity in the long-wavelength region (400-550 nm) with the absorption tail extending to *ca.* 600 nm is clearly a manifestation of the influence of strong intermolecular interactions on the energetics of the system in the aggregated state.[25,33] While pronounced effect of the intermolecular interactions of this kind is uncommon in most molecular systems such as naphthalene or anthracene, considering the dipolar nature of the present system the prominent effect observed in this case can be attributed primarily to the dipole-dipole interaction. The crystal structure data of the molecule (vide infra) not only confirms the

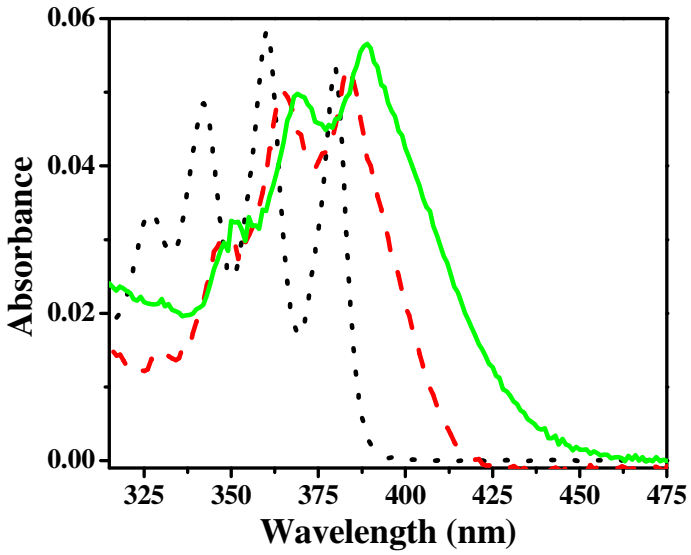

Fig. 3.6. Absorption profile of ADMA in dimethyl sulfoxide (–), tetrahydrofuran (---), and anthracene in cyclohexane (···).

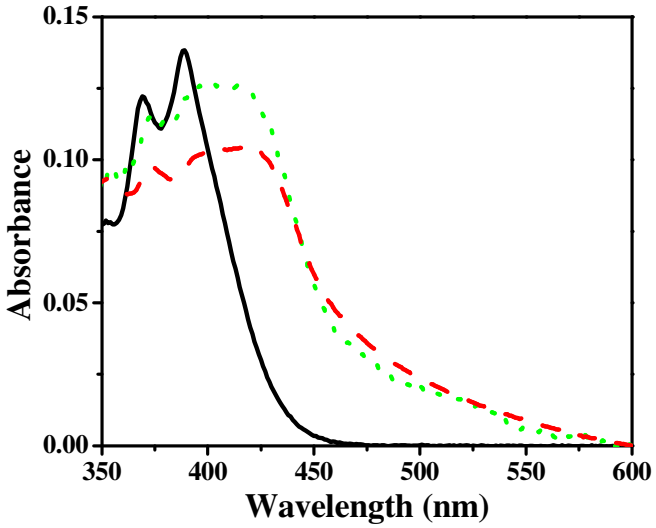

Fig. 3.7. Absorption spectra of ADMA in dimethyl sulfoxide solution (–), solid state (····) and colloidal state (---).

involvement of this nature of the intermolecular interaction, but in addition, it points to the involvement of weak van der Waals interaction in the formation of the bulk materials. Very little difference in the absorption spectral behavior of the colloidal aggregates and thin films could be observed. Additional insight into the nature of intermolecular interaction can be obtained from further analysis of the spectral features. While the broad absorption with long tail is due to the formation of the aggregates,[33] the progressive rise of the baseline with decrease of wavelength is due to Mie scattering effect.[51,52] We have monitored the aggregation process by measuring the absorption of the colloid solution at different time intervals, allowing it to age with time for about 1 h (Fig. 3.8). The interesting feature is the increased absorbance in the longer wavelength region with a peak around 425-430 nm region. As the absorption band arising out of the intermolecular interaction is red-shifted with respect to that of the unassociated molecule, the

intermolecular interaction involved in the formation of colloidal aggregates or bulk material is best ascribed in terms of J-type (parallel end-to-end stacking of dipoles) aggregation.[53] Usually, the absorption bands due to the J-type aggregates are intense and narrow.[54] The broadness and less intense nature of the absorption of the ADMA nanoparticles is possibly due to some disorder in the packing of the aggregates.[55-57]

3.3.2. Fluorescence

ADMA exhibits a structured emission band in nonpolar solvent such as cyclohexane. However, the structure disappears in moderate polar solvents like THF. With further increase in polarity of the medium, the emission band shifts toward longer wavelength (Fig. 3.9). This emission behavior is consistent with the literature.[49] It is generally believed that, in highly nonpolar medium such as in cyclohexane, the emission originates from the LE state, but with increase in polarity of the medium the emitting state changes to a CT state. Interestingly, in a highly polar solvent, DMSO, in addition to the strong CT band (λ^{max} = 600 nm), a weak emission (λ^{max} = 420 nm) from the LE state is also observed, making this system dual fluorescent. A higher sensitivity of the fluorescence peak position of ADMA on the polarity of the medium compared to absorption is due to a larger dipole moment of the CT state compared to the ground state dipole moment.[50]

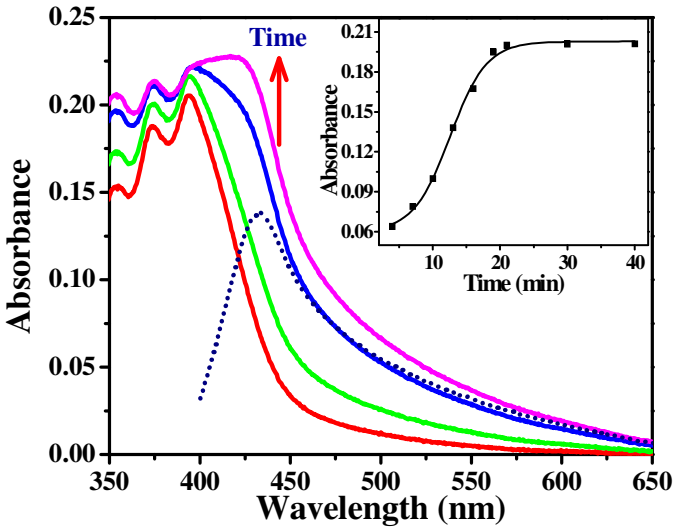

Fig. 3.8. Evolution of the absorption spectra with ageing of the ADMA aggregates at different times (4, 10, 21, and 40 min). Inset shows the variation of the optical density at 420 nm. This time dependent variation is found to be very similar at other wavelengths where an increased absorbance due to aggregation is observed.

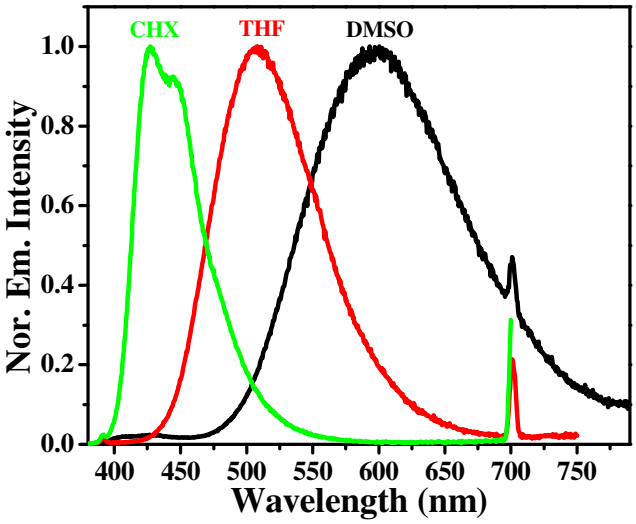

Fig. 3.9. Emission spectra (λ_{ex}= 350 nm) of ADMA in dimethylsulfoxide (DMSO), tetrahydrofuran (THF) and cyclohexane (CHX).

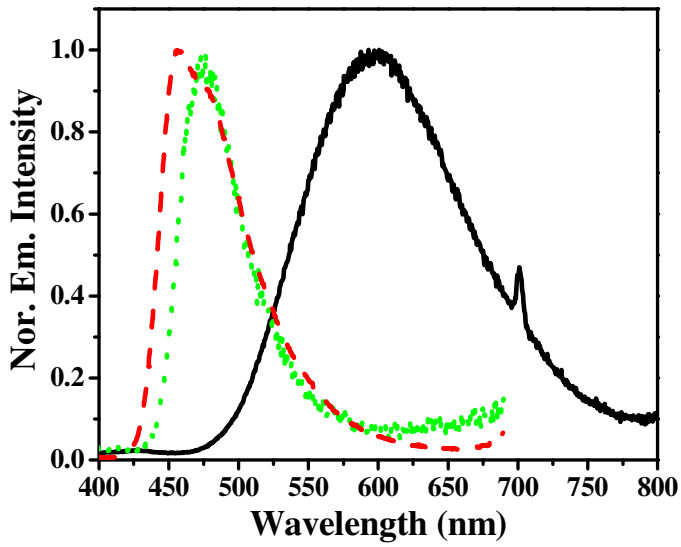

Fig. 3.10. Emission spectra (λ_{ex}= 350 nm) of ADMA in dimethyl sulfoxide solution (–), solid state (····), and colloidal state (---).

Figure 3.10 compares the spectral behavior of ADMA in the molecular state with that in the aggregated state. As can be seen, the fluorescence spectra in the aggregated and solid state look rather similar, but they differ drastically from the spectrum in DMSO. The solid ADMA shows a single emission (λ^{max} = 475 nm) which is blue-shifted when compared to solution. The stable colloidal aggregates exhibit a much narrower emission with maximum at 458 nm and a shoulder at 476 nm (Fig. 3.10). We found out that the ageing of the ADMA colloidal aggregates can be conveniently monitored by following the time-dependent changes of the fluorescence spectra (Fig. 3.11). Soon (5-7 min) after the injection of the DMSO solution of ADMA to water, the emission maximum is observed at 485 nm. However, as the time progresses the band shifts toward blue with development of structure. Huge hypsochromic shift (~140 nm) of the emission band of

the colloidal nanoparticles relative to the emission maximum in DMSO is observed. This large shift cannot be explained simply by taking into account the solvatochromic nature

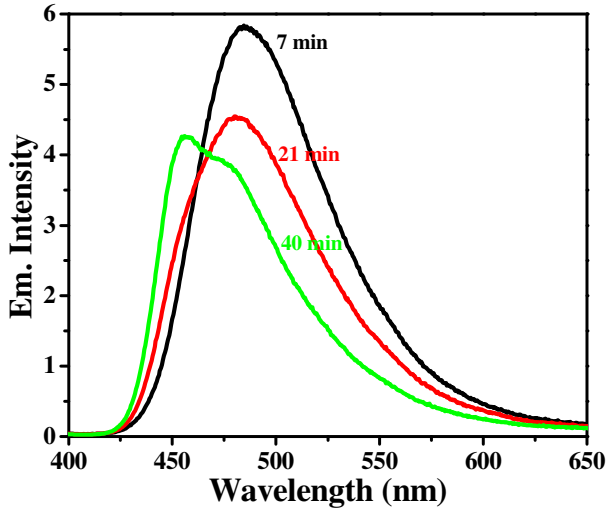

Fig. 3.11. Evolution of the emission spectra (λ_{ex}= 350 nm) with ageing of the ADMA aggregates at different times.

of the emission band. In fact, the passage of molecules from DMSO to water should have resulted in a red shift as the emitting state of ADMA is more polar than the ground state.[48,50] One can attempt to explain the spectral shift considering the structural rigidification of the molecule, as has been done in the past.[52,58,59] For example, if the two ring systems adopt a mutually perpendicular conformation in the aggregated/solid state, the charge transfer between the two rings is prevented and LE-like emission is then expected for the aggregate. Since the passage of the molecules from solution to the colloidal state removes the solvent shell from each molecule and creates a nonpolar/less polar environment, one can also expect fluorescence spectrum of the kind observed in the aggregated state when this is indeed the case. While a number of explanations of this kind

can be offered for the interpretation of the spectral data of the aggregates, the right interpretation must take into account the intermolecular interactions, which is evident from the absorption spectral data, involved in the formation of the aggregate. Strictly speaking, intermolecular interactions make the aggregate a new entity with its own energy levels. It is evident from the absorption spectral features that the lowest excited state of the aggregate is lower in energy compared to the corresponding molecular species as a result of J-type interaction. As the absorption maximum due to the aggregate appears at ~430 nm, the emission maximum is expected at wavelength higher than this. Hence, there is nothing unusual to observe the emission maximum of the aggregate at 458 nm, especially when intramolecular charge transfer in the aggregated or solid state is absent due to structural rigidity and unfavorable conformation of the two ring systems.

3.4. Fluorescence quantum yield and lifetime

Aggregation of the dye molecules often leads to a reduction in the fluorescence efficiency of the system.[60,61] However, as stated earlier, aggregation-induced emission enhancement is observed for molecular systems in which internal motion is responsible for rapid nonradiative decay of the fluorescent state.[22,26–28] For ADMA, the fluorescence quantum yields in DMSO and aggregated state have been estimated according to the procedure described in *chapter 2.7*, are 0.23 and 0.13, respectively. There can be a number of reasons for this decrease of fluorescence efficiency of the present system. A lowering of energy of the first excited state on aggregation can increase the internal conversion rate (due to a smaller S_1-S_0 energy gap) leading to a decrease of in fluorescence efficiency of the system. It is also possible that as ADMA transforms from the molecular state to the colloidal state or solid state, the nonradiative deactivation process is enhanced because of increased intermolecular interactions.[62-64] Nevertheless, ADMA is quite fluorescent in the aggregated state and is suitable for its possible

fluorescence applications in this form. The fluorescence lifetime of ADMA parallels the trend observed for the fluorescence quantum yield. The lifetime of ADMA in DMSO is estimated to be 13.9 ns (Fig. 3.12), whereas in the colloidal state the lifetime is 8.6 ns (Table 3.1). During the ageing process the average lifetime of the colloids decreases to 3.8 ns. The fluorescence of ADMA in its different states, as observed by naked eye, is illustrated in the captured photograph shown in Fig. 3.13.

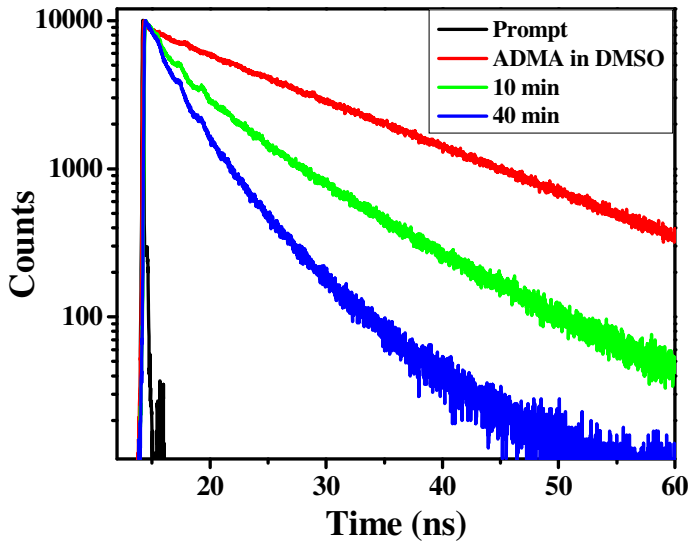

Fig. 3.12. Fluorescence decay profiles of ADMA in DMSO collected by monitoring emission at 600 nm (λ_{ex}= 374 nm) and ADMA colloids collected at different times by monitoring the emission at 485 nm (λ_{ex}= 374 nm).

Table 3.1. Fluorescence decay parameters[‡] of ADMA in DMSO and 100 µL colloid at different time intervals (λ_{ex}= 374 nm).

	τ_1	τ_2	τ_3	τ_{avg}	χ^2
DMSO[a]	0.32 (0.8)	14.08 (99.2)	-	13.9	1.21
Colloid[b]					
10min	4.84 (39.0)	10.8 (51.0)	1.3 (10.0)	8.6	1.71
40min	2.24 (56.3)	5.9 (43.7)	-	3.8	1.92

[‡]τ values are in ns. Values in parenthesis indicate relative amplitudes. Emission monitoring wavelengths (a) λ_{em}= 600 nm, (b) λ_{em}= 475nm

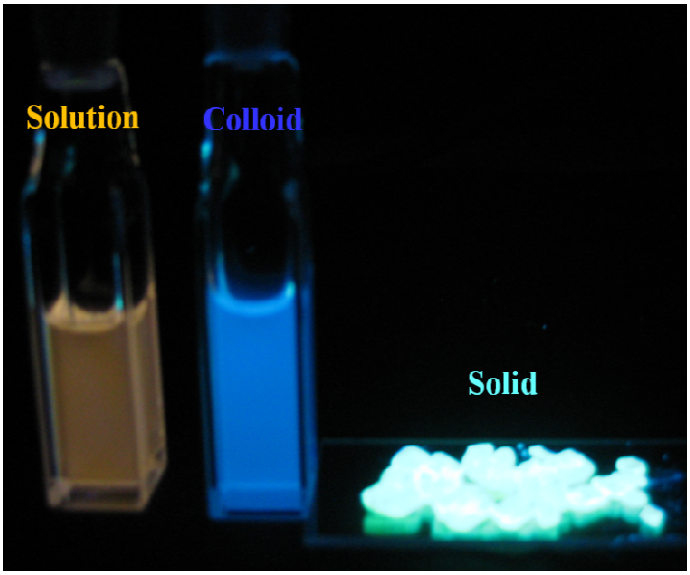

Fig. 3.13. Fluorescence of ADMA in different states; solution (in DMSO), colloidal and solid state.

3.5. Crystal structure

ADMA is fairly soluble in most of the common organic solvents. Greenish yellow crystals, obtained by slow evaporation of the ethyl acetate solution of ADMA were used for data collection. The essential crystallographic data are presented in Table 3.2. The crystal belongs to monoclinic (*C*2/*c*) space group. The ORTEP diagram with atom numbering scheme and some of the packing interactions in the solid state have been depicted in Figure 3.14. The dihedral angle between the phenyl and anthryl planes is found to be 71.65°. Parallel and antiparallel arrangements of the molecules have been observed and these are stabilized by edge-to-face C-H…π intermolecular interactions. Apart from long distance dipole-dipole interaction, these are found to be the leading interactions in crystal packing. Two kinds of C-H…π interactions are identified in the crystal structure. In the antiparallel configuration, the aminomethyl C-H of one molecule interacts with the π-cloud of the phenyl ring of another antiparallel molecule (C-H…π = 3.06 Å). In the parallel configuration, the aminomethyl C-H of one molecule interacts with the π-cloud of the anthryl ring of another parallel molecule (C-H…π = 2.92 Å) and these are shown in Figure 3.14. The crystal structure provides insight into the nature of intermolecular interactions involved in the aggregation. The observed parallel and antiparallel arrangements of the molecules are reflections of the way the molecules self-assemble themselves spontaneously in forming larger aggregates. The structural data depicted in Figure 3.14 shows that these aggregates consist of one-dimensional array of molecules wherein the dipoles of the individual monomers are aligned parallel to the line joining to their centers. This is what is commonly termed as J-type (end-to-end or head-to-tail arrangement) aggregate.[53]

Table 3.2. Data collection and structure refinement details of crystal structure of ADMA.

	ADMA
Formula	C22 H19 N
Formula wt	297.38
Crystal system	monoclinic
Space group	C2/c
a (Å)	16.476 (2)
b (Å)	8.6752 (11)
c (Å)	22.834 (3)
α (°)	90
β (°)	99.198 (2)
γ (°)	90
V ($Å^3$)	3221.8 (7)
Z	8
F(000)	1264
ρ_{calcd} (g cm^{-3})	1.226
μ (mm^{-1})	0.071
Temperature (K)	298 (2)
λ [A]	0.71073
Crystal size	0.08 x0.22 x0.27
Color, habit	Greenish yellow, Plate
Absorption correction	Multi-scan
T_{min}, T_{max}	0.981,0.994
Total no. of reflections	14067
No. of unique reflections	2850
No. of. obs. reflections	1961
θ_{max} (°)	25.05
No. of parameters	210
R indices (obs. Data): *R*, R_w	0.0927, 0.0603
R indices (all data): *R*, R_w	0.1474, 0.1279
GOF	1.02
$\Delta\rho_{max}$, $\Delta\rho_{min}$ (e/$Å^3$)	0.149, -0.137

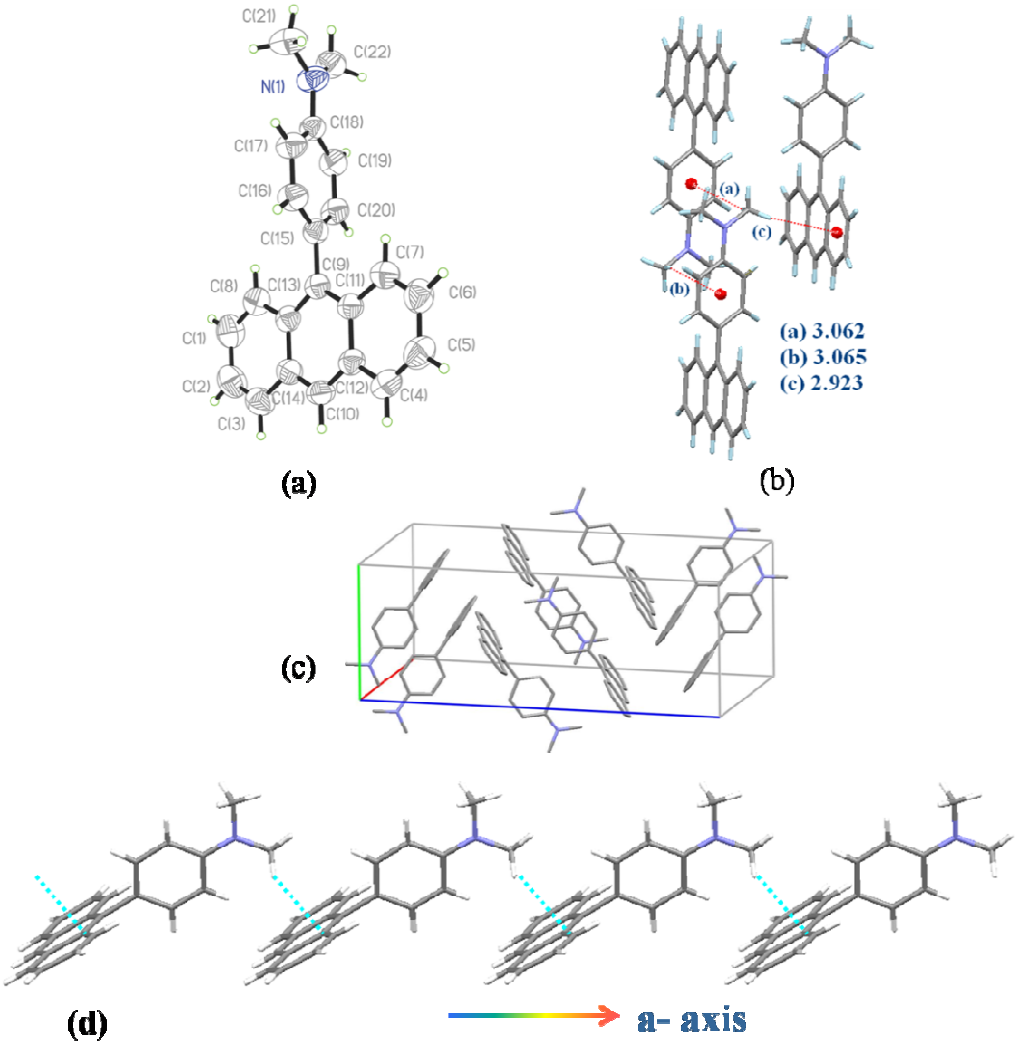

Fig. 3.14. (a) ORTEP diagram of ADMA with atoms represented by thermal ellipsoids at 50 % probability level, N(1)-C(18) bond length = 1.376 (9) Å. (b) C-H….π interactions, (c) packing diagram (all H-atoms are omitted for clarity), and (d) end-to-end arrangement of molecules in the solid state.

3.6. Conclusion

Self-assembled aggregates of a dipolar molecule, ADMA, have been prepared in aqueous medium by the reprecipitation method, and the optical absorption and fluorescence properties of these well-characterized aggregates have been studied. Aggregation gives rise to new absorption band, which contributes to the broadening of the spectral envelope. These aggregates have been found to be quite fluorescent and the emission spectrum is characterized by features that suggest absence of the intramolecular charge transfer interaction, which dominates the optical properties of ADMA in its molecular form, in the aggregated state. The nature of the intermolecular interaction in the aggregated and solid states has been identified as J-type from the head-to-tail molecular assembly in the solid state and from the spectral features.

References

(1) Alivisatos, A. P. *Science* **1996**, *271*, 933.
(2) Empedocles, S. A.; Bawendi, M. G. *Science* **1997**, *278*, 2114.
(3) Bruchez, M.; Moronne, M.; Gin, P.; Weiss, S.; Alivisatos, A. P. *Science* **1998**, 2013.
(4) Michalet, X.; Pinaud, F.; Lacoste, T. D.; Dahan, M.; Bruchez, M. P.; Alivisatos, A. P.; Weiss, S. *Single Mol.* **2001**, *2*, 261.
(5) Hagfeldt, A.; Gratzel, M. *Chem. Rev.* **1995**, *95*, 49.
(6) Schlamp, M. C.; Peng, X.; Alivisatos, A. P. *J. Appl. Phys.* **1997**, *82*, 5837.
(7) Shipway, A. N.; Katz, E.; Willner, I. *Chem. Phys. Chem.* **2000**, *1*, 18.
(8) Wohltjen, H.; Snow, A. W. *Anl. Chem.* **1998**, *70*, 2856.
(9) Chen, W.; Tu, X.; Guo, X. *Chem. Commun.* **2009**, 1736.
(10) Cheon, J.; Lee, J.-H. *Acc. Chem. Res.* **2008**, *41*, 1630.
(11) Fan, J.; Li, H.; Jiang, J.; So, L. K. Y.; Lam, Y. W.; Chu, P. K. *Small* **2008**, *4*, 1058.
(12) Kamat, P. V. *J. Phys. Chem. C.* **2007**, *111*, 2834.
(13) Soo, J. L.; Doo, R. B.; Won, S. H.; Shim, S. L.; Jong, H. J. *Eur. Jour. Inorg. Chem* **2008**, 1559.
(14) Chatterjee, S.; Gottschalk, P.; Davis, P. D.; Schuster, G. B. *J. Am. Chem Soc.* **1988**, *110*, 2326.
(15) Gilman, P. B. *J. Photogr. Sci. Eng.* **1974**, *18*, 418.
(16) Thirtle, J. R.; Zwick, D. M. *Color Photography In Kirk-Othmer:Encyclopedia of Chemical Technology*, 3 ed.; John Wiley&Sons: New York, 1979; Vol. 6.
(17) Oh, J.-W.; Kumazaki, S.; Rubtsov, I. V.; Suzumoto, T.; Tani, T.; K., Y. *Chem. Phys. Lett.* **2002**, *352*, 357.
(18) Maeda, M.; *Laser Dyes*; Academic Press: Tokyo, 1984.
(19) Shank, C. V.; Ippen, E. P. *Dye lasers*, Schafer, F. P. ed.; Springer- Verlag: Heidelberg, 1973.
(20) Sainudeen, Z.; Chandra Ray, P. *J. Phys. Chem. A.* **2005**, *109*, 9095.
(21) Wurthner, F.; Yao, S.; Debaerdemaeker, T.; Wortmann, R. *J. Am. Chem. Soc.* **2002**, *124*, 9431.
(22) An, B. K.; Kwon, S. K.; Jung, S. D.; Park, S. Y. *J. Am. Chem. Soc.* **2002**, *124*, 14410.
(23) An, B. K.; Kwon, S. K.; Park, S. Y. *Angew. Chem. Int. Ed.* **2007**, *46*, 1978.
(24) Toal, S. J.; Jones, K. A.; Magde, D.; Trogler, W. C. *J. Am. Chem. Soc.* **2005**, *127*, 11661.
(25) Patra, A.; Hebalkar, N.; Sreedhar, B.; Sarkar, M.; Samanta, A.; Radhakrishnan, T. P. *Small* **2006**, *2*, 650.
(26) Jang, S.; Kim, S. G.; Jung, D.; Kwon, H.; Song, J.; Cho, S.; Ko, Y. C.; Sohn, H. *Bull. Korean. Chem. Soc.* **2006**, *27*, 1965.
(27) Liu, Y.; Tao, X.; Wang, F.; Dang, X.; Zou, D.; Ren, Y.; Jiang, M. *J. Phys. Chem. C.* **2008**, *112*, 3975.
(28) Qian, Y.; Li, S.; Zhang, G.; Wang, Q.; Wang, S.; Xu, H.; Li, C.; Li, Y.; Yang, G. J. *J. Phys. Chem. B.* **2007**, *111*, 5861.

(29) Wang, F.; Han, M. Y.; Mya, K. Y.; Wang, Y.; Lai, Y. H. *J. Am. Chem. Soc.* **2005**, *127*, 10350.
(30) An, B. K.; Lee, D. S.; Park, Y. S.; Song, H. S.; Park, S. Y. *J. Am. Chem Soc.* **2004**, *126*, 10232.
(31) Lim, S. J.; An, B. K.; Jung, S. D.; Chung, M. A.; Park, S. Y. *Angew. Chem. Int. Ed.* **2004**, *43*, 6346.
(32) Lim, S. J.; An, B. K.; Park, S. Y. *Macromolecules* **2005**, *38*, 6236.
(33) Chen, J.; Law, C. C. W.; Lam, J. W. Y.; Dong, Y.; Lo, S. M. F.; Williams, I. D.; Zhu, D. B.; Tang, B. Z. *Chem. Mater.* **2003**, *15*, 1535.
(34) Chen, J.; Peng, H.; Law, C. C. W.; Dong, Y. Q.; Lam, J. W. Y.; Williams, I. D.; Tang, B. Z. *Macromolecules* **2003**, *36*, 4319.
(35) Luo, J.; Xie, Z.; Lam, J. W. Y.; Cheng, L.; Chen, H.; Qiu, C.; Kwok, H. S.; Zhan, X.; Liu, Y.; Zhu, D.; Tang, B. Z. *Chem. Comm.* **2001**, 1740.
(36) Ren, Y.; Lam, J. W. Y.; Dong, Y.; Tang, B. Z.; Wong, K. S. *J. Phys. Chem. B.* **2005**, *109*, 1135.
(37) Zhang, X.; Xiaohong, Z.; Meng, X.; Shi, W.; Lee, C. S.; Lee, S. T. *Angew. Chem. Int. Ed.* **2007**, *46*, 1525.
(38) Zhang, X.; Xiaohong, Z.; Zou, K. *J. Am. Chem. Soc.* **2007**, *129*, 3527.
(39) Zhang, X.; Yuan, G.; Li, Q.; Wang, B.; Zhang, X.; Zhang, R.; Chang, J. C.; Lee, C.; Lee, S. *Chem. Mater.* **2008**, *20*, 6945.
(40) Briseno, A. L.; Mannsfeld, S. C. B.; Reese, C.; Hancock, J. M.; Xiong, Y.; Jenekhe, S. A.; Bao, Z.; Xia, Y. *Nano Lett.* **2007**, *7*, 2847.
(41) Zhao, L.; Yang, W.; Ma, Y.; Yao, Y.; Lib, Y.; Liub, H. *Chem. Commun.* **2003**, 2442.
(42) Zhao, Y. S.; Wu, J.; Huang, J. *J. Am. Chem. Soc.* **2009**, *131*, 3158.
(43) Zhao, Y. S.; Xiao, D.; Yang, W.; Peng, A.; Yao, J. *Chem. Mater.* **2006**, *18*, 2302.
(44) Okada, T.; Fugita, T.; Kobuta, M.; Masaki, S.; Mataga, N. *Chem. Phys. Lett.* **1972**, *14*, 563.
(45) Grabowski, Z. R.; Rotikeiwicz, K.; Rettig, W. *Chem. Rev.* **2003**, *103*, 3899.
(46) Herbich, J.; Kapturkiewicz, A. *Chem. Phy.* **1993**, *170*, 221.
(47) Kajimoto, O.; Hayami, S.; Shizuka, H. *Chem. Phys. Lett.* **1991**, *177*, 219.
(48) Baumann, W.; Petzke, F.; Loosen, K. D. *Z. Naturforsch. A.* **1979**, *34A*, 1070.
(49) Siemiarczuk, A.; Grabowski, Z. R.; Krowczynski, A.; Asher, M.; Ottolenghi, M. *Chem. Phys. Lett.* **1977**, *51*, 315.
(50) Okada, T.; Kawai, M.; Ikemachi, T.; Mataga, N. *J. Phys. Chem.* **1984**, *88*, 1976.
(51) Cox, A. J.; DeWeerd, A. J.; Linden, J. *Am. J. Phys.* **2002**, *70*, 620.
(52) Kasai, H.; Kamatani, H.; Okada, S.; Oikawa, H.; Matsuda, H.; Nakanishi, H. *Jpn. J. Appl. Phys.* **1996**, *35*, L221.
(53) Mishra, A.; Behera, R. K.; Behera, P. K.; Mishra, B. K.; Behera, G. B. *Chem. Rev.* **2000**, *100*, 1973.
(54) Knapp, E. W. *Chem. Phys.* **1984**, *85*, 73.
(55) Eisfeld, A.; Briggs, J. S. *Chem. Phys.* **2002**, *281*, 61.
(56) Ilharco, L. M.; Brito de Barros, R. *Langmuir* **2000**, *16*, 9331.
(57) Rossi, U. D.; Daehne, S.; Reisfeld, R. *Chem. Phys. Lett.* **1996**, *251*, 259.

(58) Kasai, H.; Kamatani, H.; Yoshikawa, Y.; Okada, S.; Oikawa, H.; Watanabe, A.; Itoh, O.; Nakanishi, H. *Chem. Lett.* **1997**, 1181.
(59) Xiao, D.; Xi, L.; Yang, W.; Fu, H.; Shuai, Z.; Fang, Y.; Yao, J. *J. Am. Chem. Soc.* **2003**, *125*, 6740.
(60) Birks, J. B. *Photophysics of Aromatic Molecules*; John Wiley & Sons: London, 1970.
(61) Turro, N. J. *Modern Molecular Photochemistry*, 1 ed.; Benjamin/ Cummings Publishing Company, Inc.: California, 1978.
(62) Bhongale, C. J.; Chang, C.-W.; Lee, C.-S.; Diau, E. W.-G. *J. Phys. Chem. B.* **2005**, *109*, 13472.
(63) Li, S.; He, L.; Xiong, F.; Li, Y.; Yang, G. *J. Phys. Chem. B.* **2004**, *108*, 10887.
(64) Oelkrug, D.; Tompert, A.; Gierschner, J.; Egelhaaf, H.-J.; Hanack, M.; Hohloch, M.; Steinhuber, E. *J. Phys. Chem. B.* **1998**, *102*, 1902.

Chapter 4

Controlled Fabrication and Optical Properties of Highly Fluorescent Nano/Micro-particles of Dipolar Molecular System, 4-(9-Anthryl)-N,N-Dimethylaniline

The morphologies and optical properties of the aggregated state of a highly fluorescent electron donor-acceptor molecule, 4-(9-anthryl)-N,N-dimethylaniline (ADMA), fabricated in the presence of additives such as surfactants, polymer and ionic liquids, has been studied by various imaging, UV-vis and steady-state and time-resolved fluorescence techniques. It is demonstrated that the sizes and shapes of the aggregates of ADMA can be tuned by the surfactants, but not by the other additives described above. The various morphologies captured in this work are shown to be the consequence of preferential adsorption of the surfactants to specific crystallographic planes of ADMA. Only those crystallographic surfaces grow that are not influenced by the surfactants. Aggregation leads to a progressive shift of the UV-vis absorption towards the longer wavelength. The nano/micro-structures of ADMA have been found to be strongly fluorescent and they exhibit somewhat structured fluorescence with the emission peak position highly blue-shifted (by ~50 nm) when compared with that in homogeneous tetrahydrofuran solution. It is inferred that the anthryl and phenyl ring systems are locked in an orthogonal/near-orthogonal conformation due to the structural constraint imposed by the rigidity of the aggregated state which results in a higher fluorescence quantum yield of the nano/microstructures. The fluorescence lifetime imaging microscopy (FLIM) studies not only allow discrimination of almost identical particles, but it also makes it possible to differentiate the various segments of a given particle whose fluorescence intensity image does not show any contrast.

4.1. Introduction

There has been considerable interest in recent years on the aggregated states of organic molecular systems because of their interesting optical and electronic properties, which make them suitable for practical applications as field effect transistors,[1] sensors,[2-4] optical waveguides,[5,6] and lasers.[7,8] The large diversity of organic molecular systems, ease of materials synthesis and tunablity of the optical properties provide great

opportunities in this regard. The various design strategies identified for controlling the sizes and shapes of the aggregates (essentially nano- or micro-structures of the organic systems), and hence, their properties, include control of temperature, addition of surfactants and other additives, sonication, etc. Most of these design strategies and the optoelectronic properties of various one-dimensional nanostructures of organic molecular systems have been described in two excellent reviews.[9,10]

Despite the importance of the electron donor-acceptor (EDA) molecules in various theoretical studies and practical applications,[11-16] the aggregated state of these systems has not been explored in detail.[17-19] As optical properties of the EDA molecules are extremely sensitive to the environment, one can expect significant changes of these properties in the aggregated state, which in turn is expected to broaden the utility of these substances. As the strength and direction of the dipole-dipole interaction and molecular geometry play important roles in the formation of these one or semi-two dimensional organic nanostructures,[18,19] the simplest approach to obtain different morphologies with interesting optical properties is to play with the constituent donor and acceptor moieties of the EDA molecules. Considering these aspects, we have recently embarked upon studies on the aggregates of molecular systems of this class and studied the interactions responsible for the self-aggregation in 4-(9-anthryl)-N,N-dimethylaniline (ADMA, Chart 4.1),[20] a molecule which is strongly fluorescent, exhibits interesting photophysical/ fluorescence behavior involving twisted intramolecular charge transfer (TICT) process and solvent induced electron transfer reaction.[21-23] This study showed that neither the morphologies and nor the optical responses of the aggregates could be controlled without using any stabilizer. As potential application of a system is dependent on our ability to tune the size, shape and property of the system and also on its stability, we explore here the effect of various additives such as the surfactants, polymers and ionic liquids and other experimental conditions on the sizes and shapes and optical responses of the

various aggregates. As can be seen, we have been able to capture the various stages of the aggregation process, which gives us an opportunity to study the properties of the mesoscopic particles. Another interesting aspect of this work is the study of the aggregated state of these systems by the FLIM technique, which not only shows that almost identical looking particles can be different, but it also highlights the spatial/segmental heterogeneity of any given particle.

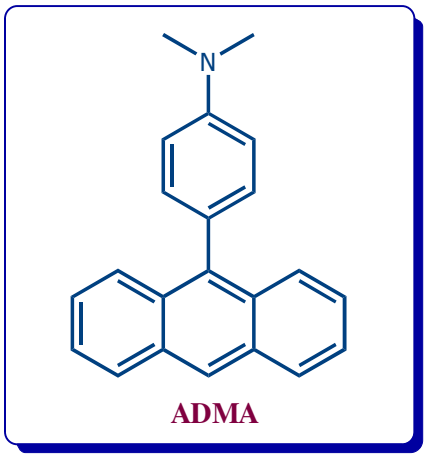

Chart 4.1. Molecular structure of 4-(9-anthryl)-N,N-dimethylaniline

4.2. Effect of cationic surfactant (CTAB)

4.2.1. Fabrication of nanoparticles

Figure 4.1 shows typical atomic force microscope (AFM) images of the ADMA nanostructures prepared by injecting different quantities of standard stock solution (ADMA in THF, 2.7 mM) to 10 mL of CTAB/water (0.5 mM) solution. As can be seen, the morphologies of the aggregates vary quite a lot depending on the condition. A rod-like morphology is changed to a plate- or sheet-like one when an increased amount of the stock solution is injected. The measured dimensions of these nanostructures obtained

from AFM analysis are summarized in Table 4.1. The morphologies and their dimensions were further confirmed by SEM (Fig. 4.2) and TEM (Fig. 4.3). The crystallinity of the nanostructures was confirmed by both TEM analysis and powder X-ray pattern (Fig. 4.4). Some of the diffraction peaks of different particles match well with the powder X-ray pattern of ADMA and sharp peaks of these nanostructures clearly indicate their crystalline nature.

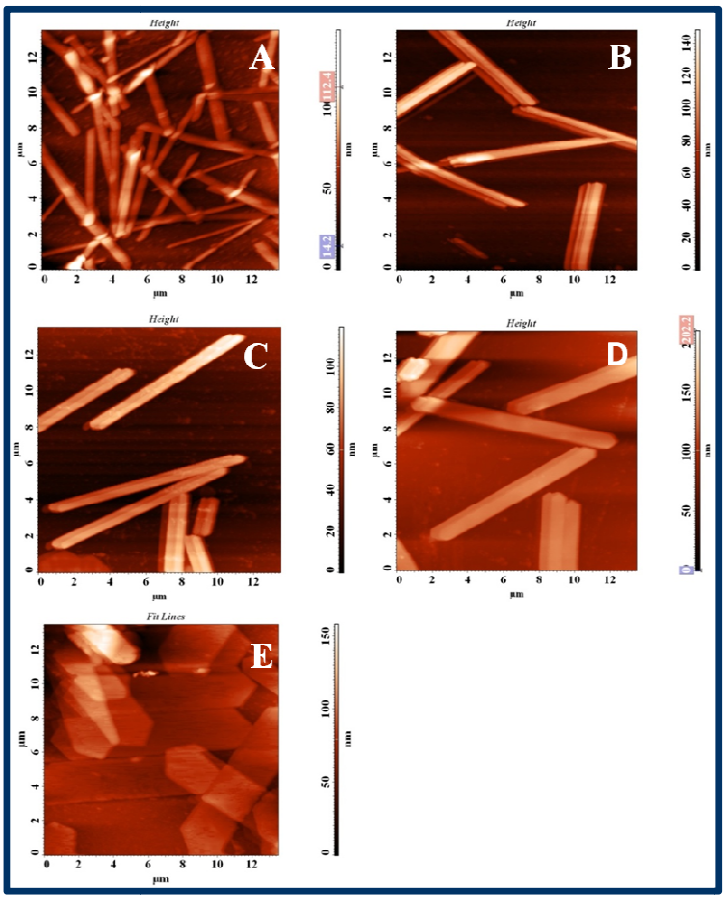

Fig. 4.1. AFM images of ADMA colloids prepared in 10 mL of CTAB solution (0.5 mM) by injecting 100 µL (A), 300 µL (B), 500 µL (C), 700 µL and 1 mL (E) of 2.7 mM THF solution.

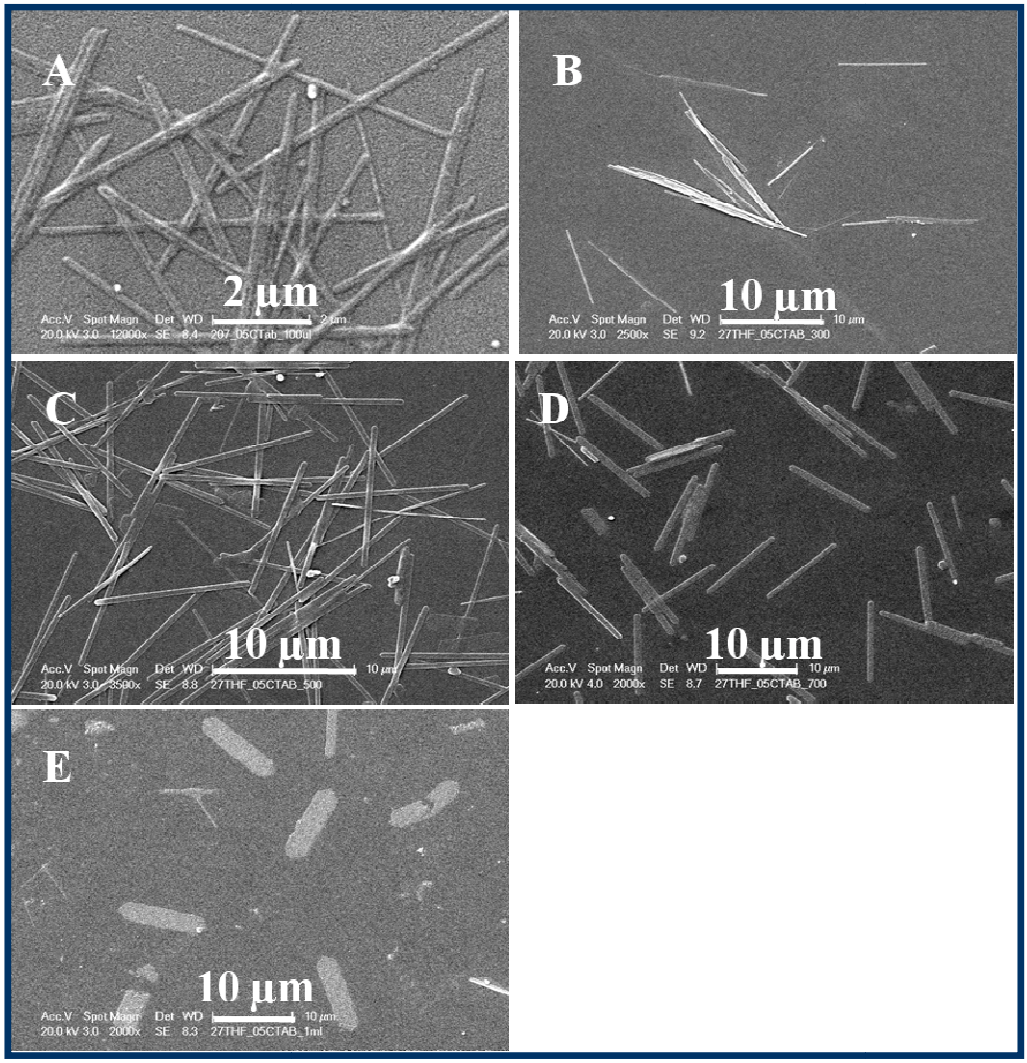

Fig. 4.2. SEM images of ADMA colloids prepared in 10 mL of CTAB solution (0.5 mM) by injecting 100 µL (A), 300 µL (B), 500 µL (C), 700 µL and 1 mL (E) of 2.7 mM THF solution.

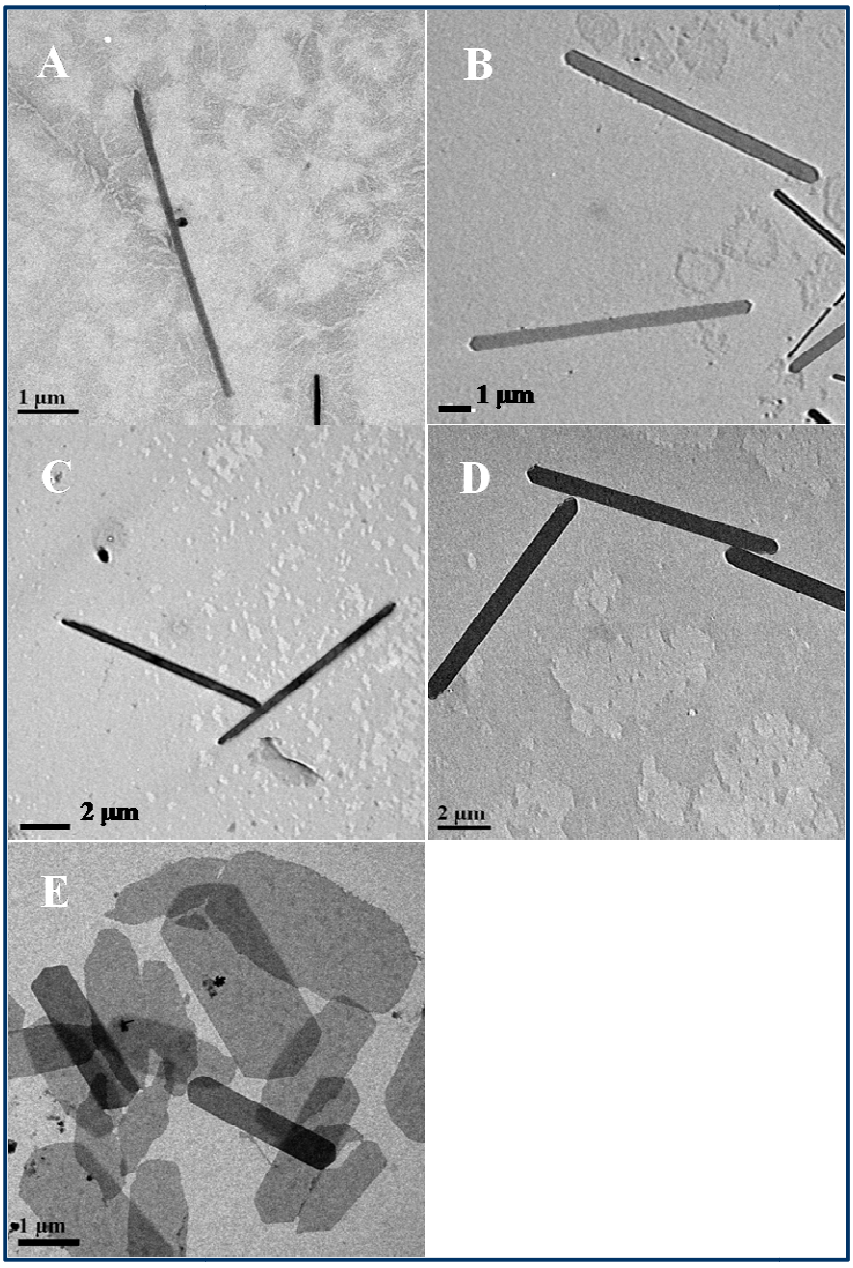

Fig. 4.3. TEM images of ADMA colloids prepared in 10 mL of CTAB solution (0.5 mM) by injecting 100 µL (A), 300 µL (B), 500 µL (C), 700 µL and 1 mL (E) of 2.7 mM THF solution.

Table 4.1. Dimensions of the different nanostructures obtained in CTAB (0.5 mM) solution, as estimated from the AFM analysis.

Sample	Length (µm)	Width (µm)	Height (nm)
100 µl	6.0- 8.5	0.2-0.25	20-30
300 µl	6.0 - 8.5	0.2-0.25	20-30
500 µl	7.5 – 10.5	0.3 - 0.6	25-50
700 µl	9.0 -10.5	0.75-1.2	40-50
1 ml	10.0 - 11.5	2.5-3.5	30-40

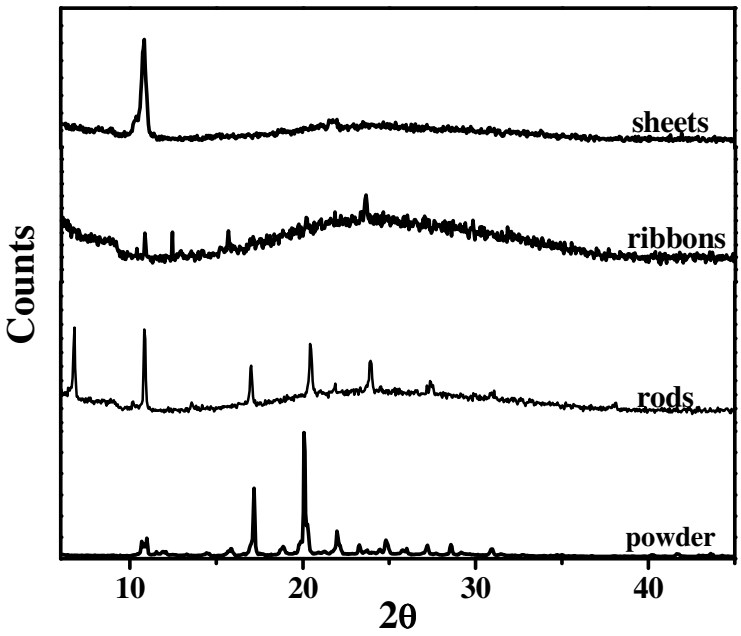

Fig. 4.4. Powder X-ray data of the nanorods, ribbons and sheets. Powder X-ray pattern of ADMA also given for the comparison.

4.2.2. Steady state absorption & fluorescence

Figure 4.5 compares typical electronic absorption spectra of the different nanostructures with those of ADMA in homogeneous solutions. It is evident that the spectral behavior of these nanostructures of ADMA is distinctly different from that of the molecular system in the homogeneous solutions. Interestingly, even though the morphologies of the aggregates in the presence and absence of the surfactants are very different, the spectral features of the different aggregates obtained in the presence of surfactants are found to be quite similar to those obtained without any surfactants.[20] A significant increase of the absorbance in the long wavelength region (400-550 nm) with the absorption tail extending up to *ca.* 600 nm is clearly a manifestation of the strong

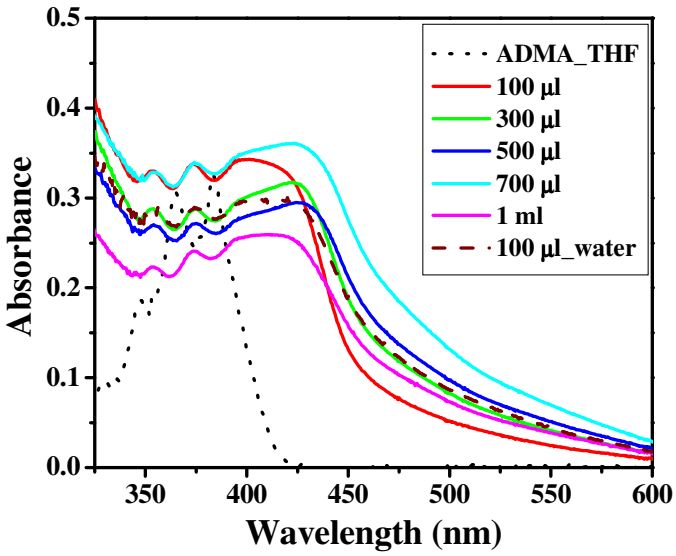

Fig. 4.5. Electronic absorption spectra of ADMA colloids prepared by injecting 0.1- 1 ml of ADMA /THF (solid lines) in CTAB solution (0.5mM). The absorption spectra of ADMA in THF (dotted line) and 100 µl colloids prepared only in water (dash line) are also shown.

intermolecular interactions on the energetics of the system in the mesoscopic regime.[18,24] Even though pronounced effect of the interactions of this kind is uncommon for molecular systems that are nonpolar or less polar in nature (such as naphthalene or anthracene), considering the dipolar nature of the present system, the prominent effect observed in this case can be attributed primarily to the dipole-dipole interaction. The broad absorption with long tail is clearly due to the presence of various nanostructures and progressive rise of the baseline with decrease of wavelength is due to Mie scattering effect.[25,26] The new distinct absorption band at ~ 420-430 nm is evidently due to J-type aggregation of the molecule in the mesoscopic regime.[20] As the band due to the aggregate overlaps with that due to the anthryl unit and hence, could not be clearly resolved, the peak positions due to the various aggregates have been obtained by deconvolution of the broad band using a multi-peak Lorentzian fitting tool (Fig. 4.6). This analysis revealed

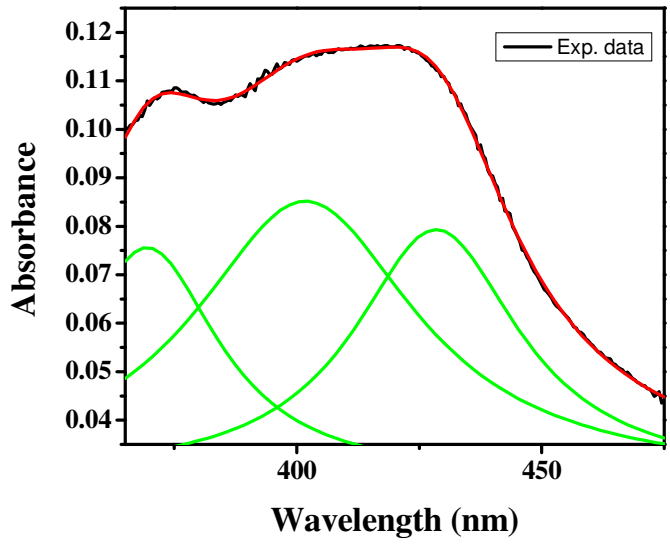

Fig. 4.6. Deconvolution of absorption spectrum of 100 µl colloid (black solid line) using multi-peak Lorentzian function.

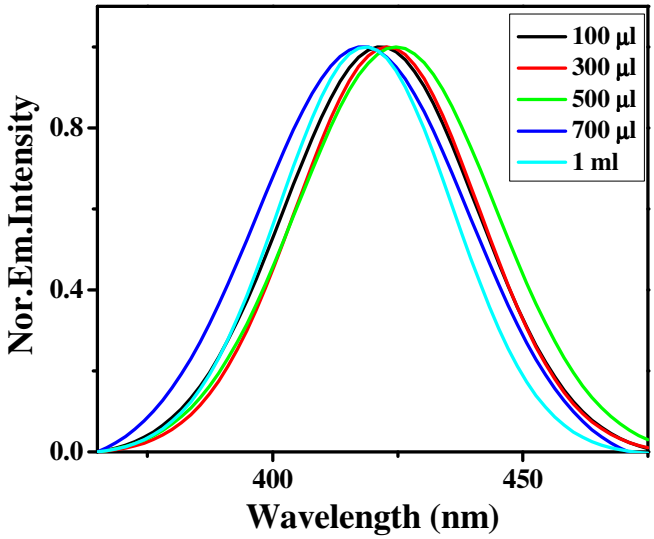

Fig. 4.7. J-type aggregate band of the nanostructures obtained from the deconvolution of each experimental curve using multi-peak-Lorentzian fitting tool.

the peak position due to the aggregate at around 420 nm. Small, but prominent changes of the J-type aggregate band position were observed and these changes can be attributed to the size effects, as already observed in some molecular systems (Fig. 4.7).[26-30] This size-dependent optical property of these nanostructures differs from the so-called quantum confinement effect, frequently observed with semiconductor nanoparticles whose sizes are between 1 and 10 nm.[31,32] Moreover, the observation cannot be explained in terms of Mie scattering as it is the peak position which is affected here, not the width. Nakanishi and coworkers attributed increasing surface area leading to lattice softening and electric field effect of the surrounding media on the surface of the crystalline aggregates to explain the size dependence of the optical properties of the perylene microcrystals[26] Perhaps a similar reasoning can be used to account for the present results. One must note however that the size dependence of the optical property of organic micro/nanocrystals is not yet completely understood.

Figure 4.8 compares the steady state emission spectrum of ADMA in THF with those of the aggregates obtained in the presence of CTAB. In THF, the emission maximum appears at around 508 nm. The emission peak due to the aggregates appears at around 455 nm indicating a large hypsochromic shift (~50 nm) of the emission band due to the nanostructures compared to its homogeneous solution (ADMA/THF). Several factors can contribute to this shift. Rigidification of the molecular structure on aggregation, as already observed in the absence of any surfactant,[20] can contribute to this. This rigidification is evident from the narrow and structured nature of the band. If the two ring systems of the molecule adopt a mutually perpendicular or near-perpendicular conformation in the aggregated/solid state, the charge transfer between the two is prevented or restricted and one can then expect a structured and blue-shifted LE-like emission. It is also possible that on passage of the molecules from homogeneous solution

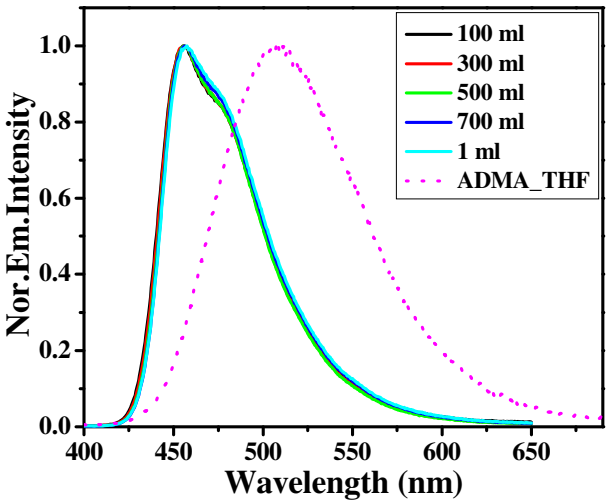

Fig. 4.8. Steady-state fluorescence spectra of the ADMA colloids obtained by injecting 0.1 - 1 ml ADMA /THF (solid lines) in 0.5mM CTAB solution. The emission spectrum of ADMA in THF (dotted line) is also shown for comparison.

to the aggregated state, the solvent shell from each molecule is removed creating a nonpolar or less polar environment. This may also lead to the observed fluorescence behavior. One can also explain the spectral behavior of these aggregates by considering the intermolecular interactions. As the absorption maximum due to the J-type aggregates appears at ~420-430 nm, the emission maximum is expected at a higher wavelength and the observed emission maximum at 456 nm for the nanostructures is in accordance with this expectation. The emission property does not change with the morphology perhaps suggests that the regular arrangement of the molecules is very similar in the various forms of aggregates.

Table 4.2. Fluorescence decay parameters[‡] and quantum yields of the various nanostructures of ADMA along with those for the molecular form of ADMA in THF (λ_{ex} = 375 nm).

Sample	τ_1 (a_1)	τ_2 (a_2)	τ_{avg}	χ^2	Φ_f
THF[a]	1.22 (0.1)	7.55 (0.9)	6.92	1.16	0.42
Colloids[b]					
100µl	2.12 (0.14)	5.01 (0.86)	4.61	1.07	0.32
300µl	2.53 (0.12)	5.87 (0.88)	5.47	1.09	0.38
500µl	2.83 (0.12)	6.06 (0.88)	5.67	1.08	0.41
700µl	2.20 (0.13)	5.87 (0.87)	5.39	1.07	0.56
1 ml	1.99 (0.11)	5.17 (0.89)	4.82	1.09	0.58

[‡]τ values are in ns. (a) λ_{em} = 500 nm (b) λ_{em} = 475 nm

4.2.3. Fluorescence quantum yield and lifetime

As can be seen from Table 4.2, the fluorescence quantum yields of most of these nanostructures are reasonably high. Compared to a homogeneous solution of ADMA in THF, the nanorods have a slightly lower quantum yield. The nanoribbons and nanosheets possess relatively higher quantum yields. The emission quantum yield of a system usually decreases in the solid/aggregated state.[33-35] Most of the aggregates, which are reported to fluoresce strongly in the aggregated/solid state,[36-41] possess no well-defined morphologies and very few systems with well-characterized morphologies are available.[42] There are a few donor-acceptor molecules with well-defined morphologies. However, the fluorescence quantum yield of which has not been measured.[43,44] The present system represents one of the first examples of highly fluorescent 1D and semi-2D nanostructures of a donor acceptor molecule. These fluorescence quantum yields of 1D and semi-2D nanostructures are comparable with few classical compounds that were used in organic light emitting diodes (OLED).[45] The fluorescence quantum yield of the particles increases with increasing particle size presumably due to structural rigidification in the aggregated state. Laser scanning confocal fluorescence microscopic experiments show that intense blue fluorescence is indeed due to these nanostructures (Fig. 4.9). The fluorescence decay profiles (Fig. 4.10) of ADMA in THF and in the aggregated state are multiexponential. The average lifetimes in homogeneous solution (THF) and various aggregated states are collected in Table 4.2. The fluorescence lifetime increases with increase in the particle size. However, for much larger particles such as the sheets, the lifetime values are slightly lower. The increase of the lifetime of the microcrystals with size is probably due to the change in the rigidity of the crystal lattice. Hence, the fluorescence lifetime variation in nanoribbons and nanosheets can perhaps be attributed to the softening of the crystal lattice.[26,46]

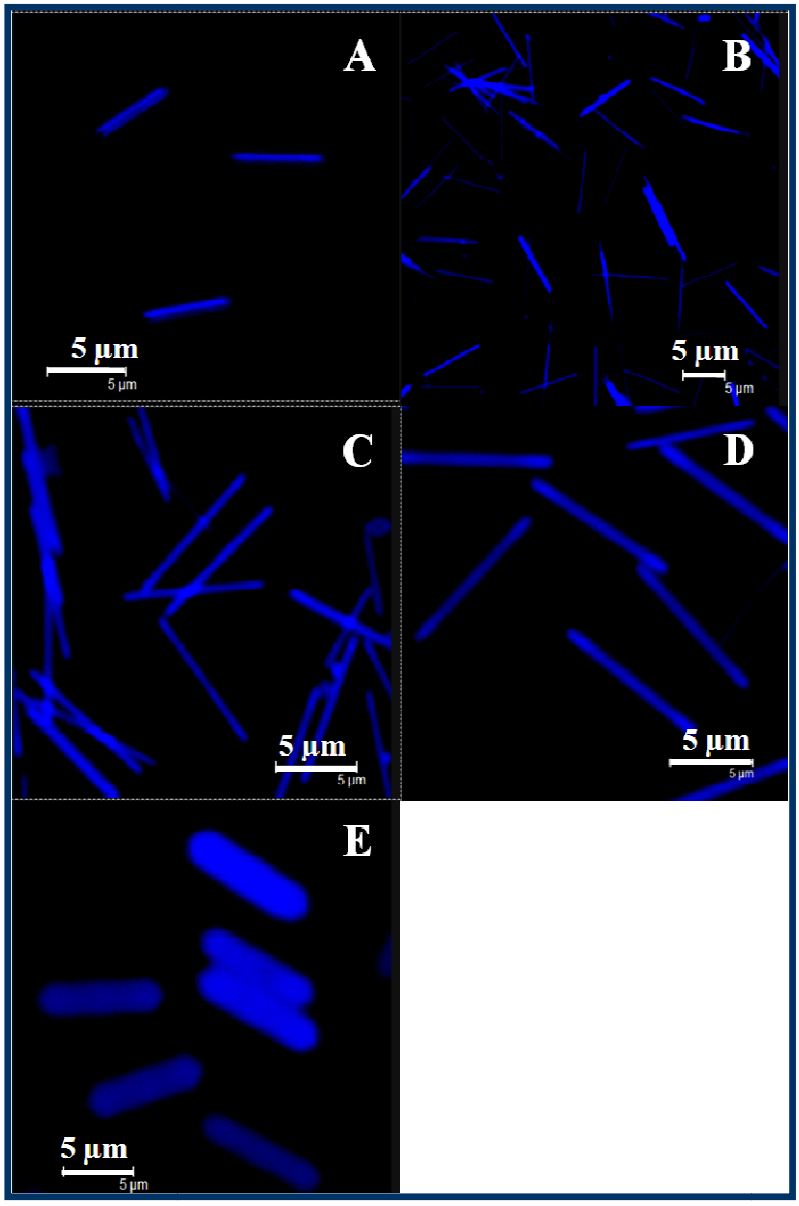

Fig. 4.9. Laser scanning confocal fluorescence microscope images of ADMA colloids prepared in 10 mL of CTAB solution (0.5 mM) by injecting 100 µL (A), 300 µL (B), 500 µL (C), 700 µL and 1 mL (E) of 2.7 mM THF solution.

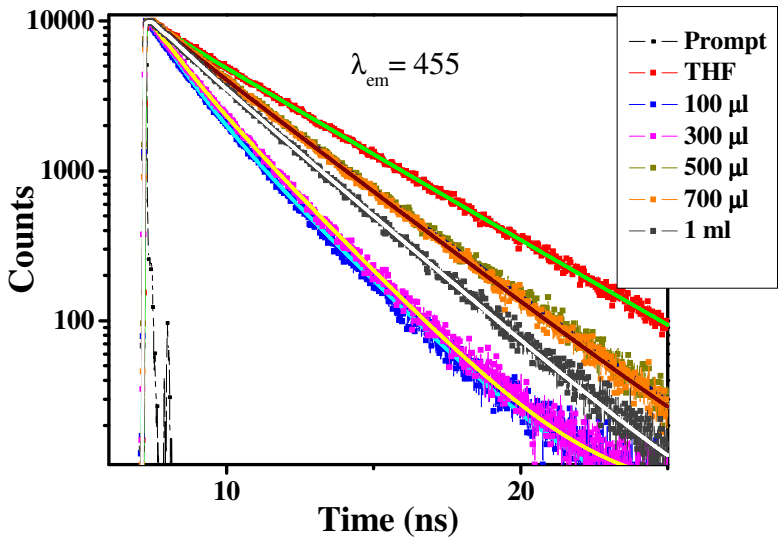

Fig. 4.10. Fluuorescence decay curves of the various nanostructures of ADMA along with that in THF collected by monitoring the emission at 455 nm (λ_{ex}= 375 nm).

4.2.4. Fluorescence lifetime imaging microscope (FLIM) study

The individual nano-/micro-particles have also been examined using a picoseconds time-resolved fluorescence lifetime imaging microscope (FLIM), which allows construction of images of the particles based on their fluorescence lifetimes. The results of these measurements, which have been carried out using a time-resolved confocal fluorescence microscope (PicoQuant Microtime 200), are depicted in Figure 4.11 along with the fluorescence intensity images of these particles for comparison. The top panel shows the fluorescence intensity images and bottom panel shows the FLIM images of the same set of particles of three different types (rods, ribbons and plates/ sheets). The fluorescence intensity images suggest that the particles of any given type lying in the confocal plane are very similar. However, unlike the intensity images, the FLIM images of the particles show good contrast and reveal much more details about the nature of these particles. In this context, we consider the following observation, to be quite

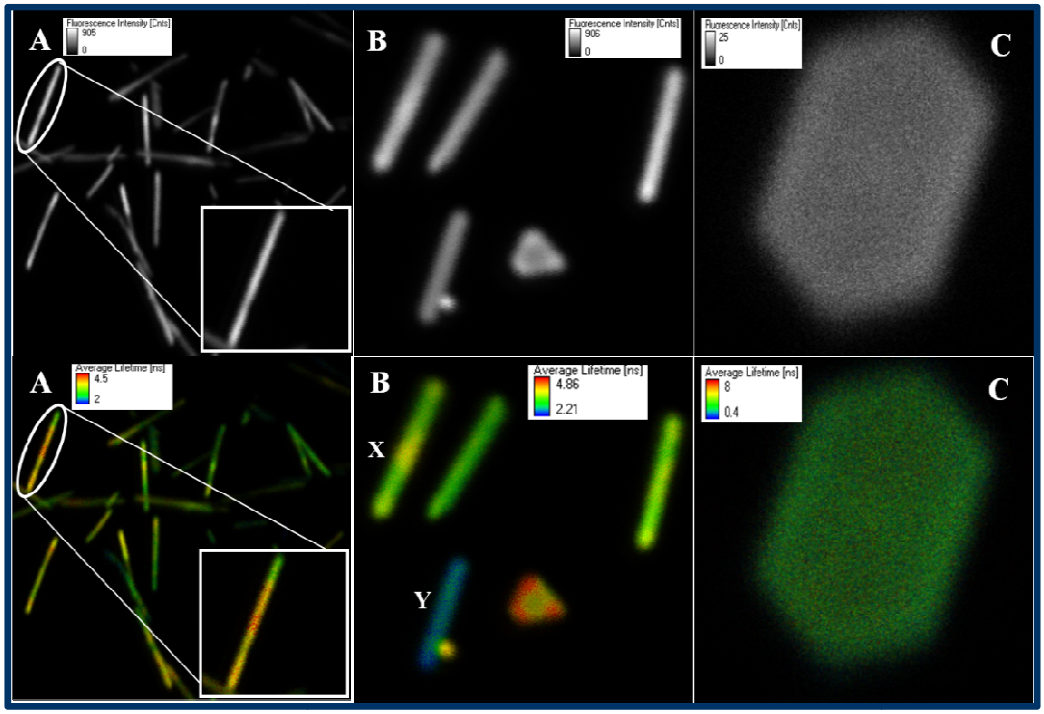

Fig. 4.11. Fluorescence intensity images (upper pannel) and FLIM images (lower pannel) of nanorods (A), nanoribbons (B) and nanosheets (C). Inset image shows the different segments has different lifetime. Scale bar for A: 15×15 µm, B: 14×14 µm, C: 8×8 µm.

significant. First, the rod, which is circled and zoomed in block A of figure 4.11, hardly shows any contrast in its intensity image. Interestingly, the distinct colors of the two ends of this rod in its FLIM image clearly suggest that the fluorescence lifetime of one end of this particle is different from the rest of the rod by nearly 1 ns. Considering the fact that the time resolution of this measurement is around 100-125 ps, the lifetime difference of 1 ns is quite significant and has to be taken seriously. Second, if we focus our attention on two particles labeled X and Y in block B of the same figure and compare their images in the top and bottom panel, we find that the fluorescence intensity images of X and Y are very similar, but the colors of the FLIM images of the particles (blue and green) suggest a

lifetime difference of around 1 ns, which is quite significant. At this stage we are unable to comment on the factors that contribute to this difference of lifetime. One approach to find this out could be to record the fluorescence spectral features of the individual particles and/or different segments of any given particle. This however requires a setup in which a spectrograph is coupled with the present time-resolved facility. As we do not have this facility this issue cannot be addressed currently.

4.3. Effect of anionic (SDS) and neutral surfactant (TX-100)

Figure 4.12, which depicts the AFM and SEM images of the ADMA nanostructures prepared in the presence of SDS, suggests that the morphologies of the nano-/micro-particles of ADMA are very similar to those obtained in presence of CTAB. Interestingly, the neutral surfactant (TX-100) under similar condition forms plates and ribbons (Fig. 4.13). No rod or sheet-like morphologies are observable in this case. Surprisingly, the optical properties of the various nanostructures obtained in presence of SDS or TX-100 were found to be quite similar to those obtained in presence of CTAB.

As the surfactant concentration maintained in all cases (0.5 mM) was lower than the CMC of CTAB and SDS, but was higher than that of TX-100,[47] the morphological difference in the later case can be due to the formation of micelle, which provides a physical template for the nanostructures. Reports of fabrication of anisotropic organic

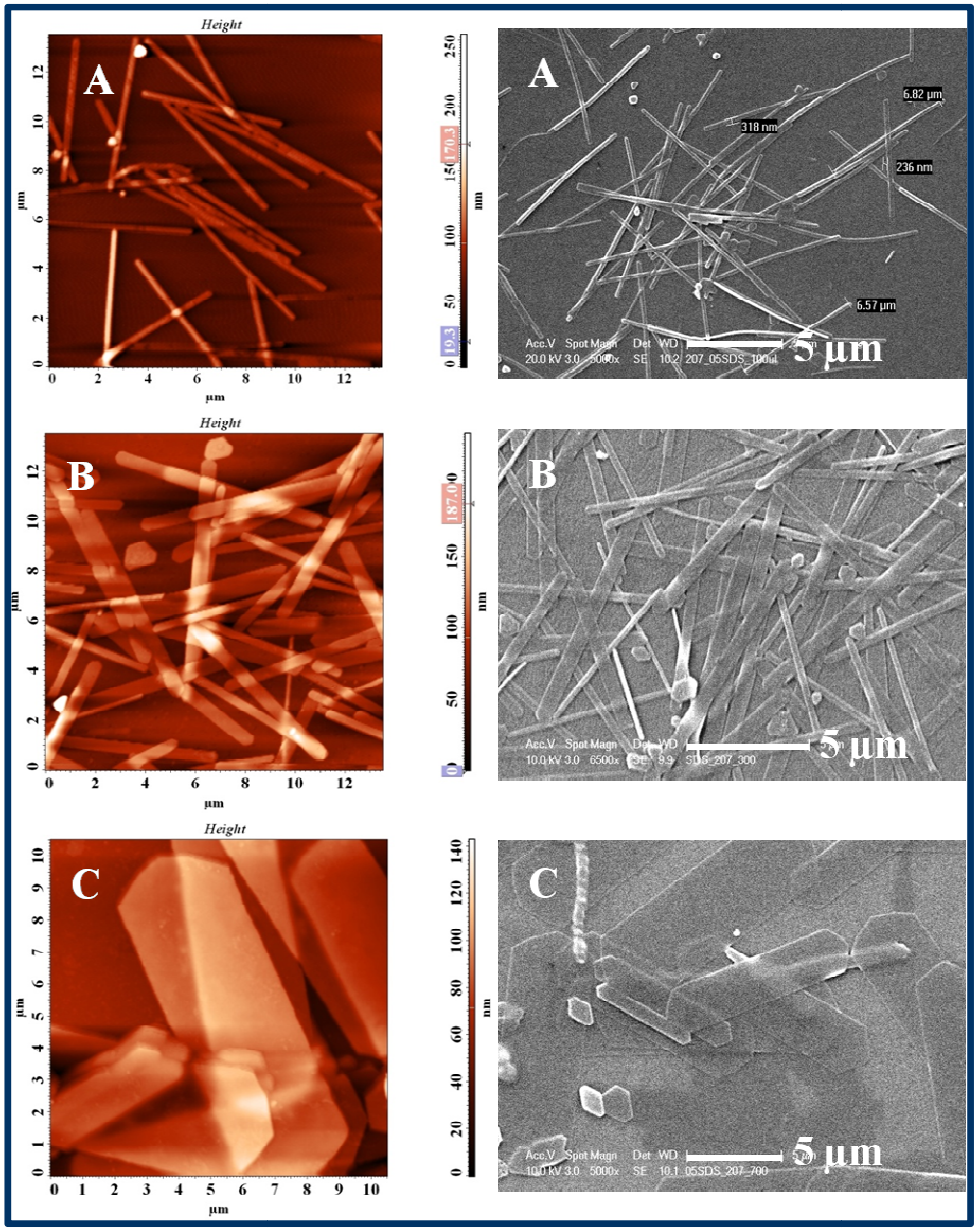

Fig. 4.12. AFM (left column) and SEM (right column) images of 100 µl (A), 700 µl (B) and 1 mL (C) colloids in the presence of SDS (0.5mM).

nanostructures in the presence of surfactants where the surfactants act both as a template[48-51] and a stabilizer[43]are available. In order to determine whether TX-100 acts as a stabilizer or provides a micellar template, experiments were carried out with less concentrated TX-100 solution (0.1 mM TX-100) such that surfactant concentration is maintained below the CMC. Even under this condition the formation of well-defined particles similar to those obtained earlier indicates that the surfactant acts as a stabilizing agent. The progressive change of the morphology on variation of the various experimental conditions, as observed in the case of CTAB and SDS, however could not be realized. This difference is most likely due to the difference of the zeta potential of the nanostructures in the two cases. The zeta potential, which is a measure of the extent of stabilization of colloidal particles, is generally lower (-10 to +10 mV) for aggregates in the presence of neutral surfactants compared to anionic and cationic surfactants (≥10 mV).[52,53] We think a lower zeta potential of the particles in TX-100 solution prevents the tunability of morphology.

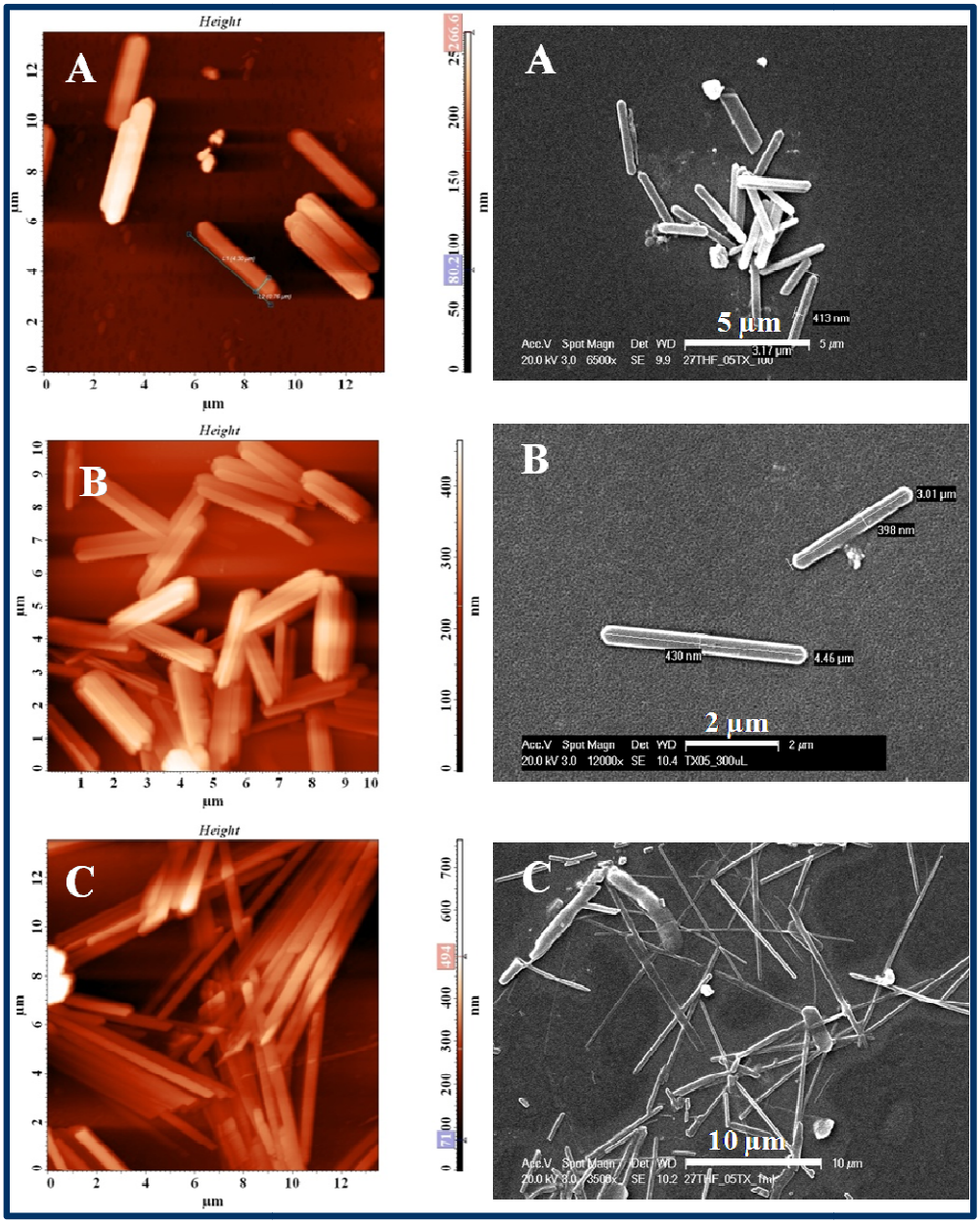

Fig. 4.13. AFM (left column) and SEM (right column) images of 100 µl (A), 700 µl (B) and 1 mL (C) colloids in the presence of TX-100 (0.5 mM).

4.4. Effect of ADMA and surfactant concentrations

We found that the sizes of the aggregates and their morphologies can also be tuned by varying the concentration of ADMA/THF solution, which is injected for the preparation of the aggregates. For example, when 100 µL of 27 mM ADMA/THF solution (instead of 2.7 mM) is injected to 10 mL of 0.5 mM CTAB/water, nanorods with larger dimensions are obtained, particle size distribution becomes broader and mixed morphologies are observed (Fig. 4.14). However, only the nanorods are obtained in CTAB/water when the injection volume is decreased. Similar results are observed in the presence of 0.5 mM SDS/water (Fig. 4.15). The effect of surfactant concentration on the morphology of the particles is also investigated. With increasing surfactant concentration, it is found that the rod-like particles assume a plate-like morphology (Fig. 4.16).

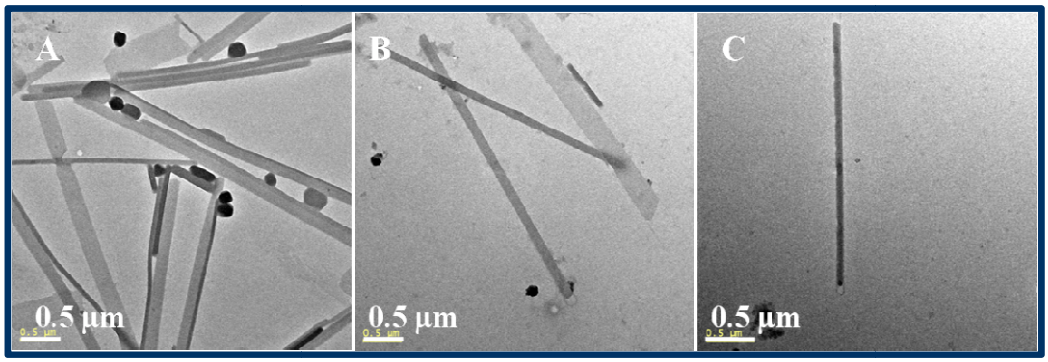

Fig. 4.14. Transmission electron microscope (TEM) images of 100 µl (A), 50 µl (B) and 25 µl (C) colloids in the presence of CTAB (0.5 mM) prepared by injecting a high concentration (27 mM) of ADMA/THF.

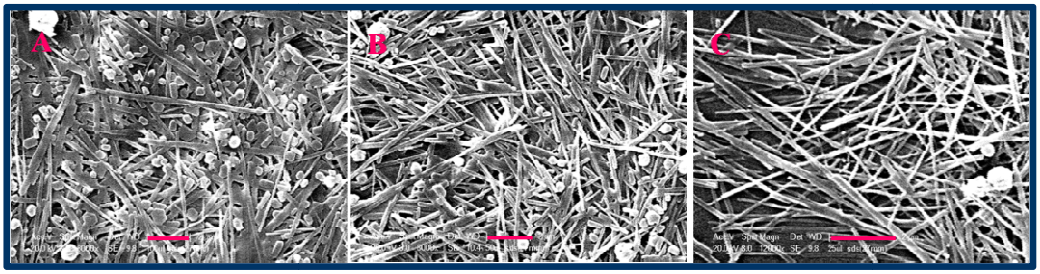

Fig. 4.15. SEM images of 100 µl (A), 50 µl (B) and 25 µl (C) colloids obtained in the presence of SDS (0.5 mM) by injecting a high concentration (27 mM) of ADMA/THF. Scale bars are 2 µm.

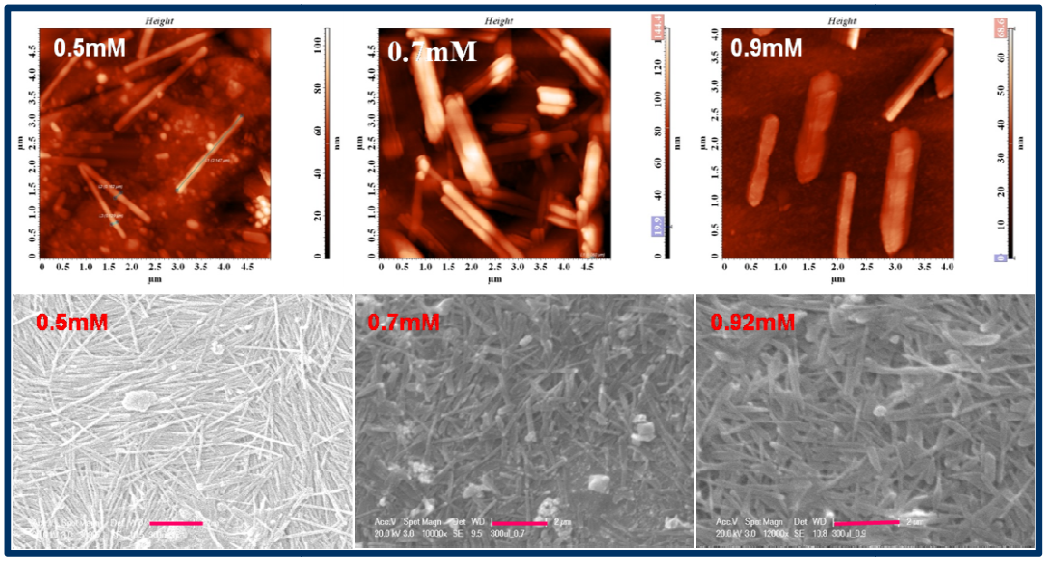

Fig. 4.16. Atomic force microscope (above) and scanning electron microscope (below) images of 300 µl (2 mM ADMA/THF) in presence of 0.5, 0.7, 0.92 mM CTAB/water. Scale bars are 2 µm.

4.5. Effect of other additives

We have also studied the influence of a polymer (PVA), an electrolyte (NaCl), an ionic salt ([BMIM][Cl]) and a room temperature ionic liquid ([BMIM][BF_4]) on the morphology of the aggregates (Fig. 4.17). Interestingly, none of these additives help formation of well-defined morphologies like those obtained in presence of the surfactants. In the presence of PVA, some scissor-shaped structures were formed. In the presence of [BMIM][Cl] and [BMIM][BF_4] spherical nanoparticles were observed. Ultra-long belts can be synthesized by a self assembly process in which one drop of 1 mM ADMA solution in ethylacetate is placed onto a cleaned glass slide and the solvent is allowed to evaporate (Fig. 4.18). On the other hand, under similar experimental condition, a hexane solution of ADMA gave relatively smaller size nanoplate and rod-like morphologies (Fig. 4.18). This difference can perhaps be explained considering the different vaporization rate of the two solvents. Rapid vaporization of hexane does not allow the formation of ultra-long belts. The absorption and fluorescence properties of these aggregates are found to be quite similar to those obtained in surfactant solutions.

4.6. Possible mechanism for the growth of the nanostructures

In the absence of surfactant, ADMA generally forms irregular particles having no definite shape and whose sizes vary between 200-500 nm (Fig. 4.19.). Under some specific conditions, however, rods and plates can also be observed along with the shapeless particles. Unlike those prepared earlier in DMSO/water,[20] the colloids prepared in THF/water without any surfactant are not stable beyond 2-3 days. Interestingly, most of the stable nanostructures reported here are obtained only in the presence of surfactants, not with the other additives. A surfactant can influence the aggregation process in two possible ways. Depending upon the concentration, the surfactant can self-assemble into

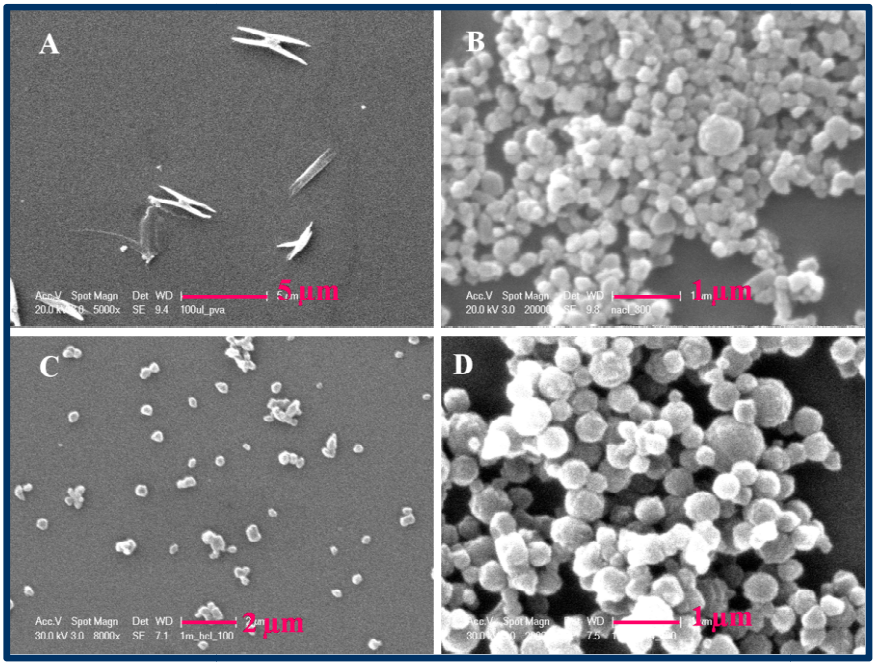

Fig. 4.17. SEM images of the nanostructures obtained in the presence of (A) PVA (B) NaCl (C) [BMIM][Cl] and (D) [BMIM][BF_4].

micellar aggregates and provide physical templates for aggregation of nanoparticles.[54-56] Using these soft micelle templates organic molecular 1D nanostructructures have been previously synthesized.[48-51] However, we do not consider this to be the case here as the surfactant concentrations used in most of the present experiments are lower than the CMC of the micelles. The role of the surfactant is clearly not to provide a template for aggregation, but to act as a stabilizer,[57-60] where it serves mainly as an aggregation preventer by attaching itself with the aggregate and then providing a layer around the aggregate. The surfactant also plays a crucial role as crystal habit modifier,[61] by preferentially getting adsorbed to selected surfaces and hence promoting the growth of the other surfaces. The issue of how different morphologies of the aggregates are obtained under various conditions can perhaps be understood by considering the solvent

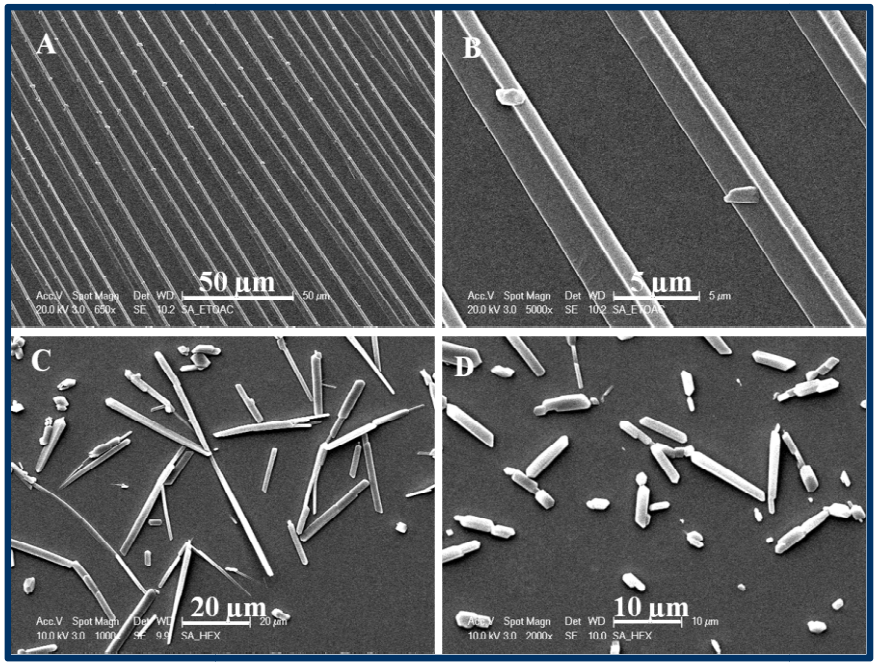

Fig. 4.18. SEM images of ultra-long belts and plates obtained on slow evaporation of ADMA/ethylacetate (2.7×10^{-6} M; A & B) and ADMA/hexane (2.7×10^{-6} M, C & D) on glass substrate.

composition or solubility of the molecule of interest at the time of the nucleation process, a mechanism formulated recently.[43] Essentially, a change of the solubility influences the super-saturation profile during the nucleation process and then the growth kinetics in different directions. The solvent composition can also influence the relative order of the surface energy when the surfactant molecules preferentially adsorb onto specific surfaces.[62] As the growth rate of a crystal surface is strongly dependent on the surface energy, one can expect differential growth rate of different surfaces leading to various morphologies.

In order to understand the formation of nanoparticles, we have monitored the growth process as function of time. Figure 4.20 shows the growth of the nanorod (100 µl of 2

mM THF solution to 10 ml of 0.5 mM CTAB) by depicting the TEM images were recorded at various stages of its growth. It is seen that 4 minutes after the injection, small particles with dimension 5-10 nm are formed. Interestingly, after 10 minutes, we observe partially grown nanorods and a little fraction of small particles. Fully grown nanrods also can be noticed, but their fraction is very small. These results suggest that small particles are the precursor of nanorods and with time these small particles combine to form rod-like morphology. The sample prepared after 20 minutes contains fully-grown nanorods.

In this growth process, the influence of the surfactants at the early stage is different from that at later stages. In the early stages, the surfactants modulate the solubility of the injected substance in the bad solvent (water). That in turn influences the nucleation of the particles, which is primarily driven by the hydrophobic nature of the molecular system and poor solubility in aqueous medium. The dipolar nature of the molecular system also helps in this nucleation process. The small nuclei then associate with each other to form larger rods through intermolecular interactions primarily driven by strong C-H…π interactions, which is indicated from single crystal X-ray studies.[20] Because of the directional nature of this interaction, the particles grow in one direction. The different shapes and long term stability of the particles can then be explained considering adsorption of the surfactant molecules onto the selective surfaces of the crystalline particles at later stages.

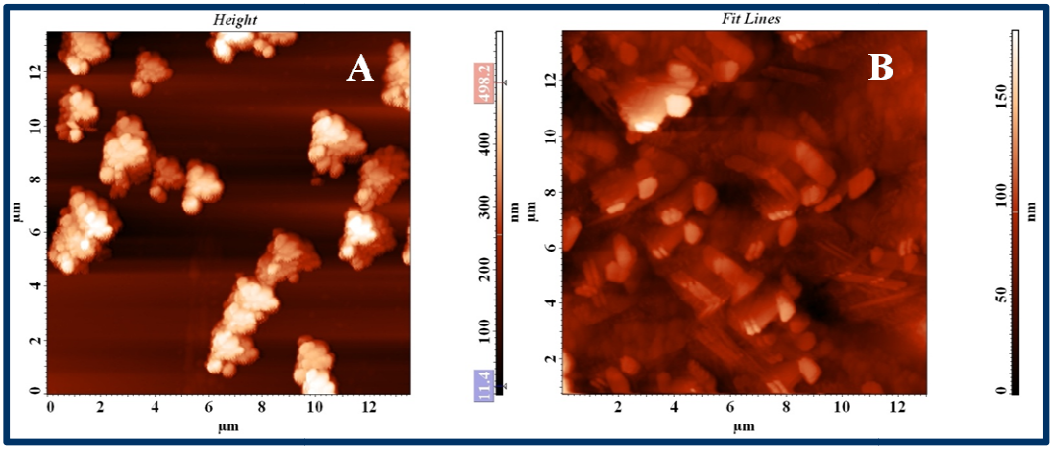

Fig. 4.19. Atomic force microscope images of 100 µl colloidal nanoparticles prepared in absence of surfactants by injecting 2.7 mM (A) and 2 mM (B) ADMA/THF solution into 10 ml of water.

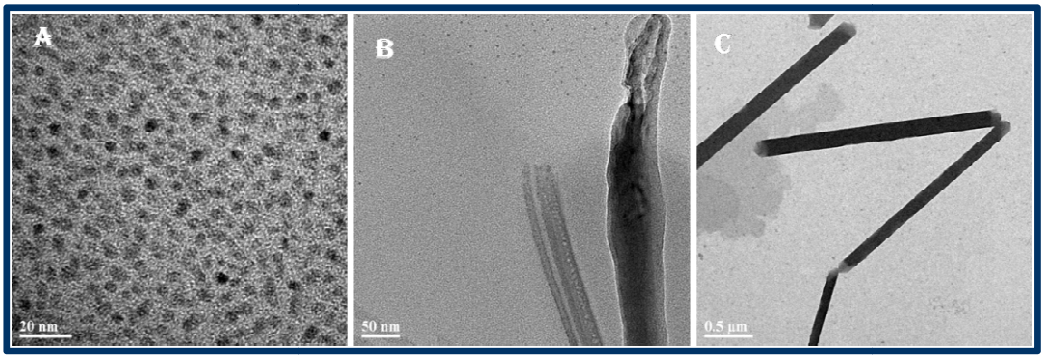

Fig. 4.20. Transmission electron microscope (TEM) images of nanorod growth process collected at 4 min (A), 10 min (B) and 20 min. (C).

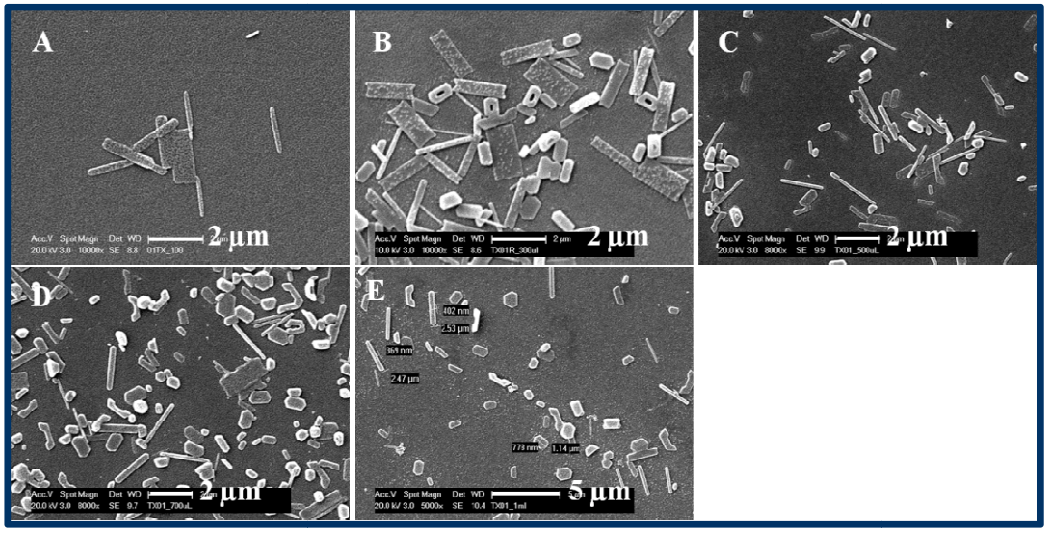

Fig. 4.21. SEM images of 100 µL (A), 300 µL (B), 500 µL (C), 700 µL and 1 mL (E) colloids prepared in the presence of 0.1 mM TX-100 solution.

4.7. Nonlinear optical properties

As size dependent nonlinear optical properties of the nano-/micro-particles are reported,[63] we considered measurement of the nonlinear optical response of these well-defined nanoparticles. However, our attempts of the measurement of the second harmonic generation ability of the aggregated structures by hyper Raleigh scattering studies were not successful mainly due to the highly fluorescent nature and broad absorption of these samples with the latter covering a large wavelength range that includes 532 nm (the 2nd harmonic of the excitation laser wavelength of 1064 nm). Semi-empirical Hatree-Fock level calculations reveal that the ADMA has polarizability (α) of 19.80 $\times 10^{-23}$ (e.s.u) and first hyperpolarizability (β) 3.19 $\times 10^{-30}$ (e.s.u). These nonlinear optical parameters values are reasonably high when compared to the push-pull stilbene and benzene derivatives.[64]

4.8. Conclusion

It is shown that the surfactants can be employed to tune the size and shape of the aggregates of the electron donor acceptor molecule, ADMA and it has indeed been possible to obtain a variety of morphologies for a single molecular system by controlling the experimental conditions and by capturing the different stages of the aggregation process, which allows study of the optical properties of these aggregates. It is suggested that the surfactants prevent the growth of certain surfaces by attaching onto them. Only those crystallographic surfaces grow, which do not show any affinity towards the surfactants. The fact that the fluorescence response of ADMA in the aggregated state is widely different from that in its molecular form is interesting and it widens the scope of this system in various fluorescence applications. Interestingly, even though the fluorescence response of ADMA in the molecular state is highly sensitive to the environment, its various aggregates of different shapes show properties that are remarkably similar. With variation of the size of aggregates some variation of the optical properties could however be observed. The high fluorescence quantum yield of ADMA in the aggregated state, which is attributed to the structural rigidity and unfavorable conformation of the two ring systems, also makes this system particularly attractive. Investigation on the growth process of the nanorods suggests that the C-H…π interaction is the leading driving force for the formation of various nano-/micro-structures. The FLIM studies have been used to distinguish particles with almost identical fluorescence intensity images. Moreover, using these measurements, it has even been possible to resolve the spatial heterogeneity of the individual particles.

References

(1) Briseno, A. L.; Mannsfeld, S. C. B.; Reese, C.; Hancock, J. M.; Xiong, Y.; A. Jenekhe, S. A.; Bao, Z.; Xia, Y. *Nano Lett.* **2007**, *7*, 2847.
(2) Che, Y.; Yang, X.; Loser, S.; Zang, L. *Nano Lett.* **2008**, *8*, 2219.
(3) Huang, Y.; Quan, B.; Wei, Z.; Liu, G.; Sun, L. *J. Phys. Chem. C* **2009**, *113*, 3929.
(4) Naddo, T.; Che, Y.; Zhang, W.; Balakrishnan, K.; Yang, X.; Yen, M.; Zhao, J.; Moore, J. S.; Zang, L. *J. Am.Chem.Soc* **2007**, *129*, 6978.
(5) Takazawa, K.; Kitahama, Y.; Kimura, Y.; Kido, G. *Nano Lett.* **2005**, *5*, 1293.
(6) Zhao, Y. S.; Xu, J.; Peng, A.; Fu, H.; Ma, Y.; Jiang, L.; Yao, J. *Angew. Chem., Int. Ed.* **2008**, *47*, 7301.
(7) O'Carroll, D.; Lieberwirth, I.; Redmond, G. *Nat. Nanotechnol.* **2007**, *2*, 180.
(8) Zhao, Y. S.; Peng, A.; Fu, H.; Ma, Y.; Yao, J. *Adv. Mater.* **2008**, *20*, 1661.
(9) Zhao, Y. S.; Fu, H.; Peng, A.; Ma, Y.; Liao, Q.; Yao, J. *Acc. Chem. Res.* **2010**, *43* 409.
(10) Zhao, Y. S.; Fu, H.; Peng, A.; Ma, Y.; Xiao, D.; Yao, J. *Adv. Mater.* **2008**, *20*, 2859.
(11) Chemla, D. S.; Zyss, J. *Optical Properties of Organic Molecules and Crystals*, Academic Press: New York.
(12) Fabbrizzi, L.; Poggi, A. *Chem. Soc. Rev.* **1995**, *24*, 197.
(13) Samanta, A. *J. Phys. Chem. Lett.* **2010**, *1*, 1557.
(14) Maeda, M. *Laser Dyes*, Academic Press: New York.
(15) Lakowicz, J. R. *Principles of Fluorescence Spectroscopy*, 2 ed.; Kluwer/Plenum Publishers: New York.
(16) Samanta, A. *Proc. Indian Natn. Aci. Acad.* **2003**, *69A*, 95.
(17) Zhang, X.; Xiaohong, Z.; Meng, X.; Shi, W.; Lee, C. S.; Lee, S. T. *Angew. Chem. Int. Ed.* **2007**, *46*, 1525.
(18) Patra, A.; Hebalkar, N.; Sreedhar, B.; Sarkar, M.; Samanta, A.; Radhakrishnan, T. P. *Small* **2006**, *2*, 650.
(19) Patra, A.; Anthony, S. P.; Radhakrishnan, T. P. *Adv. Fun. Mate.* **2007**, *17*, 2077.
(20) Kanaparthi, R. K.; Sarkar, M.; Samanta, A. *J. Phys. Chem. B* **2009**, *113*, 15189.
(21) Grabowski, Z. R.; Rotikeiwicz, K.; Rettig, W. *Chem. Rev.* **2003**, *103*, 3899.
(22) Herbich, J.; Kapturkiewicz, A. *Chem. Phy.* **1993**, *170*, 221.
(23) Kajimoto, O.; Hayami, S.; Shizuka, H. *Chem. Phys. Lett.* **1991**, *177*, 219.
(24) Chen, J.; Law, C. C. W.; Lam, J. W. Y.; Dong, Y.; Lo, S. M. F.; Williams, I. D.; Zhu, D. B.; Tang, B. Z. *Chem. Mater.* **2003**, *15*, 1535.
(25) Cox, A. J.; DeWeerd, A. J.; Linden, J. *Am. J. Phys.* **2002**, *70*, 620.
(26) Kasai, H.; Kamatani, H.; Okada, S.; Oikawa, H.; Matsuda, H.; Nakanishi, H. *Jpn. J. Appl. Phys.* **1996**, *35*, L221.
(27) Zhao, Y. S.; Xiao, D.; Yang, W.; Peng, A.; Yao, J. *Chem. Mater.* **2006**, *18*, 2302.
(28) Xiao, D.; Xi, L.; Yang, W.; Fu, H.; Shuai, Z.; Fang, Y.; Yao, J. *J. Am.Chem.Soc* **2003**, *125*, 6740.
(29) Fu, H.-B.; Yao, J. *J. Am. Chem. Soc. 2001, 123,* **2001**, *123*, 1434.
(30) Fu, H.; Loo, B.-H.; Xiao, D.; Xie, R.; Ji, X.; Yao , J.; Zhang, B.; Zhang, L. *Angew. Chem. Int. Ed.* **2002**, *41*, 962.

(31) Chang, Y. K.; Hsieh, H. H.; Pong, W. F.; Tsai, M.-H.; Chien, F. Z.; Tseng, P. K.; Chen, L. C.; Wang, T. Y.; Chen, K. H.; Bhusari, D. M.; Yang, J. R.; Lin, S. T. *Phys.Rev. Letters* **1999**, *82*, 5377.
(32) Hanamura, E. *Phys.Rev. B* **1988**, *37*, 1273.
(33) Bhongale, C. J.; Chang, C.-W.; Lee, C.-S.; Diau, E. W.-G. *J. Phys. Chem. B.* **2005**, *109*, 13472.
(34) Li, S.; He, L.; Xiong, F.; Li, Y.; Yang, G. *J. Phys. Chem. B.* **2004**, *108*, 10887.
(35) Oelkrug, D.; Tompert, A.; Gierschner, J.; Egelhaaf, H.-J.; Hanack, M.; Hohloch, M.; Steinhuber, E. *J. Phys. Chem. B.* **1998**, *102*, 1902.
(36) An, B. K.; Kwon, S. K.; Jung, S. D.; Park, S. Y. *J. Am. Chem. Soc.* **2002**, *124*, 14410.
(37) Jang, S.; Kim, S. G.; Jung, D.; Kwon, H.; Song, J.; Cho, S.; Ko, Y. C.; Sohn, H. *Bull. Korean. Chem. Soc.* **2006**, *27*, 1965.
(38) Kim, H.-J.; Lee, J.; Kim, T.-H.; Lee, T. S.; Kim, J. *Adv. Mater.* **2008**, *20*, 1117.
(39) Liu, Y.; Tao, X.; Wang, F.; Dang, X.; Zou, D.; Ren, Y.; Jiang, M. *J. Phys. Chem. C.* **2008**, *112*, 3975.
(40) Qian, Y.; Li, S.; Zhang, G.; Wang, Q.; Wang, S.; Xu, H.; Li, C.; Li, Y.; Yang, G. J. *J. Phys. Chem. B.* **2007**, *111*, 5861.
(41) An, B.-K.; Kwon, S.-K.; Park, S. Y. *Angew. Chem. Int. Ed.* **2007**, *46*, 1978.
(42) Lei, Y.; Liao, Q.; Fu, H.; Yao, J. *J. Am. Chem. Soc.* **2010**, *132*.
(43) Zhang, X.; Yuan, G.; Li, Q.; Wang, B.; Zhang, X.; Zhang, R.; Chang, J. C.; Lee, C.; Lee, S. *Chem. Mater.* **2008**, *20*, 6945.
(44) Zhang, X.; Zhang, X.; Wang, B.; Zhang, C.; Chang, J. C.; Lee, C.-S.; Lee, S.-T. *J. Phys. Chem. C* **2008**, *112*, 16264.
(45) Mattoussi, H.; Murata, H.; Merritt, C. D.; Iizumi, Y.; Kido, J.; Kafafi, Z. H. *J. Appl. Phys.* **1999**, *86*, 2642.
(46) Kasai, H.; Kamatani, H.; Yoshikawa, Y.; Okada, S.; Oikawa, H.; Watanabe, A.; Itoh, O.; Nakanishi, H. *Chem. Lett.* **1997**, 1181.
(47) Kalyanasundaram, K. *Photochemistry in microheterogeneous systems*; Academic Press: Orlando, 1987.
(48) Fu, H.; Xiao, D.; Yao, J.; Yang, G. *Angew. Chem. Int. Ed.* **2003**, *42*, 2883
(49) Hu, J.-S.; Guo, Y.-G.; Liang, H.-P.; Wan, L.-J.; Jiang, L. *J. Am. Chem. Soc.* **2005**, *127*, 17090.
(50) Jia, W.; ZuoLun, Z.; JunWei, Y.; JingYing, Z.; Yue, W. *Chinese Sci.Bull.* **2007**, *52*, 1307.
(51) Zhang, X.; Zhang, X.; Shi, W.; Meng, X.; Lee, C.; Lee, S. *J. Phys. Chem. B* **2005**, *109*, 18777.
(52) Chaudhuri, R. G.; Paria, S. *J. Colloid Interface Sci.* **2010**, *343*, 439.
(53) Sau, T. K.; Murphy, C. J. *Langmuir* **2005**, *21*, 2923.
(54) Andersson, M.; Pedersen, J. S.; Palmqvist, A. E. C. *Langmuir* **2005**, *21*.
(55) Petit, C.; Lixon, P.; Pileni, M.-P. *J. Phys. Chem.* **1993**, *97*.
(56) Setua, P.; Chakraborty, A.; Seth, D.; Bhatta, M. U.; Satyam, P. V.; Sarkar, N. *J. Phys. Chem. C* **2007**, *111*, 3901.

(57) Murphy, C. J.; Sau, T. K.; Gole, A. M.; Orendorff, C. J.; Gao, J.; Gou, L.; Hunyadi, S. E.; Li, T. *J. Phys. Chem. B* **2005**, *109*, 13857.
(58) Kuo, C.-H.; TChiang, T.-F.; Chen, L.-J.; M.H., H. H. *Langmuir* **2004**, *20*, 7820.
(59) Joseph, D.; Geckeler, K. E. *Langmuir* **2009**, *25*, 13224.
(60) Khanal, B. P.; Zubarev, E. R. *Angew. Chem. Int. Ed.* **2009**, *48*, 6888
(61) Jun, Y. W.; Choi, J. S.; Cheon, J. *Angew. Chem., Int. Ed.* **2006**, *45*, 3414.
(62) Sigman, M. B.; Jr. Ghezelbash, A.; Hanrath, T.; Saunders, A. E.; Lee, F.; Korgel, B. A. *J. Am. Chem. Soc.* **2003** *125*, 16050.
(63) Patra, A.; Venkatram, N.; Narayana Rao, D.; Radhakrishnan, T. P. *J. Phys. Chem. C* **2008**, *112*, 16269.
(64) Cbeng, L.-T.; Tam, W.; Stevenson, S. H.; Meredith, G. R. *J.Phys.Chem* **1991**, *95*, 10631.

Chapter 5

Multiple Morphologies of a Weakly Dipolar Molecule and their Optical Properties

In this chapter, we have probed the fabrication and luminescence properties of various nano/microstructures (rods, ribbons, tubes, rhombus crystals, hexagonal and rhombus plates) of an electron donor-acceptor molecule, 9-(4-cyanophenyl)carbazole (CPC). Nanoparticles with a wide variety of shapes have been fabricated from CPC merely by varying the solvent and temperature. The nano/microstructures of CPC are found to be fluorescent. They exhibit structured fluorescence with the emission peak position blue-shifted when compared with that in homogeneous tetrahydrofuran and acetonitrile solutions. Single crystal X-ray analysis and theoretical calculations have been carried out to identify supramolecular interactions and their impact on the nanocrystallization. The large shape diversity is attributed to the multiple modes of weak intermolecular interactions afforded by the molecule and the influences of solvent and temperature on growth kinetics.

5.1. Introduction

Inorganic and semiconductor nanoparticles have been the focus of extensive investigation because of their interesting optical, magnetic, electronic and thermoelectric properties, which are ideally suited for various applications.[1-3] However, nanomaterials based on small functional organic molecules have received much less attention even though these materials offer a number of advantages (such as ease of synthesis, tunable optical properties, high luminescence yield, etc) over most of their inorganic counterparts. In recent years, however, fluorescent organic nanomaterials have attracted considerable interest because of their exciting optoelectronic properties.[4,5] As these properties are often dependent on the size and shape (morphology) of the nanomaterials, and most of the applications require nanostructures with specific morphology, one of the major goals of current research has been the fabrication of nanoparticles of well-defined

morphology for specific applications. This explains the motive behind synthesis of one-dimensional (1D) fluorescent organic nanoparticles (rods, wires, tubes) for nanoscale device application as optical waveguides, chemical sensors, lasers and field-effect transistors.[4,5]

Organic molecules are commonly held together by weak van der Waals or hydrogen bonding forces in their aggregates state. As controlling the morphology of their nanoparticles requires manipulation of these forces and influencing the growth kinetics of the surfaces, it is important to understand the nature of intermolecular interactions that contributes to the morphology of the aggregated state. When it comes to the nanoparticles of organic molecules comprising electron donor and acceptor moieties, the dipolar interactions play the most important role during the early part of the nucleation process. These interactions often lead to 1D or semi-2D nanostructures unless specific template or additive is used to regulate the size and shape of the aggregate.[6,7] We attempt to explore whether it is possible to modulate the various intermolecular interactions to control the growth of nanoparticles in a desired manner. In order to accomplish this objective we realized that the molecular system should be such that its dipolar interaction with the solvents is not overwhelmingly larger than the other intermolecular interactions and the molecule should devoid of too many sites that can participate in relatively strong hydrogen bonding interaction. Considering these aspects, we have chosen N-(4-cyanophenyl)carbazole[8] (CPC, Chart 5.1), which is a weakly dipolar system (μ_g= 2.45 D)[8] comprising two nitrogen atoms and no other functional group to involve in strong intermolecular interactions. It is important to note that many molecular materials which contain carbazole moiety serve as hole (p-type) transporter in organic filed effect transistors (OTF).[9,10] In this chapter we demonstrate that a large variety of morphologies of the nanoparticles of this dipolar system can indeed be fabricated without using any physical template. Additionally, optical properties of these morphologies have been

studied by electronic absorption and steady state and time resolved fluorescence techniques.

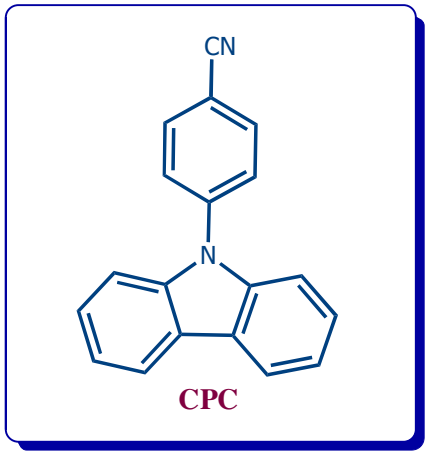

Chart 5.1. Molecular structure of N-(4-cyanophenyl)carbazole (CPC)

5.2. Fabrication of nano/microparticles

5.2.1. Fabrication at room temperature (RT, 22 °C)

Nano/microparticles of CPC were fabricated at room temperature by rapid mixing of two solvents. Different amounts of CPC in THF or ACN were injected into ultra-pure water under ultra-sonication, the latter continued for 2 more minutes after completion of injection. The samples were kept as such without disturbing for 45 minutes. During this period the solution became turbid indicating the formation of the nano/micro-aggregates. Further evidence of the nano/microaggregates formation was obtained from laser light scattering. When a red laser light passed through the colloidal solution and homogeneous CPC solution, only the colloidal solution scattered the laser light (Fig. 5.1), confirming the formation of aggregates. The aggregates which were prepared only under stirring (not under sonication) were subsequently analyzed with scanning electronic microscope

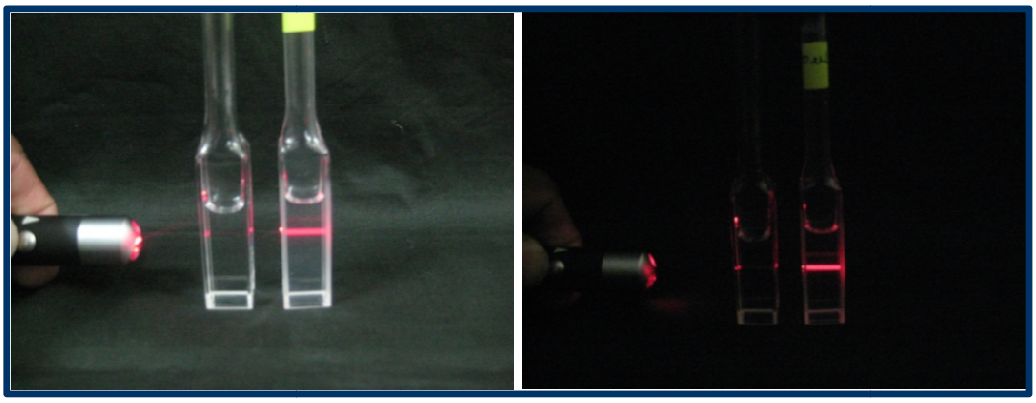

Fig. 5.1. Scattering of colloid in bright (left) and dark (right) environment. Homogeneous solution of CPC in ACN (left side cuvette) is also placed for the comparison with colloidal solution (right side cuvette) scattering.

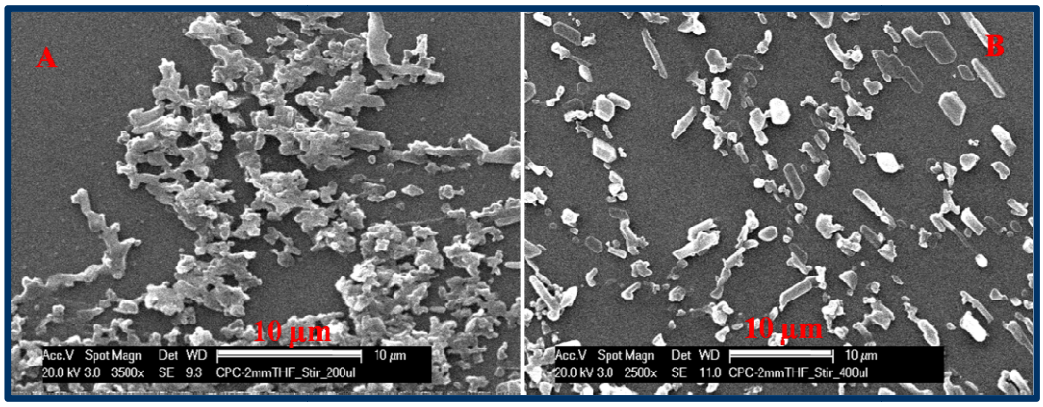

Fig. 5.2. SEM images of CPC colloids prepared at room temperature using 2 mM THF solution (A) 200 µL (B) 400 µL under vigorous *stirring*.

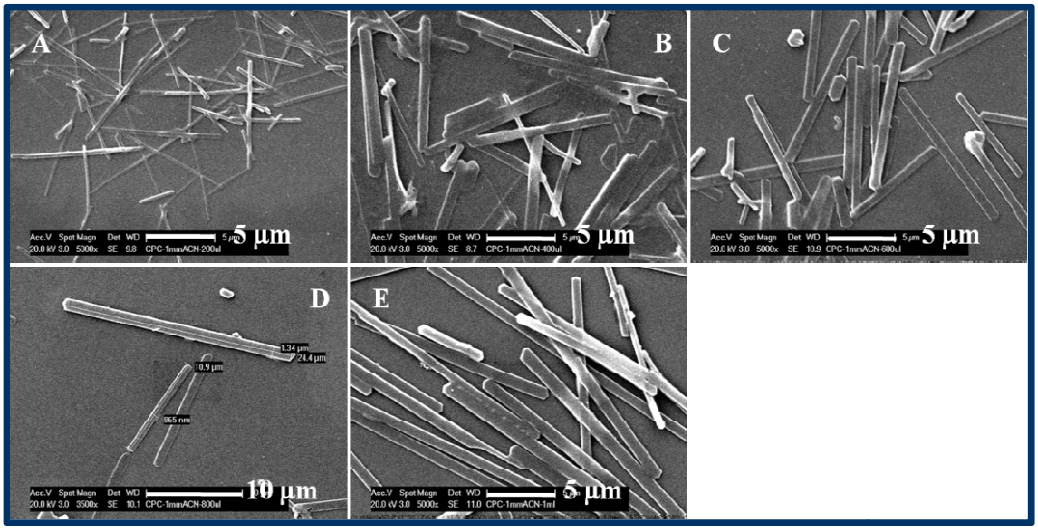

Fig. 5.3. SEM images of CPC colloids; 200 µL (A), 400 µL (B), 600 µL (C), 800 µL (D) and 1 mL (E) colloids prepared at room temperature by injecting 1 mM ACN solution to 10 mL of water under *ultra-sonication*.

(SEM) and found that these aggregates do not have any regular shape and size (Fig. 5.2). However, irrespective of the concentration of the CPC solution, well-defined morphologies of the particles were observed under ultra-sonication. Hence, further experiments were carried out with the aggregates obtained under ultra-sonication.

Figure 5.3 represents typical SEM images of self-assembled CPC nanostructures obtained by injecting different quantities (100 -1000 µL) of 1 mM ACN solution into 10 mL of water. These SEM images clearly suggest that the morphologies are strongly dependent on the amount of injected solution. Injection of a small quantity (200 µl) leads to rods formation, while larger quantities (400 µl, 600 µl, 800 µl and 1 ml) tend to form ribbon-like morphology. The sizes of the rods and ribbons can be varied by changing the stock solution. For example, under an identical condition (ultra-sonication, 10 mL water), 2 mM ACN solution, forms bigger size particles (figure 5.4). Interestingly, when 600 µL was injected, tubular morphology was noticed (Fig. 5.4).

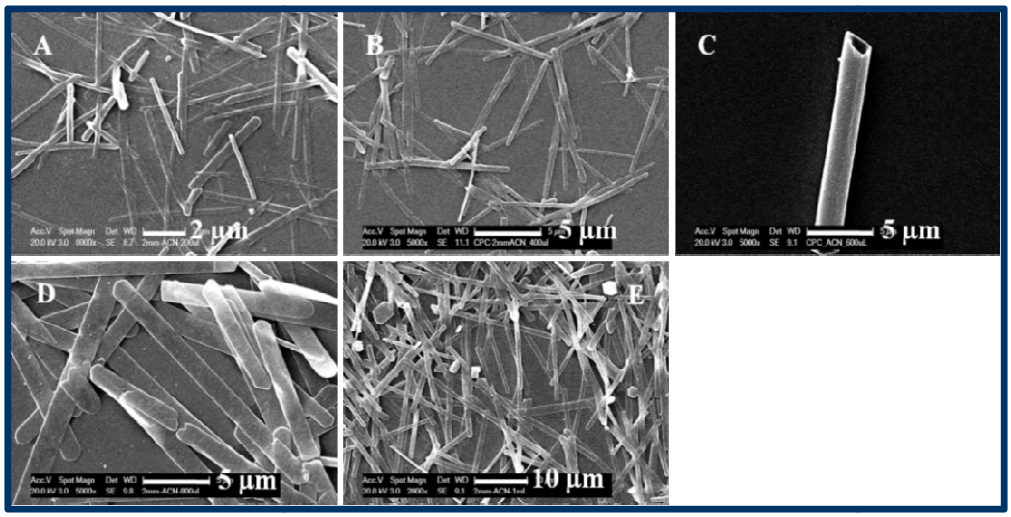

Fig. 5.4. SEM images of CPC colloids prepared at room temperature by injecting 200 µL (A), 400 µL (B), 600 µL (C), 800 µL (D) and 1 mL (E) of ACN solution (2 mM) to 10 mL of water.

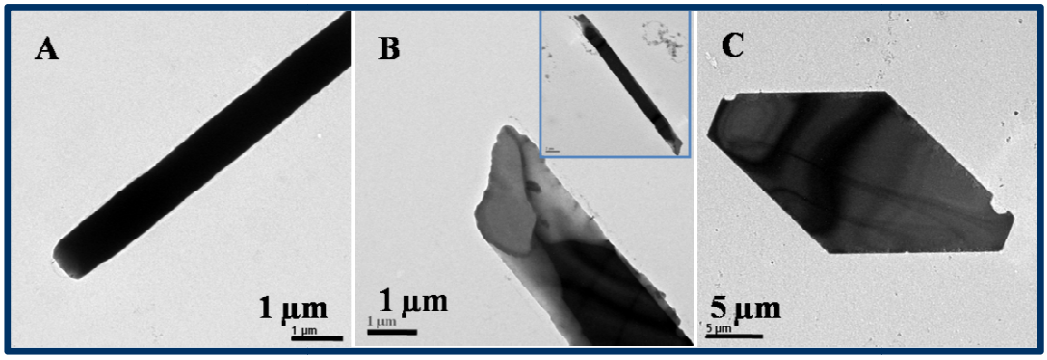

Fig. 5.5. TEM images of the ribbon (A), tube (B) and rhombus plate (C).

However, we were not successful in the reproduction of these interesting nanotubes. In most of these experiments we were ended up with ribbon-like morphology rather than

nanotubes. The ribbons obtained using 1 mM ACN solution were also confirmed by transmission electron microscope images (Fig. 5.5).

In many crystallization experiments, the solvent is used as crystal habit modifier.[11-15] Hence, THF solutions were also used keeping the other conditions (2 min. sonication, 10 mL water, 22°C) identical. The use of THF solutions led to the formation of very interesting 2D-nanoparticles (Fig. 5.6). As can be seen in the figure, using a small quantity (100 µL) of CPC stock solution, rhombus flakes along with a small fraction of rhombus crystals were obtained. When a larger amount of the stock solution (600 µL) is used hexagonal plates were obtained (Fig. 5.6). Notably, all these 2D plates are found to be monodispersed with micron dimensions and by changing the concentration of initial stock solution, the size of the particles could be tuned.

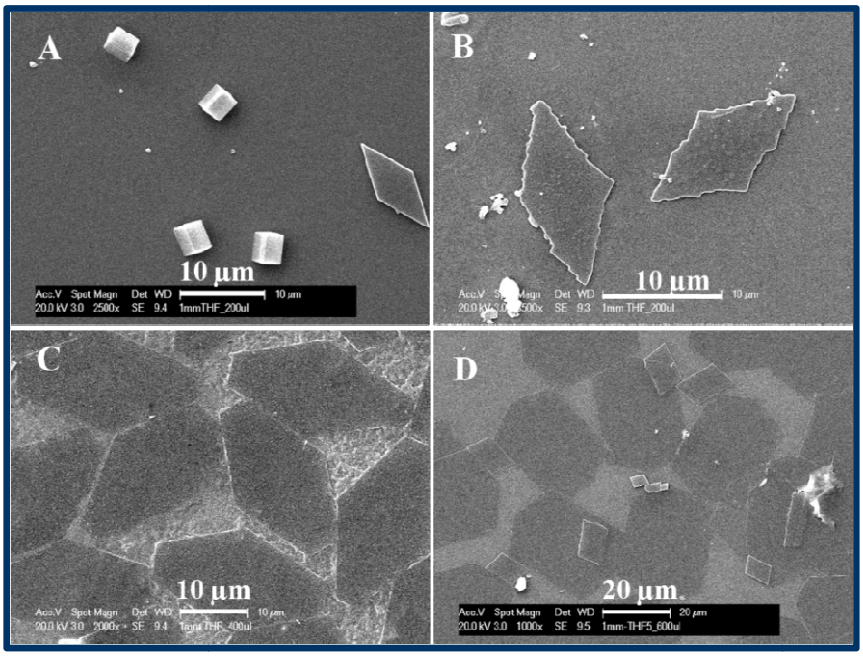

Fig. 5.6. SEM images of 100 µL (A), 200 µL (B), 400 µL (C) and 600 µL (D) CPC colloids prepared at room temperature by injecting 1mM THF solution to 10 mL of water.

5.2.2. Fabrication at low temperature (LT, 2-5 °C)

The morphologies of the CPC nanostructures found to be sensitive to the temperature at which they are fabricated. As shown in Fig. 5.4, the tubular morphology obtained at RT was not reproducible. However, when the reprecipitation experiment was carried out at 5 °C (under ultra-sonication) nearly monodisperse nanotubes are obtained in a reproducible manner. As shown in figure 5.7, when 100 µL (1 mM ACN) solution is injected to 10 mL of water, the rhombus crystals were formed with a small fraction of tubes. However, under identical conditions with increasing the quantity of the stock solution nearly monodispersed nanotubes were obtained and the particle size was

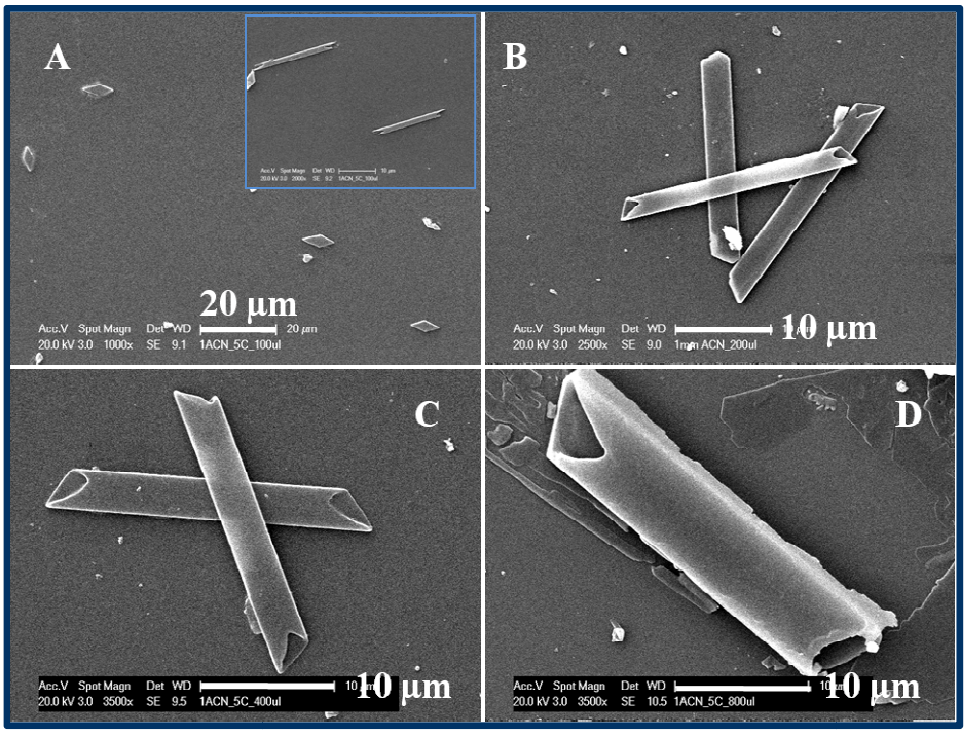

Fig. 5.7. SEM images of 100 µL (A) 200 µL (B), 400 µL (C) and 600 µL (D) CPC colloids prepared at 2-5 °C by injecting 1 mM, ACN solution to 10 mL of water.

found to increase with the amount of injected solution. On the other hand, more concentrated solution (2 mM) yielded mixed morphologies (Fig. 5.8). However, with 200 µL, highly monodispersed rhombus crystals were obtained. Thus the nanotubes and rhombus crystals, which could not be obtained at RT, in a reproducible manner, are generated at LT without any difficulty. Few molecules are known to give tubular morphology and among them the number of dipolar molecules that forms nano-/micro-tubes without using any hard or soft template is very few.[7,16] As the tubular morphology is known to be useful for the light waveguiding property,[17] the nanotube formation and their size-control would be an interesting feature of the present system for practical application.

On the other hand, when THF solutions are injected (instead of ACN solutions) under identical conditions the temperature hardly has any influence on the morphology of the nanostrcutures (Fig. 5.9). When 200 µL solution is injected the rhombus crystals are formed which turn to 2D rhombus plates with the addition of 400 µL. Higher quantities (600 µL, 800 µL and 1 mL) lead to the formation of hexagonal plates Fig. 5.9. Similar results are observed with the higher concentration (2 mM) of the stock solution (Fig. 5.10). Rod, plate and tubular natures are confirmed by the TEM images (Fig. 5.5). One open end of the tube is shown in the inset, to highlight the hollow nature of the nanotube.

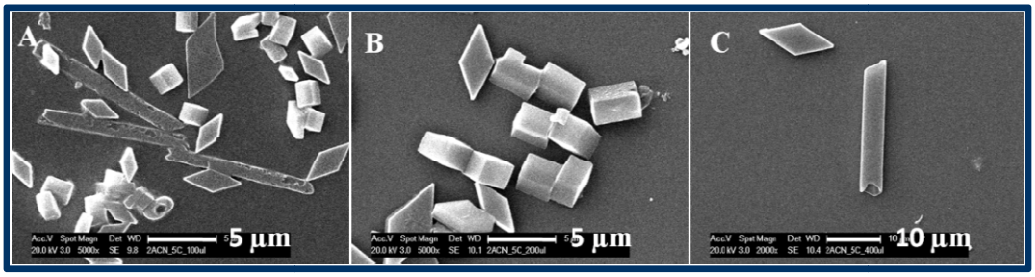

Fig. 5.8. SEM images of 100 µL (A) 200 µL (B), 400 µL (C) CPC colloids prepared at LT by injecting 2 mM ACN solution to 10 mL of water.

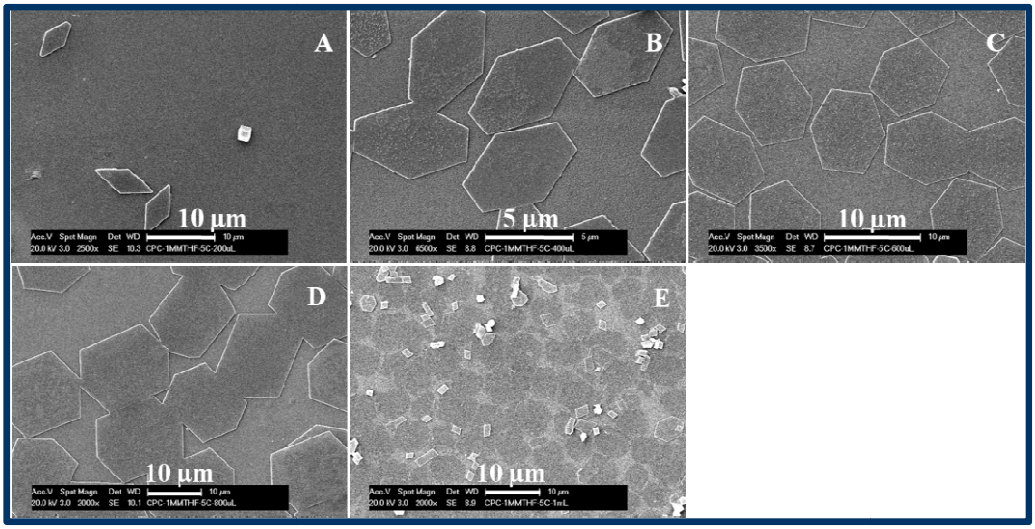

Fig. 5.9. SEM images of 200 µL (A), 400 µL (B), 600 µL (C), 800 µL (D) and 1mL (C) colloids prepared by injecting 1mM THF solution to 10 mL of water at 2-5 °C.

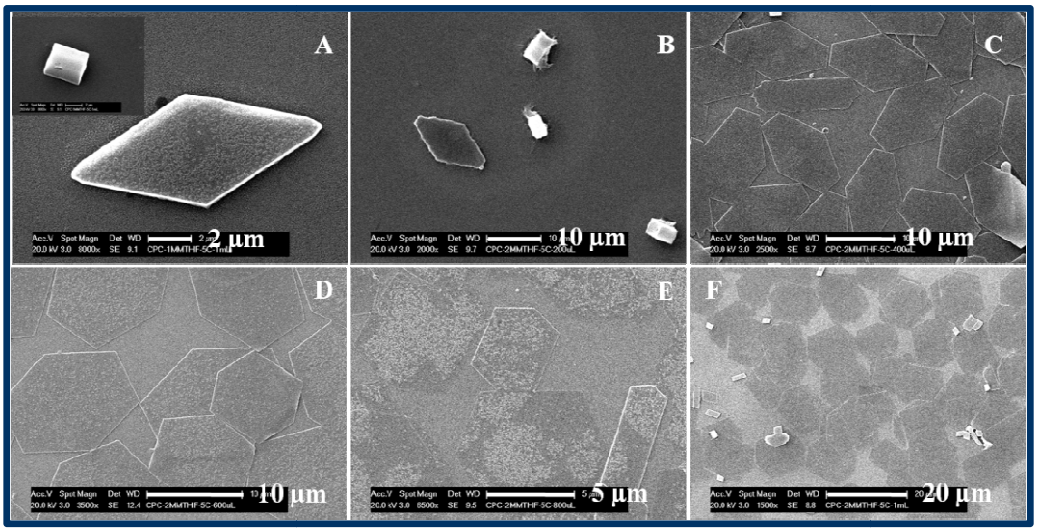

Fig. 5.10. SEM images of 100 µL (A), 200 µL (B), 400 µL (C), 600 µL (D), 800 µL (E) and 1mL (F) colloids prepared at low temperature (2-5 °C) by injecting 2mM THF solution to 10 mL of water.

5.3. Steady-state absorption and fluorescence

Figure 5.11 depicts the absorption and fluorescence spectra of CPC in three solvents of different polarities. The spectral data of the system is consistent with the literature.[18,19] As can be seen in figure, the electronic absorption spectrum of CPC which is characterized by two bands, is not sensitive to the polarity of the medium.

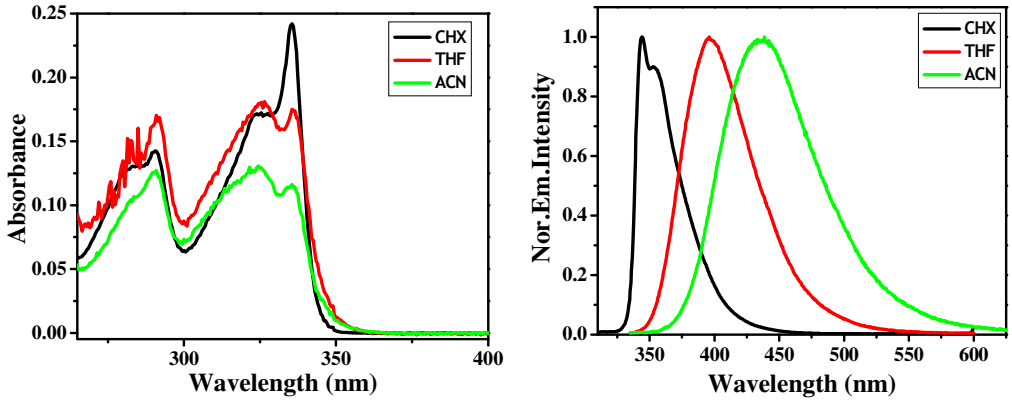

Fig. 5.11. Absorption and fluorescence spectra of CPC in cyclohexane (CHX), tetrahydrofuran (THF) and acetonitrile (ACN).

The fluorescence spectrum of CPC is characterized by a single band. In nonpolar solvents like, cyclohexane the fluorescence is somewhat structured emission (Fig. 5.11). With increasing the polarity of the medium, the emission band loses its vibrational structure and shifts towards longer wavelength (Fig. 5.11). In ACN, the emission band is centered at 435 nm and the full width at half maxima (FWHM) is 4300 cm^{-1}, which is typical for emission from the twisted intramolecular charge transfer (TICT) states.[18] Even though the emitting state of CPC was assigned to a TICT state, on the basis of time-resolved microwave dielectric loss studies the dipole moment of the emitting state was found to be low and hence, the emitting state was assigned to LE character even in polar solvents.[8] In a much recent work, Zachariasse and coworkers assigned CT character to

the emitting state.[20] According to them, the LE state is not observable for CPC for two reasons; (i) very fast CT reaction rate compared to the radiative rate of the LE state, (ii) direct excitation of CT state from the S_0 ground state, bypassing LE.

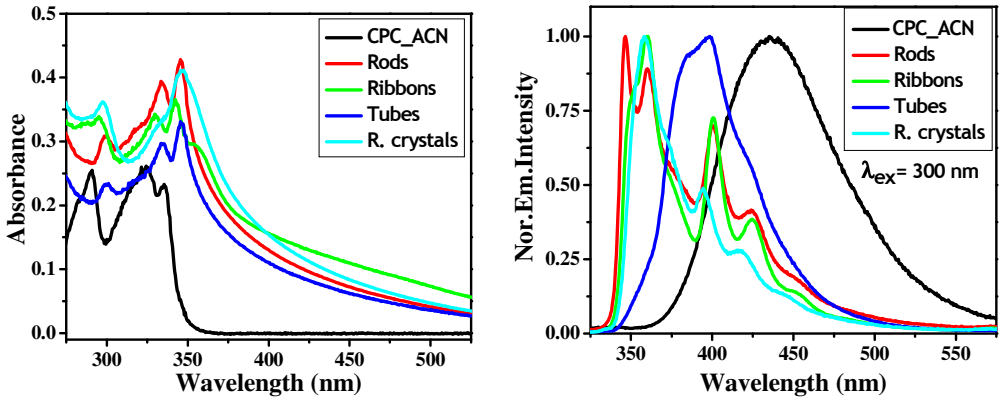

Figure 5.12. Absorption and fluorescence emission behavior of CPC nanostructures prepared using ACN solutions.

Figure 5.12 compares the absorption and fluorescence emission spectra of some of the nanostructures with that of the molecule in homogeneous solution. One can easily notice that the spectral behavior of nanostructures is distinctly different from that of the molecular form. While the absorbance due to molecular form is negligible beyond 350 nm, the absorption due to the nanoparticles extended up to ~ 600 nm. This is a reflection of strong intermolecular interactions in the mesoscopic regime,[21,22] the major contribution of which comes from the dipole-dipole interaction. The broad absorption with long tail is clearly due to the presence of various nanostructures with different energies and progressive rise of the baseline in the longer wavelength region with decrease of wavelength is due to Mie scattering effect.[23,24] A sharp absorption band due to the aggregates was observed at longer wavelength region centered at ~345 nm. The main absorption band of the nanostructures is red-shifted compared to the homogeneous ACN

solution of CPC. The red-shift suggests that these are J-type aggregates. The absorption spectra of 2D-nanoparticles (rhombus and hexagonal plates) are found to be distinctly different from the 1D-nanoparticles (Fig. 5.13). This is however not surprising as energetics of the aggregates are expected to depend on the morphologies.

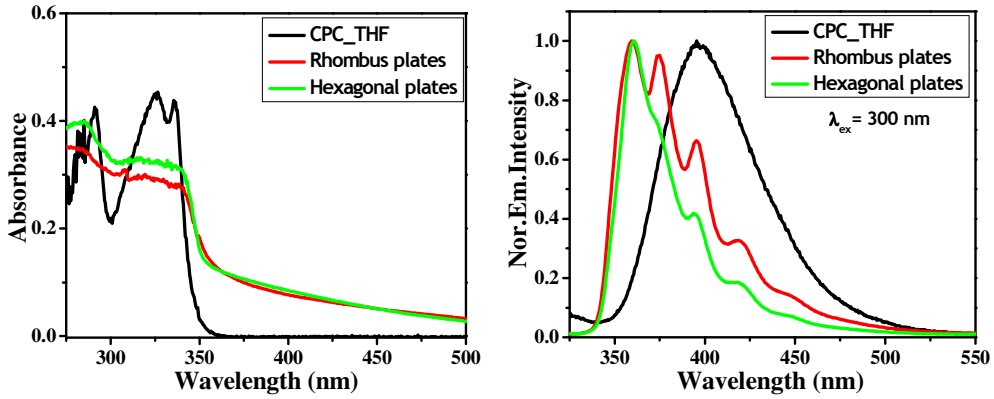

Fig. 5.13. Absorption and fluorescence emission behavior of CPC nanostructures prepared using THF solutions.

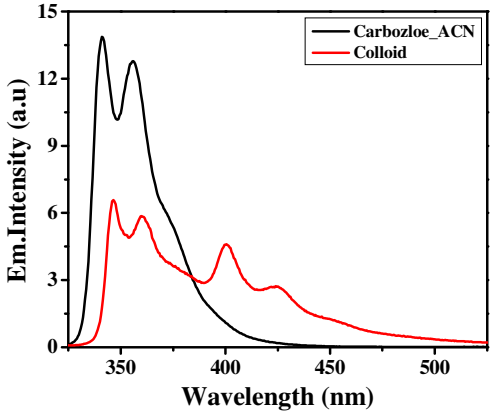

Fig. 5.14. Fluorescence spectrum of nano/microrods (red line) is compared with the fluorescence spectrum (black line) of carbazole in ACN.

The emission spectra of the nanostructures are blue-shifted compared to the fluorescence emission in homogeneous ACN/THF solution (Fig. 5.12 & 5.13). This vibrational structure of the emission band of the aggregates is presumably due to structural rigidification of molecule on the passage from its molecular form to microcrystal, as already seen in a few molecular systems.[22,25-27] Further evidence of this structural rigidification was obtained from the comparison of the spectral behavior of the aggregates with that of only carbazole molecule in neat ACN (Fig. 5.14). The emission spectrum of carbazole matches with the left part (325-375 nm) of the nanostructures emission, indicating that the carbazole moiety of CPC is decoupled from the benzonitrile moiety in the nanostructures. However, the longer wavelength region of the emission (375-525 nm) of the nanostructures, which is absent in homogeneous solution, suggests that this portion of the emission arises from the intermolecular interactions due to the close proximity of the molecules in the nanostructures. Although the absorption spectra of rods, ribbons and tubes look similar, fluorescence emission spectrum due to the nanotubes differs from the others (figure. 5.12).

Laser scanning confocal fluorescence microscope images of some of the nanostructures are collected in figure 5.15. As can be seen, all the nanoparticles give blue fluorescence, suggesting that the fluorescence emission in colloidal state is indeed due to the nano/microstructures, not from the CPC monomers.

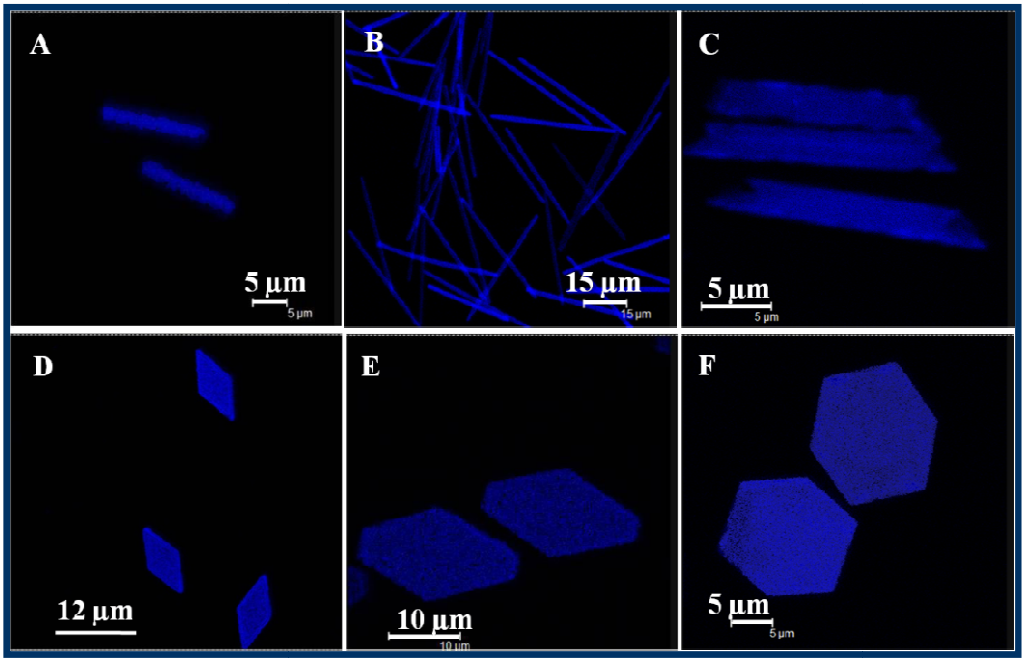

Fig. 5.15. Laser scanning confocal fluorescence microscope images of the rods (A), ribbons (B), tubes (C), rhombus plates (D) & (E) and hexagonal plate (F).

5.4. Fluorescence lifetime imaging microscope (FLIM) study

The excited state lifetimes of CPC monomers and its colloidal solutions were measured by recording the fluorescence decay profiles using time-correlated single photon counting (TCSPC) setup, by exciting the samples with a diode laser (331 nm). Typical decay profiles of CPC in two solvents (ACN and THF) along with their single-exponential fits are shown in figure 5.16. In homogeneous solutions, CPC has fairly long lifetimes (Fig. 5.16).[8] The decay profiles of the nanostructures are found to be bi-exponential. The fluorescence decay parameters along with the average lifetimes are collected in Table 5.1. As can be seen, the average lifetimes of the nanoparticles are much longer than those in its homogeneous solution. In the solid state or colloidal state, because of the enhanced intermolecular interactions, the nonradiative rate increases thus

decreasing the fluorescence lifetime.[28-30] The lifetimes of free standing nanoparticles (individual) were also measured with a picoseconds time-resolved fluorescence lifetime imaging microscope (FLIM), which gives spatially resolved fluorescence intensity images and fluorescence lifetime images (Fig. 5.17) constructed from the lifetimes of individual particles (Table 5.1). Notably, free standing nanoparticles possess much higher lifetime than the nanoparticles in solution.

Table 5.1. Fluorescence decay parameters of CPC in solution and different nanostructures

Sample	τ_1	τ_2	χ^2	τ_{avg} (ns)	
				TCSPC	FLIM
THF	6.16	-	1.11	-	-
ACN	7.66	-	1.04	-	-
Rod	0.33 (0.41)	1.35 (0.59)	1.28	0.97	4.50
Ribbon	0.55 (0.29)	2.06 (0.71)	1.26	1.58	4.02
Tube	0.46 (0.17)	1.93 (0.83)	1.23	1.68	4.18
Rhombus plate	0.59 (0.26)	1.72 (0.74)	1.18	1.42	3.82
Hexagonal plate	0.82 (0.32)	2.03 (0.67)	1.14	1.63	3.65
Rhombus crystal	0.54 (0.33)	2.22 (0.67)	1.51	1.67	4.06

The quantities in the parenthesis indicate relative amplitudes

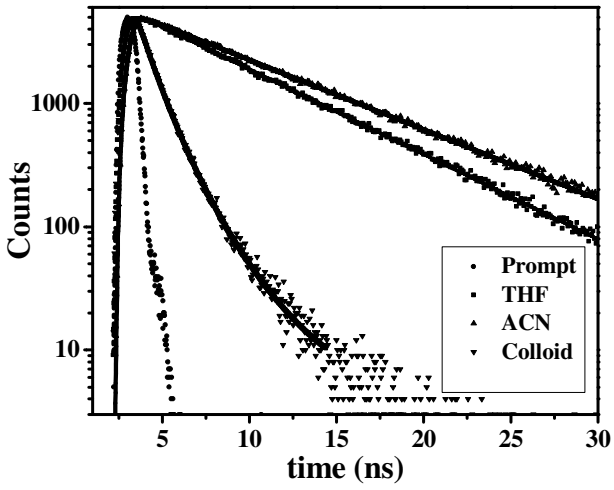

Fig. 5.16. Fluorescence decay behavior of CPC in ACN and THF and in colloidal state.

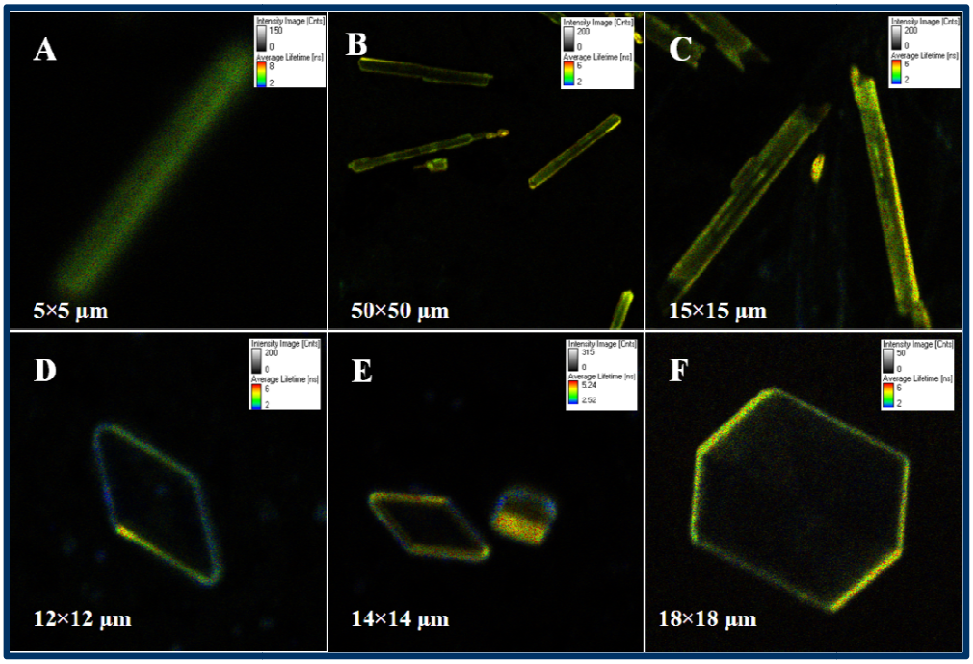

Fig. 5.17. FLIM images of rods (A), ribbons (B), tubes (C), rhombus plates (D), rhombus crystals (E) and hexagonal plates (F).

As the FLIM sample preparation involves drying of the solvent under high vacuum, the solvent interaction with the aggregates is eliminated in these measurements. Perhaps this contributes to a longer lifetime of these species.

5.5. Crystal Structure and theoretical calculations

The formation of 1D and 2D-nanostructures on changing the injected solution is quite interesting, especially for the EDA molecules, where the aggregation process is primarily driven by strong dipolar interactions. In order to find out the origin of such large morphology diversity, we examine the interactions involved in the aggregation of the molecular system, from the crystal packing diagram of the molecule.[31] As the two aromatic ring systems are twisted by 45.7° they are not electronically decoupled completely. The packing diagram reveals both parallel head-to-tail dimer motifs (J-type interaction)[32] in which the two individual dipoles are stabilized by *weak* C-H…π interaction (3.03 Å, J1-dimer, Fig 5.18) and anti-parallel motifs (H-type interaction),[32] which are stabilized by relatively *strong* C-H…π (2.67 Å, H-dimer, Fig.5.18) and non-classical C-H…N H-bonding (2.54 Å, J2-dimer, Fig.5.18) interactions. We think these intermolecular interactions are operational at the mesoscopic regime and responsible for the formation of nanoparticles. As the strongest interaction is along the a-axis, the crystal and nanostructures are expected to grow in this direction. However, one must not ignore the remaining interactions, which contribute to the growth of the nanostructures in other directions giving 2D or 3D morphologies depending on the situation.

Additional insight into the formation of the nanostructures can be obtained from the energetics of the supramolecular motifs. Molecular motifs (dimer, trimer, tetramer etc.) identified in the single crystal X-ray analysis were modelled (*vide* section 2.9) to understand energetics of the motifs, thus the nano/microparticles. *Ab-initio* calculations (single point energy) of each motif were performed and the obtained energies are

tabulated in Table 5.2. An increase in the number of the molecules in a motif increases the total energy, which, however, is lower than the sum energy of the molecules. This finding is indicative of increasing cooperative binding interactions with the number of molecules in the crystal lattice. The stabilization/binding (E_s) energies have been

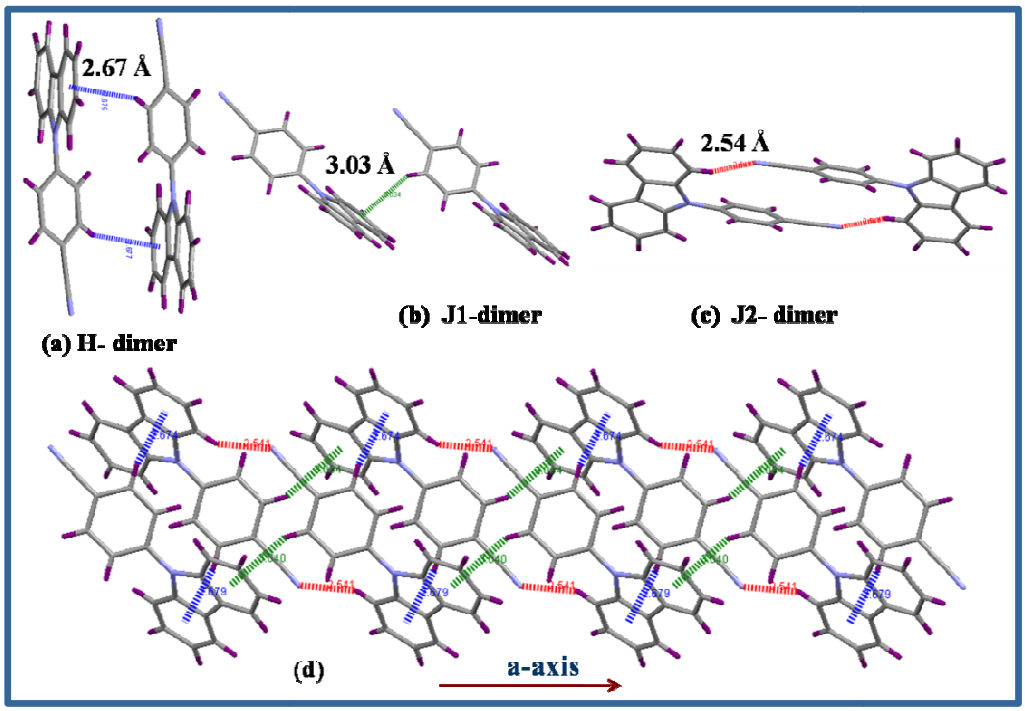

Fig. 5.18. Supramolecular interactions identified in the CPC crystal and the molecular arrangement driven by these interactions.

calculated from the computed total energies of the motifs (*vide* section 2.9). A plot of the binding energy versus the number of molecules involved in the motifs is shown in Fig. 5.19. Motifs which are associated with the C-H…N intermolecular interactions (J2) are more stable compared to the others. The highest stabilization energy of the J2-dimer is

perhaps a reflection of the strong interaction due to the short distance (2.54 Å) between the interacting atoms compared to the others. A plot of stabilization energy against 1/N is shown in Fig. 5.19. The stabilization energy for infinite lattice, estimated from this plot by extrapolating the fitted data to 1/N = 0, is 1.97 kCal mol^{-1}. Considering the stabilization energies of these aggregates, it appears that the J2-dimers are the main building blocks of the observed nanostructures.

Table 5.2. Computed energies (B3LYP/6-31+G*) of the CPC molecule and the motifs

CPC molecule/ Motif		Energy (eV)	E_S (kCal mol^{-1})
Molecule	-	-22870.5266	-
H-Aggregate	Dimer	-45741.0810	-0.32
	Tetramer	-91482.2259	-0.68
	Hexamer	-137223.0801	-0.74
J1-Aggregate	Dimer	-45741.0417	0.131
	Tetramer	-91482.1226	-0.094
	Hexamer	-137223.2171	-0.221
J2-Aggregate	Dimer	-45741.1595	-1.22
	Tetramer	-91482.3485	-1.40
	Hexamer	-137223.5843	-1.63

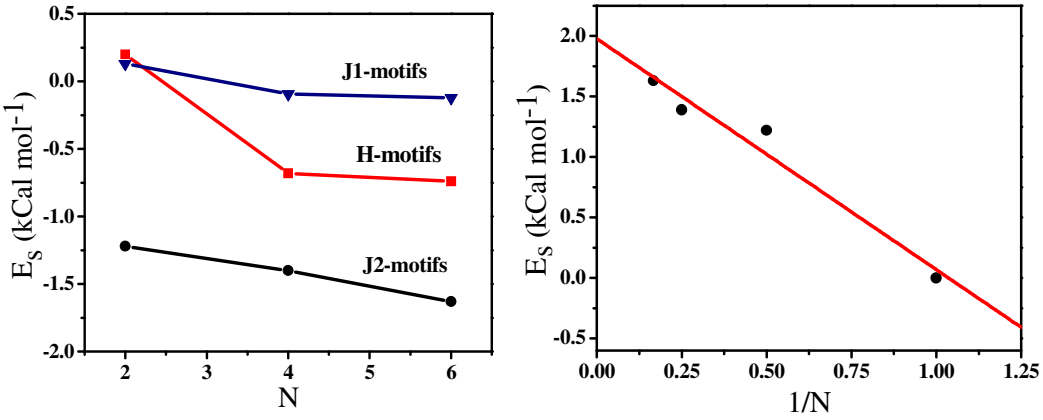

Fig. 5.19. (a) Stabilization energy (E_s) of the different motifs (dimer, tetramer and hexamer) against the number of molecules (N) involved. (b) Plot of E_s versus 1/N. The fitted line is extrapolated to find out E_s for the infinite lattice.

5.6. Mechanism for the formation of nanoparticles

We note that a change of solvent affects the solubility of a molecule, which influences the degree of its supersaturation and the relative velocities of nucleation. These two parameters influence the growth/inhibition of different crystallographic surfaces in different directions giving various morphologies. The morphology can also be influenced if the solvent interacts with specific surfaces; which happens in some cases.[12,33-38] Considering these fundamentals, we propose a mechanism for the formation of the various morphologies observed with CPC. As illustrated in the following Scheme, the building blocks of the nanostructures, which are obtained from the intermolecular interactions, can arrange either in 1D or 2D fashion depending on the solubility in mixed solvent system (water/THF and water/ACN). As ACN is more polar than THF, the solubility of CPC in the two solvents is very different. This solubility difference, which affects the supersaturation profile during the nucleation process and consequently, the growth kinetics in different directions, explains the formation of nanorods and

nanoribbons in ACN and 2D plates in THF. The solubility is indeed a major factor in determining the morphology, is evident from the fact that when the solubility is changed by varying the temperature instead of the solvent, similar dramatic changes in the morphology (*i.e.* rods/ribbons to tubes) is observed in ACN. However, with the THF solution, we did not observe such difference on changing the temperature presumably due to the fact that the dielectric constant of THF is not sensitive with temperature as that of ACN[39] and hence, the solubility of CPC at different temperatures is not very different.

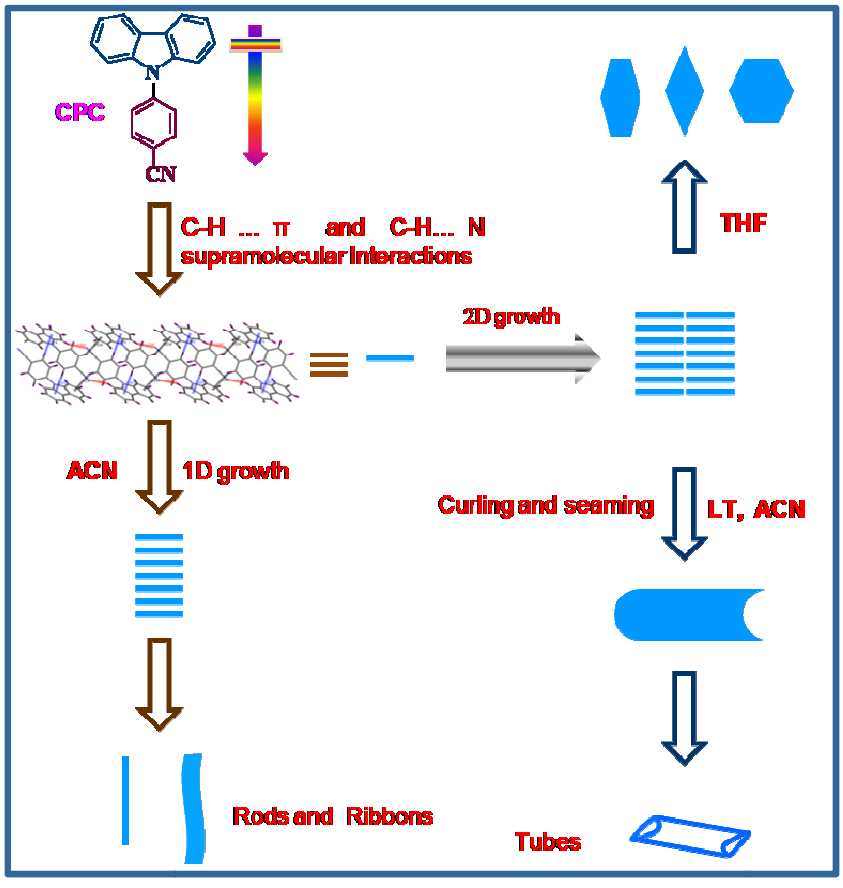

SCHEME

SEM images of the nanotubes collected after 10 minutes of growth clearly shows the presence of partially grown tubes in addition to the fully grown tubes indicating that the sheets or flakes roll into seamless tubes (Fig. 5.20), because such transformation lowers the high surface energy of the sheets/plates.[7,16]

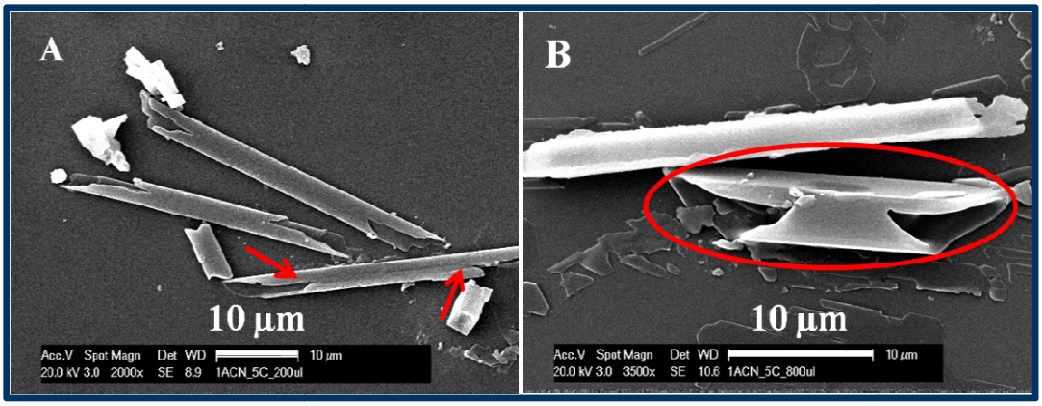

Fig. 5.20. SEM images of the nanotubes collected during its growth (10 minutes after injecting the 1 mM ACN solution).

5.7. Conclusion

In summary, it is shown that the weak supramolecular interactions and solubility of a dipolar molecule can be modulated by suitably changing the solvent and/or temperature to obtain a wide variety of nanostructures of the same molecular system without using any template or additive. The diversity of the nanostructures of CPC coupled with its fluorescent nature makes it an ideal system for practical applications, some of which are currently being explored.

References

(1) Hu, J.; Li, L.-S.; Yang, W.; Manna, L.; Wang, L.-W.; Alivisatos, A. P. *Science* **2001**, *292*, 2060
(2) Heath, J. M. *Acc. Chem. Res.* **1999**, *32 (Nanoscale materials special issue)*, 387.
(3) Alivisatos, A. P. *Science* **1996**, *271*, 933.
(4) Kim, F. S.; Ren, G.; Jenekhe, S. A. *Chem. Mater.* **2011**, *23*, 682.
(5) Zhao, Y. S.; Fu, H.; Peng, A.; Ma, Y.; Liao, Q.; Yao, J. *Acc. Chem. Res.* **2010**, *43*, 409.
(6) Zhang, X.; Zhang, X.; Wang, B.; Zhang, C.; Chang, J. C.; Lee, C.-S.; Lee, S.-T. *J. Phys. Chem. C* **2008**, *112*, 16264.
(7) Zhang, X.; Zhang, X.; Zou, K.; Lee, C.-S.; Lee, S.-T. *J. Am. Chem. Soc.* **2007**, *129*, 3527.
(8) Samanta, A.; Saha, S.; Fessenden, R. W. *J. Phys. Chem. A* **2001**, *105*, 5438.
(9) Shirota, Y. *J. Mater. Chem.* **2000**, *10*, 1.
(10) Li, J.; Liu, D.; Li, Y.; Lee, C. S.; Kwong, H. L.; Lee, S. *Chem. Mater.* **2005**, *17*, 1208.
(11) Das, K.; Panda, S. K.; Chaudhuri, S. *J. Crys.Growth* **2008**, *310*, 3792.
(12) Zhou, J.; Zhao, G.; Songb, B.; Hana, G. *Cryst.Eng.Comm.* **2011**, *13*, 2294.
(13) Zhu, G.; Liu, P.; Zhou, J.; Bian, X.; Wang, X.; Li, J.; Chen, B. *Mater.Lett.* **2008**, *62*, 2335.
(14) Kelly, R. C.; Rodrıguez-Hornedo, N. *Org.Process Res.Dev.* **2009**, *13*, 1291.
(15) Van der Heijden, A. E. D. M.; Geertman, R. M.; Bennema, P. *J. Phys. D: Appl. Phys.* **1991**, *24*, 123.
(16) Zhao, Y. S.; Yang, W.; Xiao, D.; Sheng, X.; Yang, X.; Shuai, Z.; Luo, Y.; Yao, J. *Chem. Mater.* **2005**, *17*, 6430.
(17) Zhao, Y. S.; Xu, J.; Peng, A.; Fu, H.; Ma, Y.; Jiang, L.; Yao, J. *Angew. Chem. Int. Ed.* **2008**, *47*, 7301
(18) Grabowski, Z. R.; Rotikeiwicz, K.; Rettig, W. *Chem. Rev.* **2003**, *103*, 3899.
(19) Rettig, W.; Zander, M. *Chem.Phys. Lett.* **1982**, *87*, 229.
(20) Galievsky, V. A.; Druzhinin, S. I.; Demeter, A.; Mayer, P.; Kovalenko, S. A.; Senyushkina, T. A.; Zachariasse, K. A. *J. Phys. Chem. A* **2010**, *114*, 12622.
(21) Chen, J.; Law, C. C. W.; Lam, J. W. Y.; Dong, Y.; Lo, S. M. F.; Williams, I. D.; Zhu, D. B.; Tang, B. Z. *Chem. Mater.* **2003**, *15*, 1535.
(22) Patra, A.; Hebalkar, N.; Sreedhar, B.; Sarkar, M.; Samanta, A.; Radhakrishnan, T. P. *Small* **2006**, *2*, 650.
(23) Cox, A. J.; DeWeerd, A. J.; Linden, J. *Am. J. Phys.* **2002**, *70*, 620.
(24) Kasai, H.; Kamatani, H.; Okada, S.; Oikawa, H.; Matsuda, H.; Nakanishi, H. *Jpn. J. Appl. Phys* **1996**, *35*, L221.
(25) Kanaparthi, R. K.; Sarkar, M.; Samanta, A. *J. Phys. Chem. B* **2009**, *113*, 15189.
(26) Kasai, H.; Kamatani, H.; Okada, S.; Oikawa, H.; Matsuda, H.; Nakanishi, H. *Jpn. J. Appl. Phys.* **1996**, *35*, L221.
(27) Kasai, H.; Kamatani, H.; Yoshikawa, Y.; Okada, S.; Oikawa, H.; Watanabe, A.; Itoh, O.; Nakanishi, H. *Chem. Lett.* **1997**, 1181.

(28) Bhongale, C. J.; Chang, C.-W.; Lee, C.-S.; Diau, E. W.-G. *J. Phys. Chem. B.* **2005**, *109*, 13472.
(29) Li, S.; He, L.; Xiong, F.; Li, Y.; Yang, G. *J. Phys. Chem. B.* **2004**, *108*, 10887.
(30) Turro, N. J. *Modern Molecular Photochemistry*, 1 ed.; Benjamin/ Cummings Publishing Company, Inc.: California, 1978.
(31) Saha, S.; Samanta, A. *Acta. Cryst. C* **1999**, *55*, 1299.
(32) Mishra, A.; Behera, R. K.; Behera, P. K.; B. K. Mishra; G. B. Behera. *Chem.Rev.* **2000**, *100*, 1973.
(33) Chung, H. R.; Kwon, H. E.; Oikawa, H.; Kasai, H.; Nakanishi, H. *J. Crys. Growth* **2006**, *294*, 459.
(34) Chung, H.-R.; Kwon, E.; Oikawa, H.; Kasai, H.; Nakanishi, H. *J.Cryst.Growth* **2006**, *294*, 459.
(35) Lucky, A. R.; Sui, R.; Lo, J. M. H.; Charpentier, P. A. *Cryst.Growth.Design* **2010**, *10*, 1598.
(36) Luo, Y.; Lin, J. *J. Colloid and Inter. Sci.* **2006**, *297*, 625.
(37) Stoica, C.; Verwer, P.; Meekes, H.; van Hoof, P. J. C. M.; Kaspersen, F. M.; Vlieg, E. *Cryst.Growth.Design* **2004**, *4*, 765.
(38) Zhang, X.; Yuan, G.; Li, Q.; Wang, B.; Zhang, X.; Zhang, R.; Chang, J. C.; Lee, C.; Lee, S. *Chem. Mater.* **2008**, *20*, 6945.
(39) Reichardt, C. *Solvents and Solvent Effects in Organic Chemistry*; Wiley-VCH: Weinheim, 1988; Vol. 3rd Ed.

Chapter 6

Self-Assembled 2-Dimensional Nano/microplates of a Fluorescent Molecule

Two structurally related anthracence derivatives, namely, 9,10-bis(4-cyanophenyl)anthracene (BCPA) and 9-(4-cyanophenyl)anthracene (CPA) have been synthesized and their optical properties studied. These systems exhibit very high fluorescence quantum yield in the homogeneous solutions. Aggregation of the systems has been probed in the absence and presence of additives. These investigations reveal that BCPA forms well-defined two-dimensional (2D) nanoplates while CPA gives aggregates with no well-defined shape. Photophysical properties of the BCPA nanoplates have been studied and compared to its homogeneous solution. These studies reveal that the optical properties of the nanoplates are significantly different from those of the molecular form of BCPA.

6.1. Introduction

Recently, highly ordered 2D or 3D hierarchical nanostructures have demonstrated as promising candidates for potential applications.[1-3] For example, self-organization of a fullerene derivative forms macroscopic globular flower-like objects (3D). Surfaces coated with these objects have been found to be superhydrophobic in nature and they act as non-wetting surfaces in micro/nano-electromechanical systems.[4] Li and coworkers reported highly ordered 3D micro/nanosized hierarchical structures of a simple intramolecular charge transfer (ICT) molecule.[5] On the other hand, 2D nanosheets (square and rhombus) of perylene have been fabricated by soft-template method and these can be used as 2D waveguides.[6] In a much recent work, rhombus and hexagonal plates of rubrene have been fabricated, which show morphology dependent waveguiding behavior.[7] However, compared to the low-dimensional architectures (0D and 1D), the 2D and 3D nanoparticles of small fluorescent organic functional molecules have not received much attention yet.

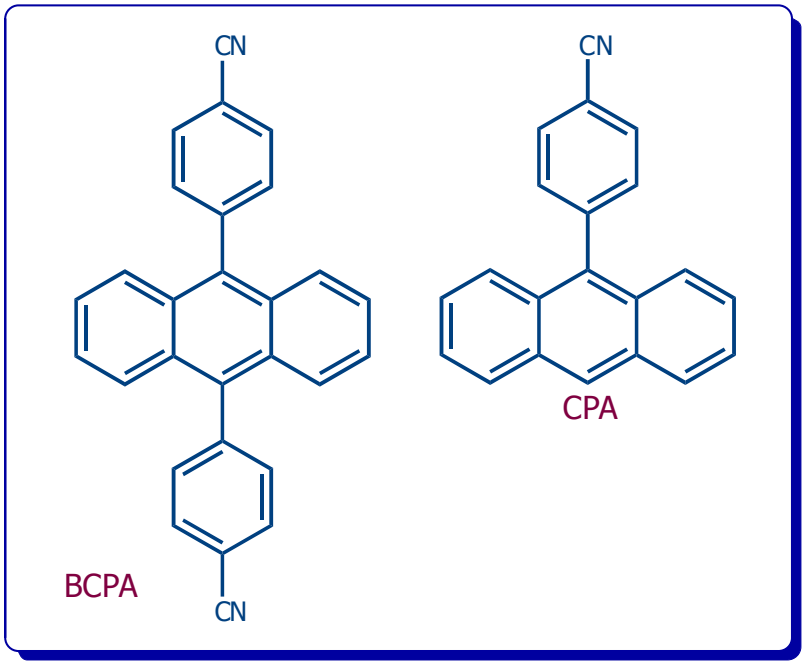

Chart 6.1 Molecular structure of 9,10-bis(4-cyanophenyl)anthracene (BCPA) and 9-(4-cyanophenyl)anthracene (CPA).

In most cases, supramolecular architectures with controlled size, shape, and properties are derived from tailor-made organic molecules.[8-11] For example, by modulating the intermolecular interactions, various morphologies have been fabricated for tailor-made ICT molecular systems.[10,11] Although the morphology is determined by the growth kinetics, the direction and strength of the intermolecular interactions play crucial role at the initial stages of supersaturation and nucleation. Strong dipolar molecule ADMA (μ_g=5.0 D) forming mainly the 1D nanostructures (Chapter 4), while weakly dipolar molecule, N-(4-cyanophenyl)carbazole (CPC, μ_g= 2.45 D) offers a large variety of morphologies. Considering these aspects, in order to explore the role of weak intermolecular interactions, we have purposefully designed 9,10-bis(4-

cyanophenyl)anthracene (BCPA, Chart 6.1) for the fabrication of 2-D nanoparticles. Additionally, we have synthesized 9-(4-cyanophenyl)anthracene (CPA, Chart 6.1) to understand some of our results. In BCPA, two benzonitrile moieties are linked covalently at the 9- and 10-positions of anthracene. Although the molecule is symmetric ($\mu_g \approx 0$), the two –CN groups present in the benzonitrile moieties are expected to take part in supramolecular interactions between the adjacent molecules. Density functional theory calculations combined with single crystal X-ray structure analysis on the present system in fact substantiates some of our assumptions. Two supramolecular interactions have been identified which are found to be bidirectional.

6.2. Results and discussion

6.2.1. Thermal stability

Both molecular systems, BCPA and CPA, were prepared by following palladium catalyzed Suzuki-coupling reaction procedure (*vide* section 2.3). Differential scanning calorimeter (DSC) measurements indicate very high melting point for BCPA (431°C, Fig. 6.1) compared to CPA (118-120 °C). Such high thermal stability of organic molecule is quite rare. Thermo-gravimetric analysis (TGA) which confirmed this observation (Fig. 6.1), indicate that BCPA melting and decomposition occurs between 400 °C and 475 °C. A much higher melting point of BCPA compared to CPA is clearly a reflection of better crystal packing for the more symmetrical molecule, BCPA.

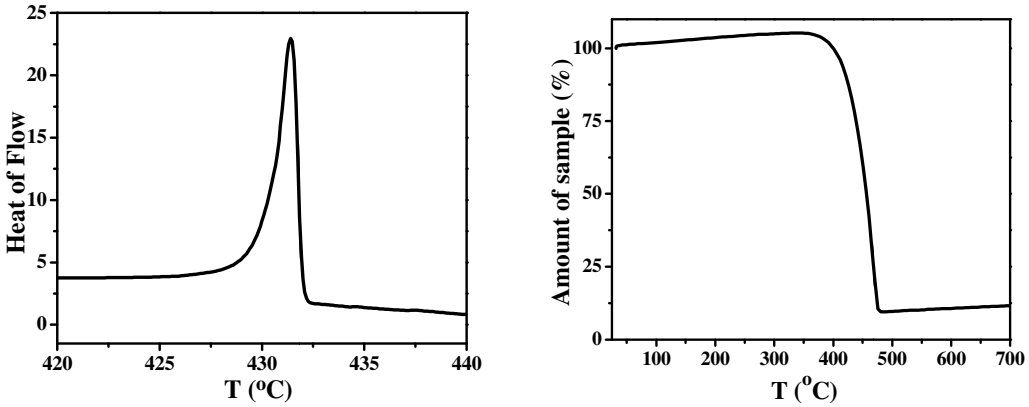

Fig. 6.1. Thermal properties of BCPA. (a) DSC and (b) TGA curves.

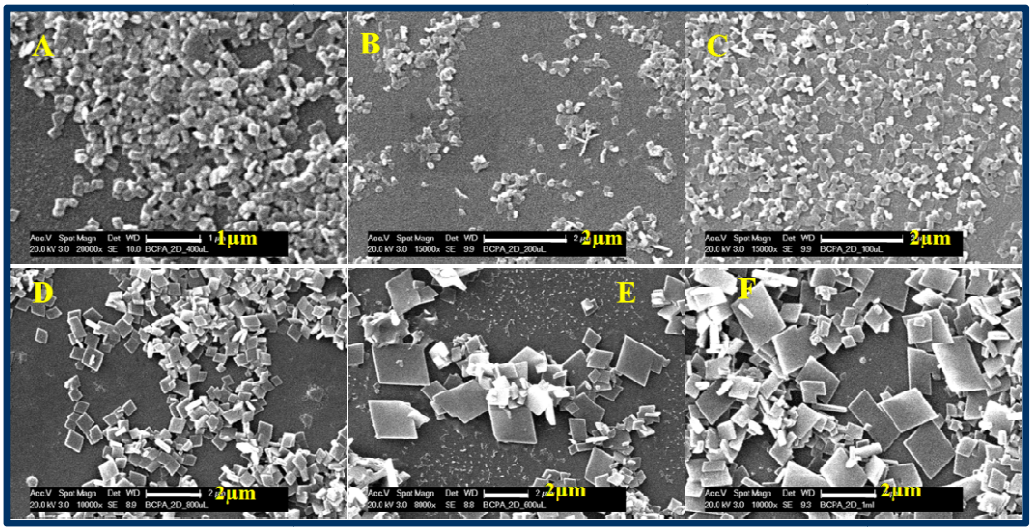

Fig. 6.2. SEM images of 100 µL (A), 200 µL (B), 400 µL (C), 600 µL (D), 800 µL (E) and 1 mL (F) colloids prepared at room temperature by injecting 2 mM DMSO solution of BCPA to 10 mL of water under *ultra sonication*.

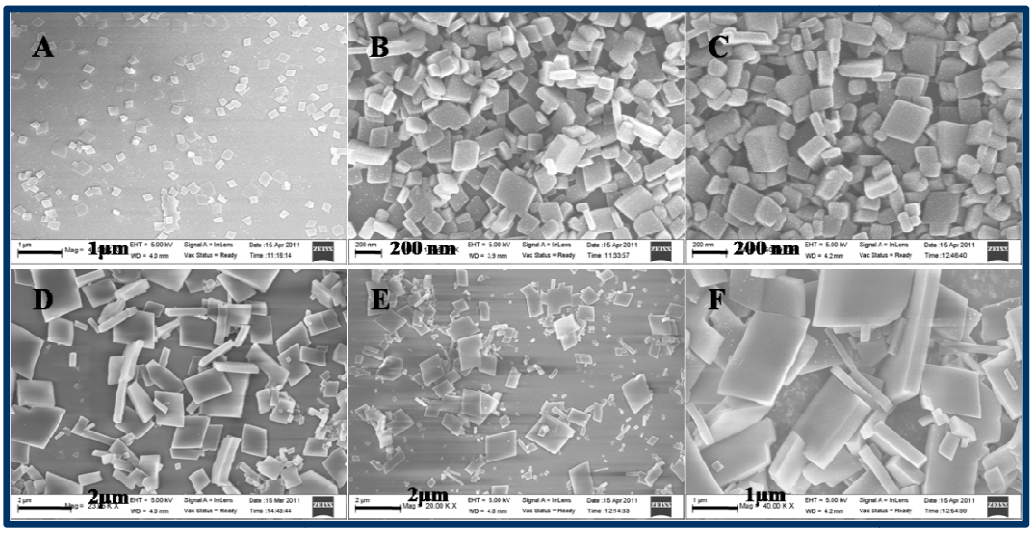

Fig. 6.3. FESEM images of 100 µL (A), 200 µL (B), 400 µL (C), 600 µL (D), 800 µL (E) and 1 mL (F) colloids prepared at room temperature by injecting 2 mM DMSO solution of BCPA to 10 mL of water under *ultra-sonication.*

6.2.2. Nanoparticles fabrication and characterization

Self-assembled nanoparticles of BCPA were fabricated at room temperature by rapidly injecting the DMSO (good solvent) solution of the sample into water (bad solvent). Figure 6.2 & 6.3 depict the SEM and FESEM images of BCPA colloids prepared by injecting different amounts (100-1000 µL) of 2 mM solution in DMSO to 10 mL of MilliQ-water under ultra-sonication. With 100 µL addition, BCPA forms well-defined rhombus and rectangular nanoplates with narrow (80-200 nm) size distribution. Increasing the amount of the injected solution (200-600 µL), the particle dimension increase slightly but the morphology remains same. With even larger quantity (800-1000 µL) of the solution, the size of particle increases further and the size distribution becomes broader.

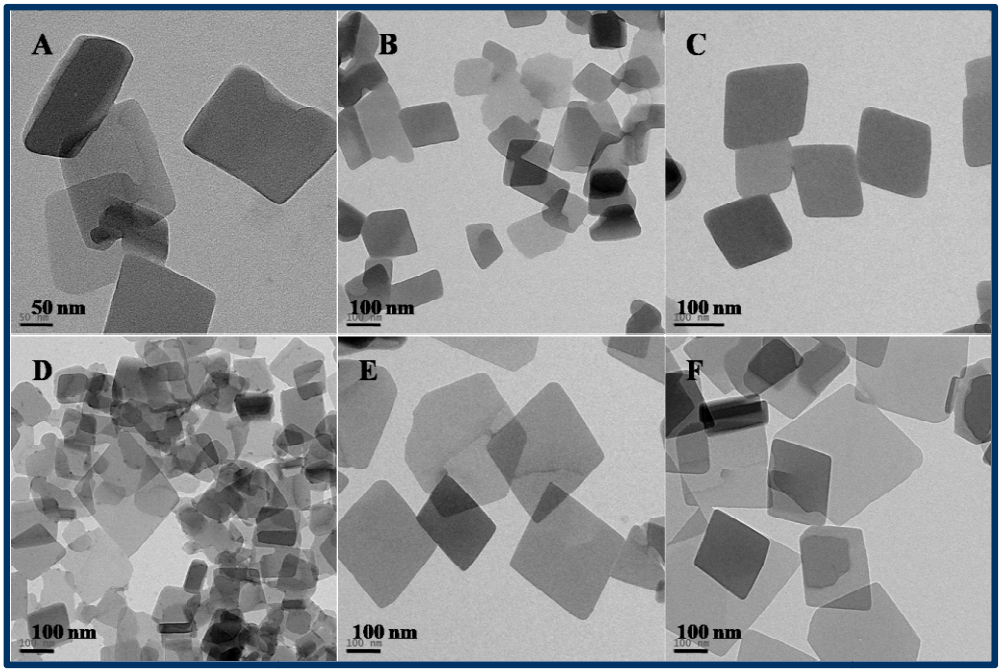

Fig. 6.4. TEM images of 100 µL (A), 200 µL (B), 400 µL (C), 600 µL (D), 800 µL (E) and 1 mL (F) colloids prepared at room temperature by injecting 2 mM DMSO solution of BCPA to 10 mL of water under *ultra sonication*.

These colloidal samples are found to be quite stable and no precipitation could be observed over a long period.

The nanoparticles have also been prepared by changing the experimental conditions such as initial concentration and solvent system. The size and morphology of the nanoparicles have been further confirmed with transmission electron microscope images (Fig. 6.4). Figure 6.5 illustrates the morphology and size distribution of the nanoparticles prepared under stirring instead of sonication. Although well-defined nanoparticles were observed under stirring condition, the size distribution is found to be broader as compared to the nanoparticles obtained under sonication. Hence, all the other nanoparticles were prepared under sonication. On the other hand, change of the initial concentration of

BCPA slightly affects the dimensions of the nanoparticles, while the morphology remains the same. Figure 6.6 which show the FESEM images of the nanoparticles prepared from 1 mM DMSO solution (instead of 2 mM solution) confirm this statement. We intended to perform experiments with higher concentration of BCPA solution. However, because of low solubility of BCPA, concentrations higher than 2 mM could not be used for the preparation of the nanoparticles. Figure 6.7 depicts the FESEM images of nanoparticles prepared by injecting different quantities of 1 mM THF solution to 10 mL of water under ultra-sonication. In this case, the particle shape is more irregular than the previous case with a small fraction of the rhombus plates. With increasing the quantity of the solution, the fraction of rhombus plates increases. Similar experiments with 1 mM acetone solution reveal that the acetone/water combination is not good for the fabrication of nanoplates (Fig. 6.8).

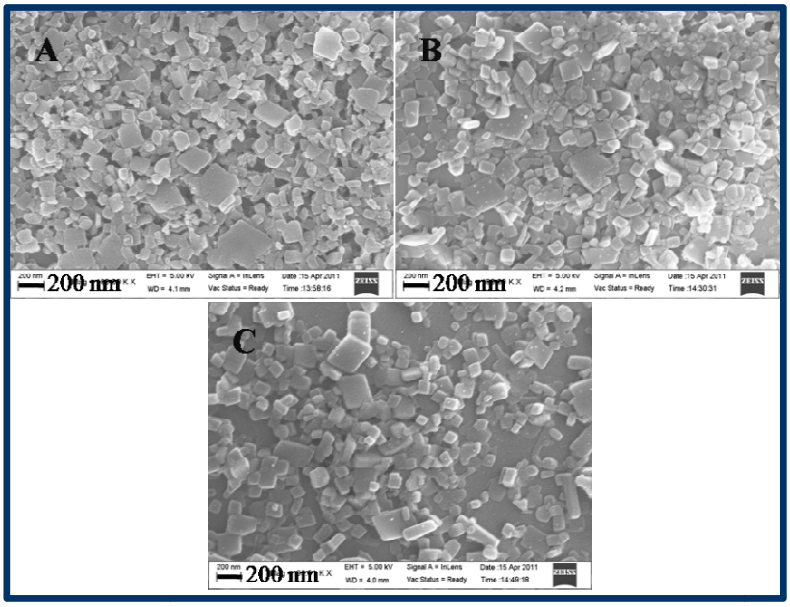

Fig. 6.5. FESEM images of 100 µL (A), 200 µL (B), 400 µL (C) colloids prepared at room temperature by injecting 2 mM DMSO solution of BCPA to 10 mL of water under *stirring*.

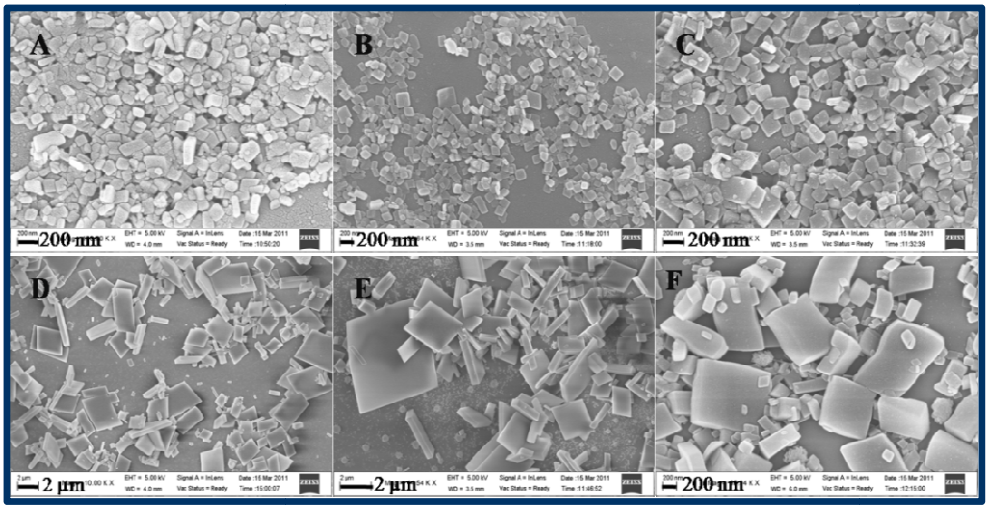

Fig. 6.6. FESEM images of 100 µL (A), 200 µL (B), 400 µL (C), 600 µL (D), 800 µL (E) and 1 mL (F) colloids prepared at room temperature by injecting 1 mM DMSO solution of BCPA to 10 mL of water under *ultra-sonication.*

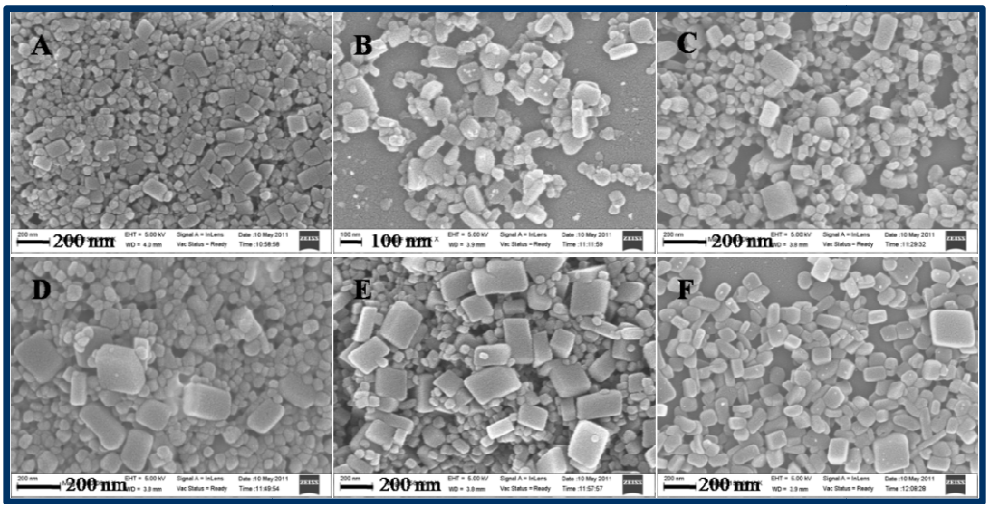

Fig. 6.7. FESEM images of 100 µL (A), 200 µL (B), 400 µL (C), 600 µL (D), 800 µL (E) and 1 mL (F) colloids prepared at room temperature by injecting 1 mM THF solution of BCPA to 10 mL of water under *ultra-sonication.*

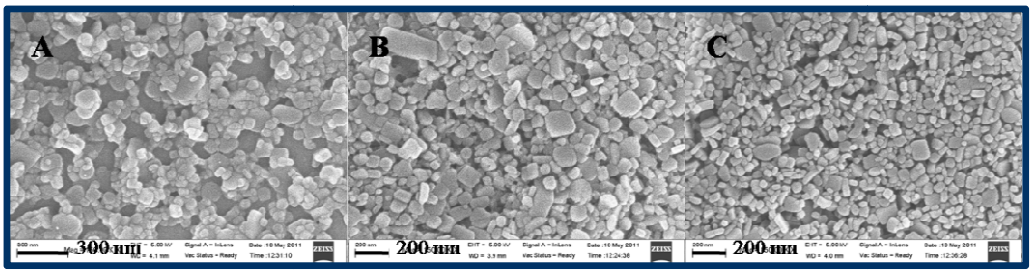

Fig. 6.8. FESEM images of nanoaprticles prepared using 1 mM acetone solution of BCPA in 10 mL of water.

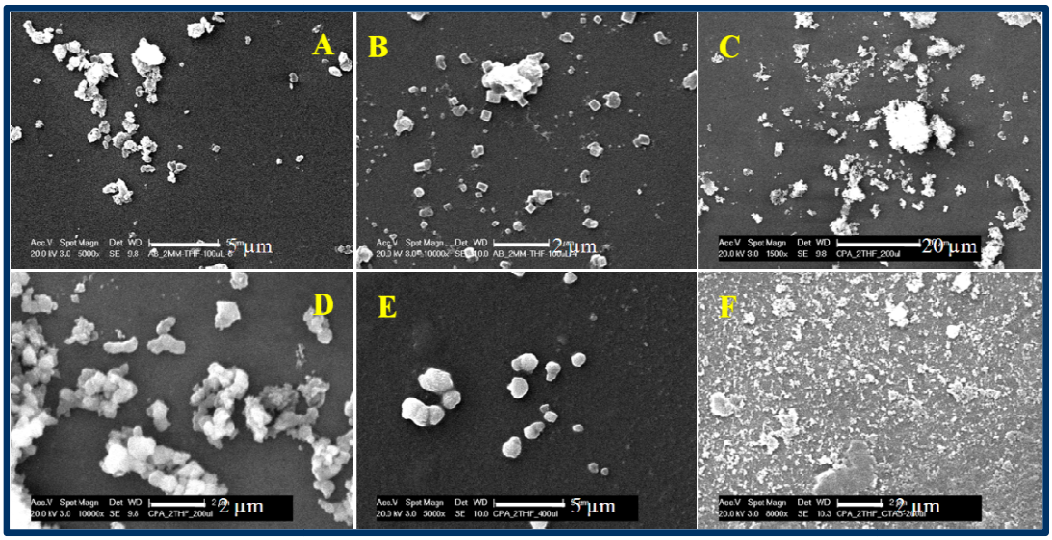

Fig. 6.9. CPA aggregates prepared from 2 mM THF solution by injecting 100 µL (A&B), 200 µL (C&D), 400 µL (E) and in presence of CTAB.

Self-assembled aggregates of CPA have also been prepared by injecting different quantities of 2 mM THF solution to 10 mL of water. Figure 6.9 represents the SEM images of the obtained nanoparticles. Unlike BCPA, CPA forms both regular and

irregular shaped aggregates. Our efforts by changing the initial concentration, solvent system and use of surfactants to synthesize well-defined nanoparticles were not fruitful.

6.2.3. Photophysical behavior in homogeneous solution

UV-vis absorption: The photophysical properties of the two systems have been studied in homogeneous solution by varying the polarity of the medium. Figure 6.10 depicts the electronic absorption spectra of BCPA and CPA in three different solvents at room temperature. The absorption spectrum of BCPA is a combination of the spectral features of the constituent phenyl and anthracene moieties. The low energy absorption band of BCPA, which is shown in the figure, is characterized by a structured band in the 310–430 nm region, is a typical signature of the S_0-S_1 (π-π^*) transition of the anthracene moiety. As the vibrational levels in the first excited electronic state of anthracene are well separated, the vibrational structure is clearly seen in the π- π^* electronic transition. With increasing the polarity of the medium the absorption peaks move towards red (Table 6.1). On the other hand, the absorption spectra of CPA are very similar to those of BCPA. However, for CPA the solvent polarity dependent shift of the peaks towards the longer wavelength is found to be slightly more pronounced. This observation is indicative of a more polar nature of the molecule. The density functional theory calculations, on the optimized geometries of the two molecules show that CPA (μ_g= 5.18 D) is more polar than BCPA (μ_g= 0.001 D).

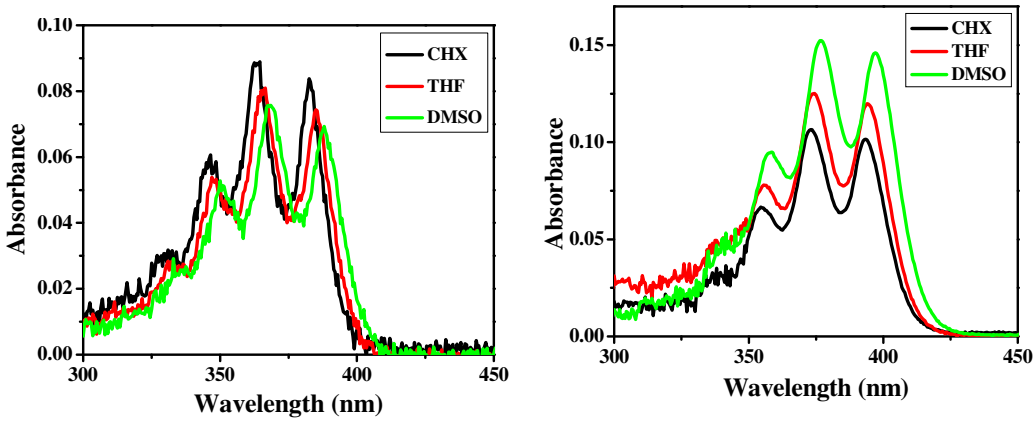

Fig. 6.10. Electronic absorption spectra of BCPA (left) and CPA (right) in cyclohexane (CHX), tetrahydrofuran (THF) and dimethyl sulfoxide (DMSO).

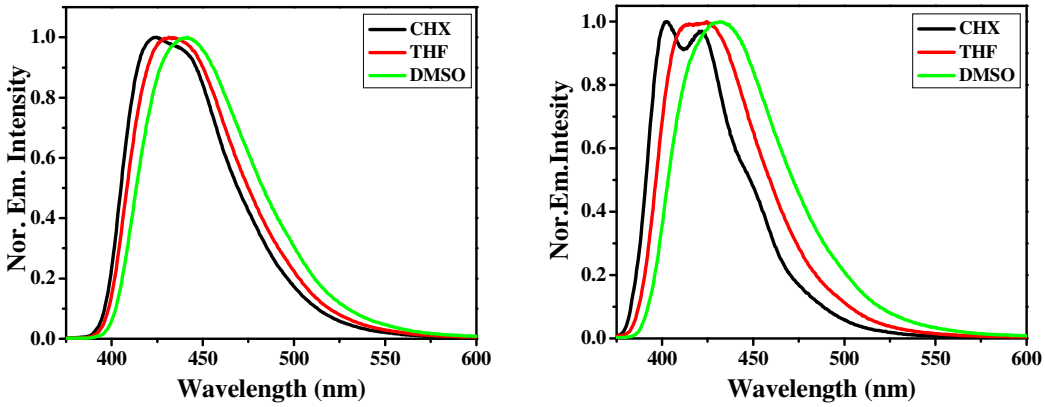

Fig. 6.11. Fluorescence spectra (λ_{ex}=350 nm) of BCPA (left) and CPA (right) in cyclohexane (CHX), tetrahydrofuran (THF) and dimethyl sulfoxide (DMSO).

Fluorescence emission: Figure 6.11 shows the fluorescence emission spectra of BCPA and CPA in three different solvents. The fluorescence spectra of both the systems are somewhat structured in nonpolar solvent, hexane. The structured nature however,

disappears with increasing polarity of the medium. As can be seen, at room temperature, BCPA gives a single fluorescence emission band in all solvents and fluorescence spectrum is not excitation wavelength dependent. The fluorescence emission shows bathochromic shift with increasing polarity of the medium. CPA also exhibit a single fluorescence band in all the solvents and excitation wavelength dependence of the emission behavior could not be observed. With increasing the polarity of the medium, a more red shift of the emission maxima is observed. A more pronounced solvent effect on the emission spectrum of the systems compared to the absorption spectra is indicative of a more polar nature of the emitting state of the two systems. This observation and the fact that the absorption spectra of the systems are structured while the emission spectra are broad indicate enhanced conjugation in the excited state of the molecule which is achieved by a decrease of the twist angle of the two ring systems.

Table 6.1. Fluorescence quantum yields and lifetimes of BCPA and CPA in different solvents.

Solvent	λ_{max}^{abs}	λ_{max}^{em}	Φ_f	λ_{max}^{abs}	λ_{max}^{em}	Φ_f
	BCPA			CPA		
CHX	373	425	0.79	364	404	0.34
THF	374	433	0.78	366	420	0.38
DMSO	376	440	0.72	369	432	0.58

6.2.4. Photophysical behavior of nanoplates

Figure 6.12 compares the absorption and emission spectra of BCPA nanoplates (prepared from 100 µL of 1 mM DMSO solution) with those in its molecular form. As can be seen, the structured absorption band of the molecular form of BCPA commenced from 425 nm, whereas the absorption due to the nanoplates starts from a much longer wavelength region (600 nm onwards) in the form of rise of the baseline. Interestingly, the structured region of the absorption spectra is not affected. The long tail is clearly due to the formation of the molecular aggregates, and the progressive rise of the baseline with decrease of wavelength is due to Mie scattering effect.[12-15] As far as the fluorescence spectra are concerned, the emission spectra of the nanoplates are not very different from those in its homogeneous solution (in DMSO and CHX). Interestingly, the emission spectrum of the nanoplates is slightly more structured, which could be due to structural rigidification as already observed in few other systems.[16] We believe that the two aromatic ring systems are also locked in an orthogonal conformation in the nanoplates.

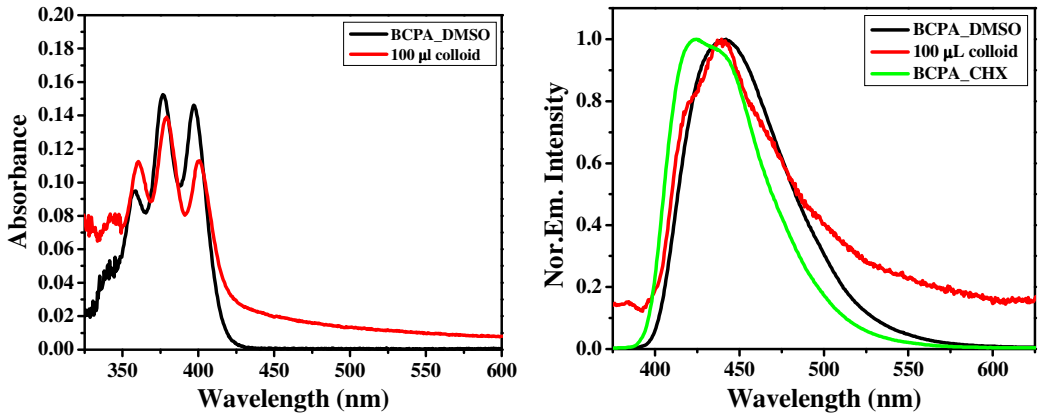

Fig. 6.12. Electronic absorption (left) and fluorescence emission spectra (λ_{ex}=350 nm; right) of 100 µl colloid prepared from 1mM DMSO solution, compared with that of BCPA in neat DMSO and cyclohexane.

6.2.5. Fluorescence lifetime and quantum yields

Fluorescence decay behavior of the two molecular systems and BCPA nanoparticles have been measured using time-correlated single photon counting technique and decay parameters are collected in Table 6.2. It is evident that the lifetimes of CPA are more sensitive to the polarity of the medium compared to BCPA. The fluorescence efficiency and lifetime of CPA increase with increasing solvent polarity. Most electron donor-acceptor (EDA) systems show a monotonic decrease of the fluorescence efficiency with increase in the solvent polarity[17-19] primarily due to lowering of the energy gap between the ground and the emitting state in polar media and consequent enhancement of the nonradiative rate. However, for the present system as the extent of the stabilization of the emitting state with polarity is not much (clearly due to not so polar nature of the state), this argument is not applicable. The changes in lifetime and fluorescence quantum yield can be due to mixing of an otherwise high-lying state in polar environment. On the other hand, BCPA lifetime and fluorescence quantum yield are not influenced by the solvent polarity. This is in accordance with the expectation. The short fluorescence lifetime of the BCPA nanoplates (0.45-0.65 ns) as compared to BCPA in homogeneous solution is presumably due to the enhanced intermolecular interactions in the nanoparticles, which is observed in few other molecular sysytems.[20,21]

We have also measured the lifetime and fluorescence quantum yield of free standing particles (prepared upon drying the solvent from colloidal solution) using fluorescence lifetime imaging microscope (FLIM, *vide* section 2.5.2). Figure 6.13 depicts the FLIM images of the nanoplates prepared from 100 μL and 1 mL stock solution (2 mM DMSO). In the case of 100 μL, due to the smaller size of the nanoplate (80-200 nm) the exact morphology could not be captured. However, measurements on particles located at different regions suggest longer lifetimes (2.7-3.5 ns) of these particles

compared to the colloidal particles. A shorter lifetime of the nanoplates in colloidal solution is due to the presence of the solvent.

Table 6.2. Fluorescence decay parameters† of the systems and nanoparticles collected by exciting the samples at 375 nm.

System	Solvent	τ_1	τ_2	τ_3 (ns)	τ_{avg}	χ^2
BCPA‡	CHX	4.62	-	-	-	1.06
	THF	4.74	-	-	-	1.36
	DMSO	4.98	-	-	-	1.47
CPA‡	CHX	2.82	-	-	-	1.11
	THF	3.67	-	-	-	1.43
	DMSO	4.54	-	-	-	1.19
Nanoplates‡	100 µL	0.06 (8.3)	0.32 (62.7)	0.84 (29)	0.45	1.09
	1 mL	0.05 (6.6)	0.47 (76.4)	1.76 (17)	0.65	1.28

† values are in ns; ‡ monitored at corresponding fluorescence emission maxima.

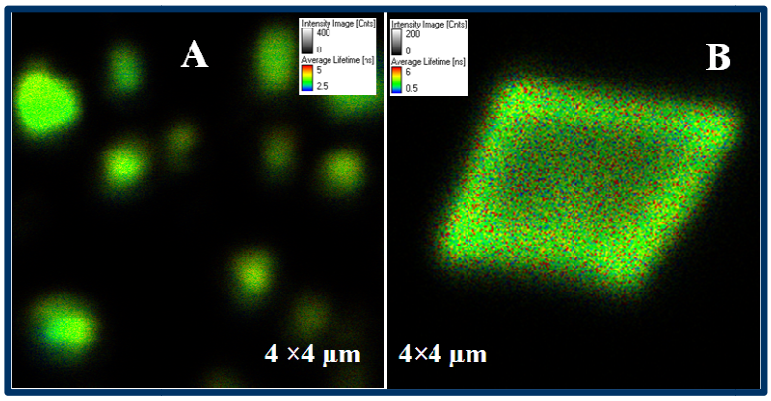

Fig. 6.13. FLIM images of nanoplates prepared from 100 µL (A) and 1 mL (B) of 2 mM DMSO.

6.3. Crystal structure and theoretical calculations

BCPA is sparingly soluble in most of the common organic solvents. Pale yellow crystals, obtained by slow evaporation of a dilute ethylacetate solution of BCPA were used for data collection. The essential crystallographic data are presented in Table 6.3. The crystal belongs to triclinic space group *p-1* with two halves of the molecule forming the asymmetric unit. The ORTEP diagram of the asymmetric unit and full molecule

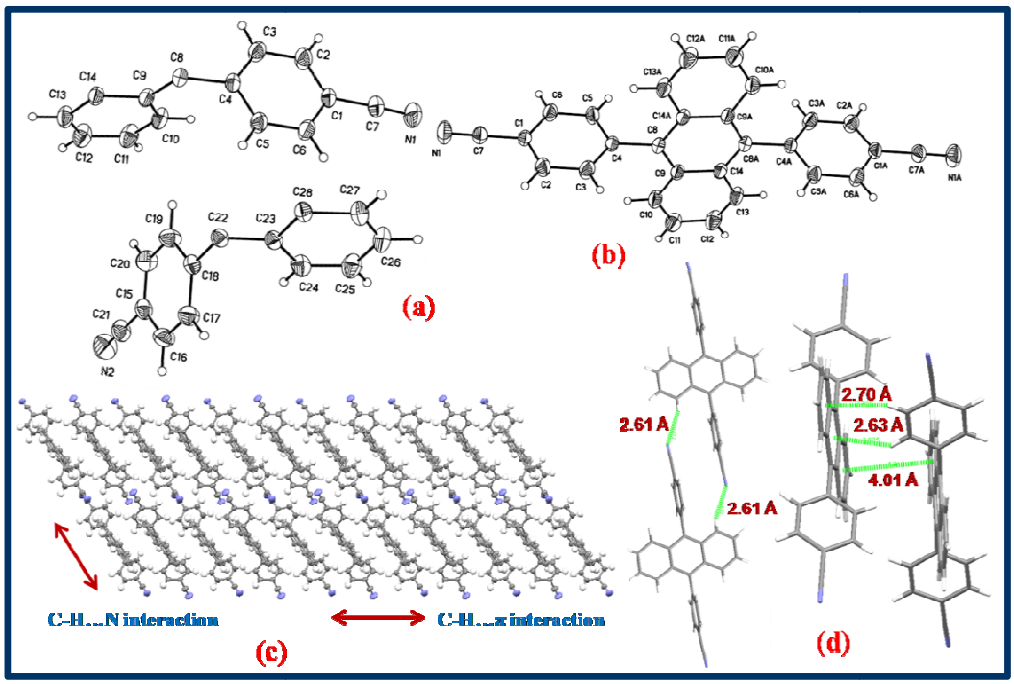

Fig. 6.14. ORTEP diagram of BCPA asymmetric unit (a) and full molecule (b) with atoms represented by thermal ellipsoids at 35 % probability level, C(4)-C(8) bond length = 1.501 (9) Å. (c) representation of intermolecular interactions (d) C-H…N and C-H…π interactions.

Table 6.3. Data collections and structure refinement details of crystal structure of BCPA and CPA.

	CPA	**BCPA**
Formula	C21 H13 N	C28 H16 N2
Formula wt	279.32	380.43
Crystal system	Monoclinic	triclinic
Space group	C 2/c	p-1
a (Å)	15.24(2)	9.28 (9)
b (Å)	10.46(15)	10.56 (10)
c (Å)	19.50(3)	11.43 (10)
α (°)	90	105.11 (8)°
β (°)	100.81(2)	103.43 (8)°
γ (°)	90	102.05 (8)°
V ($Å^3$)	3058.2(8)	1009.25 (16)
Z	8	2
F(000)	1168.0	396
ρ_{calcd} (g cm^{-3})	1.213	1.252
μ (mm^{-1})	0.070	0.074
Temperature (K)	298	298 (2)
λ [Å]	0.71073	0.71073
Crystal size	0.28×24×17	0.48×0.36×0.24
Color, habit	Greenish yellow, block	Pale yellow, Plate
Absorption correction	Multi-scan	Multi-scan
T_{min}, T_{max}	0.980, 0.988	0.966,0.983
Total no. of reflections	3754	7446
No. of unique reflections	3628	4129
No. of. obs. reflections	2399	2847
θ_{max}, θ_{min} (°)	2.13, 28.17	26.4, 3.3
No. of parameters	251	272
R indices (obs. Data): *R*, R_w	0.056, 0.151	0.041, 0.110
R indices (all data): *R*, R_w	0.151, 0.136	0.111, 0.105
GOF	1.05	1.07
$\Delta\rho_{max}$, $\Delta\rho_{min}$ ($e/Å^3$)	0.18, -0.30	0.18, -0.15

with atom numbering scheme and some of the packing interactions in the crystal lattice have been depicted in Figure 6.14. The dihedral angle between the phenyl and anthryl planes is found to be 83-85°, suggesting that anthracene moiety is decoupled from the cyanophenyl moieties. Two different interactions are seen to be responsible for the crystal packing. The C-H…N interaction and (2.61 Å) C-H…π interactions (2.73 Å, 2.63 Å) are the two major intermolecular interaction identified. A weak π-π interaction (4.01 Å) between π-cloud of one anthracene moiety with that of the another anthracene ring system is also observed.

The crystal structure provides insight into the nature of intermolecular interactions involved in the 2-D nanoplates formation. As shown in Figure 6.14, the individual molecules are held together by strong C-H…N interaction in one direction and in another direction, they are glued with C-H…π interaction. Thus the 2D molecular network is the result of bidirectional nature of the intermolecular interactions. As the nanoplates are a kind of tiny single crystals these interactions should operate at the mesoscopic regime as well.

CPA is highly soluble in most of the organic solvents. Greenish yellow crystals, grown by slow evaporation of dilute ACN solution of CPA were used to collect the single crystal X-ray data and the essential crystallographic parameters are collected in Table 6.3. The crystal belongs to monoclinic space group *C2/c* with eight individual molecules forming the asymmetric unit. The ORTEP diagram of the molecule with atom numbering scheme and asymmetric unit are depicted in Figure 6.15. The dihedral angle between the phenyl and anthryl moieties is found to be 73.6°.

Nanoparticles can be visualized as the association of molecular motifs such as dimer, trimer, tetramer and higher oligomers. In order to understand the 2-D morphologies of BCPA, some of the molecular motifs, which are identified in the single crystal X-ray analysis were modelled using Gaussian 03 package. An increase in the number of the

molecules in a motif increases the total energy, which, however, is lower than the sum energy of the molecules. This finding is indicative of increasing cooperative binding interactions with the number of molecules in the crystal lattice (Table 6.4). Stabilization/binding energy of these motifs were calculated using the procedure described in section 2.7. The stabilization energy of J-motifs increases with number of molecules. However, it is evident from the data shown in Table, the H-motifs are not stable. Considering the stabilization energies of the two motifs, it can perhaps be concluded that the J-motifs are the major building blocks of the nanoplates.

Table 6.4. Computed energies (B3LYP/6-31+G*) of the BCPA molecule and the motifs.

Molecule/ Motif		Energy (eV)	E_S (kCal mol^{-1})
Molecule	--	-32265.5592	--
H-Aggregate	Dimer	-64530.9716	1.69
	Trimer	-96796.4413	1.89
	Tetramer	-129061.8712	2.10
	Pentamer	-161327.4073	1.79
J-Aggregate	Dimer	-64531.1434	-0.28
	Trimer	-96796.7415	-0.49
	Teramer	-129062.3577	-0.69
	Pentamer	-161328.2846	-2.25

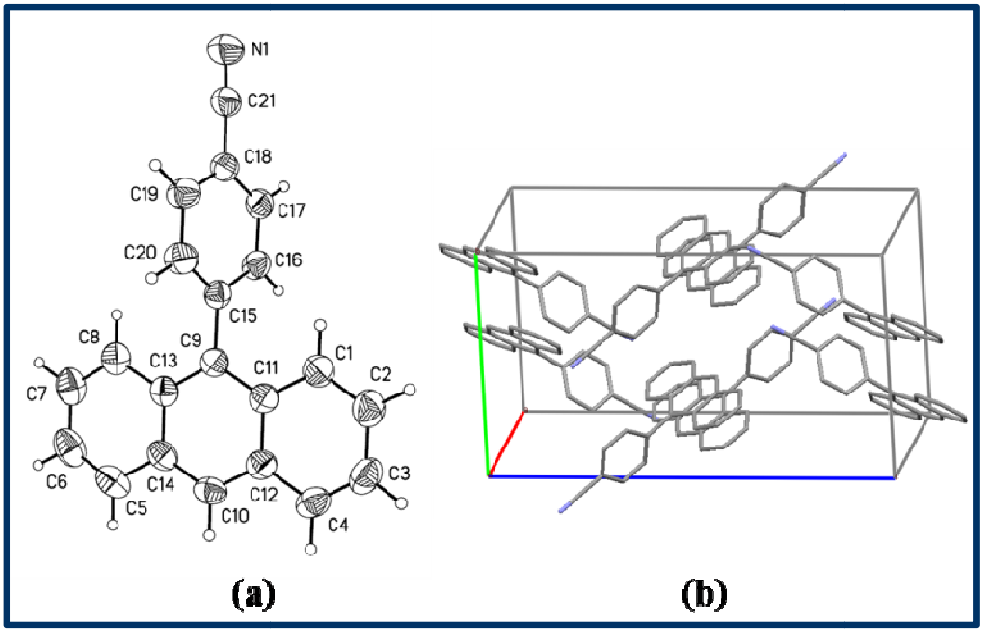

Fig. 6.15. ORTEP diagram of CPA with atoms represented by thermal ellipsoids at 35 % probability level, C(9)-C(15) bond length = 1.482 (9) Å. (b) packing diagram (all H-atoms are omitted for clarity).

6.4. Conclusion

Highly fluorescent molecular systems comprising of electron donor and acceptor moieties have been prepared by simple Suzuki-coupling reaction. Well-defined 2D nanoplates (with narrow size distribution) of one of the molecular system BCPA, have been fabricated by following the simple reprecipitation method and their absorption and fluorescence properties have been studied. The nanoplate formation of BCPA has been accounted with the help of the bidirectional nature of weak intermolecular interactions the evidence of which is obtained from the single crystal X-ray analysis. The high fluorescence efficiency of these 2D nanoparticles can make these substances useful in application.

References

(1) Lin, S. C.; Lin, T. F.; Ho, R. M.; Chang, C. Y.; Hsu, C. S. *Adv. Funct. Mater.* **2008**, *18*, 3386.
(2) Yu, P.; Zhang, X.; Wang, D.; Wang, L.; Ma, Y. *Crystal Growth & Design* **2009**, *9*, 528.
(3) Cao, F.; Shi, W.; Zhao, L.; Song, S.; Yang, J.; Lei, Y.; Zhang, H. *J. Phys. Chem. C* **2008**, *112*, 17095.
(4) Nakanishi, T.; Michinobu, T.; Yoshida, K.; Shirahata, N.; Ariga, K.; Mohwald, H.; Kurth, D. G. *Adv. Mater.* **2008**, *20*, 443.
(5) Xu, J.; Zheng, H.; Liu, H.; Zhou, C.; Zhao, Y.; Li, Y.; Li, Y. *J. Phys. Chem. C* **2010**, *114*, 2925.
(6) Lei, Y.; Liao, Q.; Fu, H.; Yao, J. *J. Phys. Chem. C* **2009**, *113*, 10038.
(7) Huang, L.; Liao, Q.; Shi, Q.; Fu, H.; Mab, J.; Yao, J. *J. Mater. Chem.* **2010**, *20*, 159.
(8) Zubarev, E. R.; Sone, E. D.; Stupp, S. I. *Chem. Eur. J.* **2006**, *12*, 7313.
(9) Che, Y.; Datar, A.; Balakrishnan, K.; Zang, L. *J. Am. Chem. Soc.* **2007**, *129*, 7234.
(10) Zhang, X.; Zhang, X.; Wang, B.; Zhang, C.; Chang, J. C.; Lee, C.-S.; Lee, S.-T. *J. Phys. Chem. C* **2008**, *112*, 16264.
(11) Zhang, X.; Zhang, X.; Zou, K.; Lee, C.-S.; Lee, S.-T. *J. Am. Chem. Soc.* **2007**, *129*, 3527.
(12) Chen, J.; Law, C. C. W.; Lam, J. W. Y.; Dong, Y.; Lo, S. M. F.; Williams, I. D.; Zhu, D. B.; Tang, B. Z. *Chem. Mater.* **2003**, *15*, 1535.
(13) Chen, W.; Tu, X.; Guo, X. *Chem. Commun.* **2009**, 1736.
(14) Cox, A. J.; DeWeerd, A. J.; Linden, J. *Am. J. Phys.* **2002**, *70*, 620.
(15) Kasai, H.; Kamatani, H.; Okada, S.; Oikawa, H.; Matsuda, H.; Nakanishi, H. *Jpn. J. Appl. Phys.* **1996**, *35*, L221.
(16) Kanaparthi, R. K.; Sarkar, M.; Samanta, A. *J. Phys. Chem. B* **2009**, *113*, 15189.
(17) Soujanya, T.; Fessenden, R. W.; Samanta, A. *J. Phys. Chem. A* **1996**, *100*, 3507.
(18) Saha, S.; Samanta, A. *J. Phys. Chem. A* **2002**, *106*, 4763.
(19) Saha, S.; Samanta, A. *J. Phys. Chem. A* **1998**, *102*, 7903.
(20) Bhongale, C. J.; Chang, C. W.; Lee, C. S.; Diau, E. W. G. *J. Phys. Chem. B* **2005**, *109*, 13472.
(21) Li, S.; He, L.; Xiong, F.; Li, Y.; Yang, G. *J. Phys. Chem. B* **2004**, *108*, 10887.

Chapter 7

Concluding Remarks

This chapter summarizes the results of the investigations delineated in this thesis. The scope of further studies based on the findings of the present work and challenges ahead have also been outlined.

7.1. Overview

The work embodied in the thesis has been undertaken with a two-dimensional objective: firstly, to understand how the photophysics of some EDA molecular aggregates are different from those in homogeneous solution and secondly to identify the role of intermolecular interactions in the aggregation process and hence their morphology and optical property as well. In this context, few EDA molecular systems have been identified and synthesized. Subsequently, the nano/microparticles of the systems have been fabricated under different experimental conditions. Thus, the fabrication of the nano/microparticles and their characterization using different microscopy techniques constitute major part of the thesis. Optical properties of these nano/microparticles have been studied to find out to what extent these properties are different from those in homogeneous solution. For this purpose, several instrumental techniques and methodologies, namely, NMR spectroscopy, UV-visible absorption, steady-state and time-resolved fluorescence, X-ray crystallography, atomic force microscopy, scanning electronic microscopy, transmission electronic microscopy, fluorescence microscopy, fluorescence lifetime imaging microscopy and theoretical calculations have been employed to carry out this work. The results obtained from the investigations are outlined below.

With a view to obtain insight into the aggregation behavior of EDA molecular systems, 4-(9-anthryl)-N,N-dimethylaniline (ADMA) has been probed by electronic

absorption and fluorescence spectroscopy, microscopy and crystallography. Self-assembled aggregates have been prepared by reprecipitation method under various conditions without using any stabilizing agent. Different microscopic techniques reveal spherical and plate-like morphologies of the aggregates. Intermolecular interaction in the aggregates induces remarkable change in the absorption and fluorescence properties and the formation of stable aggregates has been followed by monitoring the spectral response of the system as a function of time. Intramolecular charge transfer process, which dominates the photophysical behavior of ADMA in solution, could not be observed in the solid or aggregated state. The nature of the intermolecular interactions responsible for the formation and stabilization of the aggregates has been identified from the spectral and crystal structure data of the system.

In order to fabricate ADMA aggregates with well-defined morphologies, various additives such as surfactants, polymer and ionic liquids have been employed during the preparation of the nanoparticles. It is demonstrated that the shapes of the aggregates of ADMA can be tuned by the surfactants. The various morphologies captured under various conditions are shown to be the consequence of preferential adsorption of the surfactants to specific crystallographic planes of ADMA. Only those crystallographic surfaces grow that are not influenced by the surfactants. Aggregation leads to a progressive shift of the UV-vis absorption towards the longer wavelength and the structured fluorescence emission band towards the shorter wavelength. It is inferred that the anthryl and phenyl ring systems are locked in an orthogonal/near-orthogonal conformation due to the structural constraint imposed by the rigidity of the aggregated state. The fluorescence lifetime imaging microscopy (FLIM) studies on the aggregated particles reveal that the nano/microparticles are microscopically heterogeneous in nature.

Weakly dipolar molecule, 9-(4-cyanophenyl)carbazole (CPC) has been synthesized for the study of its aggregated state. We have been able to fabricate one and two-

dimensional (1D & 2D) nanoparticles of various morphologies such as rods, ribbons, tubes, rhombus crystals, hexagonal and rhombus plates merely by changing the solvent and temperature. Absorption spectral characteristics of the 1D and 2D nanoparticles are found to be different, while the fluorescence emission properties do not show much dependence on the morphology of the particles. The nano/microstructures of CPC show structured fluorescence emission with the emission peak position blue-shifted when compared with that in homogeneous solutions. Single crystal X-ray diffraction studies reveal the intermolecular interactions in the crystal lattice. The influence of the observed intermolecular interactions in the formation of nanoparticles is investigated by theoretical calculations on the molecular motifs. The large shape diversity of the molecular aggregates is attributed to the multiple modes of weak intermolecular interactions afforded by the molecule and the influences of solvent and temperature on growth kinetics.

Highly fluorescent molecules, 9,10-bis(4-cyanophenyl)anthracene (BCPA) and 9-(4-cyanophenyl)anthracene (CPA) have been synthesized with a view to study the morphology and optical properties of the aggregated states of the systems. Molecular aggregation behavior of the systems has been probed in the absence and presence of additives. These investigations reveal that BCPA forms well-defined 2D-nanoplates while CPA gives aggregates with no specific morphology. Interestingly the absorption spectra of the nanoplates have been found not very different from those of the molecule in the homogeneous solution. However, the fluorescence efficiency of the nanoplates significantly lower than that in its homogeneous solution. Single crystal X-ray diffraction studies on BCPA suggest bi-directional nature of the intermolecular interactions which seen to be responsible for the nanoplate morphology of the system in the aggregated state.

7.2. Future scope and challenges

Unlike the inorganic/semiconductor nanoparticles, the research on organic molecular nanoparticles is young and several things are not yet explored. Considering the potential application of the EDA molecular systems in diverse fields and the scarcity of the EDA molecular nanoparticles, it is essential that fabrication of these particles and study of their optical properties are undertaken, with a greater intensity.

Our study wherein we succeeded in fabricating well-defined morphologies such as nanorods, nanoribbons and nanosheets of ADMA in the presence of surfactant molecules and tuning the size of the nanoparticles is an interesting feature for measuring nonlinear optical (NLO) properties such as secondary harmonic generation (SHG) of these class of substances. As Hyper Raleigh scattering studies were not successful (Chapter 4), advanced techniques such as open and closed Z-scan experiments may be attempted for an investigation of the size and morphology dependent NLO properties. Moreover, one can also exploit these nanostructures for the study of their electronic and optoelectronic properties. The DFT calculations, which indicate low HOMO-LUMO gap for these molecular systems, points to the potential of the molecular aggregates as organic semiconducting material. As the 1D-nanostructures are promising candidates for future miniature electronics, current-voltage (I-V) characteristics of the nanostructures obtained in the present study can be investigated. Further, the optical waveguiding property of these nanostructures may be subjected to the investigation.

During the course of this study, a new strategy has been developed for tuning the morphology of EDA molecular systems, which tend to form 1D-nanostructures, by suppressing the dipolar interactions using weekly dipolar molecules. The morphologies of highly dipolar molecule can also be tuned by incorporating molecular components that participate in relatively strong H-bonding interactions. This approach may be applied to a

large variety of EDA molecular systems for large shape diversity and a broader range of optical properties.

Although many methods are available in the literature for the fabrication of organic nanoparticles, most of them are not suitable for large scale production. As most of the practical applications are linked to quantity of the nanoparticles, new methods are to be explored to produce gram scale quantities of the organic nanoparticles in highly pure and monodispersed form.

Most of the studies including the present work do not show much variation of the optical properties with the size and/or morphology of the particles. This is in contrast to the observations made with the inorganic or semiconductor nanoparticles. Hence, EDA molecular systems, which show size and morphology dependent optical properties, are to be developed.

Few organic molecular nanoparticles are shown as very good sensors for detecting species, which include acid, base and explosives. However, there is so far no report of organic nanoparticles used for sensing transition metal ions. Perhaps this problem could be investigated employing fluorescent EDA molecular aggregates.

Appendix

Atomic coordinates for X-ray structures reported in the thesis

Table A.1 Atomic coordinates ($\times 10^4$), equivalent isotropic displacement parameters ($Å^2 \times 10^3$) for **ADMA** (*Chapter 3*). U(eq) is defined as one third of the trace of the orthogonalized U_{ij} tensor. The anisotropic displacement factor exponent takes the form: $-2\pi^2[h^2a^{*2}U_{11}+\ldots+2hka^*b^*U_{12}]$.

Atoms	X	Y	Z	U(eq)	U11	U22	U33	U23	U13	U12
N(1)	1224(2)	7753(2)	5087(1)	66(1)	89(2)	44(1)	59(1)	4(1)	-4(1)	1(1)
C(1)	4747(2)	2448(4)	6124(1)	73(1)	60(2)	79(2)	84(2)	-7(2)	22(2)	-13(2)
C(2)	5055(2)	1123(4)	6441(1)	77(1)	54(2)	87(2)	91(2)	-10(2)	13(2)	4(2)
C(3)	4553(2)	259(3)	6714(1)	67(1)	60(2)	70(2)	70(2)	-4(2)	2(2)	10(2)
C(4)	1814(2)	-825(3)	7214(1)	61(1)	74(2)	58(2)	50(2)	9(1)	6(1)	-4(1)
C(5)	1021(2)	-444(4)	7197(1)	69(1)	69(2)	75(2)	65(2)	10(2)	16(2)	-11(2)
C(6)	706(2)	912(4)	6909(1)	66(1)	56(2)	80(2)	65(2)	1(2)	14(1)	-3(2)
C(7)	1199(2)	1843(3)	6639(1)	57(1)	58(2)	53(2)	58(2)	1(1)	5(1)	2(1)
C(8)	3951(2)	2870(3)	6096(1)	61(1)	65(2)	59(2)	60(2)	-2(1)	12(1)	-6(1)
C(9)	2563(2)	2406(3)	6349(1)	47(1)	55(2)	43(1)	42(1)	-5(1)	2(1)	-3(1)
C(10)	3180(2)	-261(3)	6966(1)	56(1)	68(2)	49(2)	49(1)	4(1)	0(1)	8(1)
C(11)	2042(2)	1481(3)	6635(1)	47(1)	54(2)	44(1)	41(1)	-5(1)	2(1)	0(1)
C(12)	2357(2)	113(3)	6944(1)	50(1)	59(2)	48(2)	40(1)	-2(1)	3(1)	0(1)
C(13)	3393(2)	1997(3)	6379(1)	49(1)	54(2)	49(1)	44(1)	-4(1)	4(1)	-3(1)
C(14)	3707(2)	648(3)	6694(1)	52(1)	54(2)	53(2)	48(1)	-4(1)	2(1)	3(1)
C(15)	2228(2)	3813(3)	6017(1)	49(1)	53(2)	45(1)	48(1)	1(1)	9(1)	-2(1)
C(16)	1707(2)	3706(3)	5480(1)	59(1)	78(2)	38(1)	57(2)	-6(1)	-1(1)	-3(1)
C(17)	1383(2)	4985(3)	5169(1)	58(1)	68(2)	47(2)	53(2)	-1(1)	-7(1)	-2(1)
C(18)	1568(2)	6467(3)	5381(1)	49(1)	58(2)	41(1)	48(1)	3(1)	8(1)	-1(1)
C(19)	2110(2)	6585(3)	5918(1)	57(1)	73(2)	39(1)	58(2)	-7(1)	6(1)	-6(1)
C(20)	2425(2)	5292(3)	6223(1)	57(1)	67(2)	51(2)	49(1)	-4(1)	-1(1)	-4(1)
C(21)	707(2)	7618(3)	4523(1)	80(1)	90(2)	63(2)	80(2)	13(2)	-14(2)	2(2)
C(22)	1467(2)	9277(3)	5296(1)	70(1)	93(2)	42(2)	74(2)	2(1)	11(2)	3(2)

Table A.2. Atomic coordinates ($\times 10^4$), equivalent isotropic displacement parameters ($Å^2 \times 10^3$) for **BCPA** (*Chapter 6*). U(eq) is defined as one third of the trace of the orthogonalized U_{ij} tensor. The anisotropic displacement factor exponent takes the form: $-2\pi^2[h^2a^{*2}U_{11}+\ldots+2hka^*b^*U_{12}]$.

Atoms	x	y	z	U(eq)	U_{11}	U_{22}	U_{33}	U_{23}	U_{13}	U_{12}
N (1)	2350(2)	10332(1)	10199(1)	66(1)	87(1)	64(1)	54(1)	7(1)	34(1)	36(1)
N(2)	3181(2)	5059(2)	-492(1)	79(1)	64(1)	69(1)	66(1)	-2(1)	-9(1)	2(1)
C (1)	3261(1)	8622(1)	8689(1)	37(1)	38(1)	34(1)	35(1)	2(1)	13(1)	10(1)
C(2)	3521(2)	7452(1)	8915(1)	52(1)	79(1)	47(1)	41(1)	17(1)	31(1)	25(1)
C(3)	3958(2)	6547(1)	8055(1)	51(1)	80(1)	39(1)	48(1)	19(1)	29(1)	28(1)
C(4)	4134(1)	6785(1)	6956(1)	35(1)	35(1)	32(1)	36(1)	4(1)	12(1)	11(1)
C(5)	3902(2)	7976(1)	6762(1)	47(1)	70(1)	44(1)	40(1)	16(1)	29(1)	26(1)
C(6)	3466(2)	8888(1)	7609(1)	46(1)	68(1)	37(1)	44(1)	16(1)	26(1)	26(1)
C(7)	2768(2)	9569(1)	9549(1)	45(1)	50(1)	43(1)	39(1)	6(1)	17(1)	14(1)
C(8)	4584(1)	5834(1)	5981(1)	36(1)	41(1)	31(1)	35(1)	6(1)	13(1)	15(1)
C(9)	3433(1)	4753(1)	4978(1)	37(1)	37(1)	31(1)	41(1)	6(1)	13(1)	14(1)
C(10)	1841(2)	4452(1)	4911(1)	47(1)	41(1)	40(1)	57(1)	4(1)	18(1)	15(1)
C(11)	751(2)	3420(2)	3932(2)	58(1)	36(1)	50(1)	76(1)	2(1)	14(1)	12(1)
C(12)	1169(2)	2622(2)	2947(2)	59(1)	41(1)	48(1)	64(1)	-9(1)	3(1)	9(1)
C(13)	2664(2)	2858(1)	2972(1)	49(1)	46(1)	42(1)	45(1)	-6(1)	9(1)	13(1)
C(14)	3860(1)	3920(1)	3987(1)	37(1)	40(1)	31(1)	38(1)	5(1)	12(1)	13(1)
C(15)	-613(2)	6597(1)	1207(1)	44(1)	38(1)	43(1)	38(1)	2(1)	6(1)	6(1)
C(16)	4(2)	7913(1)	1219(1)	52(1)	56(1)	50(1)	39(1)	13(1)	0(1)	11(1)
C(17)	1358(2)	8741(1)	2156(1)	49(1)	55(1)	39(1)	42(1)	12(1)	5(1)	5(1)
C(18)	2106(1)	8271(1)	3073(1)	37(1)	36(1)	36(1)	34(1)	6(1)	10(1)	7(1)
C(19)	1470(2)	6944(1)	3045(1)	49(1)	47(1)	43(1)	47(1)	17(1)	1(1)	4(1)
C(20)	119(2)	6110(1)	2118(1)	52(1)	48(1)	38(1)	57(1)	13(1)	6(1)	-1(1)
C(21)	2041(2)	5736(1)	245(1)	54(1)	50(1)	50(1)	46(1)	2(1)	4(1)	7(1)
C(22)	3591(1)	9169(1)	4065(1)	34(1)	36(1)	32(1)	31(1)	9(1)	9(1)	6(1)
C(23)	3580(1)	10286(1)	5048(1)	35(1)	36(1)	34(1)	33(1)	10(1)	11(1)	6(1)
C(24)	2201(2)	10606(1)	5174(1)	45(1)	38(1)	46(1)	45(1)	8(1)	11(1)	10(1)
C(25)	2209(2)	11659(1)	6151(1)	52(1)	45(1)	48(1)	62(1)	10(1)	22(1)	19(1)
C(26)	3611(2)	12473(1)	7093(1)	51(1)	56(1)	39(1)	53(1)	2(1)	22(1)	15(1)
C(27)	4957(2)	12218(1)	7014(1)	45(1)	47(1)	38(1)	39(1)	2(1)	13(1)	5(1)
C(28)	5018(1)	11125(1)	6006(1)	35(1)	39(1)	31(1)	31(1)	8(1)	12(1)	6(1)

Table A.3 Atomic coordinates ($\times 10^4$), equivalent isotropic displacement parameters ($Å^2 \times 10^3$) for **CPA** (*Chapter 6*). U(eq) is defined as one third of the trace of the orthogonalized U_{ij} tensor. The anisotropic displacement factor exponent takes the form: $-2\pi^2[h^2a^{*2}U_{11}+\ldots+2hka^*b^*U_{12}]$.

Atoms	x	y	z	U(eq)	U_{11}	U_{22}	U_{33}	U_{23}	U_{13}	U_{12}
N(1)	-2093(1)	-906(2)	1938(1)	92(1)	89(1)	101	86(1)	-25(1)	13(1)	-18(1)
C(1)	1483(1)	3070(1)	3878(1)	68(1)	71(1)	65(1)	72(1)	-3(1)	20(1)	-6(1)
C(2)	2288(1)	3577(2)	3835(1)	80(1)	78(1)	78(1)	92(1)	0(1)	35(1)	-10(1)
C(3)	2773(1)	4280(2)	4390(1)	82(1)	62(1)	75(1)	112	3(1)	24(1)	-13(1)
C(4)	2440(1)	4479(2)	4968(1)	72(1)	64(1)	60(1)	90(1)	-1(1)	6(1)	-9(1)
C(5)	56(1)	3898(2)	6322(1)	80(1)	112	63(1)	70(1)	-5(1)	26(1)	3(1)
C(6)	-754(2)	3436(2)	6372(1)	89(1)	120	75(1)	86(1)	8(1)	53(1)	8(1)
C(7)	-1251(1)	2725(2)	5829(1)	81(1)	88(1)	71(1)	92(1)	13(1)	40(1)	5(1)
C(8)	-924(1)	2475(1)	5247(1)	67(1)	69(1)	57(1)	77(1)	8(1)	23(1)	1(1)
C(9)	275(1)	2719(1)	4554(1)	54(1)	56(1)	44(1)	62(1)	3(1)	10(1)	2(1)
C(10)	1251(1)	4161(1)	5641(1)	65(1)	76(1)	48(1)	67(1)	-6(1)	4(1)	-1(1)
C(11)	1107(1)	3240(1)	4486(1)	56(1)	58(1)	46(1)	63(1)	3(1)	11(1)	1(1)
C(12)	1602(1)	3970(1)	5042(1)	59(1)	61(1)	45(1)	71(1)	2(1)	8(1)	0(1)
C(13)	-76(1)	2950(1)	5159(1)	57(1)	63(1)	43(1)	66(1)	7(1)	15(1)	5(1)
C(14)	427(1)	3681(1)	5711(1)	62(1)	79(1)	45(1)	63(1)	2(1)	18(1)	5(1)
C(15)	-228(1)	1922(1)	3986(1)	54(1)	52(1)	50(1)	60(1)	2(1)	14(1)	-2(1)
C(16)	43(1)	686(1)	3873(1)	63(1)	54(1)	55(1)	77(1)	-2(1)	5(1)	6(1)
C(17)	-419(1)	-55(1)	3346(1)	65(1)	62(1)	52(1)	81(1)	-9(1)	15(1)	3(1)
C(18)	-1164(1)	430(1)	2916(1)	58(1)	57(1)	60(1)	59(1)	-3(1)	15(1)	-6(1)
C(19)	-1450(1)	1656(2)	3022(1)	72(1)	70(1)	64(1)	74(1)	0(1)	-3(1)	8(1)
C(20)	-979(1)	2385(1)	3550(1)	70(1)	75(1)	50(1)	80(1)	-2(1)	1(1)	10(1)
C(21)	-1672(1)	-323(2)	2369(1)	68(1)	68(1)	72(1)	67(1)	-10(1)	18(1)	-9(1)